Model calculations of the groundwater flow at Finnsjön, Fjällveden, Gideå and Kamlunge

L Carlsson
A Winberg

Swedish Geological, Göteborg

B Grundfelt

Kemakta Consultant Company, Stockholm
May 1983

MODEL CALCULATIONS OF THE GROUNDWATER FLOW AT
FINNSJÖN, FJÄLLVEDEN, GIDEÅ AND KAMLUNGE

L Carlsson
A Winberg
Swedish Geological, Göteborg

B Grundfelt
Swedish Consultant Company, Stockholm

May 1983

MODEL CALCULATIONS OF THE GROUNDWATER FLOW

AT FINNSJÖN, FJÄLLVEDEN, GIDEÅ AND KAMLUNGE

L. Carlsson
A. Winberg
Swedish Geological

B. Grundfelt
Kemakta Konsult AB

ABSTRACT

Hydraulic properties and conditions were investigated for the
study sites of Fjällveden, Gideå, Kamlunge and Svartboberget.
Based on geological and tectonical conditions within the sites,
the bedrock was divided into different hydraulic units. Within
each unit relations between hydraulic conductivity and depth
were determined from hydraulic tests performed in 147 to 288
sections in 7 to 16 core-drilled boreholes in each site. The
groundwater table was constructed from topographic maps and
registration of groundwater head in 23 to 64 boreholes at each
site.

Based on the conceptual models of hydraulic units, hydraulic
conductivity versus depth and groundwater tables, the groundwa-
ter flow conditions were calculated using numerical models. The
models used were based on a finite element method in three-di-
mensions. The three study sites Fjällveden, Gideå and Kamlunge
were modelled together with the Finnsjön site. Each site was
modelled down to a depth of 1500 m. The results given as
groundwater potentials were used to calculate groundwater flow
at levels of a potential repository and to estimate trajecto-
ries and travel times for groundwater from the repository
level.

Calculation of the groundwater recharge and head distribution
along profiles coinciding with boreholes made it possible to
compare calculated results with measurements on the sites.

CONTENTS

1. BACKGROUND

The division of KBS at the Swedish Nuclear Fuel Suppy Co
(SKBF) has drawn up a broad-scope program in order to find,
during a period of 10 years or more, a location suitable for
final storage of high level nuclear waste from Swedish nuclear
power plants. Foreseen in the program, is the investigation of
10-2C locations in Sweden representing different types of bed-
rock and varying topographical conditions.

Of crucial importance for the selection of storage location is
the groundwater conditions in the bedrock. Low ground-water
flow in combination with stable geological conditions consti-
tute some of the fundamental criteria to be met by a reposito-
ry site. In determining the groundwater conditions in major
areas and down to depths beneath a potential repository, data
describing the water-conducting properties of the bedrock are
required. Models and methods for the estimation of groundwater
flow, turnover time and flow paths must also be included.

Final storage of high level nuclear waste in Sweden will be
located in crystalline bedrock. The bedrock is very old and
has undergone various stages of conversions and tectonic
events. As a result of this, there are i.a. fracture zones
with higher hydraulic conductivity than the bedrock as such.
The investigations already made and in progress, aiming at
characterising different potential areas, here called study
sites, are carried out according to the so called standard
program (Brotzen 1981, Thoregren 1982). An essential part of
this program is, after overall map studies, the determining of
existence, extension and continuity of fracture zones, ending
up in a descriptive tectonic model of a selected site. One or
more rock volumes will thus be selected for a potential loca-
tion of final storage.

The descriptive tectonic model developed in this way, has to
be quantified with regard to the groundwater conditions. This
is done by means of numerical modelling techniques using
three-dimensional models. These calculations are based on data

specifying the groundwater conducting ability and groundwater
head conditions within the bedrock and existing fracture
zones. These data are collected by means of various hydraulic
measurements and tests in the field and are processed in comp-
liance with available theories and models of groundwater flow
in crystalline bedrock.

The present report constitutes a compilation of methods and
model applications aiming at identifying the groundwater con-
ditions in crystalline bedrock. In addition, detailed results
are given related to each study site presented in Table 1.1.
The location of each study site is given in Fig. 1.1.

Table 1.1.   Study sites modelled and described in the present
              report.

Area	Bedrock	No of drill-holes	
		Deep >150 m	Shallow <150 m
Fjällveden	Veined gneiss	15	49
Gideå	Veined gneiss	13	24
Kamlunge	Gneiss, Granite	16	21
Svartboberget	Mig.gneiss	7	16

2. GEOLOGICAL-TECTONIC BACKGROUND

2.1 Investigations performed

The investigations, and the methods previously and currently
employed in investigations of potential sites for storage of
radioactive waste, are described in detail by Ahlbom, Carlsson
and Olsson (1983). Surface-geological and surface-geophysical
measurements have been made in order to identify rock type and
the occurance of fracture zones in the surficial parts of the
bedrock. These measurements provide maps of anomalies in
electrical, magnetical, and gravimetrical fields. These anoma-
lies are results i.a. of fracture zones which consequently can
be mapped in this way also in soil covered areas. Analyses of
aerial photographs, seismic investigations, and geological
mapping are other techniques used in order to map i.a. the
extention and geometry of existing fracture zones.

Drilling is performed within the different areas in order to
determine orientation and continuity of fracture zones and
rocktype boundaries as well as to investigate anomalies provi-
ded by surface investigations. The majority of the drill-holes
within an area will consequently penetrate one or more of the
zones mapped superficially. This makes it possible to determi-
ne the widths of the zones at penetrated depths and to obtain
data on the hydraulic conditions and properties of the indivi-
dual zones. A number of geophysical investigations are made in
the drill holes, the purposes of which are shown in Table 2.1.

Table 2.1.   Geophysical methods used in investigations of
              study sites.

	Fracture zones	Bedrock	Ground water
A Ground surface measurements			
Geoelectric	X	X	
Magnetic loop (Slingram)	X		
VLF	X		
Magnetic measurements	X	X	
Refraction seismic	X		
B Drill-hole measurements			
Gamma ray log		X	
Geohm	X		
Resistivity	X	X	
Self potential	X	X	X
Ind. polarisation		X	
Temperature	X	X	X
Salinity	X		X
Geochem.log			X

2.2   Tectonic models

2.2.1   General

A geological-tectonic model provides a description of existing
fracture zones as well as the geometrical extention of the
different rocktypes. The model can be of varying accuracy
depending on available data and purpose of the model. A model
aiming at indicating where there are zones which might entail
problems from a civil engineering view-point is made only to
include zones where there are crushed rock. A model intended
for groundwater calculations will also include zones which do
not necessarily entail problems from the viewpoint of enginee-

ring geology. Also considering the fact that safety analysis
for nuclear waste storage has a time span of 1,000 - 1 million
years, zones may be taken into consideration which are of
minor importance from engineering aspects.

The width of existing zones is estimated from the ground sur-
face geophysical measurements and from core mapping as well as
from drill-hole geophysical measurements. Fracture zones of
major extension as a rule have a highly varying structure. A
higher degree of fracturing in the zone than what is normal is
in these cases observed in the core. However, in certain cases
the fracturing is so extensive that the rock in the zone is
shattered to fragments (crushed zone). Within a certain zone
the number of crushed rock segments may vary in width and num-
ber.

In order to identify and map a crushed zone with regard to
location and extent it is also required that the extention of
the zone has been registered in the surface investigations, or
that it has been observed in one or more drill-holes in con-
juntion with such investigations. In rock there are also a
number of fractures as well as fracture zones and crushed seg-
ments of limited extent. These are regarded as being a part of
the "normal fracturing" of the bedrock.

The geological-tectonic models developed for the individual
study sites are intended to constitute back-up information for
the modelling of groundwater conditions in the bedrock. These
models should be subject to time aspects applicable to safety
analyses of a potential storage at a depth of approx. 500 m.
When appraising the extension and width of the fracture zones,
results obtained by hydraulic measurements in the individual
zones have therefore also been taken into consideration.

2.2.2   Fjällveden

The geological-tectonic model of the site Fjällveden comprises
in detailed scale an area of approx. 4 km^2. A regional model
covers approx. 300 km^2, including fracture zones of regional

character. The latter model has been developed from aerial
photograph studies. The detailed model is based on data from
ground surface geophysical and geological mapping and from
aerial photograph studies (Ahlbom et al 1983). For the deter-
mination of width and orientation of the various zones, data
from drillings and geophysical drill-hole loggings have been
utilized. The geological-tectonic model developed is described
in Fig. 2.2.1. Data on the individual zones are given in Table
2.2.a and in Fig. 2.2.2.

Table 2.2.a.　　Data on identified fracture zones in the Fjäll-
veden study site (ref. to Fig. 2.2.1.).

Zon no	Width m	Dip	Drill-hole	Identification
1	1-7	90	Fj 2,5,6 HFj 1,2	Field, topography,ground surface geophysics
2	9-12	80 NE	Fj 14,15 HFj 5,6,12, 30	Field, topography, ground surface geophysics
3	5-11	90	Fj 3,4,6 HFj 18	Field, topography, ground surface geophysics
4	1	80 SE	Fj 2	Topography, ground surface geophysics
5	0,5-1	80 NW	Fj 4,6,11, 12 HFJ 35	Field, topography, ground surface geophysics
6	0,2	75 SE	Fj 1 HFj 18,22,29	Field, (ground surface geop- hysics)

7	14	60 NW	Fj 9	
8	4.5	90	Fj 9, HFj 32	
9	5	75 SE	Fj 5,7 HFj 9	Field, topography, ground surface geophysics
10	5-6	70 SE	Fj 5,7	Field, topography, ground surface geophysics
11	3	90	Fj 6	Field, ground surface geophysics
Reg east zone	90	75 SW	Fj 10	Field, topography, ground surface geophysics

2.2.3 Gideå

The geological-tectonic model of the site Gideå comprises in detailed scale an area of approx. 5 km^2. The model is based on data from ground-surface geophysical and geological mappings and aerial photograph studies (Ahlbom et al 1983). The width and orientation of the various zones have been obtained from drillings and geophysical drill-hole investigations. The geological-tectonic model developed is described in Fig. 2.2.3 Data on the individual zones are given in Table 2.2.b and in Fig. 2.2.4.

A regional tectonic model of the area has been developed from aerial photograph studies. The size of this model is approx. 400 km^2.

Table 2.2.b.   Data on identified fracture zones in the Gideå
                study site (ref to Fig. 2.2.3).

Zon no	Width m	Dip	Drill-hole	Identification
1	22-24	40 SE	Gi 2,5 HGi 1,5,23 HGi 24	Field, topography, ground surface geophysics
2	11	70 NW	Gi 5 HGi 15	Field, topography, ground surface geophysics
3A	10-24	30 N	Gi 4,6,9,11 HGi 7,8	Field, topography, ground surface geophysics
3B	4-9	80 N	Gi 6,11	Field, topography, ground surface geophysics
4	10	90	Gi 4	Field, topography, ground surface geophysics
5	50	70-90 N		Field, topography, ground surface geophysics
6	1-8	70 SE	Gi 3,4,7,12	Ground surface geophysics
7	1-7	75 E	Gi 3,6	(Ground surface geophysics)

2.2.4 Kamlunge

The geological-tectonic model of the Kamlunge study site com-
prises, in detailed scale, an area of approx. 6 km^2. The
model is based on data from ground-surface geophysical and
geological mapping and from aerial photograph studies (Ahlbom
et al 1983). The width and orientation of the zones have been
obtained from drillings and geophysical drill-hole investiga-
tions. The geologic-tectonical model developed is described in

Fig. 2.2.5. Data on the individual zones are given in Table
2.2.c and in Fig. 2.2.6.

A regional tectonic model has also been developed for the
region surrounding the Kamlungekölen on the basis of aerial
photograph studies. The size of this model is approx. 625
km^2.

Table 2.2.c.   Data on identified fracture zones in the Kam-
lunge study site (ref. to Fig. 2.2.5).

Zon no	Width m	Dip	Drill-hole	Identification
1	3	90		Topography, ground surface geophysics
2	4-12	70 NW	Km 3,5,6, 9,12 HKm 1,2	Topography, ground surface geophysics
3	1-10	70 NW	Km 3,8,11, 12 HKm 14	Topography, ground surface geophysics
4	4	80 SW	Km 3	Topography, ground surface geophysics
5	4	60 NE		Topography, ground surface geophysics
6	3	85 NE		Topography, ground surface geophysics
7	3	75 NW		Ground surface geophysics
H1	4-14	0	Km 1,2,13, 14	Drillings

2.2.5 Svartboberget

The geological-tectonic model in detailed scale for the study site of Svartboberget covers approx. 5 km^2. This model is based on data from ground-surface geophysical and geological mapping and from aerial photograph studies (Ahlbom et al 1983). The width and orientation of the individual zones have been obtained from drillings and geophysical drill-hole investigations. Fig. 2.2.7 describes the geological-tectonic model developed. Data on the individual zones are given in Table 2.2.d. and in Fig. 2.2.8.

A regional tectonic model has been developed from aerial photograph studies and covers approx. 42 km^2.

Table 2.2.d.   Data on identified fracture zones in the Svartoberget study site (ref. to Fig. 2.2.7).

Zon no	Width m	Dip	Drill-hole	Identification
1	25	40 S	Sv 1	Topography
2	10-15	45 S	Sv 1,2	Topography, ground surface geophysics
3	25	45 S	Sv 1,2 HSv 2	Topography, ground surface geophysics
4	50	40 S	Sv 1,2 HSv 2	Topography, ground surface geophysics, field
5	20-40	30 S	Sv 1,2 HSv 2	Topography, ground surface geophysics
6	2	30 S	Sv 1	Topography, ground surface geophysics
7	10	65 SW	Sv 5	Topography, ground surface

				geophysics
			HSv 5	
8	5	60 Sv	Sv 3,5,6,7	Topography, ground surface
			HSv 3,10	geophysics
9	5-10	80 SW	Sv 6,7	Topography, ground surface
				geophysics
10	5-10	85 SW	Sv 6,7	Topography, ground surface
				geophysics
11	10	90	Sv 6	Topography, ground surface
			HSv 6	geophysics
12	<5	75 E		Topography, ground surface
				geophysics
13	4	75 E	Sv 4	Topography, ground surface
				geophysics
14	10-25	40 W	Sv 3,5,6	Topography, ground surface
				geophysics
15	5-30	30 W	Sv 3,4,5,6	Topography, ground surface
			HSv 3	geophysics
16	<5	70 N	HSv 7	Topography, ground surface
				geophysics
17	2	85 S	Sv 4	Topography
18	5->30	35 SW	Sv 1,3,5	Topography, ground surface
				geophysics
19	5	40 SW	HSv 11,13,14	Topography, ground surface
				geophysics

3. HYDROLOGICAL BACKGROUND

3.1 General

The groundwater conditions of a specific area are characterized by its topographical, geological and climatological conditions. The geological conditions prescribe i.a. the size and variation of the water-transmitting and water-storaging properties. In combination with the topographical conditions the geological conditions are decisive of how much water the bedrock can convey. The climatological conditions decide the amount of water available for this conveyance.

3.2 Precipitation, evaporation and runoff

Data on the magnitude and variation of the precipitation have been obtained from the SMHI (the Swedish Meteriological and Hydrological Institute) meteorological stations within and adjacent to the study sites. Evaporation and runoff data have been obtained from condensed SMHI reports (Eriksson, 1980, 1981) and by estimates reported by Ahlbom et al (1983). Mean values of precipitation, evaporation and runoff are shown in Table 3.2.a.

Table 3.2.a. Mean precipitation, evaporation and runoff in the study sites.

Site	Mean precipitation mm/year	Potential evaporat mm/year	Actual evaporat mm/year	Runoff mm/year	$1/s \cdot km^2$
Fjällveden	650	596	450	200	6.3
Gideå	765	420	410	345	11.0
Kamlunge	690	395	350	340	10.8
Svartbob.	715	528	390	325	10.1
Finnsjön	670	540	380	240	7.6
Sternö	715	617	540	175	5.5

A proportion of the precipitation is in the form of snow. In Table 3.2.b this proportion is specified as well as the annual mean temperature within the individual study sites.

Table 3.2.b.   Annual mean temperature and proportion of snow of annual mean precipitation within the study sites.

Site	Annual mean temperature ^oC	Proportion snow of annual mean precipitation %
Fjällveden	6.0	21
Gideå	2.7	33
Kamlunge	0.8	45
Svartboberget	3.5	24
Finnsjön	5.5	35
Sternö	7.4	18

3.3 Hydrological data

The study sites investigated are drained via a number of major or minor rivers and streams into lakes, seas or major inland waterways. Table 3.3 shows in condensed form hydrological data on the individual sites.

Table 3.3.   Hydrological data relating to the study sites.

Site	Draining watercourses	Recipient	Distance to recipient
Fjällveden	Nyköpingsån, Svartån	Östersjön	20 km
Gideå	Husån, Gideälven	Bottenhavet	16-19 km
Kamlunge	Kalixävlen, Sangisälven	Bottenviken	30-35 km
Svartbob.	Voxnan	Bottenhavet	80 km
Finnsjön	Forsmarksån	Bottenhavet	20 km
Sternö	-	Östersjön	-

3.4. Groundwater recharge

By groundwater recharge is to be understood the quantity of
water which is supplied to groundwater storage. The ground-
water recharge constitutes part of the amount of water infilt-
rated through a ground surface. A substantial portion of this
latter water quantity is returned to the atmosphere through
the transpiration of plants. The water quantity which proceeds
downwards (percolates), to the groundwater table, constitutes
the actual groundwater recharge after the acts of transpira-
tion, evaportion and capillary binding.

The groundwater recharge within a specific area can be deter-
mined or estimated i.a. by means of the following methods:

* Calculation based on the fluctuation of the groundwater
  table for an extended period and in consideration of the
  effective porosity of the subground.

* Calculation of the quantity of water which can form
  groundwater, based on meteorological, geological and land
  exploitation factors.

* Calculation of the quantity of water which is required,
  in consideration of existing groundwater levels, in order
  to maintain an equilibrium in the groundwater system.

Model estimates of the groundwater conditions within the study
sites implied the use of the latter method in the present
report. The results of these estimates are detailed in Chapter
8, 9, 10, and 11.

The runoff from a catchment area constitutes a measure of the
maximum groundwater recharge as distributed over the surface
of the entire area during an extended period of time. Within
an individual area, only a limited part is recharge areas
(entrance area for groundwater). The size of this part is
governed by the topographical character of the area concerned.

The groundwater recharge within a specific area has a varia-

tion within and between the individual years. Based on the variation of the groundwater table during extended periods (Nordberg and Persson 1976), Karlquist and Olsson (1983) have demonstrated that the groundwater recharge takes place during different periods of the year in different parts of the country, as shown in Fig. 3.4.1.

In Sweden the groundwater recharge has been measured and calculated for a number of areas, i.a. within the scope of the International Hydrological Program. Thus, a mean groundwater recharge of 64 mm/year has been calculated for Lappträsket, approx. 40 km north of Boden. This catchment area is approx. 1,000 km^2 and is made up of 30% mire and 65% till (Persson 1978).

Investigations made by von Brömssen (1968) indicate that the groundwater recharge expressed as an infiltration coefficient is 0.11 - 0.37 in the case of clay-rock-till areas. This coefficient denotes the groundwater recharging proportion of the precipitation.

The groundwater recharge to the bedrock constitutes part of the total groundwater recharge in a specific area. The magnitude of this has, in the case Lappträsket, been estimated at 0.3 - 25 mm per annum, based on groundwater level variations, and with an assumed effective bedrock porosity of 0.1 - 1% . Axelsson and Olsson (1979) have, setting out from modelbased estimates of the groundwater conditions at the Juktan power plant, calculated the groundwater recharge in rock mass at 5 mm/year and in fracture zones at 50 mm/year.

4. HYDRAULIC CONDUCTIVITY

4.1. Definitions

Crystalline bedrock in Sweden consists mainly of igneous and metamorphic rock types, in most areas with ages in excess of 800 mill. years. Both during the formation stage and during subsequent periods, the bedrock has experienced various tectonic events which have i.a. entailed the formation of the individual fractures and fracture zones. Between or within individual mineral grains there are also minor so called micro-fractures.

Major fractures or zones of fractures which can be followed in the terrain or on a map as lineaments, constitute inherent elements of the tectonic model made up for the different study sites (ref to Section 2.2). Other hydraulic elements in the bedrock are, besides the rock mass, dikes or strata of rock types of deviating hydraulic conductivity from the surrounding bedrock.

The water yielding ability of the bedrock is characterized by its intrisic permeability. This is a pure material constant (dimension L^2) denoting the permeability of the bedrock. Usually, the permeability of the bedrock to water is specified in terms of its viscous properties and the material constant is in this case referred to as the hydraulic conductivity. The relationship between the permeability k and the hydraulic conductivity K is expressed as :

$$K = g \rho k/\mu \qquad\qquad (4-1)$$

where μ = the dynamic viscosity (approx. $1.4\ 10^{-3}$ Pa.s) of water

ρ = the density

g = the gravity constant

To water as a percolating liquid the following applies:

$$K = 7. \ 10^6 \ x \ k \ m/s \qquad (4-2)$$

Hydraulic conductivity constitutes the material constant which in Darcy's law expresses the connection between water volume per unit of time and area, and the hydraulic gradient as:

$$K = Q/(Axi) \qquad (4-3)$$

where   Q = water volume per unit of time through an area A
         i = hydraulic gradient

In crystalline bedrock the rock material, i.e. the crystalline part, is of very low hydraulic conductivity. The low water flow in the rock material is via crystal boundaries and micro-fractures. The occurrence of fractures and fracture systems instead constitute the main flowpaths for water transport in ·the bedrock.

The hydraulic conductivity K_f of individual fractures can be described according to Navier-Stokes' equation of flow between parallell plates, generally referred to as Poiseuille flow. According to Snow (1967) this is expressed as :

$$K_f = (2b)^2 g \ \rho/(12 \ \mu) \qquad (4-4)$$

where 2b = fracture width
      μ = dynamic viscosity
      g = gravity constant

Fractures in rock have rough walls and openings of varying size and form. The fracture walls are in contact with each other on a number of points or surfaces. The groundwater flow is in this case limited to the open parts of the fractures, so-called channelling (Maini 1971). The flow in a fracture may, according to Iwai (1976), be approximated by parallell plate flow in an opening equal to the mean flowpath aperture.

Individual fractures and fracture zones of limited extension are, together with the crystalline part of the bedrock, inherent parts of what is here referred to as the rock mass. Zones

of geometrically well defined extension constitute other hyd-
raulic units outside the rock mass as shown in geological-tec-
tonic models set up.

The hydraulic conductivity of the rock mass varies depending
on the point (in space) which is measured. The rock material
with its microstructures usually has a very low hydraulic con-
ductivity compared to the conductivity of the fractures. Under
conditions of uniform fracture width (2b) and a groundwater
flow parallell to the fractures, the following relation app-
lies between the hydraulic conductivity of the fractures and
the rock mass:

$$K = 2b \, n \, K_f \qquad (4-5)$$

where $n = m/L =$ the fracture frequency

The hydraulic conductivity of the rock mass is in this case
proportional to the fracture frequency and the fracture aper-
ture in cube. By the number of fractures is to be understood
the number of hydraulically conductive fractures.

4.2 Determination methods and equipment

4.2.1 Scope

The hydraulic conductivity of the bedrock has been determined
by tests in individual drill-holes and between different
drill-holes (interference tests). The first-mentioned tests,
the water injection tests, were made in different sections of
the drill-holes. These sections were sealed off by means of
inflatable rubber packers. The length of the test sections
varied between the sites as shown in Table 4.2.a. Sections of
25 m length were tested in all of the deep drill-holes (diame-
ter 56 mm) within the sites of Fjällveden, Gideå, Kamlunge and
Svartboberget. In addition, 5 and 10 m sections were used in
parts of the drill-holes containing major fracture zones. In
the Finnsjön and Sternö sites, 2 and 3 m sections were used
exclusively.

Table 4.2.a. Number of drill-holes used for water injection
              testing in the individual normative areas.

Site	No of drill-holes tested	No of sections tested		
		25 m	5 a 10 m	2 a 3 m
Fjällveden	9	219	61	188
Gideå	11	288	86	162
Kamlunge	10	187	72	175
Svartboberget	7	147	87	-
Finnsjön	8	-	-	1625
Sternö	5	-	-	1399

Two types of equipment, steel mandrel and umbilical hose sys-
tem, respectively, were used in water injection testing. The
equipments and the test procedure principles are described in
detail by Almen et al (1983).

Interference tests were carried out in the Fjällveden, Gideå,
Svartboberget and Kamlunge sites. The purpose of these tests
was to estimate the hydraulic conductivity of a major rock
volume. The tests were conducted as pumping test at constant
rate. For practical reasons, the interference tests were con-
ducted in the upper part of the bedrock (0-150 m). The changes
in groundwater pressure caused by the pumping were registered
in various sections of adjacent drill-holes.

4.2.2 Water injection tests

The water injection tests were carried out in three consecuti-
ve phases as shown in Fig. 4.2.1:

* Packer sealing   (approx. 30 min.)
* Water injection   (approx. 120 min.)
* Pressure fall-off   (approx. 120 min.)

After completed packer sealing a constant water pressure is
applied to the tested section. This pressure is, as a rule 200

kPa (20 m water column) over the existing natural water pressure. The pressure is measured in the test section and kept constant by regulating the water flow. The water flow is registered as a function of time after start of water injection. Asssuming radial flow out in the rock from the tested section, the flow can be expressed as:

$$Q(t) = 2 K \times L \times H \times G(\alpha) \qquad (4\text{-}6)$$

where $Q(t)$ = the flow as a function of time t

K = the hydraulic conductivity of the rock (equivalent homogenous porous medium)

$G(\alpha)$ = well function at constant pressure

H = constant positive or negative pressure in tested section

L = section length

$$\alpha = (Kt)/(r_w^2 S_s) = t_D \qquad (4\text{-}7)$$

where r_w = drill-hole radius

S_s = the specific storage coefficient of the rock

Equation (4-6) pressumes that there is no skin effect. This means that the water pressure in the close vicinity rock is equally large as the water pressure in the drill-hole. In the case of skin being present, t_D is replaced with $t_D \times e^{2\ell}$ in equation (4-7) where ℓ is the skin factor defined in equaion (4-11) (Almen et al 1982). In injection tests at constant pressure there is no disturbing effect of well-bore storage.

In cases of large values of α, i.e. extended testing time and/or small values of r_w, $G(\alpha)$ can be approximated by $2/W(u)$, where $W(u)$ constitutes Theis' well function and

$$u = 0.25/\alpha \qquad (4\text{-}8)$$

In respect of values of $u < 0.01$ ($\alpha > 2.50$) equation (4-6) can be used (Lohman 1972):

$$1/Q(t) = 0.183(\log(2.25Kt/(r_w^2 S_s)) + 0.868\pounds)/(kLH_o)$$

$$(4-9)$$

Uraiet and Raghavan (1980) state that equation (4-9) can be used if $\alpha > 1000$.

Equation (4-9) is the basic equation for the evaluation of the hydraulic conductivity K for the individual tested sections during the injection phase. In a diagram $1/Q(t)$ is drawn up as a function of time according to Fig. 4.2.2. The hydraulic conductivity is thereupon calculated as (Almen et al 1982):

$$K = 0.183/(H_o L \Delta(1/Q)) \qquad (4-10)$$

where $\Delta(1/Q)$ = change during a decade of $1/Q$.

Calculation of the hydraulic conductivity can thus be made independently of the presence of skin. The presence of skin means that the drill-hole has inferior communication with the neighbouring rock (positive skin), or interacts with the rock via fractures (negative skin). The skin factor can be calculated as:

$$\pounds = 1.15((1/Q)_m / \Delta(1/Q) - \log(K/(r_w^2 S_s)) - 2.13)$$

$$(4-11)$$

where $(1/Q)_m$ = the value of $1/Q$ at time $t = 1$ minute.

When calculating the skin factor the value of S_s must be known or estimated.

A specific volume around the drill-hole is influenced during injection testing. The size of this volume is in general dependent on the hydraulic conductivity, the specific storage coefficient of the rock, and the duration of the test expressed as:

$$r_e = \sqrt{2.25 \ Kt/S_s} \qquad (4-12)$$

where r_e = the radius of the idealized influenced volume

t = testing time in seconds

The size of the influence radius at different values of hydraulic conductivity is shown in Fig. 4.2.3. In a test section the hydraulic conductivity varies, and the calculated value obtained constitutes a weighted mean value according to:

$$K = 1/L \quad \Sigma\ b_i K_i \qquad (4-13)$$

where K_i = the hydraulic conductivity in different parts b_i of the tested drill-hole section

Thus, the influence radius is not constant for a tested section but varies within the section depending on the K-values of the individual parts.

In the third and last phase of the water injection tests, the water flow to the test section is stopped and the pressure falls off and is levelled out to the water pressure prior to the start of injection. Based on the previous assumption, the residual water head H_i as a function of the time t, can be expressed (Earlougher 1977, Andersson and Carlsson 1981) as:

$$H_i = H - H_s = 2.30 \ \log((t_p + t')/t')/(4 \ \pi \ KL) \qquad (4-14)$$

where H_s = natural hydraulic head in the test section before the start of the injection test

   H = head in the test section at the time t'

   t_p = duration of the preceding water injection phase

   t' = current time after injection stop

In a so-called Horner-diagram the correlation between log $(t_p + t')/t'$) or the inverted value, and the water head H forms a straight line. In order for such a correlation to develop, the condition applies, that $t_D > 1,000$ and $t'_D > 40$ (Uraiet and Raghavan 1980):

$$t_D' = Kt'/r_w^2 S_s \qquad (4-15)$$

The hydraulic conductivity is calculated from the slope of the

straight line in the Horner-diagram as:

$$K = 0.183 \ Q_o /(\Delta H_i L) \qquad (4-16)$$

where Q_o = the injection flow at end of water injection pha-
se

ΔH_i = pressure change during a logarithmic decade.

In cases of skin and well-bore storage the correct line in the
Horner-diagram is not developed until after a certain period
of time contingent on the following condition:

$$2 \pi KLt'/(C \rho g) \ >= \ 60 + 3.5\pounds \qquad (4-17)$$

where C = the well-bore storage coefficient, i.e. volume
change per pressure change

The method according to Horner also enables the determination
of the test section's natural water head (the piezometric
pressure) by extrapolation of the straight line to infinite
time, i.e. when $(t_p + t')/t' = 1$ on the time axis (Andersson
and Carlsson 1981). The absolute value of the extrapolated
head is as a rule designated H* while the deviation from the
section's pressure before the packer sealing is designated
$\Delta H*$.

4.2.3 Interference tests

Interference tests have been performed as pumping tests in
Fjällveden, Gideå, Kamlunge and Svartboberget. Table 4.2.b
reports the drill-holes used for pumping and observations.
The tests have primarily been carried out to obtain values of
hydraulic conductivity over long distances on some of the
local fracture zones within each study site. The tests compri-
se the upper part of the zones. They have been performed for a
duration of about 40 days time of which half the time compri-
ses the recovery period, see Table 4.2.c.

Table 4.2.b.   Data on drill-holes used in pumping tests.

Site	Pumped drill-hole	Observation drill-holes
Fjällveden	HFj 8	HFj 4, 13, 14, 21, 22, 23, 28, 29
Gideå	HGi 24	HGi 1, 5, 20, 23
Kamlunge	HKm 21	HKm 1, 2, 3, 4
Svartboberget	HSv 11	HSv 8, 12, 13, 14

Table 4.2.c.   Data on the duration and rate of pumping tests in Fjällveden, Gideå, Kamlunge and Svartboberget.

Site	Pumping rate (1/h)	Duration in days Pumping	Recovery	Tested part of the bedrock
Fjällveden	6000	20	19	zone 3 and 6
Gideå	2400	18	17	zone 1
Kamlunge	2400	20	20	zone 2
Svartboberget	6000	14	8	Reg frac zone

In the observation drill-holes three sections have been sealed off by packers. All measurements of water head-changes have been carried out in a time-schedule which make transient evaluation possible.

4.3 Results

4.3.1 General

The hydraulic conductivity in the bedrock varies in space from point to point, and the medium may be regarded as highly heterogenous. This variation is of different type, large-scale,

local-scale and micro-scale. By large-scale is understood the variation in hydraulic conductivity occurring between different defined hydraulic units. The local-scale variation is constituted of the variations in hydraulic conductivity within the individual hydraulic unit. By local scale is in this context understood measurement values determined for lengths or volumes greater than the distance between individual, water--conducting fractures. The micro-scale variations are e.g. constituted of the variation in permeability along a fracture or between fractures and the crystalline part of the rock.

In a heterogenous medium the porosity P, the hydraulic conductivity K, and the specific storage coefficient S_s vary (Dagan 1979). It is not possible to obtain knowledge of the detailed distribution of the above variables with location and flow. Instead, the variables are regarded as stochastic with frequency functions determined by the measured data. This means that defined hydraulic units are regarded as statistically homogenous.

4.3.2 Hydraulic units

For each study site a descriptive hydraulic model of the bedrock has been drawn up consisting of the following hydraulic units:

> A. Regional fracture zones
> B. Local fracture zones
> C. Rock mass

In this grouping, the geological-tectonic models have formed the base for the division of the K-values. In group B data have been compiled from all local zones, irrespective of direction and width. Knowledge of the width, derived from corelog data, has been used in calculating the hydraulic conductivity of the fracture zone from the K-value obtained for the entire section tested. All measured values of hydraulic conductivity have been referred to either of the groups mentioned (hydraulic unit).

Fracture zones are of tectonically different shapes. In the Gideå site the fracture zones are, for instance, partly filled with clay, and thus have a low hydraulic conductivity. In such cases, zones of higher conductivity, connected to the fracture zones, may exist in the surrounding rock mass. In those cases, the high conductivity values have been designated to the adjacent fracture zone.

As for the regional fracture zones, a very limited number of data is available. In general, however, these zones have been assumed to possess higher hydraulic conductivity than the local fracture zones. The relationship between depth and conductivity has been assumed to be similar to that applying to the local fracture zones.

4.3.3 Effective hydraulic conductivity

ᵀn order to characterize the hydraulic properties of the different hydraulic units for model calculations, an effective hydraulic conductivity K_e has been applied based on all measurement values within each individual unit. This effective hydraulic conductivity constitutes some kind of mean value of individual conductivities measured.

Each individual measurement value represents a limited part of a hydraulic unit. The size of these parts varies and depends i.a. on the hydraulic conductivity. The interrelations between these parts are decisive to the choice of mean value estimation. Fig. 4.3.1 illustrates different relations between conductive parts of the bedrock. In Case (a) each measurement value represents bedrock strata of infinite extension. In cases of groundwater flow parallel and perpendicular, respectively, to the strata, the effective hydraulic conductivity is described by the arithmetic K_a and the harmonic K_h mean value as:

$$K_a = 1/n \sum_i^n K_i \qquad i = 1,2,\ldots,n \qquad (4\text{-}18)$$

$$K_h = n/(\sum_i^n (1/K_i)) \qquad (4-19)$$

In the different hydraulic units, the different hydraulic conductivity values are of random distribution, Case (b) in Fig. 4.3.1. The distribution of hydraulic conductivity values in large statistically homogenous formations indicate logarithmic normal distribution (Freeze 1975). Warren and Root (1961), Freeze (1975) and Dagan (1979 and 1981) have theoretically treated porous statistically homogenous media where the distribution of the hydraulic conductivity has been log-normal. This has been performed i.a. by means of Monte Carlo simulation and the utilization of stochastic differential equations. Dagan (1979 and 1981) has demonstrated that the effective hydraulic conductivity K_e of a log-normal distribution can be expressed as:

$$K_e = K_g (1 + (1/2 - 1/m) s^2) \qquad (4-20)$$

where K_g = the geometric mean value

m = 1, 2, 3 depending on the flow conditions being one-, two-, or three-dimensional

s = standard deviation of ln (K)

Corresponding results have also been reported by Gutjahr et al (1978).

4.3.4   Frequency distribution

The geometric mean value K_g may be written as:

$$K_g = (\prod_i^n K_i)^{1/n} \qquad (4-21)$$

In a log-normal distribution K_g is equal to the median value K_m. To a log-normal distribution the following applies, see Fig. 4.3.2:

$$K_a = K_g \exp (s^2/2) \quad \text{(arithmetic mean value)}$$

$$K_h = K_g \exp(-s^2/2) \text{ (harmonic mean value)}$$

where s = standard deviation of ln(K).

The hydraulic conductivity of the individual hydraulic unit has been assumed to be statistically log-normal distributed. This assumption has been tested with regard to the rock mass by dividing hydraulic conductivity values into 100 m intervals with respect to the vertical depth below the ground surface, and by drawing up the frequency distribution of the measurement values in log-normal diagrams. Figures 4.3.3, 4.3.4, 4.3.5 and 4.3.6 specify the measurement values of the individual study sites, drawn up in such diagrams. The volume of data per individual interval in the form of statistical values obtained, is specified in the Appendix.

Fig. 4.3.7 specifies the median values of the drawn-up lognormal distributions, as well as calculated geometric mean values. From the figure is evident that K_g and K_m have corresponding values within 100 m intervals down to a depth of approx. 400 m. At greater depths the observed deviation depends on the large amount of measurement data on the measurment limit (1.10^{-11} m/s), see Fig. 5.1.1, which means that the geometric mean value is greater than the median value.

The log-normal distributions shown in Figs. 4.3.3, 4.3.4, 4.3.5 and 4.3.6, have been tested using the Chi-square-test. For this purpose, statistical parameters have been obtained from the drawn-up figures. The results indicate that the assumed log-normal distribution is fullfilled in 75% of the tested intervals, Table 4.3.a.

4.3.5. Depth dependence

The hydraulic conductivity in the bedrock is dependent on the frequency, apertures, and continuity of the hydraulic fractures. Equation (4-4) expresses the hydraulic conductivity of an individual fracture on the assumption of flow between parallell plates. The corresponding expression for a rock mass of

Table 4.3.a.   Result of Chi-square-test of log-normality of
               frequency of measured values of hydraulic con-
               ductivity in the rock mass within different 100
               m intervals. Confidence degree 0.95. Varying
               degree of freedom between 1 and 5. Median values
               and statistical parameters derived from Fig.
               4.3.3, 4.3.4, 4.3.5 and 4.3.6.

Interval	Fjällveden	Gideå	Kamlunge	Svartboberget
0-100	Pos	Pos	Pos	Pos
100-200	Pos	Pos	Neg	Pos
200-300	Pos	Pos	Neg	Pos
300-400	Pos	Neg	Pos	Pos
400-500	Pos	Neg	Pos	Pos
>500	Pos	Neg	Pos	Neg

uniform fracture width and fracture frequency is given by
equation (4-5). As demonstrated in section 4.1 a ground-water
flow along a fracture is a flow along irregular channels
extending along the plane of the fracture.

The hydraulic conductivity within different hydraulic units in
the bedrock has been assumed to be log-normally distributed.
According to Neuzil and Tracy (1981) the fracture width dist-
ribution is also log-normally distributed. A fracture width
distribution which has, under original rock stress conditions,
a logaritmic normal distribution, has, under other conditions
also a logaritmic normal distribution with the same variance.
This applies provided that a change in stress normal to the
fracture will result in a reversible change in fracture aper-
ture which is proportional to the original aperture. This is a
simplification of a complex process and does not account for
the crushing of asperities or the creation of new points of
contacts, along the individual fractures.

Assuming that a linear relationship exists between changes

in stress and fracture aperture, a relationship between depth
representing the rock stress, and hydraulic conductivity may
be expressed as:

$$K = a \ Z^{-b} \quad (Z > 0) \qquad (4-22)$$

where a and b are constants
      Z = vertical depth below ground surface

In the calculations all measured values within the individual
hydraulic units have been utilized. Different flow conditions
have, moreover, been assumed in accordance with equation
(4-20). A three-dimensional flow has been assumed in the rock
mass, and two-dimensional groundwater flow in the local and
regional fracture zones, respectively.

The depth dependence of the effective hydraulic conductivity
may thus be expressed, in accordance with equations (4-20) and
(4-22), as follows:

$$K_e = c \ a \ Z^{-b} = A \ Z^{-b} \quad (Z > 0) \qquad (4-23)$$

$$c = (1 + (1/2 - 1/m) \ s^2) \qquad (4-24)$$

In Tables 4.3.b and -c, the values obtained for coefficient a,
b and c are shown in respect to rock mass and local fracture
zones within each study site. The hydraulic conductivity ver-
sus depth is shown in Figs. 4.3.8, -9, -10 and -11 in respect
to rock mass, and in Figs. 4.3.12, -13, -14 and -15 in respect
to the local fracture zones within the sites.

Values below the set measurement limit (1.10^{-11}) have been
given the value of the limit which means that the effective
hydraulic conductivity below approx. 400 m depth is strongly
influenced by the measurement limit. Medean values of the
log-normal distribution indicate that the effectice conducti-
vity in the rock mass at depth of 500 m is 0.1 - 0.5 times
lower. In the model calculations, the relationships specified
in Tables 4.3.b and 4.3.c have however been utilized.

Table 4.3.b. Coefficients a, b and c, equation (4-23) expres-
sing the relationship between depth and hydrau-
lic conductivity in rock mass within each study
site.

Site	No of data	a	-b	c	regression coefficient r^2
Fjällveden	200	$8.0 \ 10^{-4}$	2.78	1.92	0.44
Gideå	264	$2.2 \ 10^{-2}$	3.33	2.42	0.46
Kamlunge	227	$4.3 \ 10^{-3}$	3.17	1.84	0.54
Svartbob.	109	$4.8 \ 10^{-4}$	2.70	1.94	0.48

Table 4.3.c. Coefficients a, b and c, equation (4-23) expres-
sing the relationship between depth and hydrau-
lic conductivity in local fracture zones within
each study site.

Site	No of data	a	-b	c	regression coefficient r^2
Fjällveden	14	$1.7 \ 10^{-1}$	3.15	1	0.58
Gideå	24	$8.5 \ 10^{-2}$	3.33	1	0.32
Kamlunge	8	$4.0 \ 10^{-7}$	1.02	1	0.10
Svartbob.	20	$1.3 \ 10^{-3}$	2.31	1	0.33

Besides the curves in Figures 4.3.8, -9, -10 and -11 as well
as 4.3.12, -13, -14 and -15, specified confidence intervals
are presented with confidence levels 0.98 and 0.95 respective-
ly.

In the Fjällveden and Gideå sites the bedrock is composed of
alternating strata of veined gneiss and granite gneiss. Both
rock types have different permeability which means that in
local scale the bedrock exhibits anisotropic hydraulic proper-
ties. In directions parallel to the orientation of the strata,

the rock mass has a hydraulic conductivity K// obtained from
the following equation:

$$K// = a \, K(GG) + (1-a) \, K(VG) \tag{4-25}$$

where K(GG) = the hydraulic conductivity of the granite gneiss
K(VG) = the hydraulic conductivity of the veined gneiss
a = the proportion of granite gneiss

The hydraulic conductivity of the rock mass perpendicular to
the orientation of the strata is obtained from the harmonic
mean value of the hydraulic conductivity of the granite gneiss
and veined gneiss.

In the Fjällveden area the granite gneiss constitutes approx.
3 % of the rock mass. The orientation of the strata follows
the general strike and dip characteristics, i.e. northeast
strike and vertical dip. In the Gideä area, the strata are
subhorisontally layered and the proportion of granite gneiss
is 6 % . In both areas the strata are continuous over long
distances (Ahlbom et al 1983).

When estimating the hydraulic conductivity of the individual
rock types, measurement data from sections containing only
veined gneiss, have formed the basis for a relationship bet-
ween depth and effective hydraulic conductivity. In the measu-
rement sections constituted of granite gneiss and veined
gneiss the measured conductivity value has been reduced by the
hydraulic conductivity of the veined gneiss derived from the
the above mentioned relationship. Residual hydraulic conducti-
vity has been referred to the granite gneiss in accordance
with the following equation:

$$K(GG) = (K \, L - K(VG) \, L(VG)) \; / \; L(GG) \tag{4-26}$$

where   L = lenght of measurement section (25 m)
L(VG) = length of veined gneiss in the measurement sec-
tion
L(GG) = length of granite gneiss in the measurement
section

K = measured hydraulic conductivity

K(VG) = the hydraulic conductivity of veined gneiss at
specified depth derived from the depth relation
curve

Figs. 4.3.16 and 4.3.17 show the effective hydraulic conducti-
vity of veined gneiss and granite gneiss as a function of
depth in the Fjällveden and Gideå areas. The figures also spe-
cify the greatest hydraulic conductivity calculated to illust-
rate anisotropic conditions (parallel to the bedrock structu-
re). Table 4.3.d summarizes the coefficients obtained for the
different relationships according to equation (4-23).

Table 4.3.d.   Coefficients a, b and c, equation (4-23),
expressing the hydraulic conductivity versus
depth in granite gneiss, veined gneiss, and
hydraulic conductivity parallel to bedrock
structure under anisotropic conditions within
the study sites Fjällveden and Gideå.

Site and rock-type	No of data	a	-b	c	regression coefficient r^2
Fjällveden					
Veined gneiss	175	$3.38 \ 10^{-3}$	3.11	1	0.58
Granite gneiss	22	$3.32 \ 10^{-3}$	2.24	1	0.15
K parallel to bedrock structure		$2.78 \ 10^{-4}$	2.38	1	
Gideå					
Veined gneiss	164	$2.63 \ 10^{-2}$	3.39	1	0.52
Granite gneiss	85	$4.00 \ 10^{-1}$	3.49	1	0.28
K parallel to bedrock structure		$4.70 \ 10^{-2}$	3.43	1	

5. WATER TRANSMITTING PART OF THE BEDROCK

5.1 General

The occurrence and movement of groundwater in the bedrock is
highly dependent on existing fractures. Although bedrock with
a high proportion of fractures may contain much groundwater,
these fractures must be interconnected in order to mobilize
the groundwater. The rate at which the water is transmitted in
the fractures depends on the hydraulic conductivity of the
fractures, primarily on their apertures.

Bedrock containing a large proportion of fractures, i.e. with
a high frequency of fractures, may have adequate hydraulic
communication between the fractures in the surficial parts.
Under the influence of heavy loads, fractures will be less
open and will also have lesser degree of hydraulic communica-
tion with each other. This results in decreasing hydraulic
conductivity with increasing depth, see also Section 4.3.5.

Fig. 5.1.1 shows the percentage of measured 25 m sections in
the rock mass within the study sites, which have a hydraulic
conductivity less than 1.10^{-11} m/s, i.e. below the set
measurement limit. The figure also shows the mean fracture
frequency within the corresponding depth interval. Evident
from the figure is the connection between fracture frequency
and the proportion of non-conductive sections, with the excep-
tion of the site Svartboberget. The mean fracture frequency in
the rock mass at depths below 500 m is 1.8 - 2.5 fractures per
metre and the proportion of measurement values below
1.10^{-11} m/s being 63 - 71 % in the study sites.

5.2. Porosity

The part of the rock not consisting of mineral grains or other
solid matter, primarily fractures of different sizes, is
expressed as porosity. Of this porosity only a minor part is
hydraulically conductive. This part is denoted kinematic poro-
sity or flow porosity and consists of those fractures which,
on the one hand, are sufficiently open to permit water to flow

through them and, on the other hand, are in continous connection with each other as shown by the outline drawing in Fig. 5.2.1.

According to Norton and Knapp (1977) the porosity of the bedrock can be categorized as follows:

$$P(T) = P(K) + P(D) + P(R) \qquad (5-1)$$

where P(T) = total porosity
      P(K) = kinematic porosity
      P(D) = diffusion porosity
      P(R) = residual porosity

Total porosity can be calculated from density measurements on rock samples. Realistic values of kinematic bedrock porosity have only been obtained at field tests where the flow velocity of the groundwater has been examined under controlled conditions using suitably selected tracers. The total of kinematic porosity and diffusion porosity is estimated by measuring the continous pore volume in test speciments being filled with a liquid after desiccation in vacuum. It may also be estimated by aid of determinining the electric conductivity of the rock after calibration based on liquid saturation tests (Öquist 1981). Tables 5.2.a, 5.2.b, 5.2.c and 5.2.d present such measurements made on cores from Fjällveden, Gideå, Kamlunge and Svartboberget respectively.

Table 5.2.a.   Total values of kinematic and diffusion porosity measured on drill core specimens from Fjällveden. Mean values of logarithmic normal-distribution.

Rock type	No of measurements	Calculated porosity %
Gneiss	175	0.46
Granite	23	0.30
Pegmatite	21	0.33
Greenstone	15	0.03

Table 5.2.b.   Total values of kinematic and diffusion porosi-
                ty measured on drill core specimens from Gideå.
                Mean values of logarithmic normal-distribution.

Rock type	No of measurements	Calculated porosity %
Migmatite	28	0.18
Dolerite	8	0.03
Granite	14	0.20
Pegmatite	5	0.21

Table 5.2.c.   Total values of kinematic and diffusion porosi-
                ty measured on drill core specimens from Kam-
                lunge. Mean values of logarithmic normal-dist-
                ribution.

Rock type	No of measurements	Calculated porosity %
Granite	26	0.22
Amphibolite	3	0.22
Biotitic gneiss	17	0.20
Quartzitic gneiss	4	0.21
Granodiorite-diorite	5	0.13
Pyroxenite	6	0.22

Table 5.2.d.   Total values of kinematic and diffusion porosi-
                ty measured on drill core specimens from Svart-
                boberget. Mean values of logarithmic normal--
                distribution.

Rock type	No of measurements	Calculated porosity %
Migmatite	120	0.28
Migmatite gneiss	47	0.26
Graphitic migmatite gneiss	16	0.38
Migmatite granite	42	0.28
Old granite suite	1C	0.26
Greenstone	44	0.22

Knowing the above-mentioned porosities the residual porosity
can be determined. This porosity usually constitutes the major
part of total bedrock porosity.

When dissolved substances are transported with the mobilized
groundwater the kinematic porosity of the bedrock is utilized.
Dissolved substances can also be transported by diffusion,
utilizing both kinematic porosity and diffusion porosity. Such
conveyance is contingent on differences in concentration and
is therefore independent of groundwater flows.

The magnitude of kinematic porosity varies and depends on whe-
re in the bedrock the measurement is performed. In a fracture
zone the kinematic porosity is higher than in rock mass of
small fracture frequency. Table 5.2.e specifies field-test
values of kinematic porosity.

Table 5.2.e.   Field-test values of kinematic porosity (Gus-
                tafsson and Klockars 1980, Klockars et al
                1981).

Rock type	Site	Kinematic porosity %
Granodiorite, fracture	Finnsjön	0.08 - 0.09
Granitic gneiss, fracture	Studsvik	0.2 - 0.5

5.3   Fracture frequency

The fracture frequency in the bedrock has been determined on
cores from the drill-holes within each study sites. In the
zones defined in Section 2 as regional and local fracture
zones, the fracture frequency is in places so high that the
number of fractures cannot be determined. In certain cases the
fracturing has advanced so far that the rock is crushed to
fragments. The zone is in this case designated crushed zone.

In rock mass between defined local and regional zones, the
fracture rate varies. Tables 5.3.a, -b, -c and -d specify the
mean fracture frequency (fractures per metre) within different
vertical 100 m intervals in the individual study sites. The
standard deviations presented have been calculated on the
basis of fracture frequencies specified within 5 m intervals.
Drill-holes which entail an overrepresentation of fractures
due to their orientation (parallel with fracture zones) have
been excluded.

From tables 5.3a, -b, -c and -d and Figures 5.1.1 it is evi-
dent that the fracture frequency in the bedrock at depths
greater than 500 m is 1.8 - 2.5 fractures per metre. The mean
fracture frequency and the standard deviation decrease with
the depth, except in the case of the Svartboberget area, where
minor variations are observed.

When calculating the fracture frequency in local fracture zones, the number of fractures in existing crushed zones has been set at 50 fractures per metre. In Table 5.3.e the mean fracture frequency is specified for rock mass and local fracture zones within the individual sites. As shown by the table, the fracture frequency in the local fracture zones varies very little between the sites.

Table 5.3.a.   Mean fracture frequency and standard deviation within different 100 m intervals within the Fjällveden site.

Interval	No of measurements	Mean fracture frequency (fr/m)	Standard deviation
0-100	163	3.93	2.53
100-200	170	2.42	2.19
200-300	180	1.94	1.84
300-400	179	1.78	1.68
400-500	180	1.50	1.59
>500	206	1.76	1.91

Table 5.3.b.   Mean fracture frequency and standard deviation within different 100 m intervals within the Gideå site.

Interval	No of measurements	Mean fracture frequency (fr/m)	Standard deviation
0-100	254	4.76	2.66
100-200	248	5.15	3.62
200-300	218	4.58	2.82
300-400	208	4.18	2.39
400-500	209	2.78	2.45
>500	273	2.04	2.32

Table 5.3.c.   Mean fracture frequency and standard deviation
                within different 100 m intervals within the
                Kamlunge site.

Interval	No of measurements	Mean fracture frequency (fr/m)	Standard deviation
0-100	265	5.48	4.08
100-200	270	4.25	3.43
200-300	200	2.86	2.14
300-400	179	2.62	1.73
400-500	178	2.40	1.74
>500	223	2.48	1.57

Table 5.3.d.   Mean fracture frequency and standard deviation
                within different 100 m intervals within the
                Svartboberget site.

Interval	No of measurements	Mean fracture frequency (fr/m)	Standard deviation
0-100	112	2.74	1.70
100-200	122	2.60	1.66
200-300	122	1.84	1.51
300-400	103	2.06	1.49
400-500	72	2.28	3.06
>500	139	2.50	1.62

Table 5.3.e.   Mean fracture frequency (fr/m) for rock mass
                and local fracture zones within the Fjällveden,
                Gideå, Kamlunge and Svartboberget sites.

Hydraulic units	Fjällveden	Gideå	Kamlunge	Svartboberget
Rock mass	2.18	3.90	3.51	2.35
Local fracture zones	11.55	11.05	12.55	11.08

5.4 Hydraulic fracture frequency

Only a certain proportion of the fractures in the rock mass
is hydraulically conductive and thus to be referred to the ki-
nematic porosity see Section 5.2. The frequency of the hydrau-
lically conductive fractures has been calculated on the basis
of water injection tests in 2 or 3 m sections in core-drilled
holes as shown in Table 5.4.a. These calculations are based on
statistic analyses of test sections which contain one to eight
fractures.

The proportion of all test sections of a given fracture fre-
quency within a given depth interval, which have a hydraulic
conductivity less than the measurement limit, is a statistical
estimate of the probability that the test sections with the
given fracture frequency are not hydraulically conductive. By
making calculations for different fracture frequencies within
each 100 m interval, and reducing the aquired estimates to
represent one single fracture, a representative value of the
probability of one hydraulically conductive fracture in the
interval studied is obtained after weighting. Knowing the
total fracture frequency within the interval, the latter can
be converted into a hydraulic fracture frequency.

In the Fjällveden, Gideå and Kamlunge sites, calculations have
been made on measurement results from one individual drill-ho-
le, see Table 5.4.a. In the Finnsjön and Sternö areas detailed
measurements (3 m) have been made in all drill-holes.

The results of the calculations of hydraulic fracture frequen-
cy are shown in Table 5.4.b and Fig. 5.4.1-4. In the Fjällved-
en, Gideå, and Kamlunge sites the hydraulic fracture frequency
varies between 0 and 1.5 fr/m. In the Fjällveden site, the
hydraulic fracture frequency has the same depth characteris-
tics as the total fracture frequency.

The results obtained from the Finnsjön and Sternö sites, Table
5.4.c and Fig. 5.4.4, are based on a more extensive statisti-
cal material. In these cases 5 drill-holes have been used for
the calculations.

Table 5.4.a.   Drill-holes, vertical depth intervals and num-
                ber of measurement values utilized in calcula-
                ting the hydraulic fracture frequency.

Study site	Drill-hole	Vertical depth m	No of data	Measurement limit K m/s
Fjällveden	Fj2	200 - 600	126	$1.3\ 10^{-10}$
Gideå	Gi7	200 - 600	162	$1.0\ 10^{-11}$
Kamlunge	Km2	200 - 600	175	$1.3\ 10^{-10}$
Finnsjön	5 no	0 - 600	467	$2.5\ 10^{-9}$
Sternö	5 no	0 - 600	399	$4.0\ 10^{-10}$

The results obtained from the Finnsjön and Sternö sites indi-
cate a hydraulic fracture frequency varying between 0.08 and
0.93 fr/m. A decreasing frequency with depth is observed in
both sites with the exception of a slight increase in the
Finnsjön site between 400 and 600 m.

Table 5.4.b   Hydraulic fracture frequency, Nh, (fr/m) in
               Fjällveden, Gideå and Kamlunge areas, incl. 95 %
               confidence interval dNh (fr/m).

Depth inter-val	Study site					
	Fjällveden		Gideå		Kamlunge	
	Nh	+/- dNh	Nh	+/- dNh	Nh	+/- dNh
200-300	0.96	0.280	0.53	0.090	0.94	0.250
300-400	0.20	0.015	0.80	0.080	0.09	0.003
400-500	0.26	0.018	1.53	0.195	0.00	0.000
500-600	0.58	0.060	0.38	0.045	0.00	0.000

Table 5.4.c.   Hydraulic fracture frequency Nh (fr/m) in Finn-
               sjön and Sternö areas, incl. 95 % confidence
               interval dNh (fr/m).

Depth inter-val	Study site				
	Finnsjön			Sternö	
	Nh	+/- dNh		Nh	+/- dNh
0-100	0.93	0.094		0.69	0.063
100-200	0.27	0.014		0.55	0.052
200-300	0.17	0.006		0.23	0.040
300-400	0.15	0.004		0.15	0.020
400-500	0.30	0.012		0.18	0.020
500-600	0.30	0.024		0.08	0.011

The hydraulic fracture frequency in the Sternö site shows a
trend in accordance with the total fracture frequency versus
depth in the area.

The estimation of hydraulic fracture frequency is highly
dependent on the measurement limit of the equipment used when
determining the hydraulic conductivity. In the case of the
Fjällveden, Gideå and Kamlunge sites the equipment used per-
mitted the determining of hydraulic conductivity corresponding
to measurement limits of $1.30 \ 10^{-10}$, $1.0 \ 10^{-11}$ and
$1.25 \ 10^{-10}$ m/s respectively.

In the Kamlunge area, sections with a hydraulic conductivity
corresponding to the measurement limit exclusivly were obtai-
ned in the interval 400-600 m. This means that the drill-hole
is tight from the hydraulic viewpoint and consequently has a
hydraulic fracture frequency = 0 fr/m. In conjunction with the
injection tests in 25 m sections in the drill-hole concerned
(Km 2), conductivity values in excess of the measurement limit
$(1.0 \ 10^{-11}$ m/s) were noted in 50 % of the test sections.
Thus, there is a conductive proportion of the total fracture
frequency which cannot be established due to the too high mea-
surement limit when measuring 2 m sections.

In the case of the Finnsjön and Sternö sites, calculations of hydraulic fracture frequency has also been carried out using imaginary measurement limits, in order to study the dependence of the hydraulic fracture frequency on utilized measurement limit. Results are shown in Fig. 5.4.5 and 5.4.6. It is obvious from the figures that the hydraulically conductive proportion of the fractures is highly dependent on the measurement limit of the equipment used.

6. GROUNDWATER CONDITIONS

6.1 General

The groundwater flow is determined partly by hydraulic conduc-
tivity, partly by existing hydraulic head conditions. Diffe-
rences in head within a rock constitute the driving force.
These differences in head varies and are, in general, greater
in the surficial parts of the rock mass than in the deeper
situated parts. In the upper part of the bedrock the groundwa-
ter head is equal to the groundwater table.

The humid climate in Sweden in combination with the low hyd-
raulic conductivity of the bedrock implies, in general, that a
greater water quantity is available for recharge of water to
the bedrock than the quantity of groundwater run-off from the
bedrock. This means that the groundwater table is highly con-
tingent on the topographical conditions. Extended formations
of high hydraulic conductivity entail an equalization of the
topographically contingent groundwater table. Examples of this
are gravel ridges and certain permeable sandstones although
major fracture zones in basement rock may have a similar equa-
lizing effect.

The effect of the topographically contingent groundwater level
is equalized with increasing depth below the groundwater tab-
le. The distribution of hydraulic conductivity is in this con-
text of major importance. In the vertical direction there are
consequently different water pressures and, as a result, dif-
ferent hydraulic gradients. Depending on if the water pressure
increases or decreases, groundwater outflow and inflow areas,
respectively, develop. Figures. 6.1.1 and 6.1.2 show how head
differences created by the topographically contingent ground-
water level are equalized with increasing depth under the
ground surface and how this equaliztion is dependent on the
depth-related character of the hydraulic conductivity.

The groundwater table and the water head in the bedrock fluc-
tuate depending partly on climatological factors, partly on

changes in atmospheric pressure, gravity and other temporary loads. The largest fluctuations in Sweden are caused by climatological factors. The differences between the highest and lowest groundwater level are different in different types of aquiferous deposits, whereas the climatological conditions decide when these extreme values occur. Table 6.1.a indicates some guiding values on the amplitude of groundwater fluctuations during the year (Carlsson and Olsson 1979).

Table 6.1.a. Guiding values of natural change in groundwater level (calculated on material collected by the Geological Survey of Sweden). In individual cases, depending on terrain and location in groundwater flow configuration, substantial deviations from guiding values given may ensue (Carlsson and Olsson 1979).

Formation (Aquifer type)	Annual variations cm	Normal max daily variations cm
Crystalline rock covered by till	150 - 200	< 50
Limestone	100 - 200	< 20 *
Large esker (below highest shoreline)	10 - 30	< 1
Small esker	100 - 150	< 15
Extensive delta formation	10 - 30	< 1
Fine sediment (silt)	50 - 100	< 20
Sandy-silty till	150 - 200	< 50

* Max. daily variation in karstified limestone may be considerably greater. 5 - 10 m has been observed on Gotland (Fagerlind och Nordberg 1973).

6.2 Hydraulic gradient

The hydraulic gradient developed in the bedrock is contingent on the groundwater recharge and the hydraulic conductivity and boundary conditions. The ground surface represents the highest level to which the groundwater can rise after which there is an outflow of groundwater and run-off in the form of surface water.

Fig. 6.2.1 shows how the hydraulic gradient in horisontal and vertical direction changes with increasing depth beneath a circular hill of 200 m radius. The magnitude as well as the depth-dependence is influenced by the depth-dependence of the hydraulic conductivity. In the case of decreasing hydraulic conductivity with increasing depth, a slower gradient decrease is obtained than in the case of uniform conductivity.

Apart from the depth-dependence of the hydraulic conductivity, the presence of high permeable fracture zones influences the hydraulic gradient. This influence is highly contingent on topographical conditions at the fracture zones and on the continuity of the zones and their contrast to surrounding rock mass in respect to hydraulic conductivity. In many cases, fracture zones have an equalizing effect on the hydraulic gradient of intermediate rock mass (Axelsson and Carlsson 1979, Carlsson and Olsson 1979). This effect varies, however, horisontally as well as vertically.

6.3 Determination methods

The groundwater head in the bedrock has been measured by the following means:

* Registration of the groundwater table in drill-holes.

* Registration of groundwater pressure at different levels in drill-holes (piezometry).

* Calculations based on data from hydraulic tests.

The groundwater table has been continously monitored in drill-
holes by means of soundings. Packers have been installed in
the drill holes approx. 5-10 m below the groundwater table in
order to section off the upper part of the bedrock and obtain
measurement values representative to this part. In Table 6.3.a
the number of observations for each study site is specified.

Table 6.3.a.   Number of drill-holes in which groundwater head
                in bedrock has been registered within the study
                sites.

Site	Measurement by		
	sounding	gauge instrumet	piezometry
Fjällveden	60	3	2
Gideå	37	3	1
Kamlunge	35	2	2
Svartboberget	13	3	2

Piezometric measurements have been carried out by sealing off
sections in the drill-holes by means of packers. These sec-
tions were primarily zones of high hydraulic conductivity,
e.g. geometrically identified major fracture zones or crushed
parts in the holes.

The water injection tests have been performed in 2 phases.
During the initial phase a constant injection pressure has
been maintained and the injected flow rate registered. During
the subsequent phase the flow was stopped and the pressure
fall off with time was registered. The tested section's origi-
nal water pressure, i.e. the bedrock water pressure in the
section has been calculated on the basis of the results of
both phases.

Measurements and calculations indicate that the water head in
the bedrock varies with depth. In general, the pressure dif-
ferences are of the magnitude 0-10 m. Depending on if the
drill-holes are located in in-flow or out-flow areas, decrea-
sing or increasing water pressure at different depth levels
have been registered (Ahlbom et al 1983). The presence of
major fracture zones in the drill-holes in many cases implies
marked differences in head in drill-holes in locations where
major topographical differences exist.

6.4 Groundwater maps

Groundwater maps have been constructed for the individual stu-
dy sites . These maps are based on observations of the ground-
water table in existing boreholes and on topographical condi-
tions. The groundwater maps constitute back-up for numeric
model calculations of the groundwater conditions within each
site. The maps are in general showing the groundwater table
within and adjacent to the sites.

In principle, the groundwater map is a topographical map of
the individual site, although with lower levels in elevated
parts. When drawing up the maps certain assumptions have been
made from conditions measured, as follows:

* Beneath isolated hilly parts, the distance between the
  ground surface and the groundwater table is greater than
  within lower parts of the terrain.

* Along and beneath lakes the groundwater table and the sur-
  face of the lake coincide.

* Lower parts of the terrain with major water courses, more
  extensive mire and tectonic zones, constitute groundwater
  out-flow areas, and here the groundwater table coincides
  with the ground surface.

Groundwater maps for the individual sites are shown in Fig.

6.4.1, -2, -3 and -4. The areas vary topographically and thus also with regard to differences between highest and lowest groundwater level. Fig. 6.4.5, -6, -7 and -8 present hypsographical curves of the investigated sites. These curves, which indicate the proportion of an area which is over respectively under a given level, also give a relative measure of differences in groundwater head within a specific area. Of the study sites, Svartboberget has the most marked topography. The Kamlungekölen displays more extensive differences in regional scale, however.

7. SIMULATION AND PRESENTATION OF GROUNDWATER FLOW

7.1 Introduction

The preceding chapters have dealt with the site investigations
and data supply to model calculations. In the following chap-
ters, model calculation procedure and results will be presen-
ted for the sites Finnsjön, Fjällveden, Gideå and Kamlunge.
This chapter briefly describes the simulation procedure and
the presentation of input data. Results of the model calcula-
tions are given in the subsequent chapters. The model used and
the program package for input and output handling in described
by Thunvik and Braester (1980) and Grundfelt (1983).

7.2 The simulation procedure

7.2.1 General

The groundwater flow simulation is performed using a three-di-
mensional model based on the Finite Element Method (FEM)
(Thunvik and Braester 1980). The principal data needed for the
simulation of groundwater flow in an area can be divided into
the following groups:

- Geometry description of the study area
- Boundary condition
- Material properties

Using these data the model computes the ground water head
distribution. The special derivatives of the groundwater head,
the hydraulic gradients, are not neccessarily continous which
means that the solution might be non-mass conservative. This
is as far as possible circumvented by optimizing the size and
distribution of the finite elements.

An extensive package of computer programs (Grundfelt 1983) has
been designed to facilitate the preparation of input data and
to present the results in terms of isopotential lines, flow

vectors etc. This is briefly described below.

7.2.2 Finite Element Method

In FEM the modelled domain is subdivided into a number of ele-
ments. Each element is defined by a number of nodal points
located in the corners and on edges of the elements. Within
each element the unknown variable, in this case the groundwa-
ter head, is assumed to vary according to a polynomial func-
tion of the variable values at the nodal points associated
with the element. Integrating the flow equation within the
element then yields an algebraic equation. The demand for con-
tinous values of the unknown variable at the element interfa-
ces and integration for all elements, generates an algebraic
equation system where the unknowns are the head at the nodal
points.

In the current study, a finite element mesh in general con-
sists of about 200 elements and 10.000 nodal points. The com-
puter space needed to solve such an extensive equation system
is between 5000 and 8000 Kbytes.

7.2.3 Geometry description

The FEM-mesh must be adjusted to the topography of the ground-
water table and the geometry of the hydraulic units e.g. the
fracture zones of the site studied.

The basic data for the geometry description is a map of the
groundwater table and a map of the different hydraulic units
(the regional and local fractures zones) in the site to be
modelled. The map of the groundwater table is digitalized and
used to define the geometry of the top surface of the mesh.

Points defining intersections of different hydraulic units,
bends, hills, summits and other features significant for the
mesh generation are digitized from the maps of hydraulic units
and groundwater table and treated as input data to the actual

mesh generation.

The mesh is, for simplicity, first generated with a flat top-surface. The numbering of elements and nodal points are not optimal with respect to compuational effort in the FEM-model. Special programs have been devised to optimize the numbering of the elements and nodal numbers and to "mold" the mesh into the configuration of the groundwater table.

7.2.4 Boundary conditions

Two types of boundary conditions have been used:

- non-flow boundary
- prescribed head boundary

The non-flow boundary is used for the bottom surface of all study sites and for the vertical boundaries in most of the runs. In the modelling of the local area at Kamlunge, the vertical boundaries are described using prescribed head taken from a calculation on a larger region. In the modelling of the Finnsjön site some runs are made prescribing hydrostatic pressure to the vertical boundaries.

At the top surface the pressure is prescibed to be zero. This is equivalent to assigning potentials corresponding to the elevation above the sea level.

7.2.5 Material properties

The governing material property is the hydraulic conductivity. This property varies with depth as described in chapter 4. The obtained relationships for the depth variation and the derivation of the constants in the equation from field data is described in section 4.3.5. An effective hydraulic conductivity is calculated from eqv (4-23) for each element in the mesh applied in each site.

In some runs for Fjällveden and Gideå, the hydraulic conducti-
vity is assumed to be anisotropic as described in Table 4.3.d.

7.3 Presentation of input data and results

7.3.1 Presentation of the groundwater table

The groundwater table is presented both in a three-dimensional
refief plot and as a contour map. The relief plot is a picture
of the digitalized groundwater table map wheras the contour
map describes the top surface of the finite element mesh.

The contouring is made using an algorithm that utilizes the
same interpolation functions as the finite element mesh. This
means that contours, without smoothening, describe the actual
topography of the mesh´s top surface. Discontinuities in the
gradient thus appear as sharp bends in the contours. Such
discontinuities depend on the relatively coarse discretization
that can be afforded in three dimensions.

7.3.2 Presentation of the finite element mesh

All the meshes that are made in this study consist of a number
of horizontal element layers. The number of layers in each
mesh varies between 6 and 12.

As the fracture zones in many of the modelled areas are incli-
ned, the size of the elements and thus the element density may
vary with depth. However, only the element distribution at the
top surface is presented. The inclination of the fracture
zones is instead described in tabular form in the text. It has
proved intractable to present the full three-dimensional mesh
graphically as the number of lines becomes too large.

7.3.3 Presentation of results

The presentation of results is directed towards illustrating:

- The distribution of groundwater head and the flow field

- The magnitude of the flow rate in and around a potential repository

- Travel times and path lengths for particles originating from the repository

- The relevance of the results

These items are dealt with below.

Distribution of groundwater pressure and flow

The groundwater head distribution is presented as contours of the hydraulic head in vertical and horisontal cross-sections. The algorithm used for contouring is the same as described in section 7.3.1 for the presentation of the topography of the top surface of the mesh. The results are thus presented without smoothening. Discontinous gradients, representing deviations from mass conservatism in the solution, show up as sharp bends in the contours. The algorithm limits the choice of plot planes to planes coinciding with finite element faces.

The arrows in the vertical cross-sections illustrate projections on the plot plane of flow vectors. The length of the vectors are proportional to the logarithm of the Darcy velocity. The direction of the vector component perpendicular to the plot plane has been indicated using filled arrow heads for components directed out of the paper (towards the reader) and unfilled heads for components directed into the paper.

Note that the vectors shown are two-dimensional projections of the three-dimensional solution. The arrows are thus not necessarily perpendicular to the isopotential contours but rather to the three-dimensional isopotential surfaces.

The flow-rate in and around the repository

The magnitude of the calculated flow rate is presented as con-
tour plots in a plane through and parallel to the repository.
The algorithm used for contouring is a simple first order
interpolation on a regular, rectangular grid. This yields a
smoothened result.

Travel times and path lengths for particles from the repository

Trajectories have been traced from positions within the repo-
sitory to points where they exit from the mesh. The lengths of
the trajectories and the integrated travel times have been
tabulated for the trajectories.

The tracking of the trajectories is made using simple Euleran
stepping which introduces a systematic error "in the direction
of the centrifugal force". This, in comibination with the lack
of mass conservatism in the solution, causes some of the tra-
jectories to exit through non-flow boundaries instead of
through the top surface of the mesh.

The relevance of the results

The results of a groundwater flow calculation could be defi-
cient either because of insufficient data or due to a much too
simplified solution of the governing equations. The relevance
of the results are tested in three ways:

- Calculation of the groundwater formation rate (groundwater
  recharge)

- Mass balance for individual elements

- Comparison between calculated potentials and measured piezo-
  metric head distribution in drill-holes.

The groundwater recharge is calculated by summing up all positive recharges and dividing the sum with the total area of the top surface. The formation rate thus calculated is then compared with measured data or knowledge of groundwater recharge in crystalline rocks (section 3.4).

A mass balance is calculated for each element in the mesh to check the numeric quality of the solution. A relative mass balance deviation is calculated from the following equation:

$$\Delta_e = \frac{\sum\limits_i F_i}{\sum\limits_i \left| F_i \right|} \tag{7-1}$$

where: Δ_e = relative mass balance deviation for element e
F_i = the flow across element face i and the summation is made over all faces of element e

The elements are classified according to their Δ_e:s and the proportion of the elements with Δ_e < 1%, 1% < Δ_e < 10% and 10% < Δ_e < 100% are presented. The location of elements with high deviation is also discussed. These are generally found in the topmost portion of the mesh where gradients are steep and/or in the vicinty of fracture zones where the hydraulic conductivity can vary strongly.

During the site investigations piezometric head distribution has been measured in drill-holes. The groundwater potentials obtained from the model calculations have been recorded along lines corresponding to the relevant drill-holes and compared with the measured heads. These comparisons are presented graphically.

8. CALCULATED GROUNDWATER FLOW AT FINNSJÖN

8.1 Introduction

The Finnsjön site has in the context of the current study been
used to test the program package and to give experience on the
required descretization. That is, how to treat fracture zones
and how to treat the hydraulic conductivity function (see sec-
tion 4.3.5) from a numerical point of view. Three meshes cal-
led FINL, FINS and FINC have been generated covering successi-
vely smaller areas, Figure 8.1. The FINL- and FINS-meshes were
abandoned before enough experience was gained to give relevant
results. For this reason only the FINL-results are presented
below. The presentaion of results for the Finnsjö-area is less
detailed than for the other sites and does not fully comply
with the description given in Chapter 7.

8.2 Description of the FINC-mesh

The FINC-mesh covers a 1.8 km^2 triangular area bordered by
three fracture zones. The mesh contains six element layers
extending down to a depth of 1500 meters. The number of ele-
ments is 906 and the number of nodal points is 4221.

The fracture zones constituting the boundaries of the modelled
area are included in the mesh. Inside the fracture zones thin
elements have been created to increase the capability of the
mesh to represent the sharp gradients that can occur at the
interface between the rock mass and the fracture zones.

The description of the groundwater table given by the FINC
mesh is presented in Figure 8.2. This figure also shows the
location of three vertical cross-sections used for presenting
the calculated groundwater head distribution.

8.3 Results

8.3.1 General

As mentioned in section 8.1, the Finnsjö-area was merely used
to gain experience in modelling. A relatively large number of
runs were made to test the model's sensitivity to various
assumptions regarding the treatment of the hydraulic conducti-
vity versus depth and boundary conditions. Out of these runs,
five have been chosen to demonstrate the results obtained. The
selected runs are listed in Table 8.1 together with a brief
description of the runs.

As can be seen from the table the conductivity is a rather
steep function of the depth. In the FINC- and FINCL-runs this
function is evaluated directly at the integration points. The
conductivity within one element can thus vary in a wide range
especially in the topmost element layers. This is an unfavou-
rable situation from a numerical point of view. In the FINCL
run, however, the conductivity is constant for the topmost 120
metres.

In the FINCK-run an average depth is calculated for each ele-
ment and a constant conductivity value corresponding to the
function value at the average depth is assigned to the ele-
ment. The FINCHT-run treats the permeability in the same way
as the FINCK-run but has a hydrostatic boundary condition app-
lied to the vertical boundaries.

In the FINCL2-run, an alternative statistical evaluation of
the measured conductivity data has been utilized. This evalua-
tion gives a less steep permeability function than the evalua-
tion used in the runs described above.

8.3.2 Head distribution and flow field

The hydraulic heads in three cross-sections are shown in Figu-
res 8.3 - 8.5 for the five runs listed in Table 8.1.

It is obvious from the figures that the FINC-run has yielded
unreliable results from a physical point of view. Comparison
with the FINCL-run which has a constant hydraulic conductivity
in the topmost portion of the mesh, leads to the conclusion
that a prime reason for the physical results in the FINC-run
is the very steep decrease of the conductivity in the upper
part of the mesh.

As an extension of this conclusion the FINCK-run was performed
using constant hydraulic conductivity in all elements. A com-
parison between the FINCL- and the FINCK-run shows a remarkab-
le resemblance leading to the conclusion that the FINCK-app-
roach would be a feasible way to treat the hydraulic conducti-
vity function.

Table 8.1.   Definition of runs with the FINC-mesh and coeffi-
              cients used in equation (4-23).

| Run | Coefficients used in equation (4-23) | | | | Conditions at |
| | Rock mass | | Fracture zones | | vertical |
	A	-b	A	-b	boundaries
FINC (Z>25m)	$1.3 \ 10^{-2}$	2.49	0.1	2.0	Non-flow
FINCL (Z>120m)	$1.3 \ 10^{-2}$	2.49	0.1	2.0	"
FINCK x)	$1.3 \ 10^{-2}$	2.49	0.1	2.0	"
FINCHT	$1.3 \ 10^{-2}$	2.49	Not applicable		Hydrostatic pressure
FINCL2 (Z>25 m)	$7.5 \ 10^{-6}$	1.30	0.005	2.15	Non-flow

Z=depth in m

x) The function has been averaged within the elements so that
    each element has a constant permeability.

Also the FINCL2-run seems to have yielded an acceptable solution.

8.3.3 Groundwater flow at the repository level

The groundwater flow passing in the immediate vicinity of the waste canisters is a parameter of paramount interest because it is used both in the calculation of radionuclide release rates from the waste and in the migration calculations in the far-field of a repository. The Darcy velocity has therefore been recorded on a point-grid at a depth of 500 meters. Only the runs that have given meaningful results (i.e. FINCL, FINCK, FINCHT and FINCL2) are recorded. The groundwater flows and potentials at different points are tabulated in Figure 8.6. The location of the different points is given in the same figure which also shows the countour lines of the groundwater table.

The rightmost grid point (point 11) in the second row from below is situated in the eastern fracture zone. The remarkably lower flow in this point in the FINL2-run is due to the more marked decrease in hydraulic conductivity with depth in the fracture zones in this run compared to the other runs.

In FINCHT the fracture zone was assumed to have the same conductivity as the rock. This run has yielded a lower flow rate at the point in the fracture zone.

8.3.4 Groundwater recharge

The head distribution is calculated from data on the groundwater table and the hydraulic conductivity versus depth. These data are basically determined independently from each other. The groundwater recharge rate at the surface can be calculated backwards from the computed head distribution. If there is an incorrectness in the data describing the groundwater table and the hydraulic conductivity, the calculated groundwater recharge can appear unreasonable.

To check the groundwater recharge and to illustrate the location of recharge- and discharge areas the recharge rates were plotted for the runs FINCL, FINCK, FINCHT and FINCL2. These plots are shown in Figures 8.7 - 8.10. Outflow areas appear in the plots as areas with negative recharge rates.

The major discharge area is located in the northern part of the eastern fracture zone whereas most of the rest of the modelled site is a recharge area. The magnitude of the recharge rate by far exceeds the available amount of rainfall (approx. 670 mm/yr) at least in the fracture zones. In Figures 8.11 - 8.14 the recharge rates have been plotted excluding the fracture zones and the adjacent row of elements. Even though some very high values appear in the figures the values are much more reasonable in Figures 8.11 - 8.14 than in the former.

9. CALCULATED GROUNDWATER FLOW AT FJÄLLVEDEN

9.1 Modelled area

9.1.1 Groundwater table

The topography of the groundwater table at Fjällveden, Figures 9.1 and 9.2 varies between 40 m and 65 m above sea level. The lowest parts, approximately 40 m, are found in the north-eastern and south-western corners of the area. The area between these low parts is largely situated at 50-55 m with some "peaks" with altitudes of about 65 m above sea level.

9.1.2 Hydraulic units

The hydraulic units in the modelled area comprise rock mass, regional and local fracture zones. The modelled fracture zones in the Fjällveden are indicated in Figure 9.3. Table 9.1 shows a comparison between the widths and dips (inclinations) of the fracture zones as modelled with those obtained from the site investigations (compare Table 2.2a).

The zones 2 and 5 have been modelled somewhat wider than the measured widths. Zone no 5 have been attributed the transmissivities of zones 4 and 6 that run parallel with zone no 5 and which have been omitted from modelling.

The regional zones that form the boundaries of the modelled area in the southwest and northeast have been modelled 10 m wider than their measured width. They have been modelled as vertical structures.

The omitted fracture zone no 11 connects the zones no 3 and 5 and runs close to zone no 1. It was deemed to have a very limited influence on the flow conditions.

Table 9.1.   Comparison between measured and modelled fracture
             zone properties at the Fjällveden site.

Zone	Measured		Modelled	
	Width (m)	Inclination ($^{\circ}$)	Width (m)	Inclination ($^{\circ}$)
1	1-7	90		
2	9-12	80 NE	20	80 NE
3	5-11	90	10	90
4	1	80 SE	-	-
5	0.5-1	80 NW	5	80 NW
6	0.2	75-SE	-	-
7	14	60 NW	14	60 NW
8	4.5	90	5	90
9	5	75 SE	5	75 SE
10	5-6	70 SE	5	70 SE
11	3	90	-	-
Reg	90	75 SE	100	90

9.2   Modelling strategy

9.2.1 Element distribution

In general it is desirable to have the highest element density
in regions where steep hydraulic gradients prevail. In Fjäll-
veden, however, the topography is very flat. The elements have
thus been evenly distributed over the modelled area.

The total number of elements in the mesh is 1932 in 6 horizon-
tal layers. The mesh contains 8538 nodal points. Figure 9.4
shows the top surface of the mesh.

9.2.2 Fracture zones

The widths and inclinations of the modelled fracture zones are
indicated in Table 9.1. The zones are modelled with one row of
elements. The interpolation across the fracture zone is in

general linear to save nodal points. Alongside each fracture zone there is a thin element to facilitate the representation of gradients in the vicinity of the fracture zones.

9.2.3 Material properties

As described in section 4.3.5 the hydrualic conductivity has been assumed to vary with depth according to a power function (eqv. 4-23).

Three runs, one with isotropic conductivity (FJEL), one with anisotropic conductivity, (FJELA) and one run where both the rock mass and the fracture zones were treated as rock mass with isotropic conductivity (FJELB) have been performed. In the isotropic run the constants A and b in eqv. (4-23) were calculated using the geometric mean of all data available for the rock mass. In the anisotropic case the data for the two major rock types in the area (gneiss and granite gneiss, compare section 4.3.5) have been treated separately. The granite gneiss, which runs in vertical layers in a predominantly north-easterly direction, is the more permeable of the two rock types. The procedure for calculating the hydraulic conductivity in the directions parallel and perpedicular to the granite gneiss has been described in section 4.3.5. Table 9.2 gives the constants A and b in eqv. (4-23) used in the modelling. The rock mass and fracture zones are assumed to be continous down to 1500 m. The hydrualic conductivity versus depth relations given in Table 9.2 are also assumed to be valid down to this depth.

For each element the average depth has been calculated and used in eqv. (4-23) to calculate the hydraulic conductivity for the element.

Table 9.2.   Constants in equation (4-23) for the isotropic
              and anisotropic cases for Fjällveden.

Run	Rock mass		Fracture zones	
	A	-b	A	-b
FJEL (isotrop.)	$1.5 \ 10^{-3}$	2.78	0.17	3.15
FJELA (anisotrop.)				
NE-direction	$2.8 \ 10^{-4}$	2.38	"	"
NW-direction	$3.4 \ 10^{-3}$	3.11	"	"
Vertical	$2.8 \ 10^{-4}$	2.38	"	"
FJELB (isotrop.)	$1.5 \ 10^{-3}$	2.78	NA	NA

9.2.4 Boundary conditions

The boundary condition at the top surface was set to zero
prescribed pressure. This is the same as to say the potential
at the surface is the same as the elevation of the groundwater
table above the sea level. The potential distribution at the
top surface is shown in relief in Figure 9.1 and as a contour
map in Figure 9.2. Note that the contour map in Figure 9.2 is
produced using the interpolation functions that are defined by
the finite elements. The contours thus describe the actually
applied boundary condition.

The bottom surface is treated as a non-flow boundary situated
1500 meters below the sea level.

All vertical boundaries except the northwestern boundary are
defined as non-flow boundaries located on the outside of frac-
ture zones. This means that the flow is forced upwards in the-
se zones. As some of the zones are inclined, the horisontal
size of the mesh increases with depth.

The northwestern boundary is a vertical non-flow boundary run-
ning along a topographical groundwater divide.

9.3 Results

9.3.1 Head distribution and flow field

Figures 9.5 through 9.10 show the ground water potential dist-
ribution in six horisontal cross-sections at successively inc-
reasing depths. A comparison between the figures shows a clear
decrease of the hydraulic gradient with depth. The local hills
have already disappeared at depths of 260 m. At lower levels
the flow pattern is characterized by a flow inwards from the
north and south to a saddle point at approximately X=0 and
Y=600 m. From the saddle point the water is drained towards
the regional fracture zones in the northeast and southwest.

The same general pattern applies to the isotropic run (FJEL),
the anisotropic run (FJELA) and the run without permeable
fracture zones (FJELB). In the FJELA-run the anisotropy has
scewed the isopotential lines compared to the FJEL run. The
resulting gradients in the FJELA-run are, compared to those of
the FJEL-run, somewhat higher in the northern part of the area
and somewhat smaller close to the regional fracture zones.

In the FJELB run the gradients are considerably lower than in
the FJEL run. This is due to the fact that the relatively high
conductivity in the fracture zones tend to decrease the verti-
cal head drop and consequently maintain the gradient also at
greater depths.

Figure 9.11 shows the location of the 4 vertical cross-sec-
tions shown in Figures 9.12 - 9.15. Comparison of the poten-
tial distribution and flow-vectors plotted in these vertical
cross-sections confirms the above described pattern and ten-
dencies. Note that the isopotential lines and flow vectors are
projected on the plot plane (see Chapter 7). Also note that
the lengths of the vectors are proportional to the logarithm
of the flow.

9.3.2 Groundwater flow

The calculated groundwater flow has been recorded at three
levels corresponding to 400 m, 500 m and 600 m below the
ground surface. The area recorded is approximately the area
where a potential repository could be placed. The correspon-
ding flow rate distributions are shown in Figures 9.16 - 9.18.
The square-pattern that appears in the fracture zones in the
figures derives from the interpolation procedure used for con-
touring and is not relevant to the problem as such.

The flowrates in the rock mass from Figures 9.16 - 9.18 are
summarized in Table 9.3 in terms of interval and representati-
ve value. It can be concluded that the anisotropy increases
the flow rate with up to a factor 2. As could be expected the
flow rates are lower when the fracture zones are treated as
rock mass.

Table 9.3.   Flow rate $(ml/m^2 yr)$ interval and representative
              value from different runs concerning Fjällveden.

| Depth | FJEL | | FJELA | | FJELB | |
m	interval	repr.val.	interval	repr.val.	interval	repr.val
400	5-25	15	5-50	25	3-25	10
500	3-10	7	3-15	10	3-10	5
600	3-10	5	2-15	10	2-4	3

9.3.3 Trajectories and ground water travel times

Thirteen trajectories have been tracked from a depth of 500 m
depth in the FJEL and FJELB runs. The starting points of the
trajectories are located in the area of a potential reposito-
ry, Figure 9.11. The total lengths and particle travel times
for these trajectories are summarized in Table 9.4. The kine-
matic porosity (see section 5.2) was assumed to be 10^{-4}.

Table 9.4. Travel times, path lengths and average velocities along 13 trajectories in Fjällveden. Locations given in Fig. 9.11.

Trajectory no.	FJEL Length (m)	Travel time (yrs)	av.vel. (m/yr)	FJELB Length (m)	Travel time (yrs)	av.vel. (m/yr)
4	210	400	0.53	690	2 520	0.27
5	850	7 100	0.12	870	18 200	0.05
6	1 820	11 900	0.15	2 230	141 000	0.02
7	1 190	5 570	0.21	1 320	5 800	0.23
8	770	2 730	0.28	1 140	3 970	0.29
9	310	750	0.42	1 000	2 720	0.37
10	1 640	2 560	0.64	5 220	5 500	0.95
11	1 490	13 100	0.11	1 980	51 670	0.04
12	1 300	6 530	0.20	950	5 430	0.17
13	170	420	0.41	680	1 900	0.36
14	1 410	740	1.90	970	2 390	0.40
15	1 644	810	2.04	1 620	7 030	0.23
16	2 040	19 330	0.11	2 570	246 700	0.01

It should be noted that a majority of the trajectories have exited the modelled area through the vertical boundaries without reaching the top surface. This is inconsistent with the definition of the boundary conditions and is probably due to a combination of insufficient mass conservatism in the solution along the boundaries and truncation errors in the tracking routine.

The data in Table 9.4 show that the fracture zones have shortened both the trajectories and the travel times in most cases. The influence is in some cases, however, relatively small.

9.4   Relevance of results

9.4.1 Groundwater recharge

The groundwater recharge is calculated as the total recharge
across the top surface divided by the area of the top surface.
For the FJEL-run this is done both including and excluding the
fracture zones. The resulting groundwater recharges are shown
in Table 9.5.

Table 9.5.   Calculated groundwater formation rates and rec-
                 harge areas.

Run	Recharge rate (mm/yr)	Recharge area (km^2)
FJEL:		
incl. fr. zones	443	2.86
excl. fr. zones	44.8	2.74
FJELA:	4.32	2.73
FJELB:	1.77	2.21

The recharge rate for the FJEL run including fracture zones is
somewhat high. This may be due to either a too high hydraulic
conductivity in the topmost portion of the fracture zones or
to a too steep hydraulic gradient of the groundwater table in
the fracture zones. The other values lie within the interval
expected from current understanding of groundwater recharge in
crystalline rocks.

9.4.2 Mass conservatism of the solution

The procedure for calculating the mass balance is described in
Chapter 7. The portion of the elements in different deviation
intervals are given in Table 9.6.

Table 9.6.   Mass balance for Fjällveden runs.

Run	Percentage of elements deviating from mass conservatism with:		
	< 1%	1-10 %	10-100 %
FJEL	22	51	27
FJELA	22	50	28
FJELB	33	44	23

It can be seen from the table that the FJELB-run has yielded a more mass conservative solution than the other two runs. It can thus be concluded that the fracture zones contribute to deviations from mass conservatisms through the discontinuities in material properties. This can be confirmed by studying the locations in the mesh of those elements that deviate most from mass conservatism. They either appear in the vicinity of, or in the fracture zones, or they may appear close to the top surface where the gradients are higher.

9.4.3 Piezometric profiles along drill-holes

The calculated potentials for the FJEL-run have been recorded along lines which coincide with the core drill-holes Fj 2, Fj 4 and Fj 5 in Figure 9.19 together with the measured piezometric heads in the drill-holes. It should be noted that the measured data are derived from short time measurements and are thus somewhat uncertain.

10.   CALCULATED GROUNDWATER FLOW AT GIDEÅ

10.1   Modelled area

10.1.1 Groundwater table

The topography of the ground water table at Gideå (see Figures
10.1 and 10.2) varies between approximately 80 m and 120 m
above sea level.

The main part of the area constitute a plateau at a level
essentially between 110 m and 120 m. The lowest parts (80 m)
are found in the north-west corner of the modelled area whereas
the highest part (125 m) is situated on the western boundary.
This part is actually outside the area covered by the detailed
site investigations.

10.1.2 Hydraulic units

The modelled hydraulic units in the Gideå area are local frac-
ture zones and rock mass. In Figure 10.3 the modelled fracture
zones are indicated. Table 10.1 shows a comparison between the
widths and inclinations of the fracture zones as modelled with
those obtained from the site investigations (compare Table
2.2.b).

As seen from the table only two of the fracture zones are ver-
tical. In fact several of the zones are so slanted that they
intersect at depths. The zones 1 and 2 thus intersect at a
depth of about 125 m. At this depth also the zones 3A and 4
intersect.

The zones 1 and 3A cut through the vertical boundaries of the
area at a depth of 500 m. Consequently zone 3A also inter-
sects zone 5 at this depth.

The deviation between the measured and modelled fracture zone
properties are small. The most significant deviations are the

width of zone 4 and the fact that zone 8 has been reinterpre-
ted at a later stage and is no longer considered to be a frac-
ture zone. The potential consequences of these deviations are
discussed in section 10.3.1.

Table 10.1.   Comparison between measured and modelled fracture
zone properties at the study site Gideå.

Zone	Measured		Modelled	
	Width (m)	Inclination ($^{\circ}$)	Width (m)	Inclination ($^{\circ}$)
1	22-24	40 SE	25	40 SE
2	11	70 NW	15	70 NW
3A	10-24	30 N	12	30 N
3B	4-9	80 N	10	80 N
4	10	90 N	5	90
5	50	70-90 N	50	90
6	1-8	70 SE	5	70 SE
7	1-7	75 E	5	75 E
8	-	-	10	70 SW

10.2 Modelling strategy

10.2.1 Element distribution

Figure 10.4 shows the element distribution at the top surface
of the mesh. Comparing Figures 10.4 and 10.2 shows that the
element density is higher in areas with comparatively steep
gradients.

The fracture zone pattern at Gideå has substantially complica-
ted the mesh generation. The fracture zone intersections
discussed in section 10.1.2 have been dealt with through the
introduction 20 m thick element layers at the levels where the
fracture zones intersect i.e. at the depths 125 m and 500 m.
The elements in this layer that represent the fracture zone
intersection are given fracture zone permeability whereas the

rest of the elements in the layer is treated as rock mass.

The total number of elements in the mesh is 2464 divided in 8 layers out of which 2 layers are the thin layers caused by the fracture zone intersections. The number of nodal points are 10751. This mesh is, due to the complicated fracture zone pattern, the largest mesh, in terms of elements, and nodes, treated in the current study.

10.2.2 Fracture zones

The widths and inclinations of the fracture zones are indicated in Table 10.1. The strategy for modelling fracture zones is similar to that described in section 9.2.2 for Fjällveden with the additional complications described in section 10.2.1.

.

10.2.3 Material properties

The treatment of the hydraulic conductivity as a power function of the depth is described in section 4.3.5. Two runs have been made for Gideå. In the first run (GIDE) the rock mass and fracture zones have been treated as isotropic using the geometric mean of the measured hydraulic conductivities (see section 4.3.5). The site investigations indicated the occurrence of layers of more conductive granite gneiss similar to that in Fjällveden. In Gideå, however, the granite gneiss appears in horisontal layers. To illustrate this, a second run (GIDEA) was made using a higher conductivity in the horisontal (X- and Y-directions) directions than in the vertical (Z-direction).

The procedure for calculating the constants a, b and c in eqv. (4-23) is described in section 4.3.5 for both the isotropic and the anisotropic case. Table 10.2 gives the values of the constants that are used in the model calculations.

Table 10.2.   Constants in eqv 4-23 for the isotropic and ani-
               sotropic cases for the site Gideå.

Case	Rock mass		Fracture zones	
	A	-b	A	-b
GIDE	$5.0 \ 10^{-2}$	3.33	$1.38 \ 10^{-3}$	2.79
GIDEA				
X-and Y-direction	$4.7 \ 10^{-2}$	3.43		
Z-direction	$2.6 \ 10^{-2}$	3.40	$8.46 \ 10^{-2}$	3.33

For each element an average depth is calculated and used in
eqv. (4-23) to obtain the hydraulic conductivity for the ele-
ment.

10.2.4 Boundary conditions

The boundary condition at the top surface is set to zero pre-
scribed pressure i.e. the potential at top surface is equal to
the elevation of the groundwater table relative to the sea
level. The potential distribution at the top surface is shown
in Figures 10.1 and 10.2. Note that contours in Figure 10.2
represent the actually applied boundary condition as they were
produced using the interpolation functions used by the finite
elements.

The bottom surface is a non-flow boundary at 1 500 m depth
(Z = -1430 m).

The vertical boundaries are non-flow boundaries. The northern
boundary is located on the northern side of the fracture zone
5. The north-western, south-western and southern boundaries run
along topographic groundwater divides whereas the eastern boun-
dary is considered to be a symetric discharge boundary.

10.3 Results

10.3.1 Head distribution and flow field

Figures 10.5 - 10.7 show the groundwater potential distribution
in three horisontal cross-sections at Z-coordinates -150 m,
-500 m and -750 m respectively. The flow pattern is largely
governed by the recharge at the central plateau from which the
water flows radially in all directions. The major discharge
areas are in the north-east and north-west. These areas are to
a large extent covered with bogs. The cross-section at -150 m
is of about the depth were the predominance of this regional
flow pattern is established. At shallower levels there are
local inflows and outflows. This can be seen in the vertical
cross-sections in Figures 10.9 - 10.12, especially in Figure
10.12. The location of these vertical cross-sections are shown
in figure 10.8.

Comparison of the a- and b-frames in Figures 10.5 - 10.7 and
10.9 - 10.12 shows that the major effect of the anisotropy in
the b-frames is a lowering of the hydraulic gradient. As the
higher conductivity is in the horisontal directions the verti-
cal head losses should be greater in the anisotropy-run than in
the isotropic. The results are thus consistent.

When comparing the results from Gideå with those of Fjällveden
in chapter 9, it is obvious that the hydraulic gradient decrea-
ses faster with depth in Gideå than in Fjällveden. The probable
reason for this is that the slanted and vertically intersecting
fracture zones in Gideå relieve the gradients rather quickly.
The effect is similar to the above described anisotropy effect.

10.3.2 Groundwater flow

The calculated groundwater flow has been recorded at three
levels corresponding to the depths of 400 m, 500 m and 600 m
respectively. The area recorded covers the area where a poten-
tial repository could be placed. The distribution of the flow
rate is given in Figures 10.13 - 10.15. The square pattern that

appears in conjunction with the fracture zones in the anisotropy run is an artifact from the simple linear interpolation model used for contouring and has nothing to do with reality.

The flow rates from Figures 10.13 - 10.15 are summarized in Table 10.3. It can be concluded that the anisotropy as treated in these runs reduces the groundwater flow with a factor of about two as compared to isotropic conditions.

Table 10.3. Flow rate ($ml/m^2 yr$), interval and representative value in different depths of a potenital repository at the study site Gideå.

Depth	GIDE		GIDEA	
	interval	repr val	interval	repr val
400	10-50	40	10-50	20
500	10-20	15	5-15	5
600	5-10	10	2-4	3

10.3.3 Trajectories and groundwater travel times

Fifteen trajectories have been tracked from the -500 m level in the GIDE-run. The starting points of the trajectories are located in the area for a potential repository. The total length and particle travel times for these trajectories are summarized in Table 10.4. The kinematic porosity (section 5.2) is assumed to be 10^{-4}.

As for the Fjällveden area (section 9.3.3) a majority of the trajectories never reach the surface due to truncation errors and improper mass conservatism of the solution in the superficial layers.

When comparing the results in Table 10.4 with those for Fjällveden in Table 9.4, a similarity in the aquiered results is obvious.

Table 10.4.   Travel times, path lengths and average velocities
               along 15 trajectories in Gideå.

Trajectory no	Length (m)	Travel time (yrs)	Aver vel (m/yr)
2	510	990	0.52
3	740	3 010	0.25
4	800	4 600	0.17
5	570	1 800	0.32
6	770	1 470	0.52
7	1 090	4 370	0.25
8	1 716	1 140	1.51
9	762	2 730	0.28
10	1 240	9 530	0.13
11	3 610	329 000	0.01
12	1 360	1 400	0.97
13	780	2 770	0.28
14	890	1 820	0.49
15	2 300	20 000	0.12
16	1 250	1 310	0.95

10.4 Relevance of results

10.4.1 Groundwater recharge

The groundwater recharge is calculated as the total recharge
across the top surface divided by the area of the top-surface.
The resulting groundwater recharge rates are shown in Table
10.5. The values in the table are in agreement with the current
understanding of groundwater recharge in Swedish bedrock.

10.4.2 Mass conservatism of the solution

For each element a mass balance is calculated according to the
procedure outlined in Chapter 7. The portion of the elements in
different deviation intervals is shown in Table 10.6.

Table 10.5.   Calculated groundwater recharge rates and rechar-
              ge areas at Gideå.

Run	Recharge (mm/yr)	Recharge area (km^2)
GIDE	111	2.75
GIDEA	72.8	2.80

The solution in the anisotropy run (GIDEA) appears to have
somewhat less mass conservatism than the solution for the
isotropic case. The difference is, however, small and of little
significance.

The elements with high deviations are located close to the top
surface and close to fracture zones. Especially fracture zone
intersections (both horisontal and vertical) appear to have
affected the solution negatively.

Table 10.6.   Mass balance for Gideå runs.

RUN	Percentage of elements deviating from mass conservatism with		
	<1%	1-10%	10-100%
GIDE	29	53	18
GIDEA	24	57	19

10.4.3 Piezometric profiles along drill-holes

The calculated potentials from the GIDE-run have been recorded
along lines corresponding to core drill-holes Gi 3, Gi 7 and Gi
8. The potentials are plotted in Figure 10.16 together with the
measured piezometric heads from the drill-holes. The data from
drill-hole Gi 7 are obtained from long time measurements and
are therefore less uncertain than the data from the measure-

ments in the other drill-holes.

The trend in the variation of potential with depth is about the same for measured and calculated potentials.

11.   CALCULATED GROUNDWATER FLOW AT KAMLUNGE

11.1 Modelling strategy

The study site Kamlunge is located on the top of a topographi-
cally significant plateau. The topography of the groundwater
table of the plateau is shown in Figure 11.1. The slopes of the
plateau are relatively steep and may affect the flow pattern in
the study site itself. It was therefore decided to model the
hydraulic situation in two steps. The first step involves the
whole plateau. In the second step a smaller mesh is made and
the boundary conditions at the vertical boundaries of this
local mesh are prescribed head taken from the results of the
regional calculation.

The size relation between the regional and local meshes is
shown in Figure 11.2. The regional mesh is about 35 km^2. The
area covered by the local mesh is approximately 1.7 km^2.
For simplicity no fracture zones were included in the regional
mesh. The orientation of the fracture zones found in the site
investigations is such that they tend to shield the central
area from the steep gradients at the slope of the plateau rat-
her than increasing the effect of the gradients. The omission
of the fracture zones is thus justified.

In the following, first the head distribution and flow field
of the regional run (KAMR) is presented. The results of the
local mesh (KAML- and KAMS runs) are thereafter presented fol-
lowing the same pattern as has been used in Chapters 9 and 10.
Finally the results of all three runs are discussed.

11.2 The regional model

11.2.1 The KAMR-mesh

The mesh used for the regional model contains 1884 elements and
8868 nodal points. The elements are arranged in 12 layers
extending down to a depth of 1 500 m. Figure 11.3 shows the

element distribution at the top surface of the mesh. Figure
11.4 is a contour map of the groundwater table as described by
the mesh. When comparing the two figures the element density is
found to be higher in areas with steep gradients than in the
relatively flat areas on the top of the plateau.

11.2.2 Material properties

The hydraulic conductivity has been assumed to follow the
potential function of depth given in eqv. (4-23) in section
4.3.5. (the mesh contains no fracture zones). The constants
used for the rock mass are $A = 1.4 \times 10^{-3}$ and $b = -2.93$. The-
se values differ somewhat from the values given in Table 4.3.b
because they were obtained at a stage when data were incomple-
te.

11.2.3 Boundary conditions

The bottom surface and the vertical boundaries are considered
to be non-flow boundaries. A zero-pressure is applied to the
top surface, i.e. the potential at the top surface corresponds
to the elevation above sea level, Figure 11.4. It should be
noted that the vertical boundaries are located close to the
steep gradients at the plateau sides. This means that the water
is forced upwards and therefore the gradients are not allowed
to even out as in an undisturbed system.

11.2.4 Head distribution and flow field

The calculated head distributions is presented in 4 horisontal
cross sections at various depths in Figure 11.5. As could be
expected the hydraulic gradient decreases with depth. The local
hill in the southern part totally disappeared at $Z = -750$ m.

Figure 11.6 shows the location of the six vertical cross sec-
tions shown in Figure 11.7. The above mentioned disappearance
of the local hill is clearly seen in cross section no. 1 where

the flow vectors under this hill turn southwards between 600
and 800 m under the sea level. A similar pattern can be seen in
the righthand side portion of cross section 3.

The above discussed flow patterns show that there is a regional
dominance of the steep plateau side gradients on the overall
flow pattern. This does not, however, exclude that there are
more or less shallow local flow cells.

11.2.5 Trajectories and groundwater travel times.

Due to the absence of fracture zones in the KAMR-mesh, the mesh
may not represent the natural flow conditions. However, for
comparison reasons sixten trajectories have been tracked from z
= -300 m level. The starting points are indicated in Figure
11.6. They fall within the area of a potential repository. Tab-
le 11.1 gives a summary of the path lengths and travel times
along the trajectories.

A majority of the trajectories have exited through the vertical
non-flow boundaries. This is due to a combination of a non-
mass-conservative solution of the flow equation and truncation
errors in the tracking routines.

11.3 The local model

11.3.1 Hydraulic units

In the local area at Kamlunge, seven vertical or near-vertical
and one horisontal fracture zones have been modelled. Table
11.2 shows a comparison between the properties of these fractu-
re zones as modelled and as obtained from the field investiga-
tions (compare Table 2.2.c). The location of the fracture zones
are shown in Figure 11.8.

As can be seen from the table most of the zones have been
modelled slightly wider than the measured widths. This has been
done due to numerical considerations.

Table 11.1. Travel times, path lengths and average velocities along 16 trajectories in the regional area at Kamlunge.

Trajectory no.	Length (m)	Travel time (yrs)	av.vel (m/yr)
1	2 110	32 630	0.065
2	1 620	6 610	0.25
3	1 400	3 940	0.36
4	1 210	2 430	0.50
5	2 360	57 890	0.041
6	2 250	56 190	0.040
7	1 940	15 010	0.13
8	1 730	8 800	0.20
9	1 860	15 270	0.10
10	2 320	42 570	0.054
11	3 840	202 330	0.019
12	3 670	422 800	0.009
13	2 000	9 820	0.20
14	2 930	23 750	0.12
15	3 050	21 080	0.14
16	3 320	40 300	0.082

Table 11.2. Fracture zone properties as modelled and as measured in the field.

Zon no.	Measured		Modelled	
	Width (m)	Inclination ($^\circ$)	Width (m)	Inclination ($^\circ$)
1	3	90	5	90
2	4-12	70 NW	8	70 NW
3	1-10	70 NW	5	70 NW
4	4	80 SW	5	80 SW
5	4	60 NE	5	60 NE
6	3	85 NE	5	85 NE
7	3	75 NW	5	75 NE
H 1	4-14	0	10	0

11.3.2 Description of the mesh.

The topography of the groundwater table in the local area is rather flat. The elements have therefore been relatively evenly distributed over the ar ', see Figure 11.9. The fracture zones have been modelled i- ..me way as previously described for Fjällveden (section *.2.2).

Two meshes, K `L-excluding the horisontal fracture zone and KAMS inclu´. .ჳ the horisontal zone, have been generated. Both meshes u - the same areal distribution of elements but the KAMS-me৴h has one additional element layer describing the horisontal zone.

The KAML-mesh contains 2064 elements in 8 layers extending down to z = -1500 m. The number of nodal points are 9265.

The KAMS-mesh contains 2322 elements in 9 layers. The horisontal zone is represented by a 10 m thick element layer between z = -405 m and z = -415 m. The number of nodal points in the KAMSmesh is 10055.

11.3.3 Material properties

The hydraulic conductivity is assumed to be a power function of the depth as described in section 4.3.5. The values for the constants in eqv. (4-23) were set to $A = 1.41 \times 10^{-3}$ and $b = -2.93$ for the rock mass and $A = 1.2 \times 10^{-6}$ and $b = -1.16$ for the fracture zones.

11.3.4 Boundary conditions

The bottom surface of the mesh has been treated as a non-flow boundary. At the top surface the head is prescribed to be zero. This means that the potential at the surface is equal to the elevation of the ground water table above the sea level. The description of the ground water table has been taken from the

map covering he regional area (see figure 11.1). The topography
of the ground water table in the local area is described by the
top surface of the mesh as shown in Figure 11.13.

The vertical boundaries have been treated as prescribed head
boundaries. Each nodal point at these boundaries were assigned
the calculated head from the regional area (KAMR-run) at the
corresponding coordinates.

11.4   Results from the local model

11.4.1   Head distribution

Figures 11.10 through 11.12 show the head (potential) distribu-
tion in three horisonal cross secions for the KAML-and KAMS-
runs. The cross section in Figure 10.10 is located 130 m above
the horisontal fracture zone included in the KAMS whereas the
other two cross-sections are located below the zone. From the
figures it can be concluded that he hydraulic gradient decrea-
ses with depth and furthermore that the horisontal components
of the gradient is lowered by the horisontal fracture zone.

In Figure 11.13 the locations of six vertical cross sections
displayed in Figures 11.14 - 11.19 are shown. The level of the
horisontal zone is marked in the figures. The effect of the
horisontal zone is more obvious in the vertical cross sections
than in the horisontal as the gradient in the whole area is
largely directed upwards (flow direction downwards). The gra-
dient above the zone is higher in the KAMS-run than in the
KAML-run whereas the situation below the zone is the reverse.
This is most clearly seen in cross section no 1.

11.4.2   Ground water flow

The ground water flow rate has been recorded at three levels
for the potential repository area. The flow rates are shown in
contour plots in Figures 11.20 - 11.22. The cross section in
Figure 11.20 is located 105 m above the horisontal fracture

zone. The remaining two cross sections are located 5 m above
and below the zone respectively.

It can clearly be seen from the figures that the flow rates
above the zone are higher when the horisontal zone is included.
On the other hand the flow rate below the zone is lower, than
without the zone.

The flow rates from Figures 11.20-11.22 are summarized in Table
11.3.

Table 11.3.   Flow rate (ml/m^{2}yr), interval and representati-
ve value from model calculations of Kamlunge.

Depth	KAML		KAMS	
	interval	repr.val.	interval	repr.val.
450	15-30	20	20-60	50
550	8-15	10	15-30	25
570	8-20	10	4-10	6

11.4.3   Trajectories and groundwater travel times.

Sixteen trajectories have been tracked, started at the reposi-
tory level (z = 300 m) for the KAML- and KAMS runs. The star-
ting points have the same coordinates as the starting points in
the KAMR-run (see section 11.2.4 and Figure 11.6). They have
also been marked in figure 11.13.

Table 11.4 gives a summary of the path lengths and travel
times along trajectories 2-16. The tracking of trajectory no. 1
could not be completed for numerical reasons. Note that, due to
the formulation of the boundary conditions, the trajectories
exit through the vertical boundaries of the mesh and never
reach the top surface in the local area. The travel times given
in the table is thus shorter than the expected travel times to
the surface.

It should also be noted that in the KAMS run a large portion of the path length falls within the horisontal fracture zone where the velocity is high. The average velocity is thus higher than expected in the rock mass.

Table 11.4. Travel times, path lengths and average velocities along 15 trajectories in the KAML- and KAMS-runs.

	KAML			KAMS		
Trajec- tory no.	Length (m)	Travel time (yr)	av.vel. (m/yr)	Length (m)	Travel time (yr)	av.vel. (m/yr)
2	1 180	10 630	0.11	650	1 950	0.33
3	490	1 820	0.27	490	330	1.49
4	340	900	0.38	380	440	0.86
5	220	2 940	0.075	1 380	13 170	0.11
6	1 820	66 670	0.027	1 030	320	3.22
7	1 060	10 170	0.10	850	250	3.41
8	770	3 670	0.21	770	990	0.78
9	690	5 170	0.13	810	4 830	0.17
10	1 050	11 500	0.091	1 090	460	2.37
11	1 580	58 000	0.027	1 510	7 770	0.19
12	2 050	83 330	0.025	1 240	1 060	1.17
13	440	3 010	0.15	520	2 110	0.25
14	860	5 630	0.15	870	4 000	0.22
15	970	7 770	0.13	1 090	1 260	0.87
16	1 320	29 500	0.045	2 470	94 300	0.026

It can be concluded from Table 11.4 that the horisontal fracture zone has both shortened the path lengths and the travel times for particles released from the repository when situated above the zone. It also obvious that, in complicance with the conclusions in sections 11.4.1 and 11.4.2, the horisontal zone would have a lengthening effect on the path lengths and travel times if the repository was to be placed below it.

11.5 Relevance of results

11.5.1 Ground water recharge

The ground water recharge rate is calculated for the KAMR-, KAML- and KAMS-runs in the same way as for the runs described in the previous chapters. For the KAML- and KAMS-runs this is made both including and excluding the fracture zones. The results that are summarized in Table 11.5, can be said to comply with current understanding of ground water formation in crystalline rock.

Table 11.5. Calculated ground water recharge rates and recharge areas for the Kamlunge site.

RUN	Formation rate (mm/yr)	Recharge area (km^2)
KAMR	20.55	14.54
KAML		
incl.fr.zones	1.76	1.74
exkl.fr.zones	1.73	1.72
KAMS		
incl.fr.zones	1.45	1.71
exkl.fr.zones	1.42	1.69

11.5.2 Mass conservatism of the solutions

A mass balance is calculated for all elements in the KAMR-, KAML- and KAMS-runs according to the procedure described in chapter 7. The portion of the elements in various deviation intervals is tabulated in Table 11.6.

The distribution of the elements in different deviation intervals is about the same as for Fjällveden and Gideå. The regional run (KAMR) is somewhat more mass conservative than the other runs probably due to the absence of fracture zones.

Table 11.6. Mass balance for Kamlunge runs.

Run	Percentage of elements deviating from mass conservatism with:		
	< 1%	1-10 %	10 - 100 %
KAMR	32	48	20
KAML	28	51	21
KAMS	27	52	21

11.5.3 Piezometric profiles along drill-holes

The piezometric measurements at Kamlunge were not completed when this report was written.

12. INFLUENCE OF WELL DISCHARGE ON THE GROUNDWATER CONDITIONS

12.1 Background

In the area of a final repository for nuclear waste, restrictions will be set up regarding the use of drilled wells for water supply. However in the long term of land-use, water supply for domestic purposes might be located within the area or adjacent to a nuclear repository. To yield sufficient water for groups of a few houses or farms, wells for water supply would have to be located into rather high permeable part of the bedrock. On the other hand the repository will be sited within the low permeable parts of the bedrock at depth of 500 m below ground surface.

12.2 General considerations

Groundwater discharge through wells will influence the groundwater conditions in a local area in the bedrock. This influence has two basic impacts:

- It might change the groundwater head within or adjacent to the repository, thus modifying the groundwater flow from the repository.

- Water coming from the repository will enter the influence area of the well and be discharged into the water supply.

Water consumption for domestic purposes is set to around 300 l/person and day. Thus for 20 persons, 6000 l/day is required. The discharge from the well is mainly distributed during daytime. In combination with temporarily storage of water in pressure tanks, the pumping time can be estimated to be cyclic, regular or irregular. Here it is assumed to be cyclic during 12 hours per day.

For the water comsumption of 20 persons, an effective storage

volume of 75 liters is needed in a pressure tank. Due to insufficient use of the tank, the value should be reduced to 50 liters. The pump used in connection with the pressure tank has a working rate of 0.8 l/s. Thus 120 cycles of pumping per day are needed. The pumping time during each cycle will be around one minute. During this time the groundwater level in the rock surrounding the well will be lowered. During the next five minutes a recovery will take place until the next pumping period and so on for 12 hours. The influence on the groundwater head in the well after the last pumping of the day, neglecting the storage of water in the well itself, can be calculated according to:

$$h_w = \frac{Q(w)}{4 \, \Pi K \, H} \ln \frac{2.25 \, K \, t(e)}{r_w^2 \, S_s} \qquad (12\text{-}1)$$

The radius of the influence area is calculated according to:

$$r_e = \sqrt{2.25 \, K \, t_e / S_s} \qquad (12\text{-}2)$$

where h_w = drawdown in the well

H = thickness of the water yielding part of the well

K = hydraulic conductivity

S_s = specific storage of the bedrock (1.E-5 1/m)

t_e = effective pumping time

r_w = well radius

r_e = radius of influence

$Q(w)$ = well discharge during pumping

The effective pumping time t_e is calculated from:

$$t_e = \frac{t(p1).t(p2).....t(pn)}{t(r1).t(r2)....t(r(n-1))} \qquad (12\text{-}3)$$

where t(pn) = pumping time during period n

t(rn) = recovery time during period n

The effective pumping time is calculated to about 3 minutes based on the cyclic pumping assumption made above.

The relation R between the amount of water $Q(r)$ emanating from the repository and the total discharge $Q(w)$ from the well is considered as:

$$D = Q(r)/Q(w) \qquad (12-4)$$

12.3 Results

The water supply well is situated within a vertical permeable fracture. The depth of the well is 200 m and the diameter 110 mm. The hydraulic conductivity of the fracture is assumed to be constant within the upper 200 m and decreasing deeper down according to the conditions measured at the studied sites. The groundwater flow through the repository is set to 0.1 1/square-meter and year.

In Figure 12.3.1 the drawdown, influence area and ratio of groundwater from the repository to the discharge water are given. In the figure certain limitations are made. Drawdown of more than 100 meters are usually not accepted. Thus the hydraulic conductivity of the fracture zone has to be higher than about $2. \ 10^{-8}$ m/s. On the other hand, the values obtained on fracture conductivity usually are less than $5. \ 10^{-7}$ m/s.

The area of influence due to pumping will be very limited, up to 5 meters from the well. Thus no influence on the natural groundwater conditions at repository depth is expected. The factor D will be $1.2 \ 10^{-7} - 7. \ 10^{-6}$, see Figure 12.3.1, which means a dilution of 0.1 - 8 million times. A convergence of the streamlines from the repository towards the area influenced by the well will give a smaller dilution. On the other hand, the calculated groundwater flow at repository depth is on the average 0.01-0.03 $1/m^2$ and year at the sites of Fjällve-den, Gideå and Kalmunge. This means a higher dilution than the values given above.

REFERENCES

Ahlbom, K., Albino, B., Carlsson, L., Danielsson, J., Nilsson, G., Olsson, O., Sehlstedt, S., Stejskal, V., Stenberg, L. 1983: Evaluation of the Geological, Geophysical and Hydrogeological Conditions at Kamlunge. - KBS technical report TR 83-54.

Ahlbom, K., Albino, B., Carlsson, L., Nilsson, G., Olsson, O., Stenberg, L., Timje, H. 1983: Evaluation of the Geological, Geophysical and Hydrogeological Conditions at Gideå. - KBS technical report TR 83-53.

Ahlbom, K., Carlsson, L., Carlsten, L-E., Duran, O., Larsson, N-Å., Olsson, O. 1983: Evaluation of the Geological, Geophysical and Hydrogeological Conditions at Fjällveden. - KBS technical report TR 83-54.

Ahlbom, K., Carlsson, L., Gentzschein, B., Jämtlid, A., Olsson, O., Tiren, S. 1983: Evaluation of the Geological, Geophysical and Hydrogeological Conditions at Svartboberget. - KBS technical report TR 83-55.

Ahlbom, K., Carlsson, L., Olsson, O. 1983: Final Disposal of Spent Fuel - Geological, Hydrogeological and Geophysical Methods for Site Characterization. - KBS technical report TR 83-43.

Almén, K-E., Andersson, J-E., Carlsson, L. 1982: Hydrauliska tester. Del 4: Jämförande studier av olika hydrauliska metoder. - KBS arbetsrapport AR 83-02, December 1982.

Andersson, J-E., Carlsson, L. 1981: Hydraulsika tester. Del 2: Pulsrespons-tester. - KBS arbetsrapport AR 82-35. April 1981.

Axelsson, C-L., Carlsson, L. 1979: Model calculations of groundwater conditions on Sternö peninsula. - KBS technical report TR 79-10.

Axelsson, C-L., Olsson, T. 1979 : Grundvattenpåverkan vid tunneldrivning - Paranetrbestämning med numerisk modell. - Hydrogeologi vid SGU, Rapporter och meddelanden nr 14, sid 55-62.

Brotzen, O. 1981: Site Investigations for a Nuclear Waste Repository in Crystalline Rock. - Proceeding of OECD/NEA Workshop on Siting of Radioactive Waste Repositories in Geological Formations. France.

Carlsson, L., Gidlund, G., Hesselström, B. 1983: I: Evaluation of the Hydrogeological Conditions at Finnsjön. II: Supplementary Geophysical Investigations of the Sternö Peninsula. - KBS technical report TR 83-56.

Carlsson, L. Olsson, T. 1979: ALMA. Hydrauliska barriäregenskaper hos marknära bergmassor. - Programrådet för Radioaktivt avfall, Rapport 1.24, maj 1979.

Dagan, G. 1979: Models of groundwater flow in statistically homogeneous formations. - Water Resources Research, Vol 15, No 1, Feb 1979, pp 47-63.

Dagan, G. 1981: Analysis of flow through Heterogeneous random aquifers by the method of embedding matrix. 1. Steady flow. - Water Resources Research, Vol 17, No 1, Feb 1981, pp 107-121.

Earlougher, R.C., Jr. 1977: Advances in Well Test Analysis. - Soc. Pet. Engr. Monograph Series, Vol 5, SPE, Dallas 1977.

Eriksson, B. 1980: Sveriges vattenbalans. Årsmedelvärden (1931-60) av nederbörd, avdunstning och avrinning. - SMHI Rapporter RMK 18, 1980.

Eriksson, B. 1981: Den "potentiella" evapotranspirationen i
        Sverige. - SMHI Rapporter RMK 28, 1981.

Fagerlind, T., Nordberg, L. 1973: Variation of Groundwater
        Levels and a Calculation of the Effective Porosity at
        File Hajdar, Gotland. - Geol. Fören. Stockholm Förh.
        95, pp 317-327.

Freeze, R.A. 1975: A Stochastic-Conceptual Analysis of One-di-
        mensional Groundwater Flow in Nonuniform Homogeneous
        Media. - Water Resources Research, Vol 11, No 5, Oct
        1975, pp 725-741.

Gustafsson, E., Klockars, C-E. 1981: Studies on Groundwater
        Transport in Fractured Crystalline Rock under cont-
        rolled conditions using Nonradioactive Tracers. - KBS
        technical report TR 81-07. April 1981.

Grundfelt, B. 1983: GWHRT - A Finite Element Solution to
        the Coupled Ground Water Flow and Heat Transport
        Problem in Three Dimensions. - KBS technical
        report TR 83-51.

Gutjahr, A.L., Gelhar, L.W., Bakr, A.A., MacMillan, J.R. 1978:
        Stochastic Analysis of Statial Varibility in Subsur-
        face Flows. ". Evaluation and application. - Water
        Resources Research, Vol 14, No 5, Oct 1978, pp
        953-959.

Iwai, K. 1976: Fundamental Studies of Fluid flow through a
        single Fracture. - Ph.D. Thesis, Univ. of Calif. Ber-
        keley 1976.

Karlqvist, L., Olsson, T. 1983: Hydrogeologiska förutsättning-
        ar för reduktion av lakvattenbildningen vid avfall-
        supplag. - Naturvårdsverket Rapport SNV PM 1647, mars
        1983.

Klockars, C-E., Persson, O., Landström, O. 1982: The Hydraulic
        Properties of Fracture Zones and Tracer Tests with
        Nonreactive elements in Studsvik. - KBS technical
        report TR 82-10, April 1982.

Maini, T. 1971: In situ Hydraulic parameters in Jointed Rock
        -Their Measurement and Interpretation. - PH.D. Thesis
        Imp. Coll. of Sci. and Technol., London 1971.

Neuzil, C.E., Tracy, J.V. 1981: Flow through fractures. -
        Water Resources Research, Vol 17, No 1, Feb 1981, pp
        191-199.

Nordberg, L., Persson, G. 1976: On the Temporal and Regional
        Groundwater Variations in Sweden. - Nordic Hydrologi-
        cal Conference 1976, Session IV. Reykjavik september
        1976.

Norton, D., Knapp, R. 1977: Transport Phenomena in Hydrother-
        mal Systems: The Nature of Porosity. - Am,erican
        Journal of Science, Vol 1277, Oct 1977, pp 913-936.

Persson, M. 1978: Slutrapport över hydrologiska undersökningar
        i Lappträskets representativa område. - SMHI Hb-rap-
        port nr 33. Norrköping 1978.

Snow, D.T. 1968: Rock fracture spacing, openings and porosi-
        ties. - Jour. Soil Mech. and Foundation Eng. ASCE 94,
        pp 73-91.

Thoregren, U. 1982: Final Disposal of Spent Fuel - Standard
        Programme for Site Investigations. - KBS technical
        report TR 83-31.

Thunvik, R., Braester, C. 1980: Hydrothermal Conditions around
        a Radioactive Waste Repository. - KBS technical
        report 80-19.

Uraiet, A.A., Raghavan, R. 1980: Unsteady Flow to a well Pro-
        ducing at a constant Pressure. - Jour. Pet. Tech, Oct
        1980, pp 1803-1812.

Uraiet, A.A., Raghavan, R. 1980: Pressure Buildup Analysis for
        a well Produced at Constant Bottomhole Pressure. -
        Jour. Pet. Tech, Oct 1980, pp 1813-1824.

Warren, J.E. 1961: Flow in Heterogeneous Porous Media. - Jour.
        Soc. of Pet. Eng. Sept 1961, pp 153-169.

von Brömssen, U. 1968: Grundvattenbildning i geologiskt olika
        terrängavsnitt. Försök till bestämning av infiltra-
        tionskoefficienter. - Metod, Teknik, Analys 1968, sid
        33-110.

Öquist, U. 1981: Measurements of Electrical Properties of Rock
        and its Application to Geophysical Investigation of
        Ore and Waste Disposals. - Doctorial Thesis, Royal
        Institute of Technology 1981.

APPENDIX

DATA ON MEAN VALUES OF HYDRAULIC CONDUCTIVITY

Parameters obtained from graphically log-normal distribution
of measured values of hydraulic conductivity for the rock mass
within different 100 m interval. K_m = mean value, K_g =
geometric value based on measured data. Values on and below
measurement limit has been given the value of the measurement
limit ($1 \ 10^{-11}$ m/s).

FJÄLLVEDEN

Depth-interval	No of data	K_m m/s	K_g m/s
0-100	23	$5.3 \ 10^{-8}$	$4.1 \ 10^{-8}$
100-200	32	$3.8 \ 10^{-10}$	$4.9 \ 10^{-10}$
200-300	38	$9.1 \ 10^{-11}$	$9.6 \ 10^{-11}$
300-400	39	$5.6 \ 10^{-11}$	$7.4 \ 10^{-11}$
400-500	33	$4.4 \ 10^{-12}$	$4.4 \ 10^{-11}$
>500	35	$3.3 \ 10^{-13}$	$2.3 \ 10^{-11}$

GIDEÅ

Depth-interval	No of data	K_m m/s	K_g m/s
0-100	39	$5.6 \ 10^{-8}$	$3.2 \ 10^{-8}$
100-200	46	$8.9 \ 10^{-9}$	$3.0 \ 10^{-9}$
200-300	42	$3.2 \ 10^{-10}$	$2.4 \ 10^{-10}$
300-400	47	$1.4 \ 10^{-12}$	$4.0 \ 10^{-11}$
400-500	46	$4.0 \ 10^{-11}$	$3.4 \ 10^{-11}$
>500	44	$5.3 \ 10^{-14}$	$1.5 \ 10^{-11}$

KAMLUNGE

Depth-interval	No of data	K_m m/s	K_g m/s
0-100	39	$2.1 \ 10^{-8}$	$1.6 \ 10^{-8}$
100-200	45	$3.4 \ 10^{-10}$	$6.4 \ 10^{-10}$
200-300	41	$1.0 \ 10^{-11}$	$4.7 \ 10^{-11}$
300-400	33	$1.5 \ 10^{-11}$	$3.2 \ 10^{-11}$
400-500	35	$8.7 \ 10^{-12}$	$1.9 \ 10^{-11}$
>500	34	$2.6 \ 10^{-12}$	$1.7 \ 10^{-11}$

SVARTBOBERGET

Depth-interval	No of data	K_m m/s	K_g m/s
0-100	16	$2.2 \ 10^{-8}$	$1.5 \ 10^{-8}$
100-200	18	$1.1 \ 10^{-9}$	$9.5 \ 10^{-10}$
200-300	21	$3.7 \ 10^{-11}$	$7.4 \ 10^{-11}$
300-400	19	$1.0 \ 10^{-10}$	$1.3 \ 10^{-10}$
400-500	11	$1.5 \ 10^{-11}$	$1.5 \ 10^{-11}$
>500	24	$2.8 \ 10^{-12}$	$1.8 \ 10^{-11}$

Calculated arithmetic, geometric and harmonic mean values within different 100 m interval.

FJÄLLVEDEN

Depth-interval	Harmonic mean value	Geometric mean value	Arithmetic mean value
0-100	5.010^{-9}	4.110^{-8}	5.010^{-7}
100-200	4.710^{-11}	4.910^{-10}	1.510^{-8}
200-300	3.010^{-11}	9.610^{-11}	4.010^{-10}
300-400	2.010^{-11}	7.410^{-11}	5.010^{-10}
400-500	1.510^{-11}	4.410^{-11}	1.310^{-8}
>500	1.110^{-11}	2.310^{-11}	8.510^{-10}

GIDEÅ

Depth-interval	Harmonic mean value	Geometric mean value	Arithmetic mean value
0-100	1.710^{-10}	3.210^{-8}	7.310^{-7}
100-200	9.410^{-11}	3.010^{-9}	3.910^{-7}
200-300	1.910^{-11}	2.410^{-10}	1.010^{-8}
300-400	1.210^{-11}	4.010^{-11}	6.510^{-10}
400-500	9.510^{-12}	3.410^{-11}	3.610^{-9}
>500	7.810^{-12}	1.510^{-11}	4.510^{-10}

KAMLUNGE

Depth-interval	Harmonic mean value	Geometric mean value	Arithmetic mean value
0-100	$4.5 \cdot 10^{-10}$	$1.1 \cdot 10^{-8}$	$2.0 \cdot 10^{-7}$
100-200	$6.4 \cdot 10^{-11}$	$3.0 \cdot 10^{-10}$	$4.8 \cdot 10^{-9}$
200-300	$1.9 \cdot 10^{-11}$	$4.1 \cdot 10^{-11}$	$1.3 \cdot 10^{-9}$
300-400	$1.6 \cdot 10^{-11}$	$3.2 \cdot 10^{-11}$	$4.2 \cdot 10^{-10}$
400-500	$1.3 \cdot 10^{-11}$	$2.0 \cdot 10^{-11}$	$1.3 \cdot 10^{-10}$
>500	$1.2 \cdot 10^{-11}$	$1.7 \cdot 10^{-11}$	$6.9 \cdot 10^{-11}$

SVARTBOBERGET

Depth-interval	Harmonic mean value	Geometric mean value	Arithmetic mean value
0-100	$1.9 \cdot 10^{-9}$	$1.5 \cdot 10^{-8}$	$5.0 \cdot 10^{-7}$
100-200	$7.7 \cdot 10^{-11}$	$9.5 \cdot 10^{-10}$	$1.4 \cdot 10^{-8}$
200-300	$1.6 \cdot 10^{-11}$	$7.4 \cdot 10^{-11}$	$5.0 \cdot 10^{-9}$
300-400	$2.3 \cdot 10^{-11}$	$1.3 \cdot 10^{-10}$	$4.8 \cdot 10^{-9}$
400-500	$7.9 \cdot 10^{-12}$	$1.5 \cdot 10^{-11}$	$1.0 \cdot 10^{-10}$
>500	$7.3 \cdot 10^{-12}$	$1.8 \cdot 10^{-11}$	$1.5 \cdot 10^{-10}$

LIST OF FIGURES

107

Figure 1.1.   Study sites.

Figure 2.2.1.   Map of fracture zones at the ground surface
in Fjällveden.

Zone no.	Bore-hole	Borehole-interval (m)	Vertical-depth (m)	Mean fracture frequency (frac/m)
1	Fj 02	340-354	294.4 - 306.6	12.9
1	Fj 05	469-473	406.2 - 409.8	7.0
1	Fj 06	479-486	414.8 - 420.8	8.1
3	Fj 06	37-59	32.0 - 51.1	12.8
3	Fj 04	140-192	121.2 - 166.3	13.2
4	Fj 02	596-600	516.2 - 519.6	22.0
5	Fj 04	61-63	52.8 - 54.6	24.0
5	Fj 06	610-611	528.3 - 529.1	49.0
6	Fj 01	674-676	671.4 - 673.4	13.0
7	Fj 09	110 - 131	84.3 - 100.4	11.3
8	Fj 09	424 - 433	324.8 - 331.7	15.4
9	Fj 05	173 - 185	149.8 - 160.2	11.3
9	Fj 07	685 - 731	593.2 - 633.1	6.9
10	Fj 07	53 - 89	45.9 - 77.1	11.3
10	Fj 05	96 - 102	83.1 - 88.3	13.7

Figure 2.2.2.   Percentage of low (normal) fractured, highly fractured and crushed rock in the fracture zones in Fjällveden.
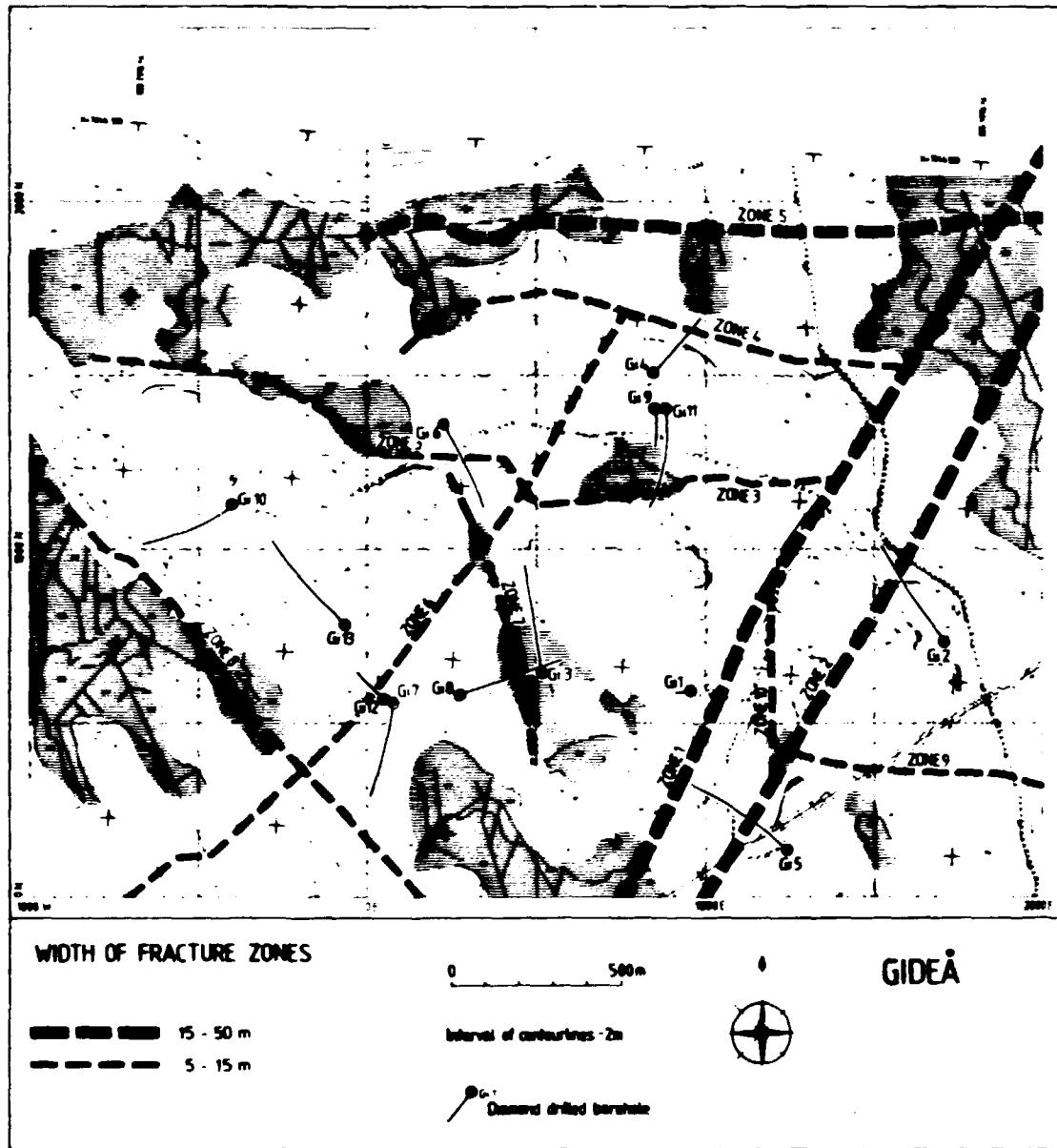
Figure 2.2.3.   Map of fracture zones at the ground surface
                 in Gideå.

	Zone no.	Bore-hole	Borehole-interval(m)	Vertical-depth (m)	Mean fracture frequency(frac/m)
	1	Gi 5	210-232	181.9-200.6	5.7
	1	Gi 2	308-335	267.6-290.1	12.5
	2	Gi 5	520-567	450.3-491.0	8.8
	3A	Gi 6	51-80	44.2-66.3	14.4
	3A	Gi 11	118-130	107.6-117.6	18.4
	3A	Gi 6	129-146	118.7-134.4	17.1
	3A	Gi 4	217-259	203.6-243.4	1.6
	3B	Gi 6	222-240	192.3-207.8	10.5
	3B	Gi 11	345-352	312.7-318.0	15.1
	4	Gi 4	606-655	569.4-615.5	10.6
	6	Gi 12	52-61	45.5-53.4	12.9
	6	Gi 7	362-397	313.5-343.8	15.6
	6	Gi 3	622-628	538.7-544.7	17.9
	6	Gi 4	670-690	629.8-648.4	10.2
	7	Gi 3	329-342	284.8-296.2	9.3
	7	Gi 6	443-452	383.8-391.4	22.1

Figure 2.2.4.   Percentage of low (normal) fractured, highly fractured and crushed rock in the fracture zones in Cideå.
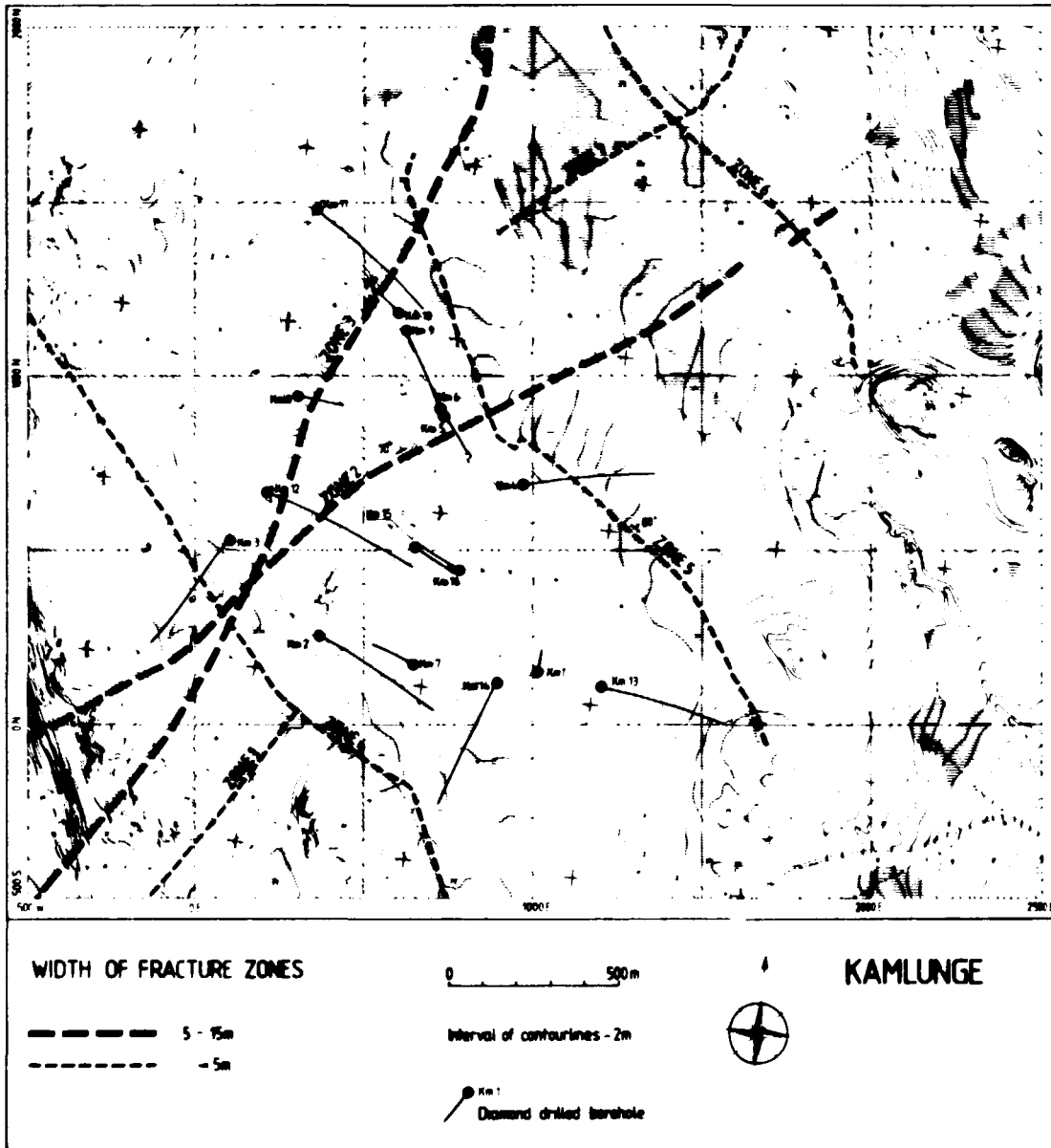
Figure 2.2.5.   Map of fracture zones at the ground surface
                 in Kamlunge.
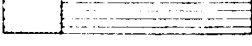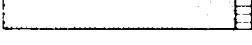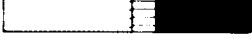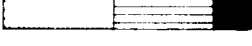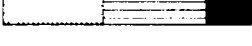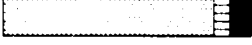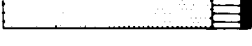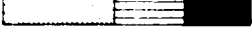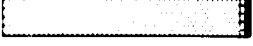
	Zone no.	Bore-hole	Borehole - interval (m)	Vertical - depth (m)	Mean fracture frequency (frac/m)
	H 1	Km 1	544-560	541.9 - 557.9	9.1
	H 1	Km 14	667-673	577.6 - 582.8	7.8
	H 1	Km 13	669-674	579.4 - 583.7	21.1
	H 1	Km 2	676-684	585.4 - 5924	6 5
	2	Km 5	47 - 53	40.7 - 45.9	31.5
	2	Km 6	86 - 94	74.5 - 81.4	1.6
	2	Km 12	195 - 210	168.9 - 181.9	7.6
	2	Km 3	313 - 337	271.1 - 291.8	15.4
	2	Km 9	414 - 425	358.5 - 368.1	18.2
	3	Km 12	52 - 80	45.0 - 53.0	12.6
	3	Km 8	63 - 89	54.6 - 59.8	18.4
	3	Km 11	324-335	280.6 - 290.1	8.7
	3	Km 3	441-450	381.9 - 389.7	23.0
	4	Km 3	507- 517	439.1 - 447.7	4.5

Figure 2.2.6.   Percentage of low (normal) fractured, highly
fractured and crushed rock in the fracture
zones in Karlunge.
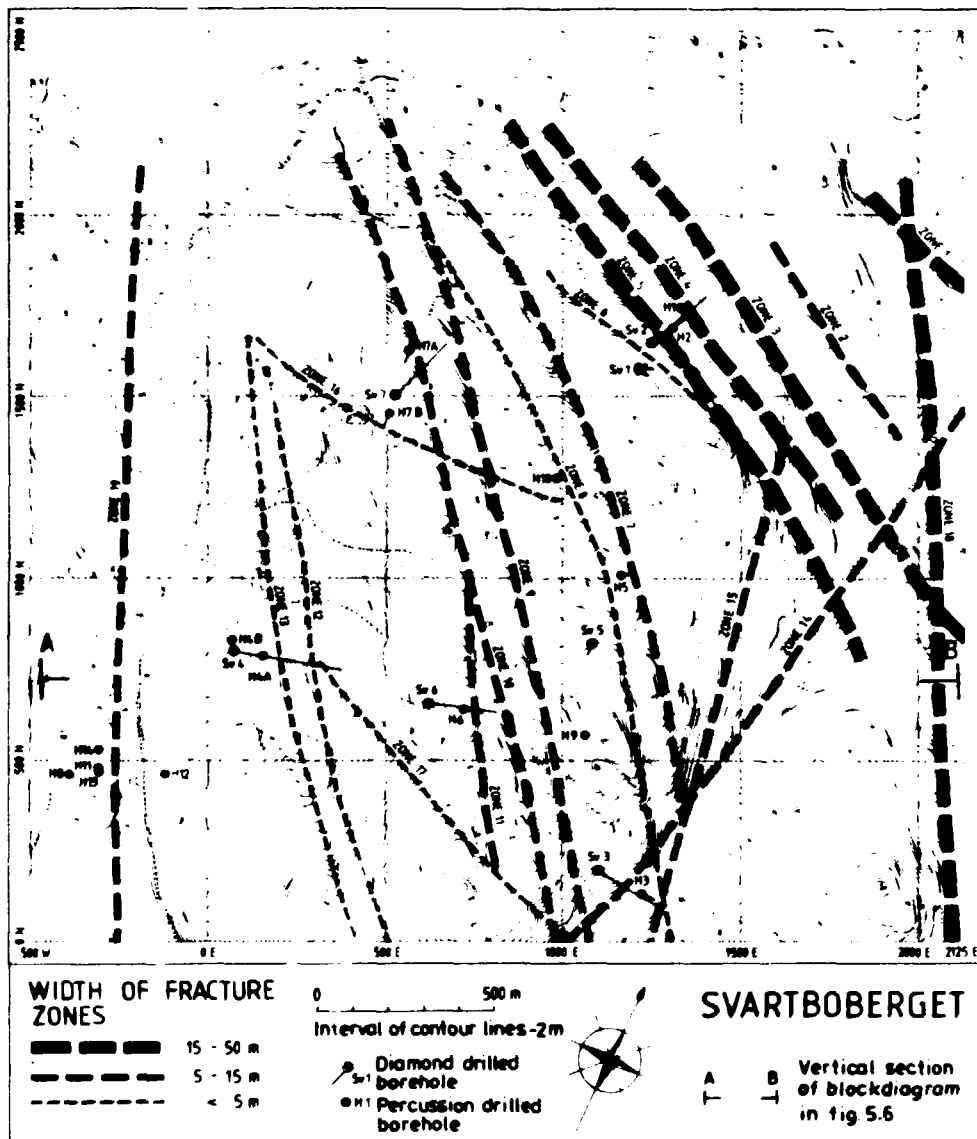
Figure 2.2.7.   Map of fracture zones at the ground surface
                 in Svartboberget.

Figure 2.2.6.   Percentage of low (normal) fractured, highly
fractured and crushed rock in the fracture
zones in Svartboberget.

Figure 3.4.1.   Regions in Sweden with similar groundwater
                 recharges. The northern region is characteri-
                 zed by dominating recharge from snow-melting.
                 In the southern region the whole winter sea-
                 son usually has groundwater recharge. After
                 Varlquist and Olsson (1983).
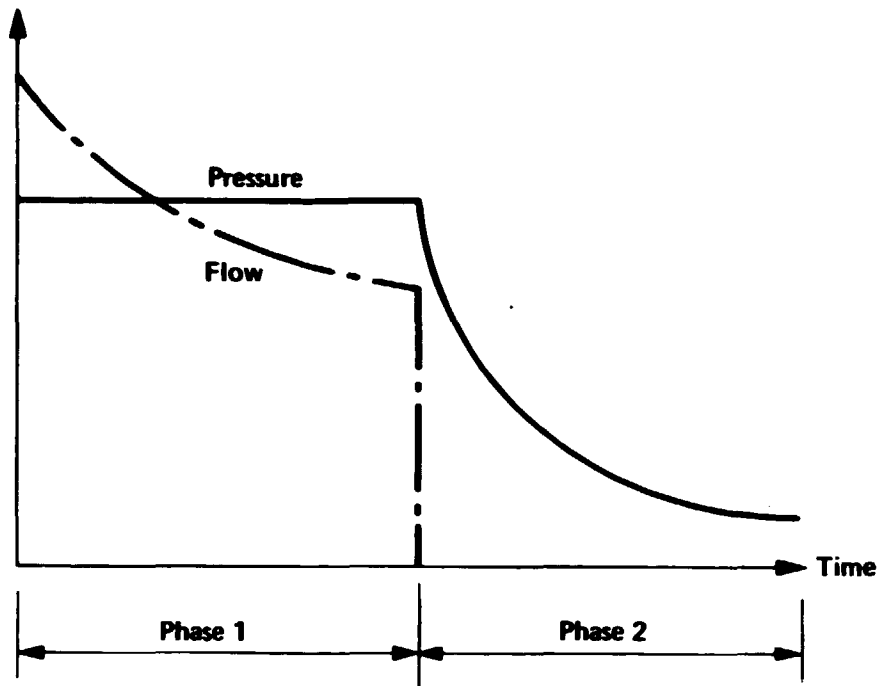
Figure 4.2.1.   Steps in the performance of hydraulic tests.
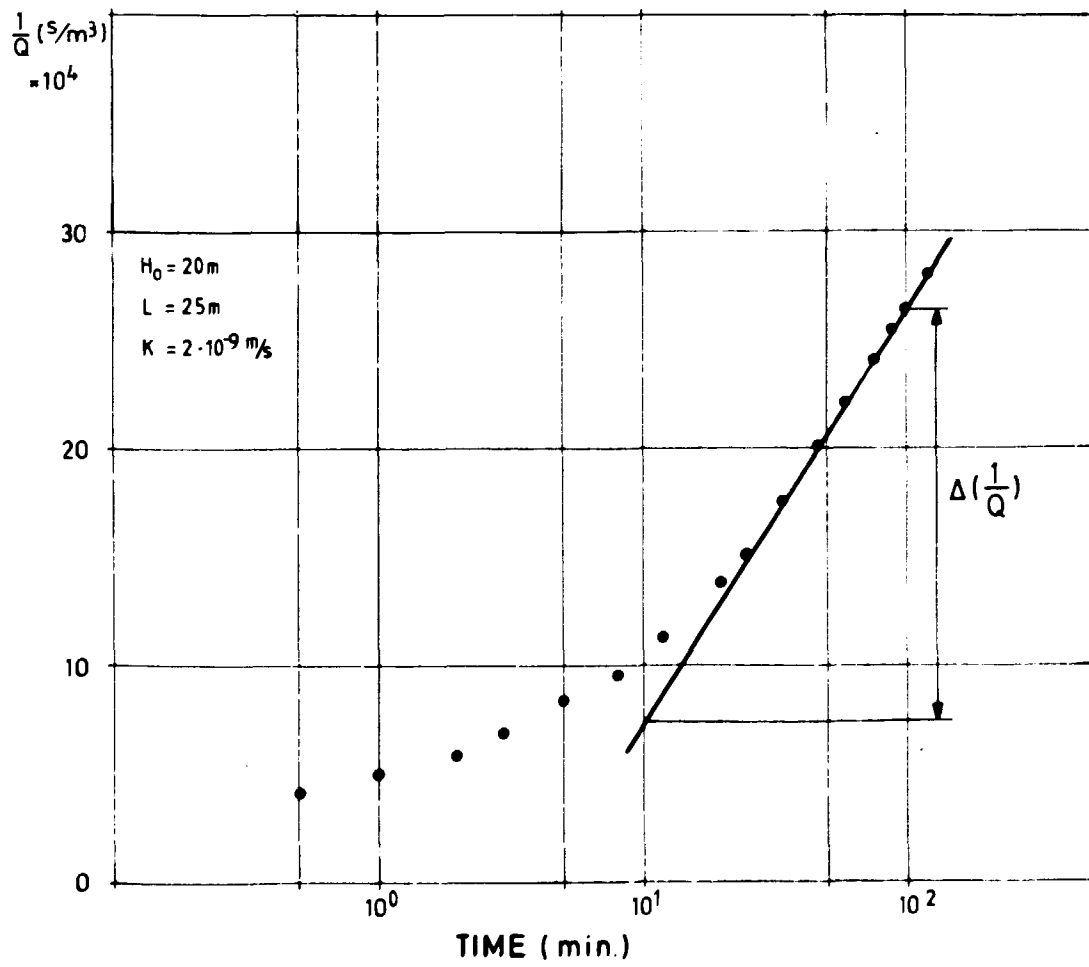
Figure 4.2.2.   Example of the evaluation of hydraulic con-
                 ductivity from water injection test with
                 constant head.
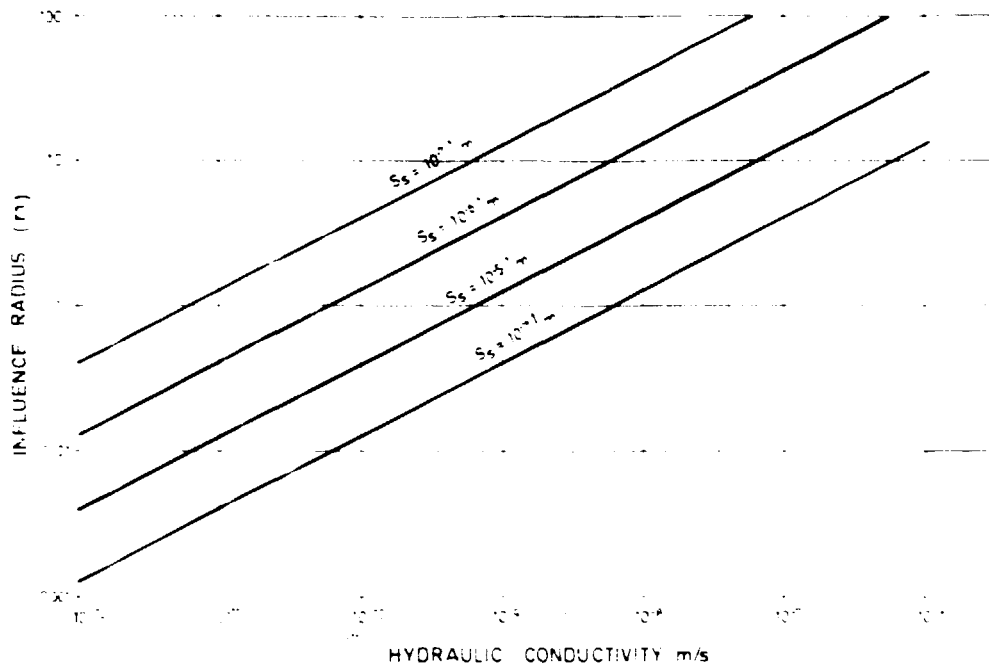
Figure 4.2.3   ladius of influence as a function of specific
storage and hydraulic conductivity. Testing
time 12(minutes.
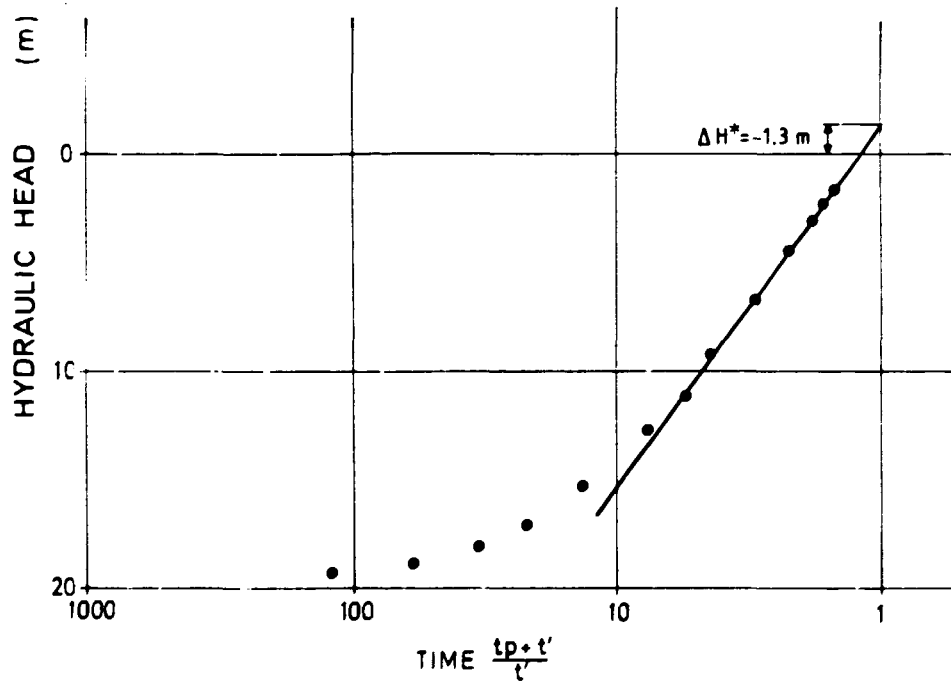
Figure 4.2.4.   Evaluation of hydraulic conductivity and pie-
zo etric head using Horner plot.
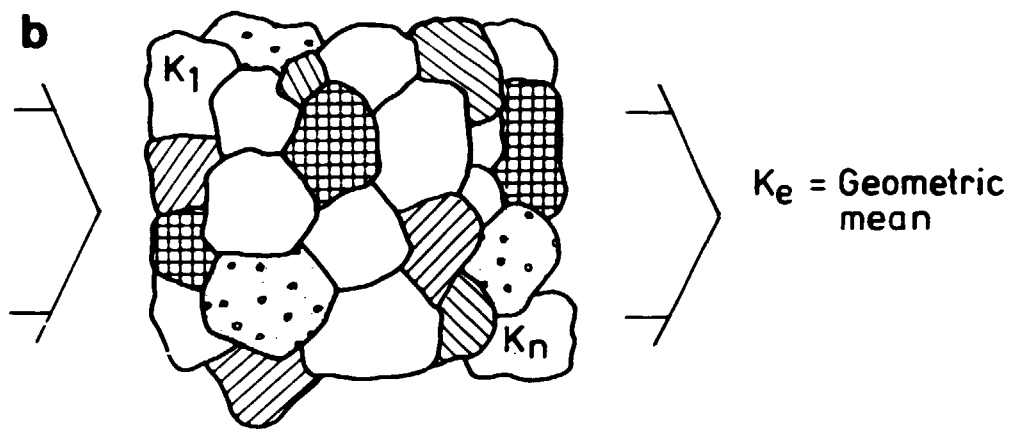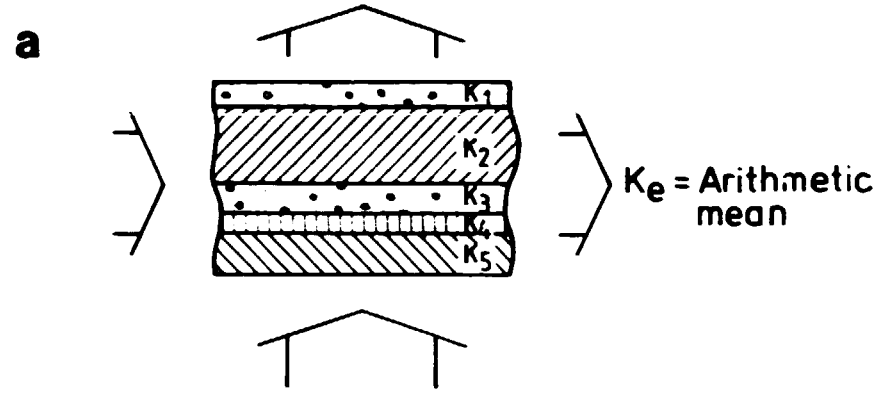
Figure 4.3.1   Estimation of the effective hydraulic conductivity K(e) by using different mean values.
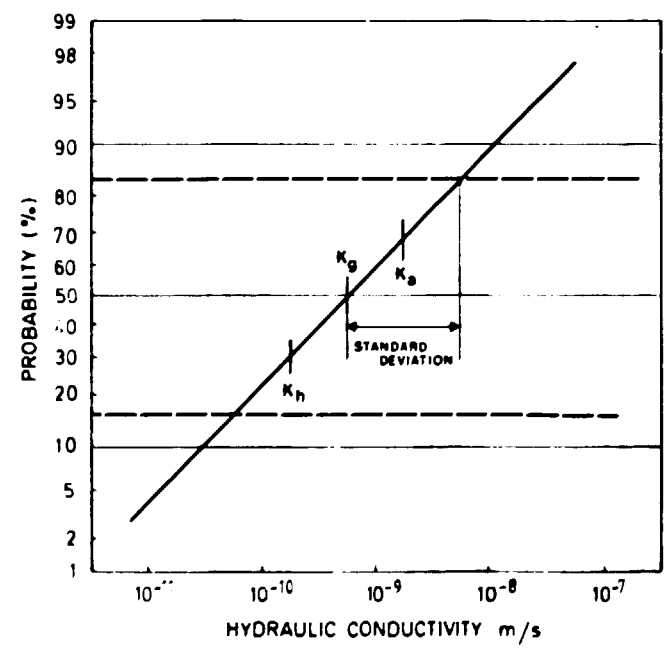
Figure 4.3.2.   Example of lognormal distribution with median value, geometric mean, arithmetic and harmonic means and standard deviation.
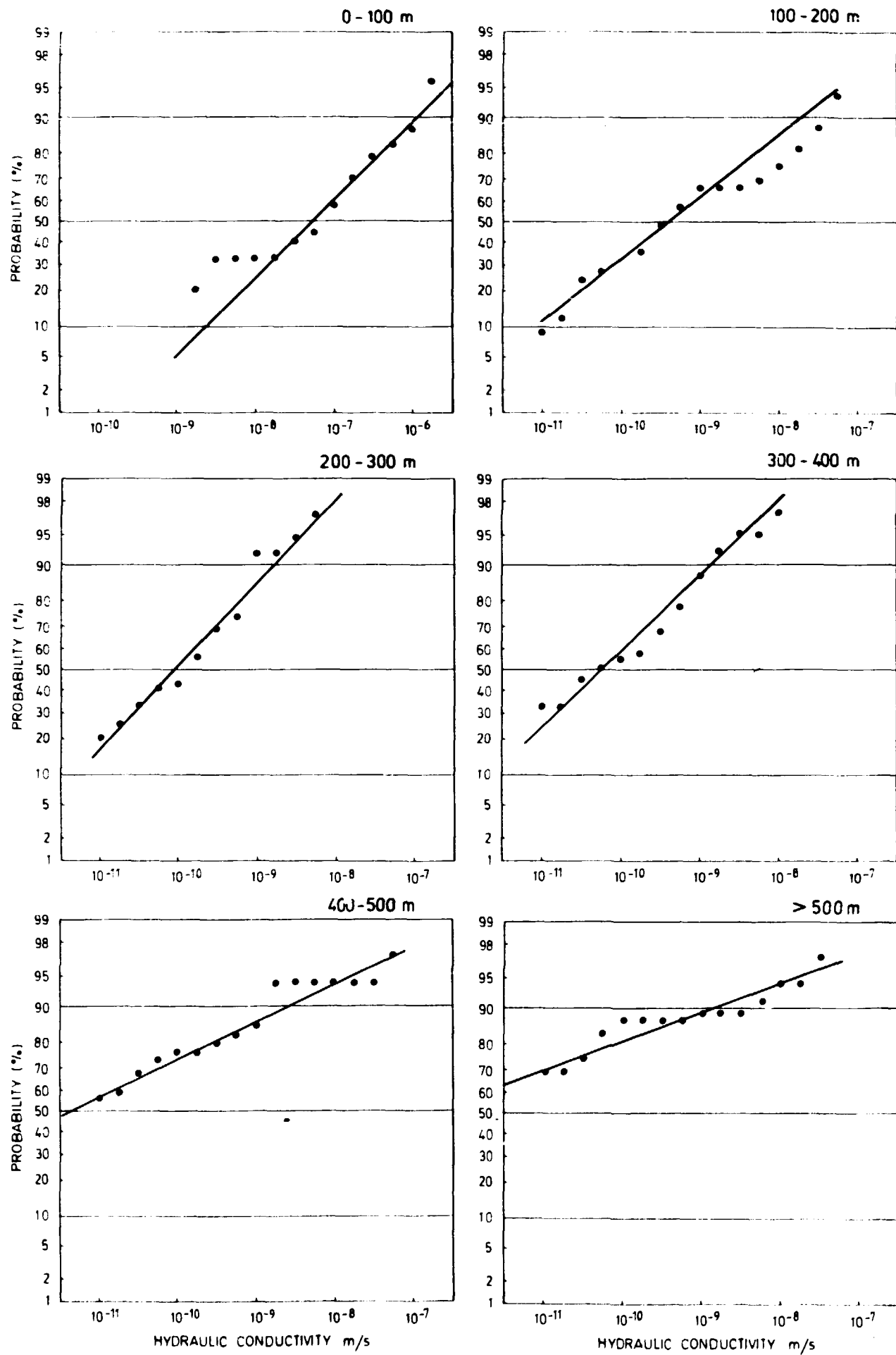
Figure 4.3.3.   Frequency distribution of measured values of
hydraulic conductivity in the rock mass of
Fjällveden.
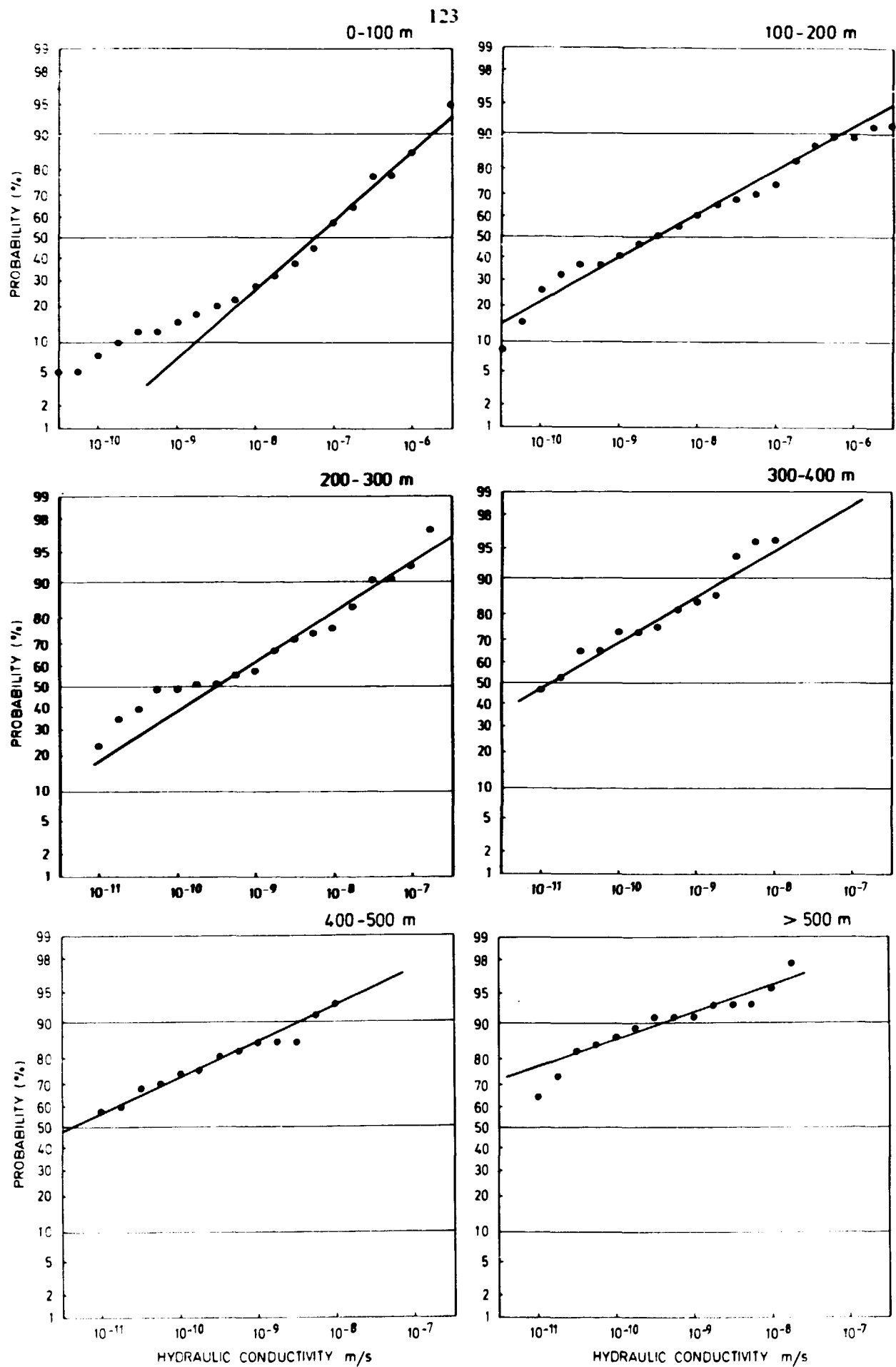
Figure 4.3.4. Frequency distribution of measured values of hydraulic conductivity in the rock mass of Gideå.
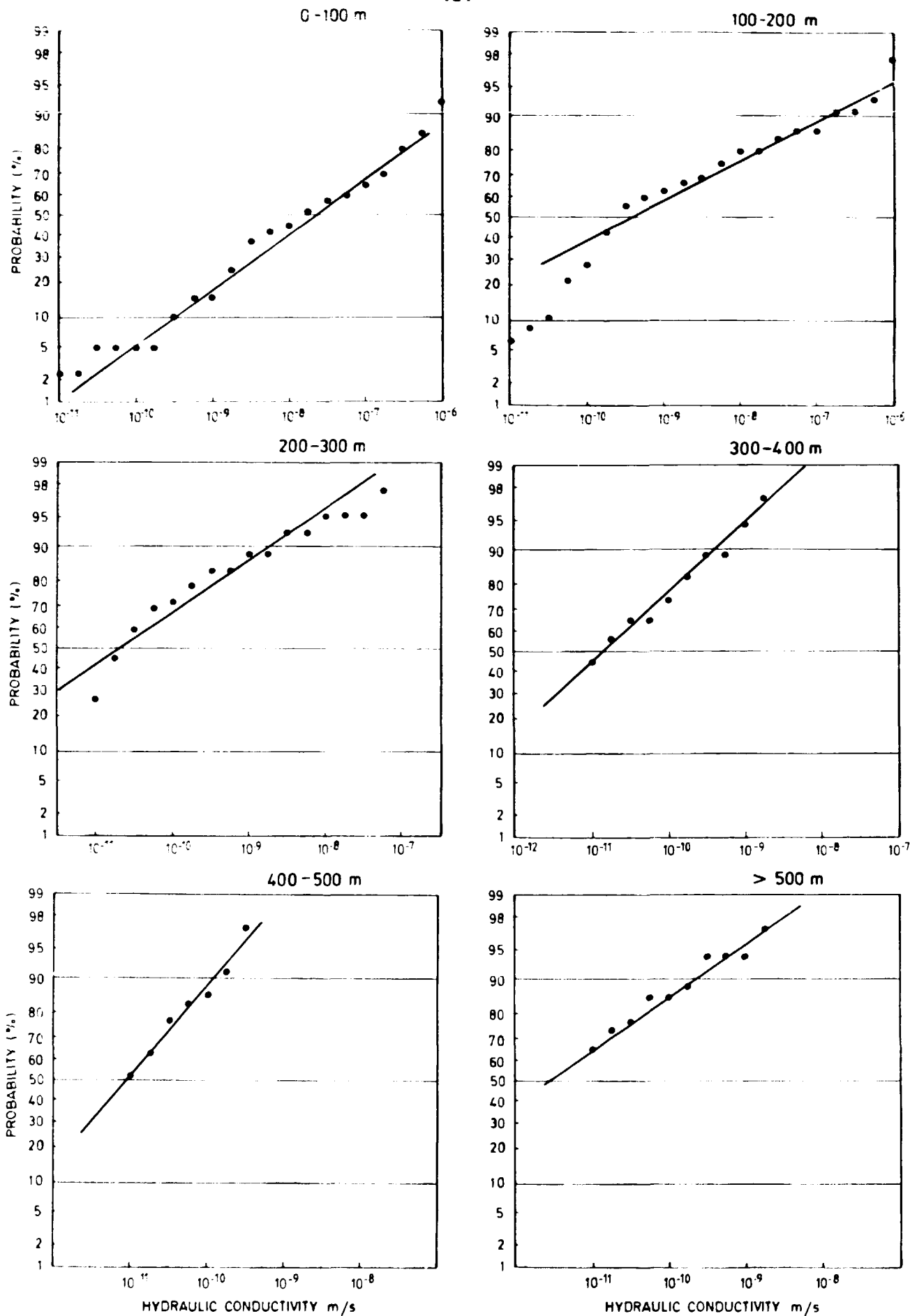
Figure 4.3.5.   Frequency distribution of measured values of
                 hydraulic conductivity in the rock mass of
                 Karlunge.
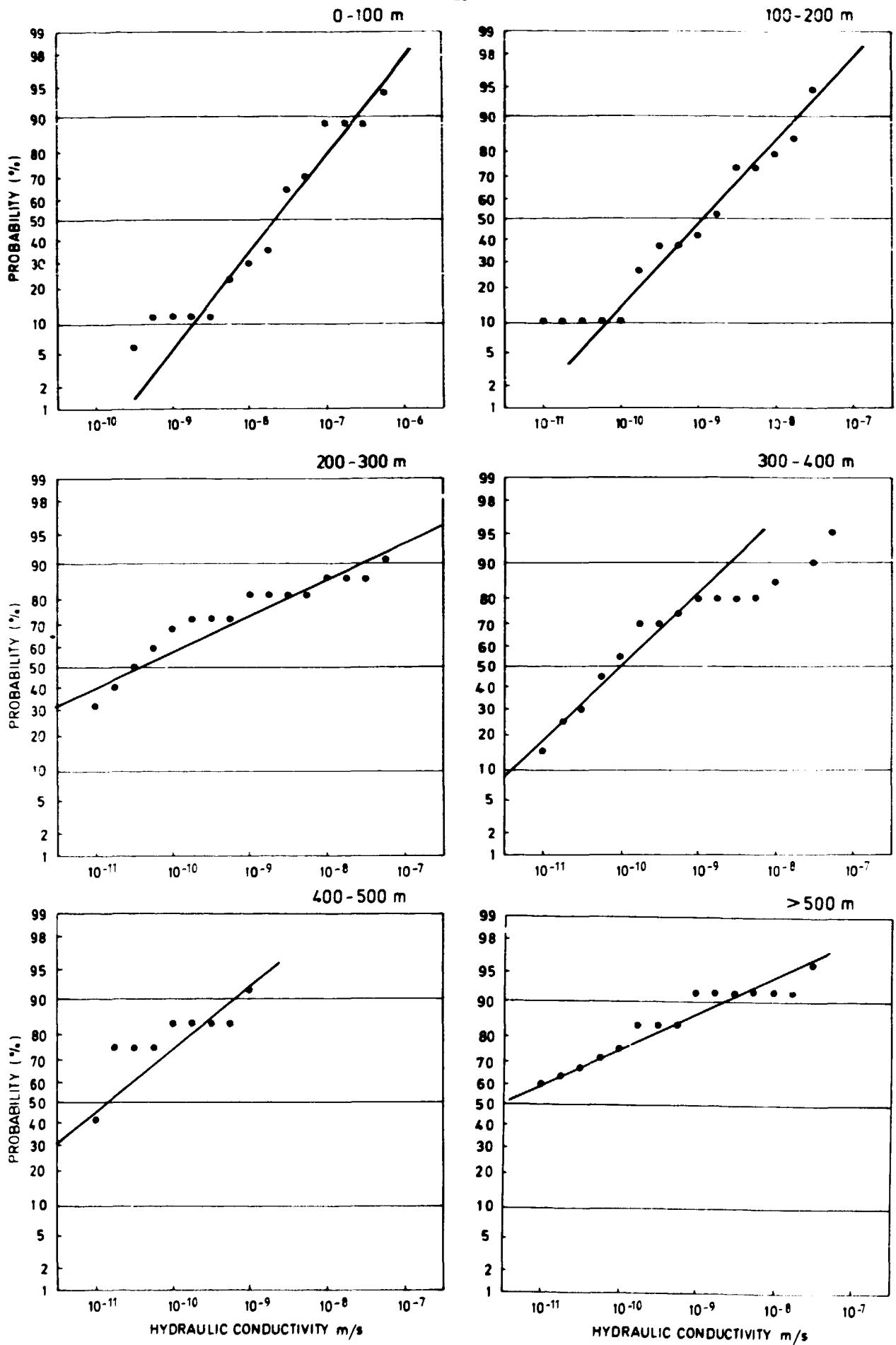
Figure 4.3.6.   Frequency distribution of measured values of
hydraulic conductivity in the rock mass of
Svartboberget.
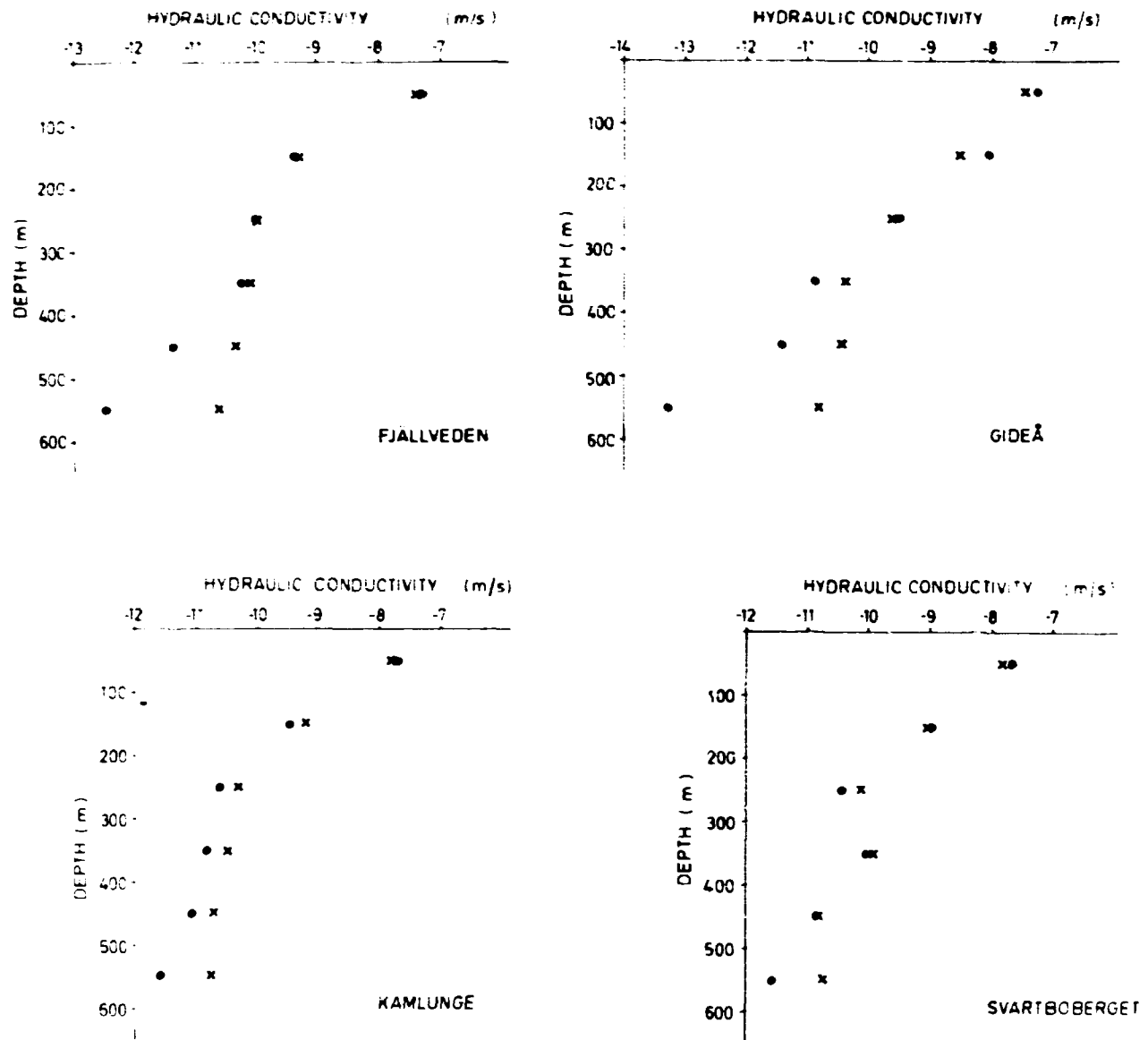
Figure 4.3.7.   Median values of the hydraulic conductivity
from lognormal distribution (●) and calcula-
ted geometric mean (X) from different 100
meter sections in the rock mass.
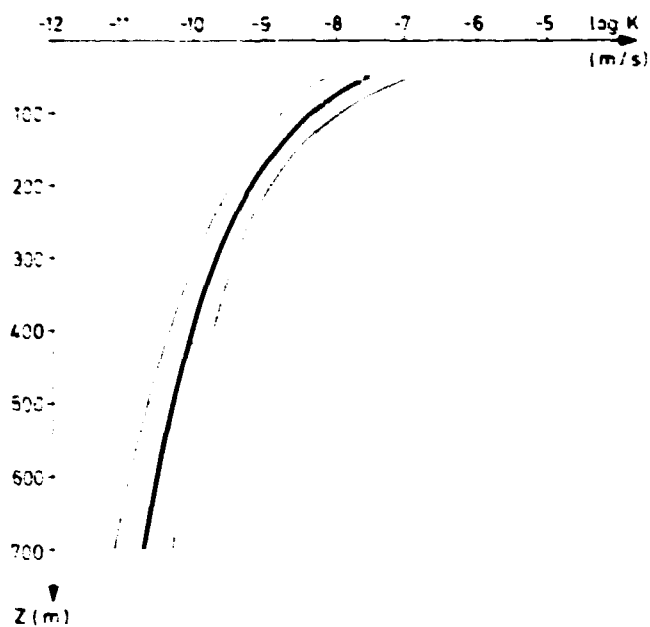
Figure 4.3.8.   Hydraulic conductivity versus depth with con-
                 fidens width of 98% for the rock mass in
                 Fjällveden assuming three-dimensional ground-
                 water flow.
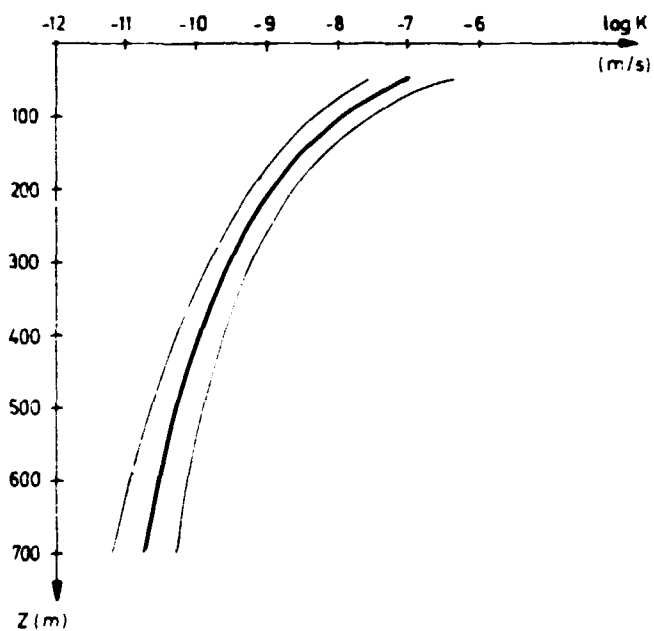
Figure 4.3.9.   Hydraulic conductivity versus depth with con-
                 fidens width of 98% for the rock mass in
                 Gideå assuming three-dimensional groundwater
                 flow.
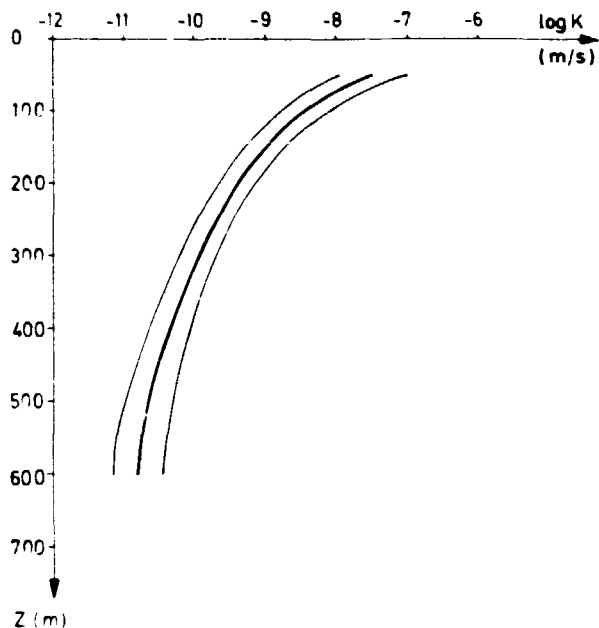
Figure 4.3.10.   Hydraulic conductivity versus depth with con-
                  fidens width of 98% for the rock mass in Kam-
                  lunge assuming three-dimensional groundwater
                  flow.
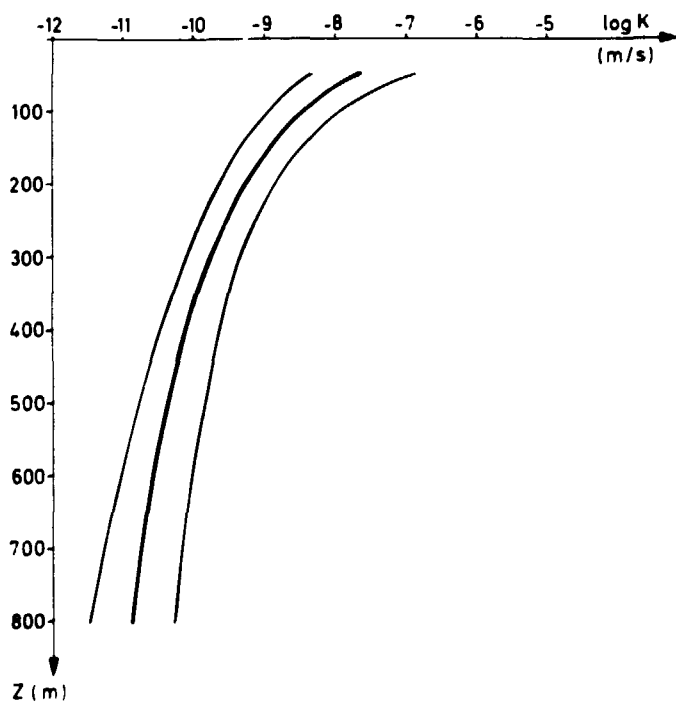
Figure 4.3.11.   Hydraulic conductivity versus depth with con-
                  fidens width of 98% for the rock mass in
                  Svartboberget assuming three-dimensional
                  groundwater flow.
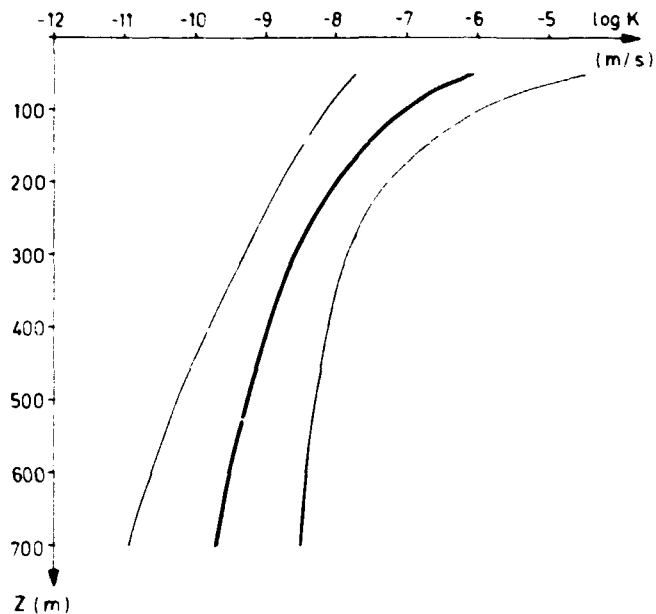
Figure 4.3.12.   Hydraulic conductvity versus depth with con-
                 fidens width of 95% for the local fracture
                 zones in Fjällveden assuming two-dimensional
                 groundwater flow.
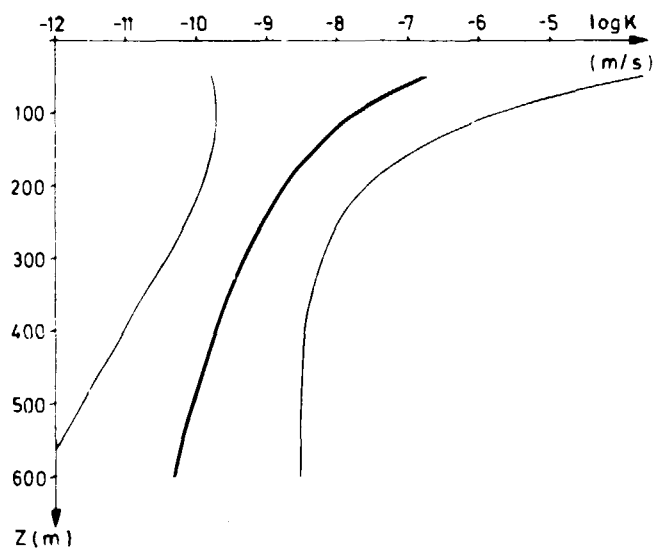
Figure 4.3.13.   Hydraulic conductvity versus depth with con-
                 fidens width of 95% for the local fracture
                 zones in Gideå assuming two-dimensional
                 groundwater flow.
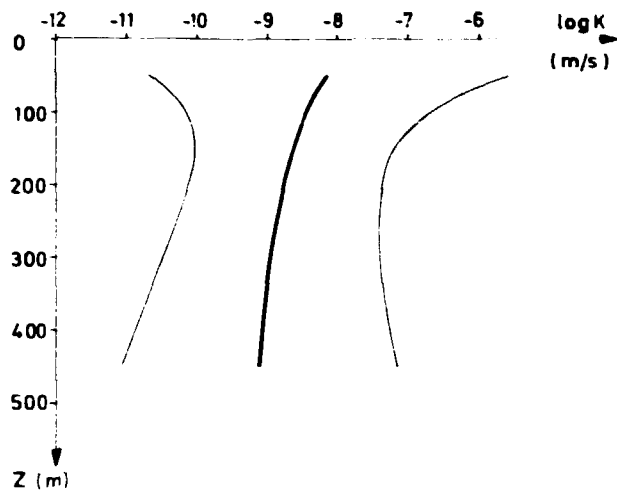
Figure 4.3.14. Hydraulic conductvity versus depth with con-
fidens width of 95% for the local fracture
zones in Kamlunge assuming two-dimensional
groundwater flow.
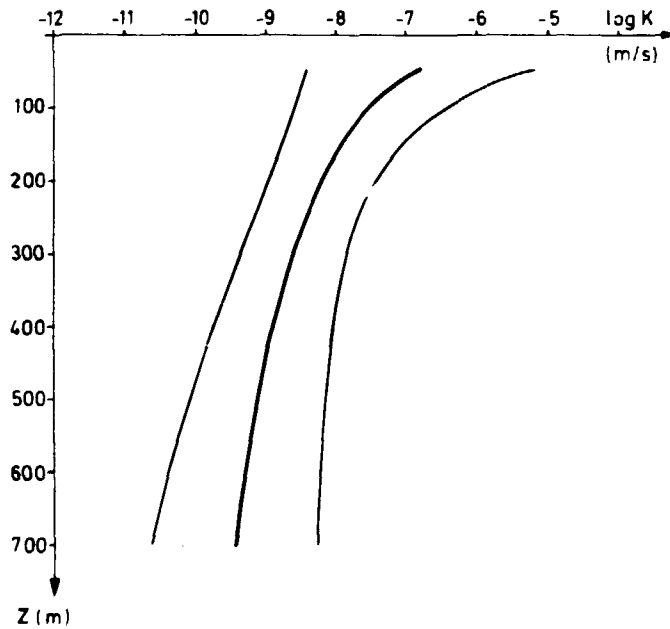
Figure 4.3.15. Hydraulic conductvity versus depth with con-
fidens width of 95% for the local fracture
zones in Svartboberget assuming two-dimensio-
nal groundwater flow.
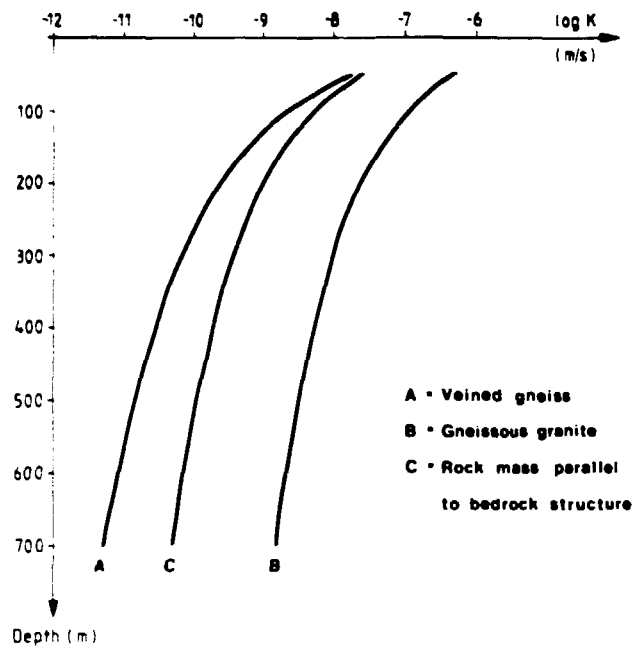
Figure 4.3.16.   Hydraulic conductivity versus depth for vei-
ned gneiss, gneissic granite and rock mass
parallel to bedrock structure in Fjällveden.
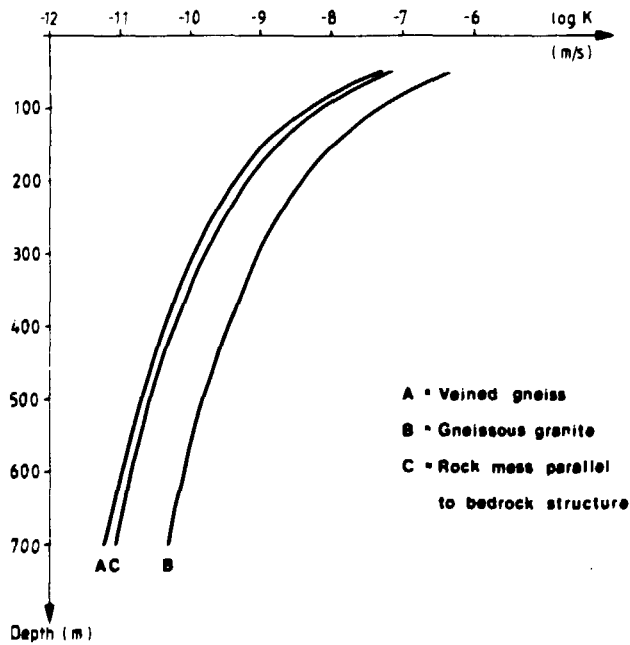
Figure 4.3.17.   Hydraulic conductivity versus depth for vei-
ned gneiss, gneissic granite and rock mass
parallel to bedrock structure in Gideå.
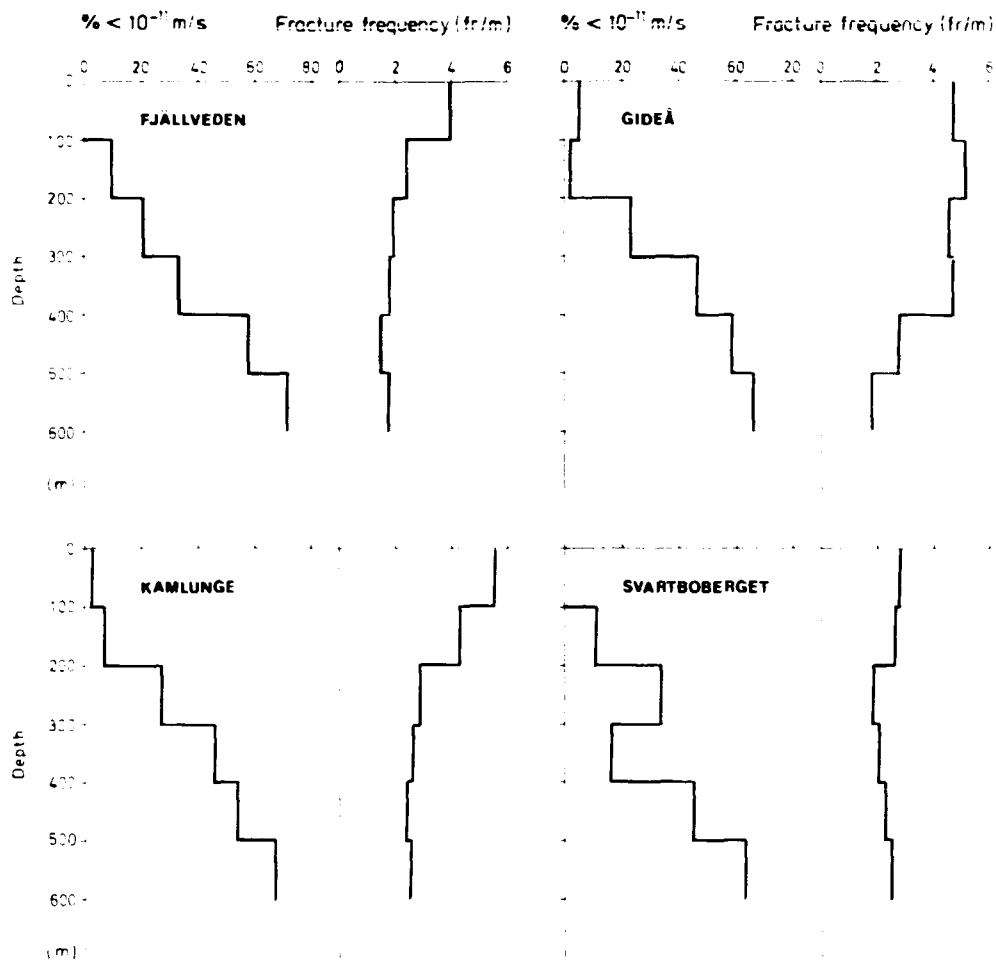
Figure 5.1.1.   Percentage of the hydraulic conductivity
                 values in the rock mass lower than 1.E-11 m/s
                 and the mean fracture frequency versus depth
                 in Fjällveden, Gideå, Kamlunge and Svartbo-
                 berget.
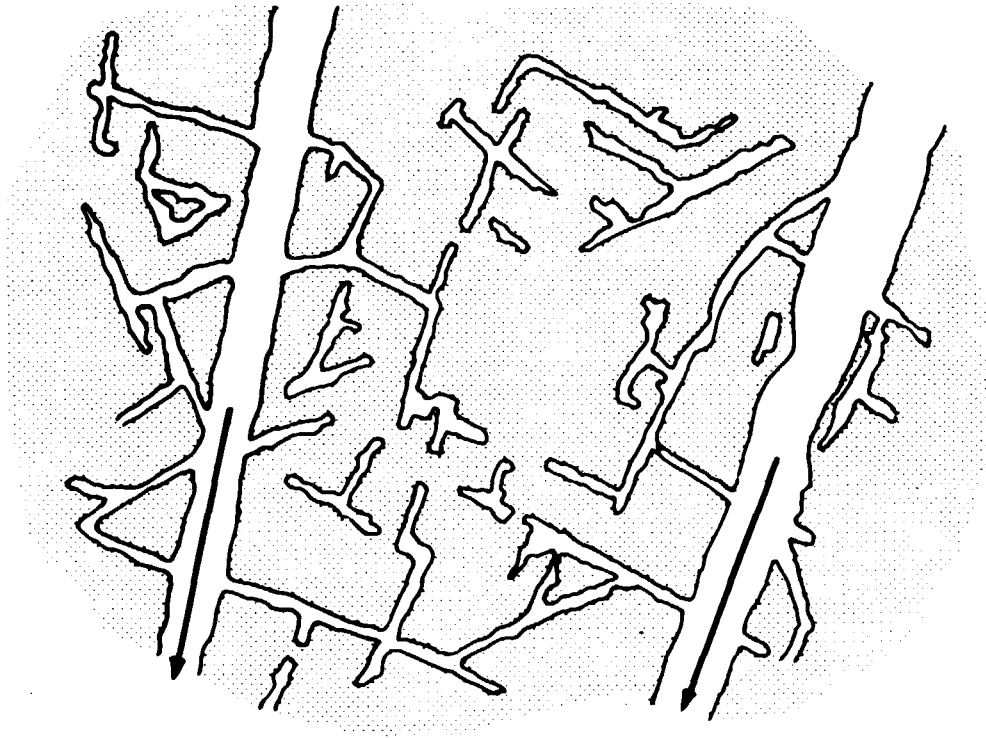
Figure 5.2.1.   Schematic representation of different fractu-
                 res and their geometric relationship in the
                 rock mass. The arrows denote fractures consti-
                 tuting the kinematic porosity (hydraulic
                 fractures). Smaller fractures connected to
                 the hydraulic fractures constitutes the
                 diffusion porosity, the remaining the residual
                 porosity. After Norton and Knapp (1977).
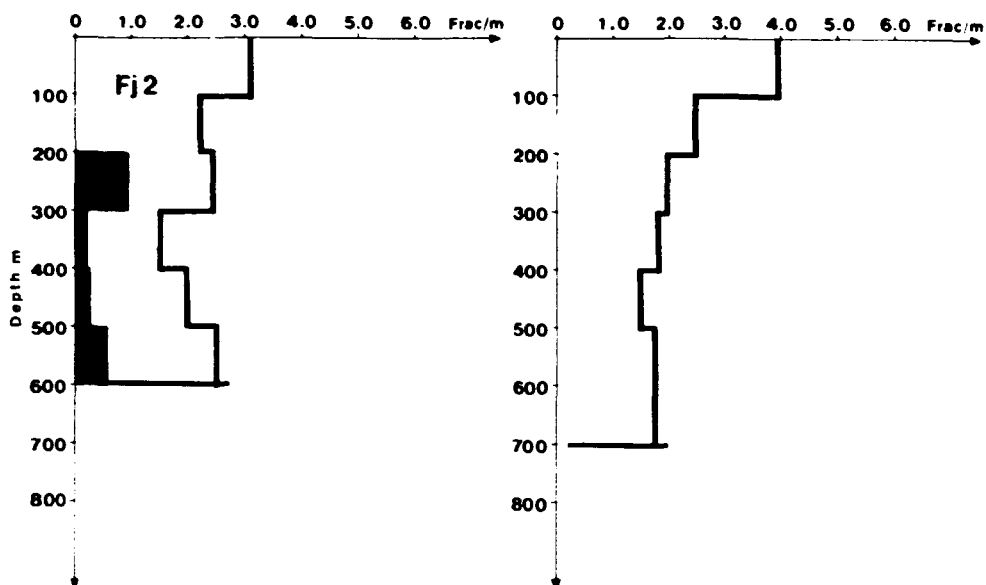
Figure 5.4.1.   Hydraulic fracture frequency and total frac-
                  ture frequency in borehole Fj 2, together
                  with total fracture frequency from all
                  core-drilled boreholes in the Fjällveden
                  area.
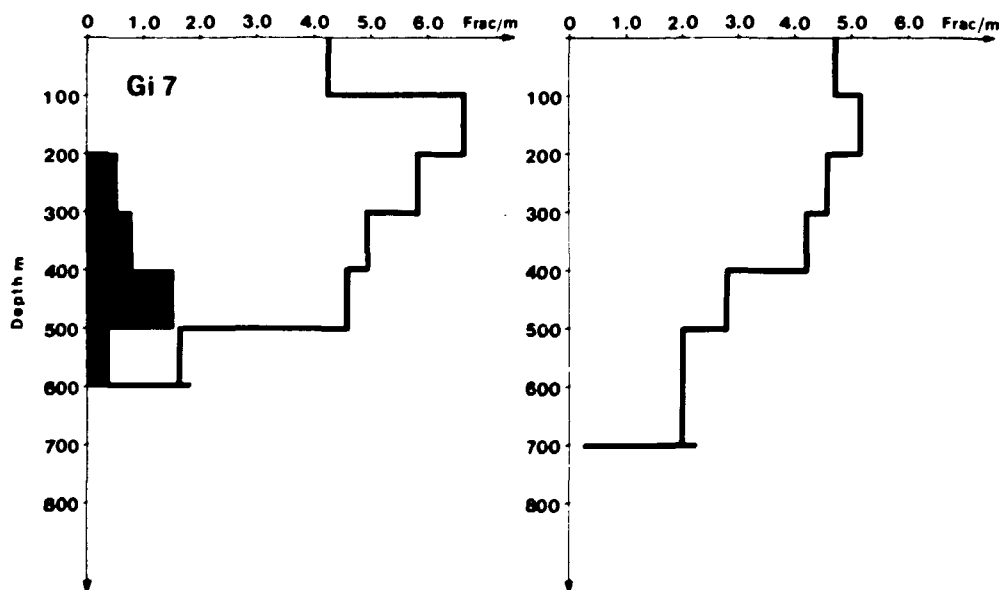
Figure 5.4.2.   Hydraulic fracture frequency and total frac-
                  ture frequency in borehole Gi 7, together
                  with total fracture frequency from all
                  core-drilled boreholes in the Gideå area.
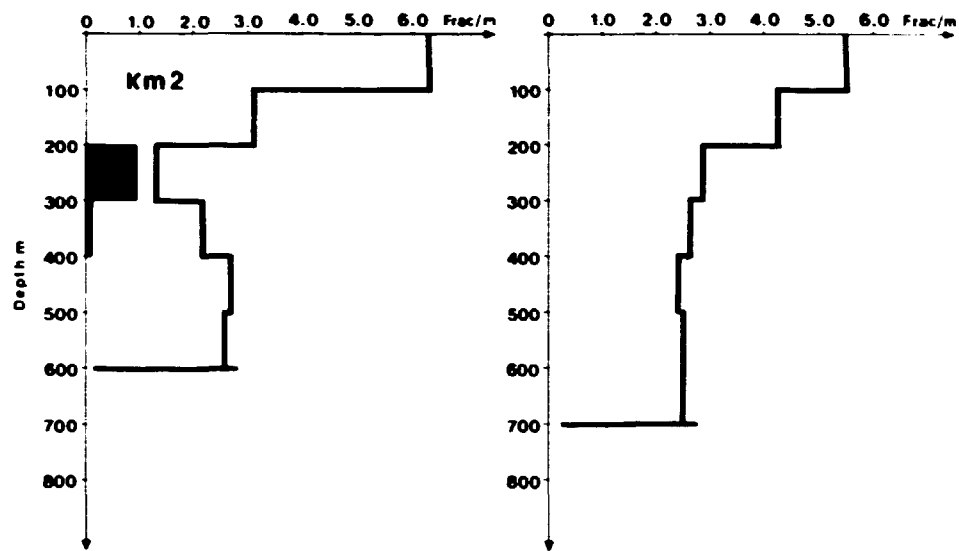
Figure 5.4.3.   Hydraulic fracture frequency and total frac-
                 ture frequency in borehole Km 2, together
                 with total fracture frequency from all
                 core-drilled boreholes in the Kamlunge area.
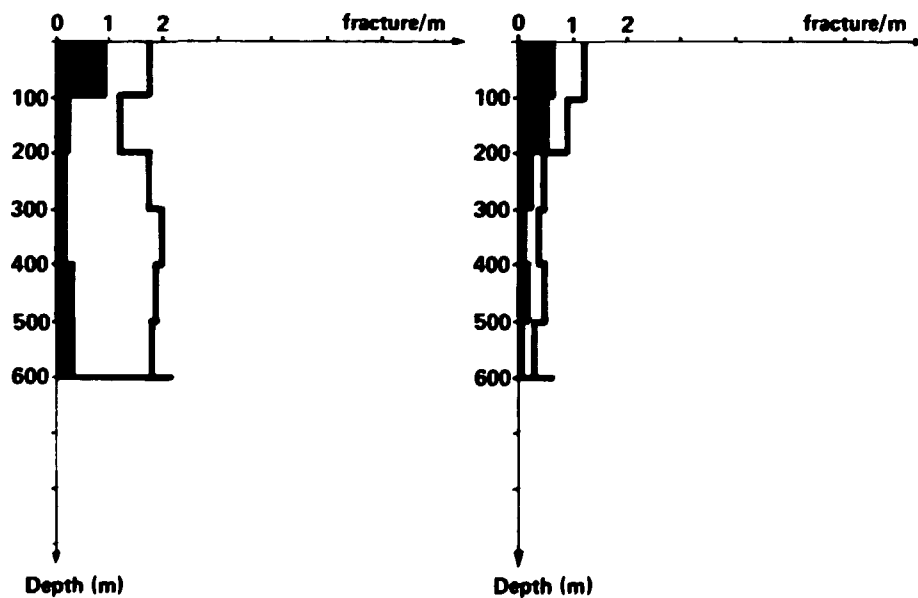
Figure 5.4.4.

Left - Hydraulic fracture frequency and total fracture fre-
    quency from the core-drilled boreholes Fi 1, Fi 2, Fi 4, Fi
    6 and Fi 7 in the Finnsjön area.
Right - Hydraulic fracture frequency and total fracture fre-
    quency from all core-drilled boreholes in the Sternö area.

PERCENTAGE HYDRAULIC CONDUCTIVE FRACTURES
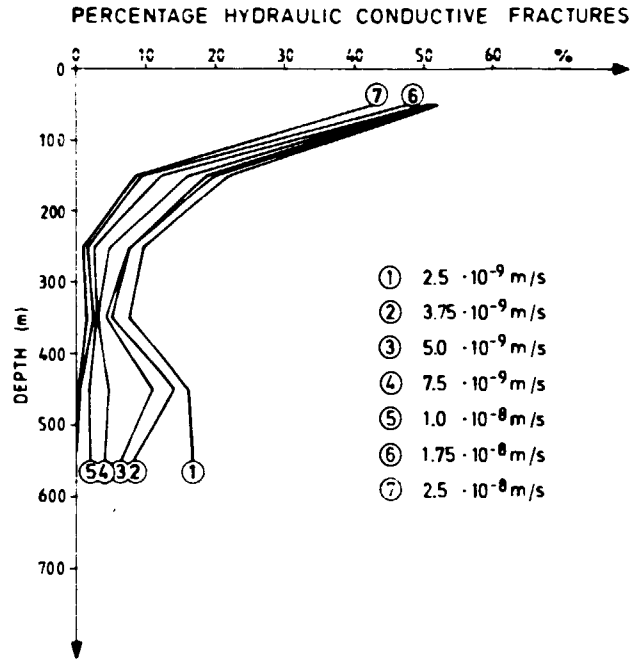
Figure 5.4.5.   Percentage of hydraulic fractures calculated
with different measuring limit in Fjällveden.

PERCENTAGE HYDRAULIC CONDUCTIVE FRACTURES
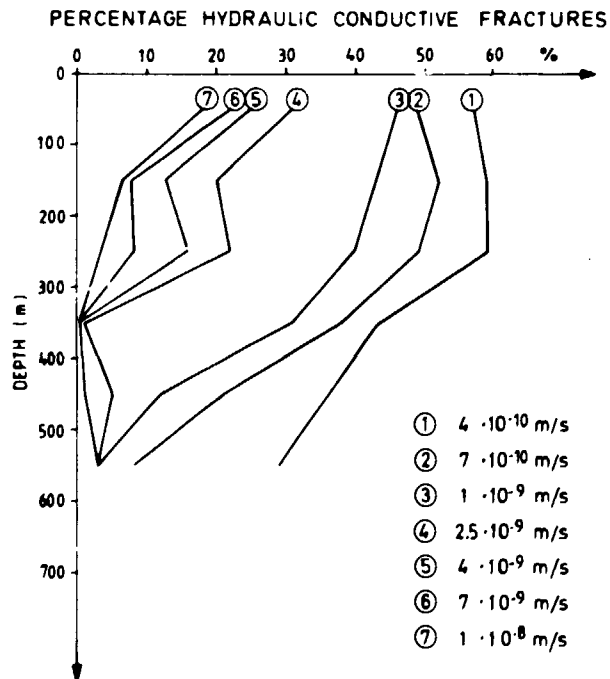
Figure 5.4.6.   Percentage of hydraulic fractures calculated
with different measuring limit in Sternö.
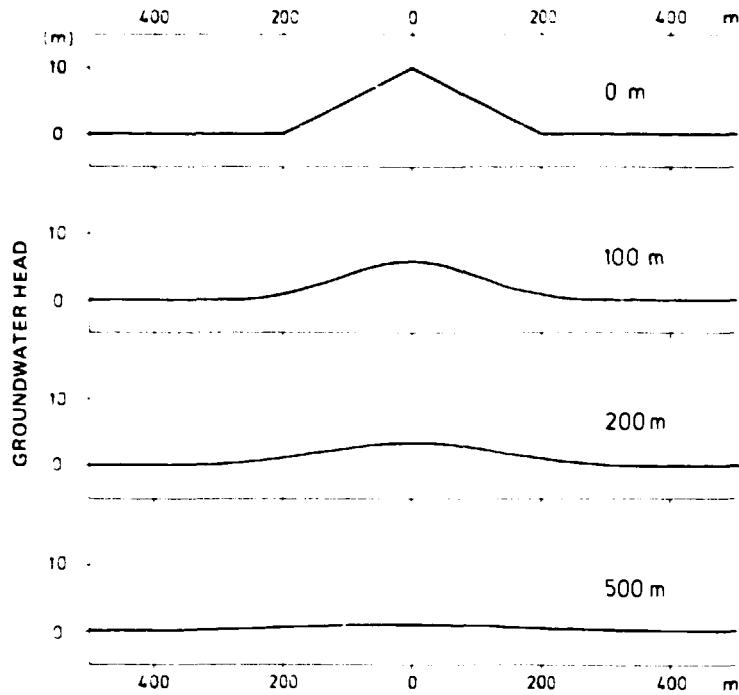
Figure 6.1.1.   Groundwater head at different depth below a
circular hill with 200 m radius. Deacreasing
hydraulic conductivity with depth.
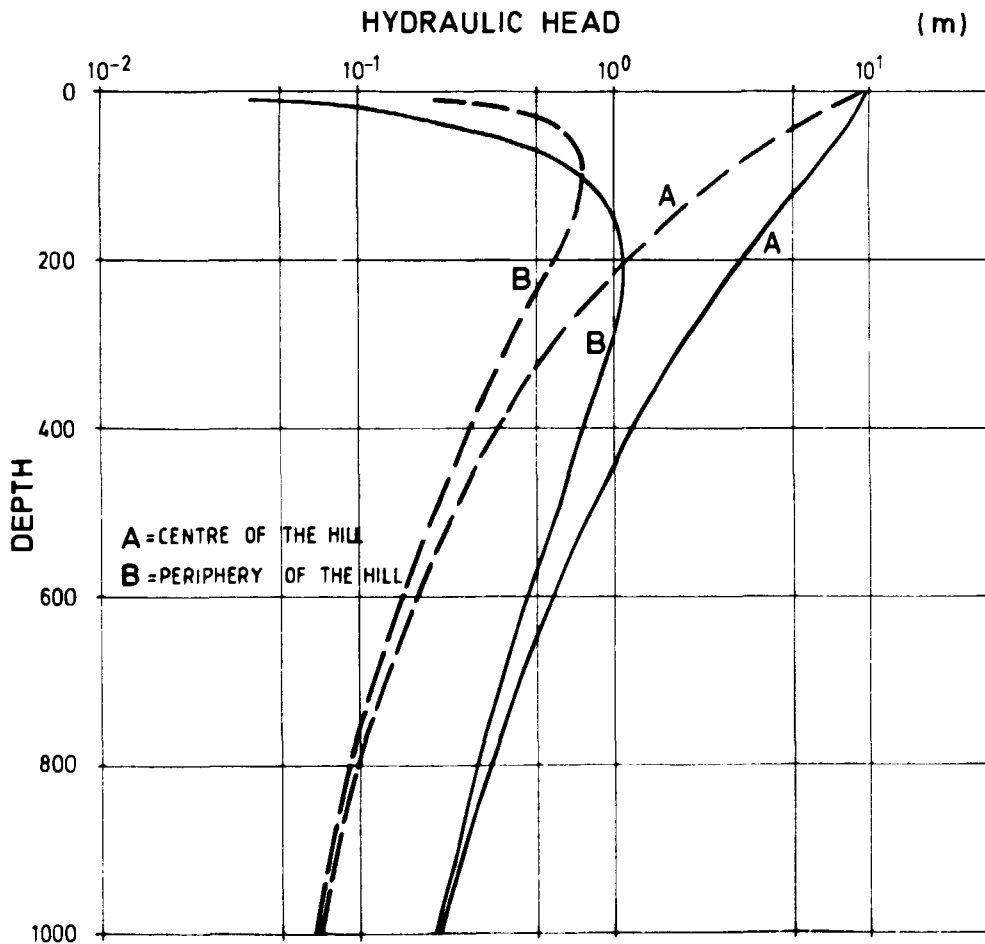
Figure 6.1.2.   Change in groundwater head versus depth below
a circular hill with 200 m radius. ――― ▪
constant hydraulic conductivity, ――――― ▪
decreasing hydraulic conductivity with depth.
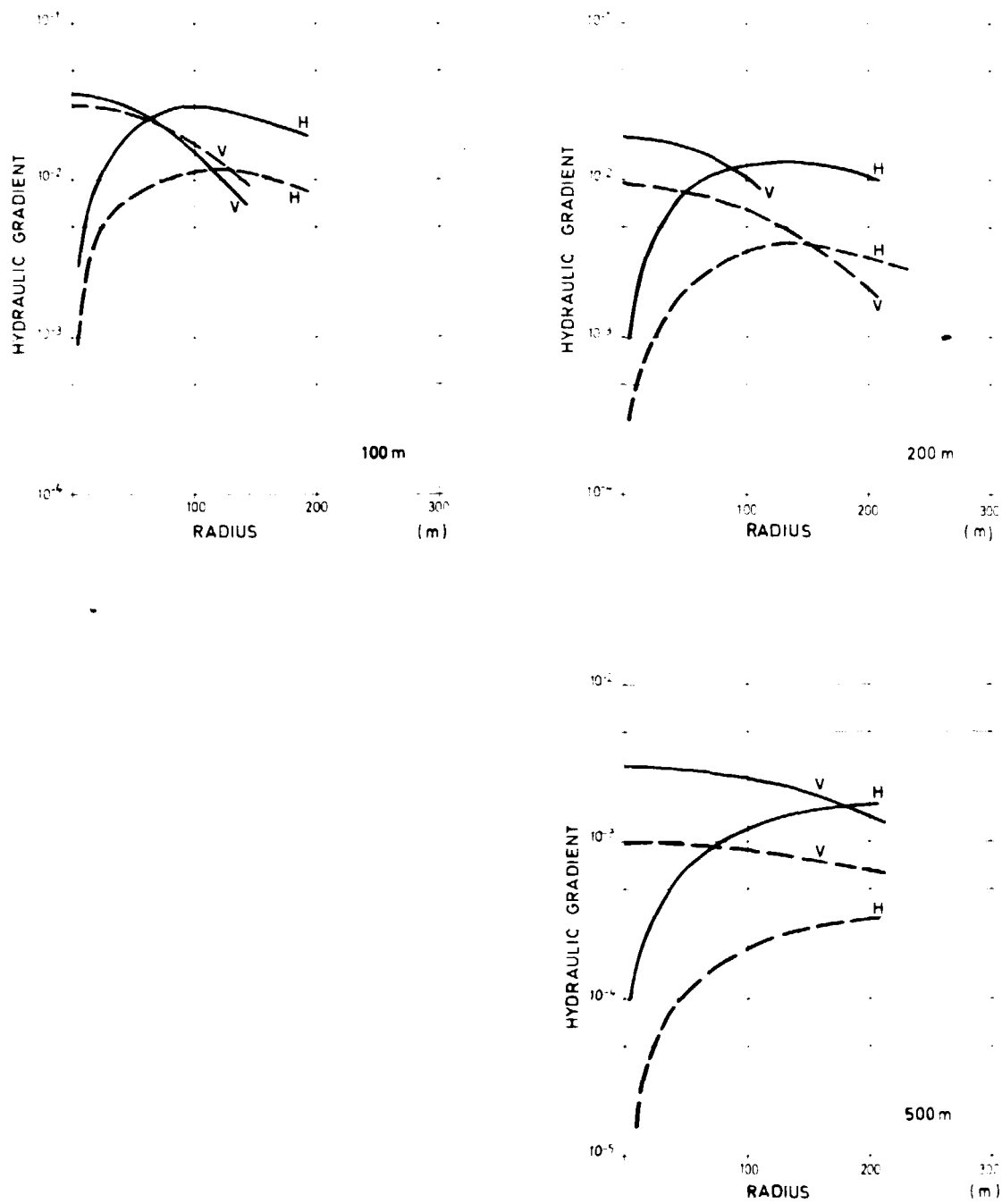
Figure 6 2.1.   Hydraulic gradient at different depth below a
                 circular hill with 200 m radius. V = vertical
                 gradient, H = horisontal gradient, ---- =
                 constant hydraulic conductivity, ——— =
                 decreasing hydraulic conductivity with depth.
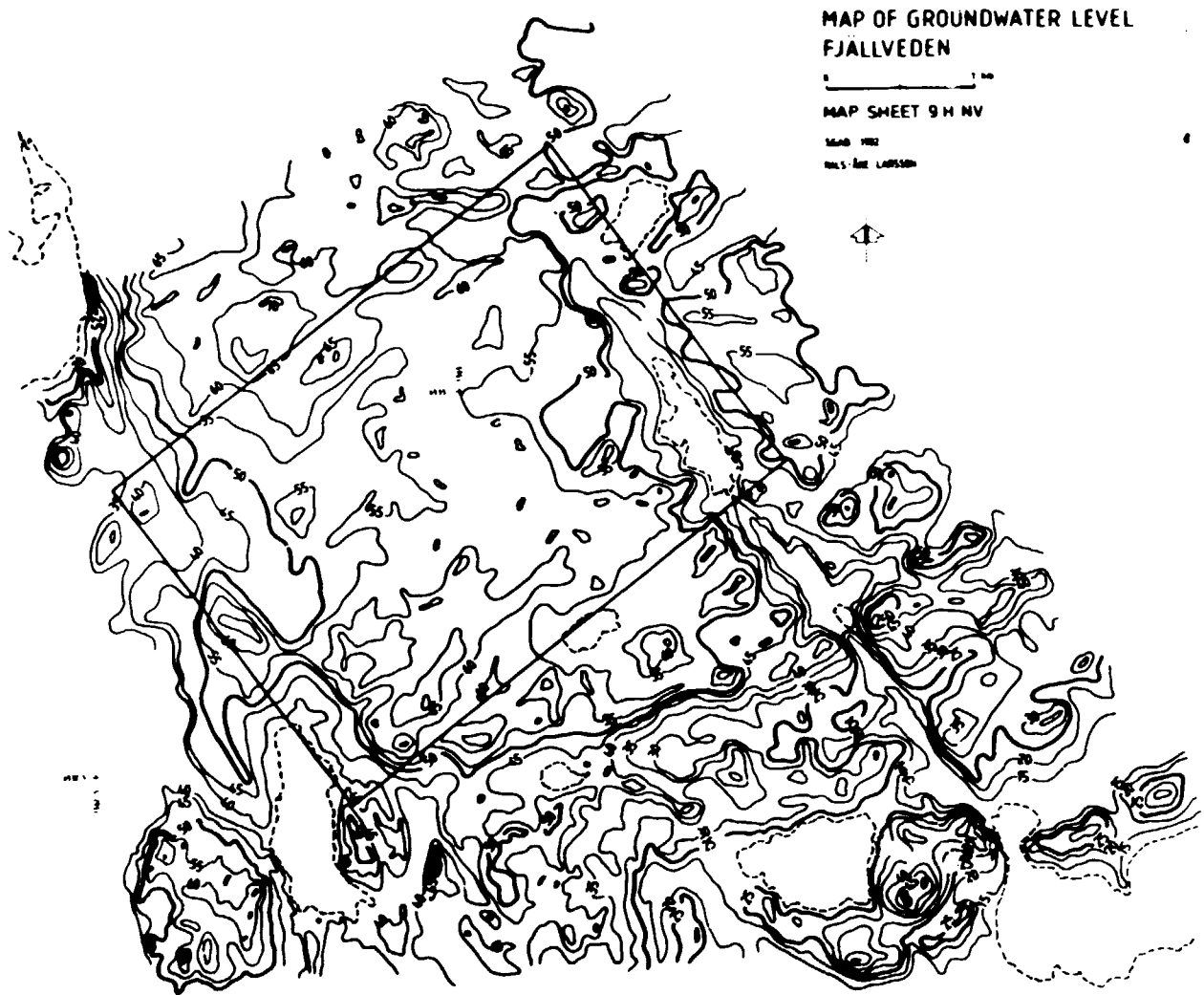
Figure 6.4.1.   Groundwater head in the upper part of the
bedrock (groundwater table) in Fjällveden.

MAP OF GROUNDWATER
LEVEL GIDEÅ

MAP SHEET 19J 8c
- -d
19J 9c
- -d

SGAB 1982
Holger Timje
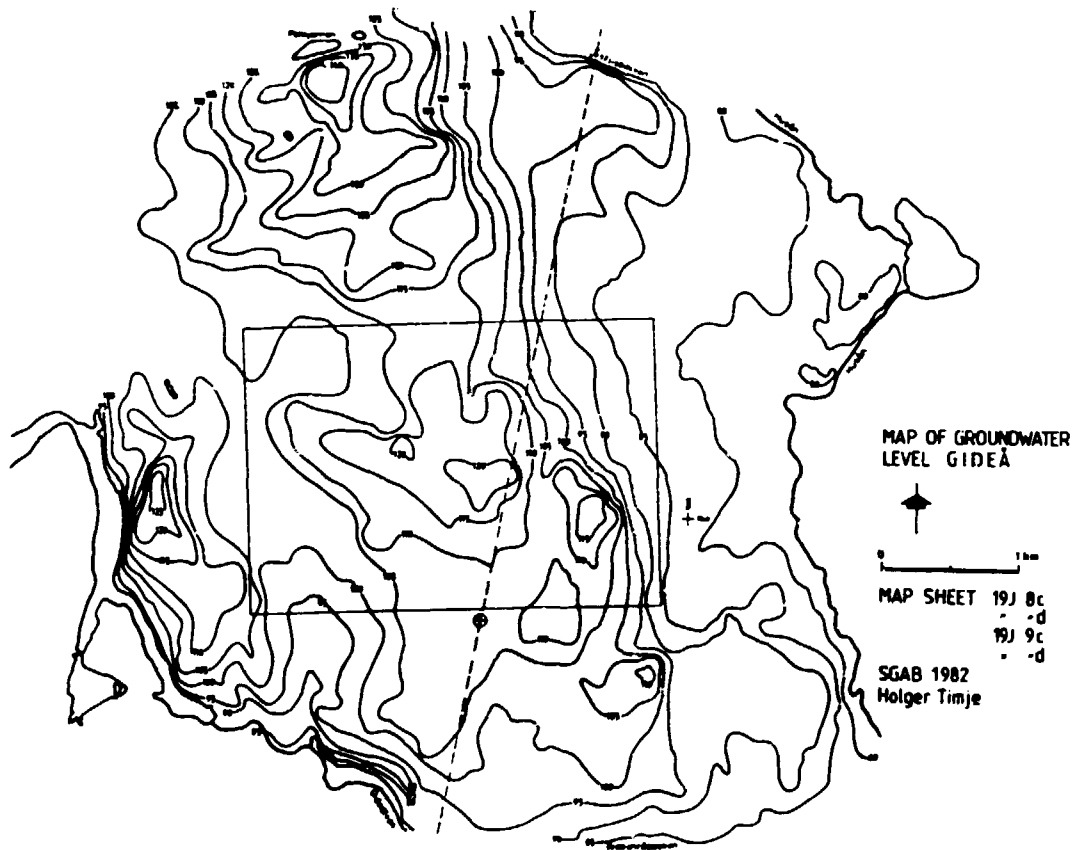
Figure 6.4.2.   Groundwater head in the upper part of the
bedrock (groundwater table) in Gideå.
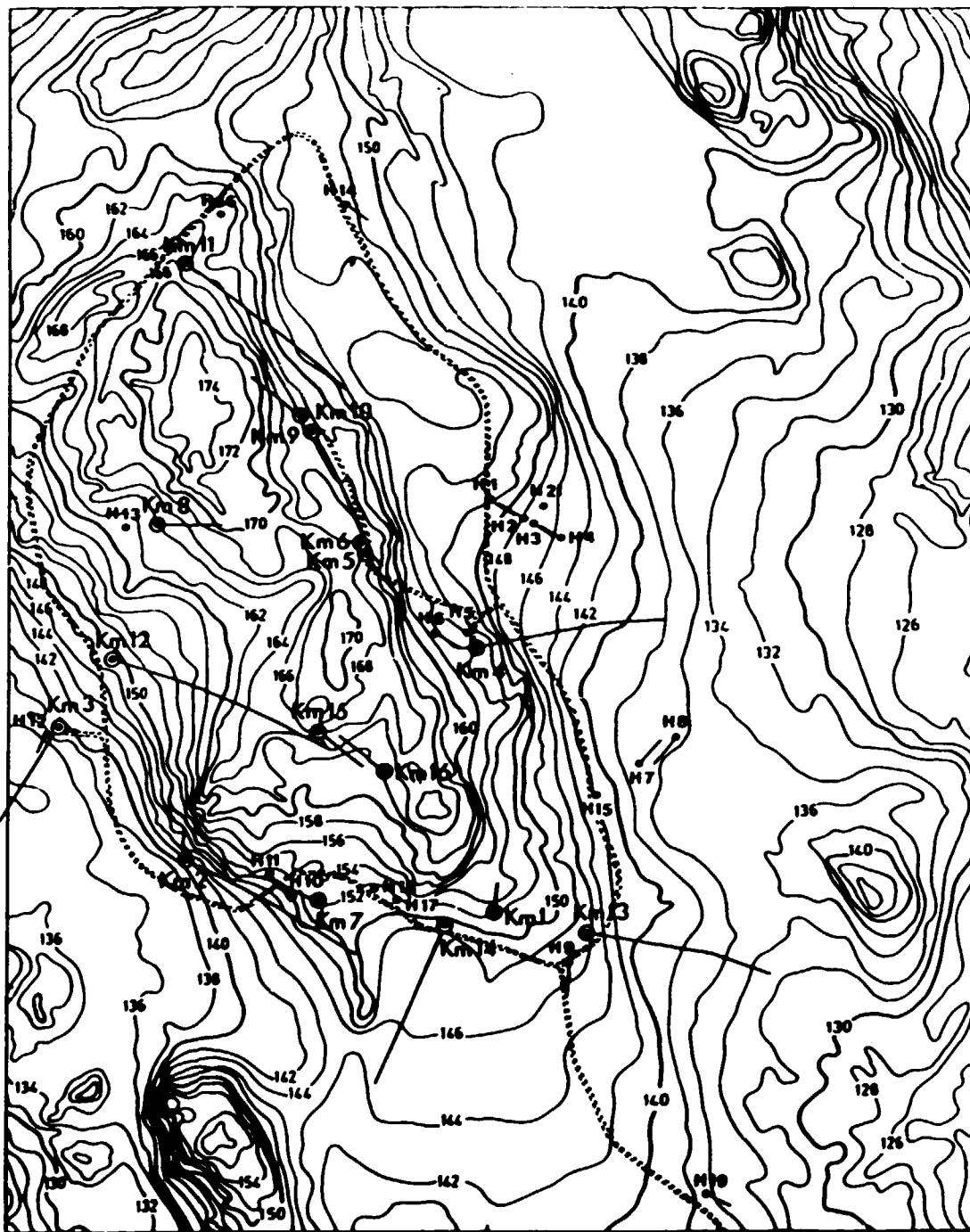
Figure 6.4.3.   Groundwater head in the upper part of the
bedrock (groundwater table) in Kamlunge.

MAP OF GROUNDWATER LEVEL
SVARTBOBERGET

MAP SHEET 15 F SO
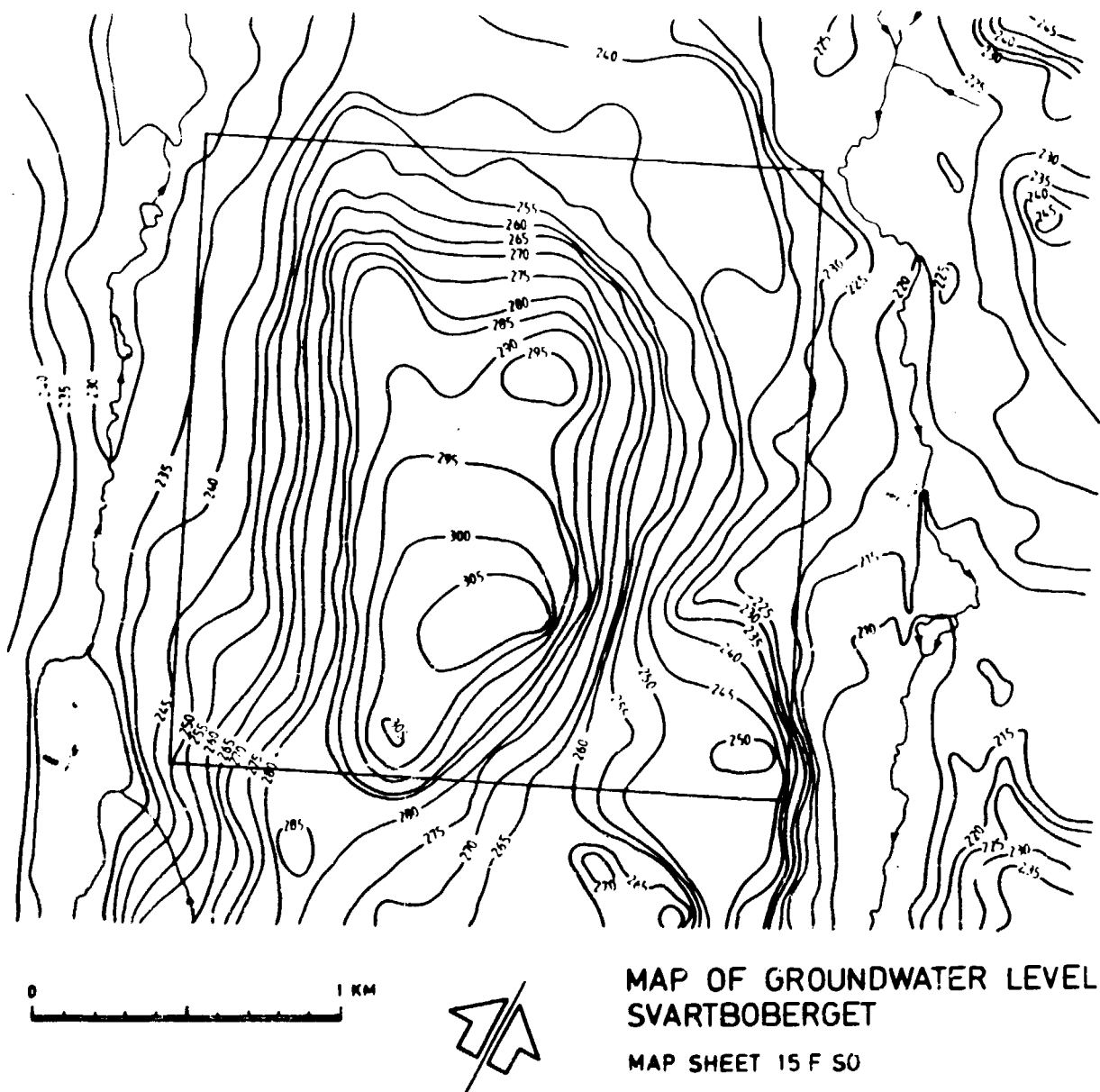
Figure 6.4.4.   Groundwater head in the upper part of the
bedrock (groundwater table) in Svartboberget.
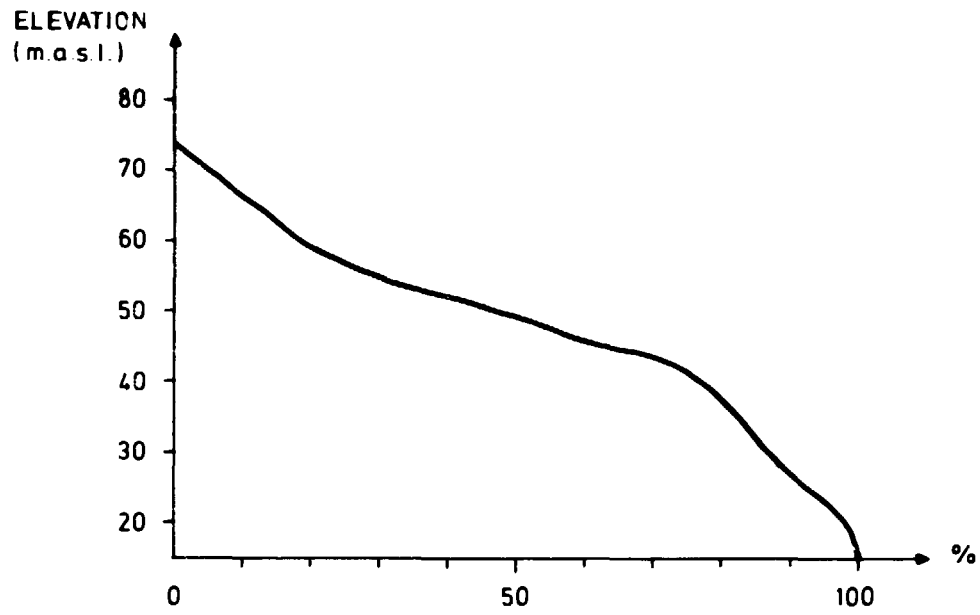
FJÄLLVEDEN

Figure 6.4.5.   Hypsographic curve of the study site
Fjällveden.
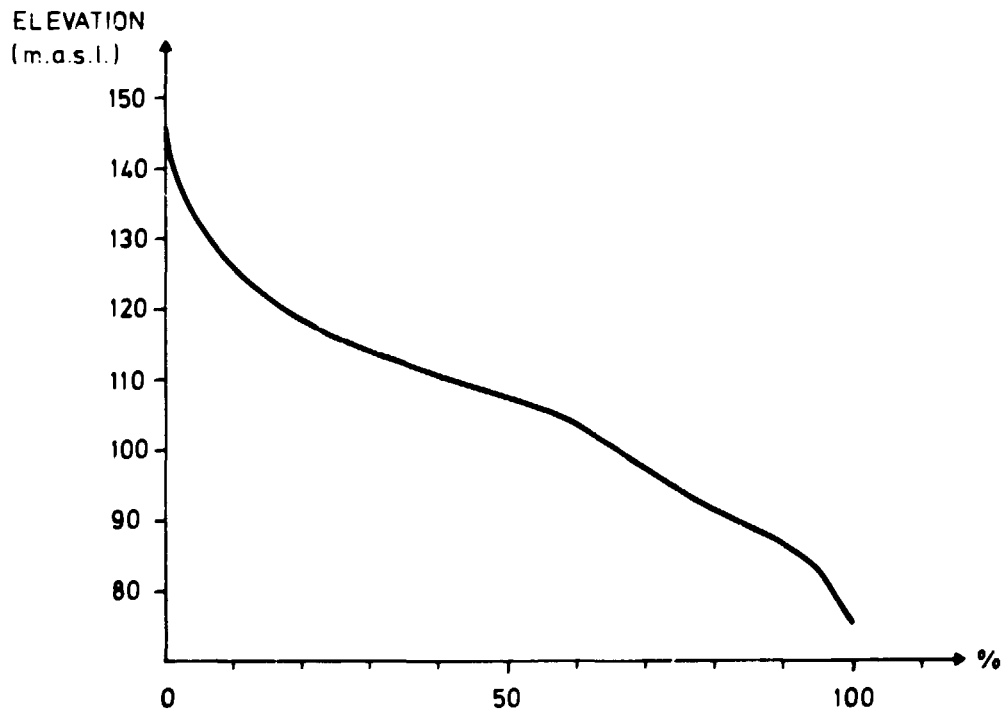
GIDEÅ

Figure 6.4.6.   Hypsographic curve of the study site
Gideä.

KAMLUNGE
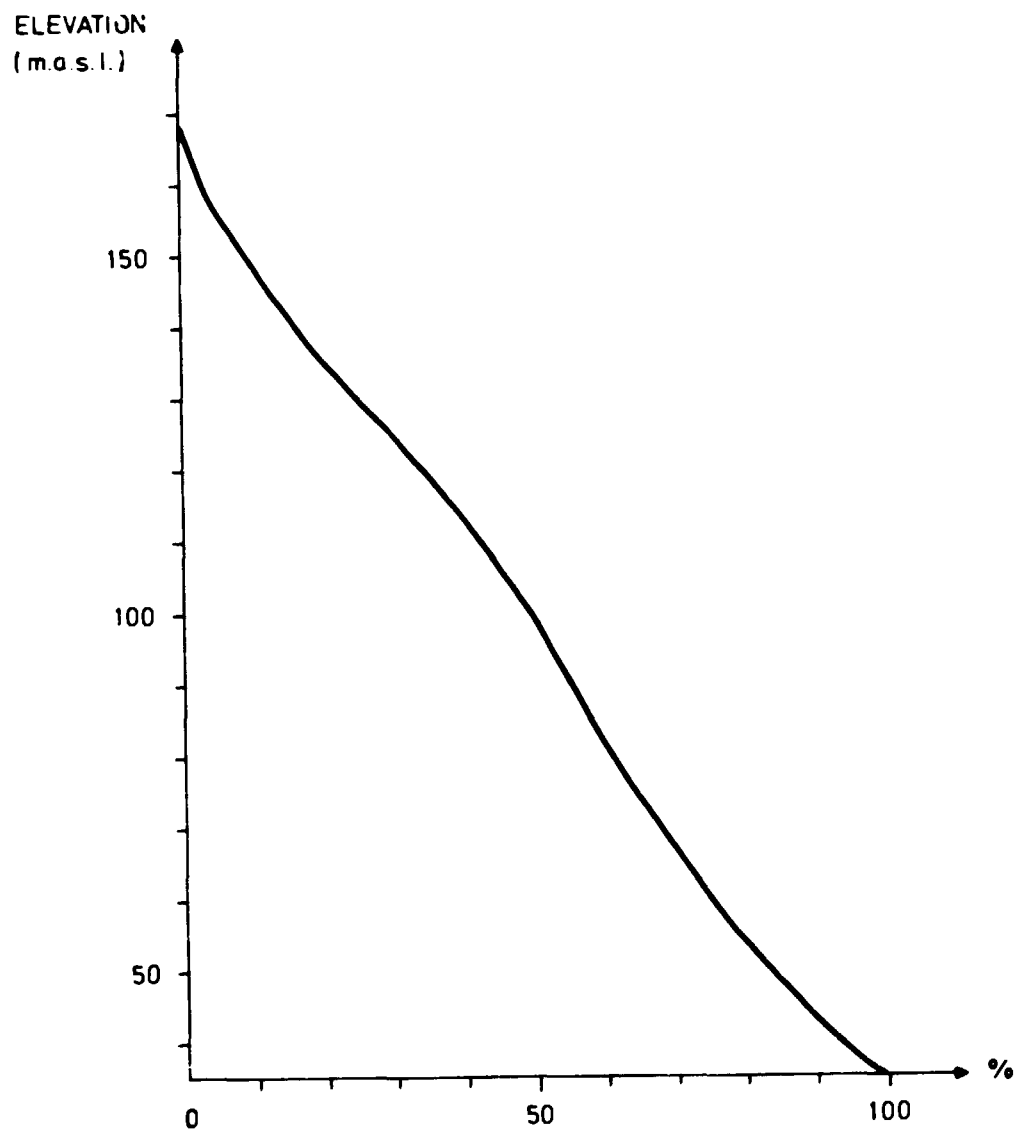
Figure 6.4.7.   Hypsographic curve of the study site Kamlunge.

SVARTBOBERGET
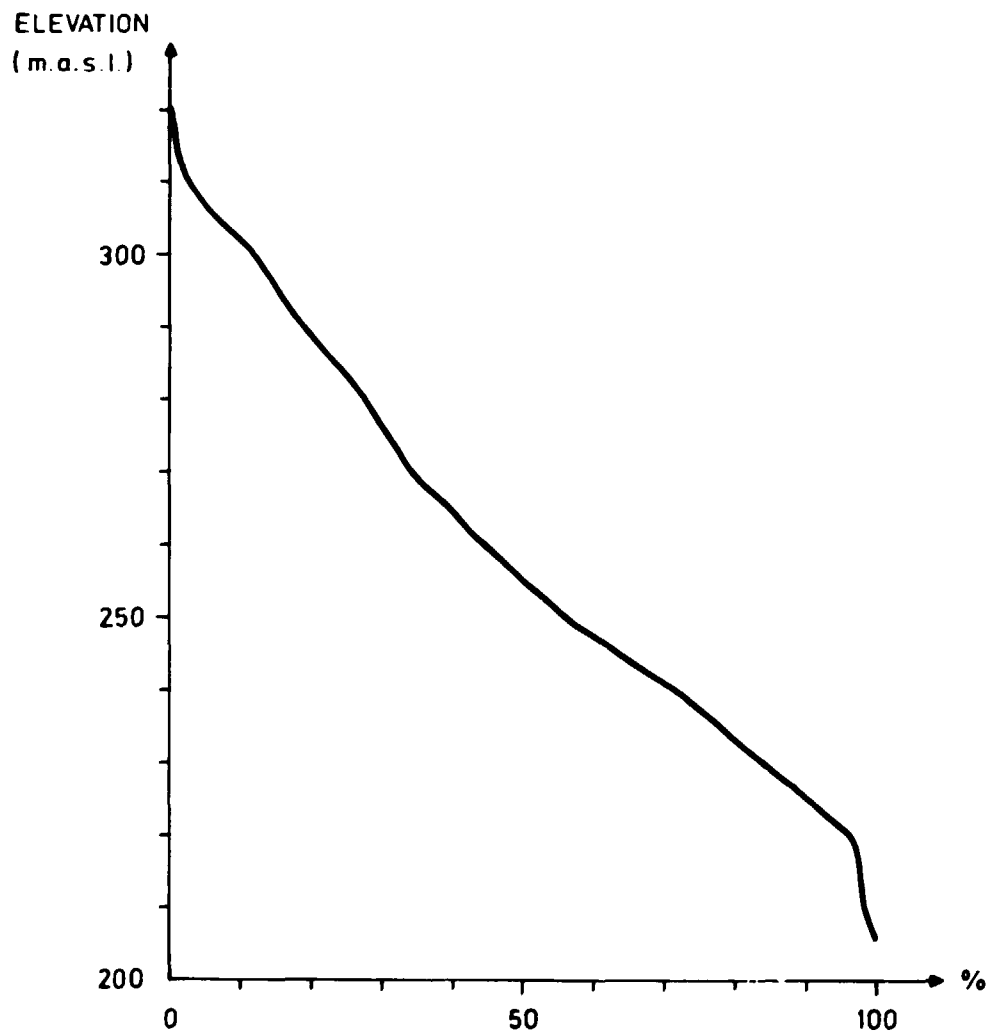
Figure 6.4.8.   Hypsographic curve of the study site
Svartboberget.
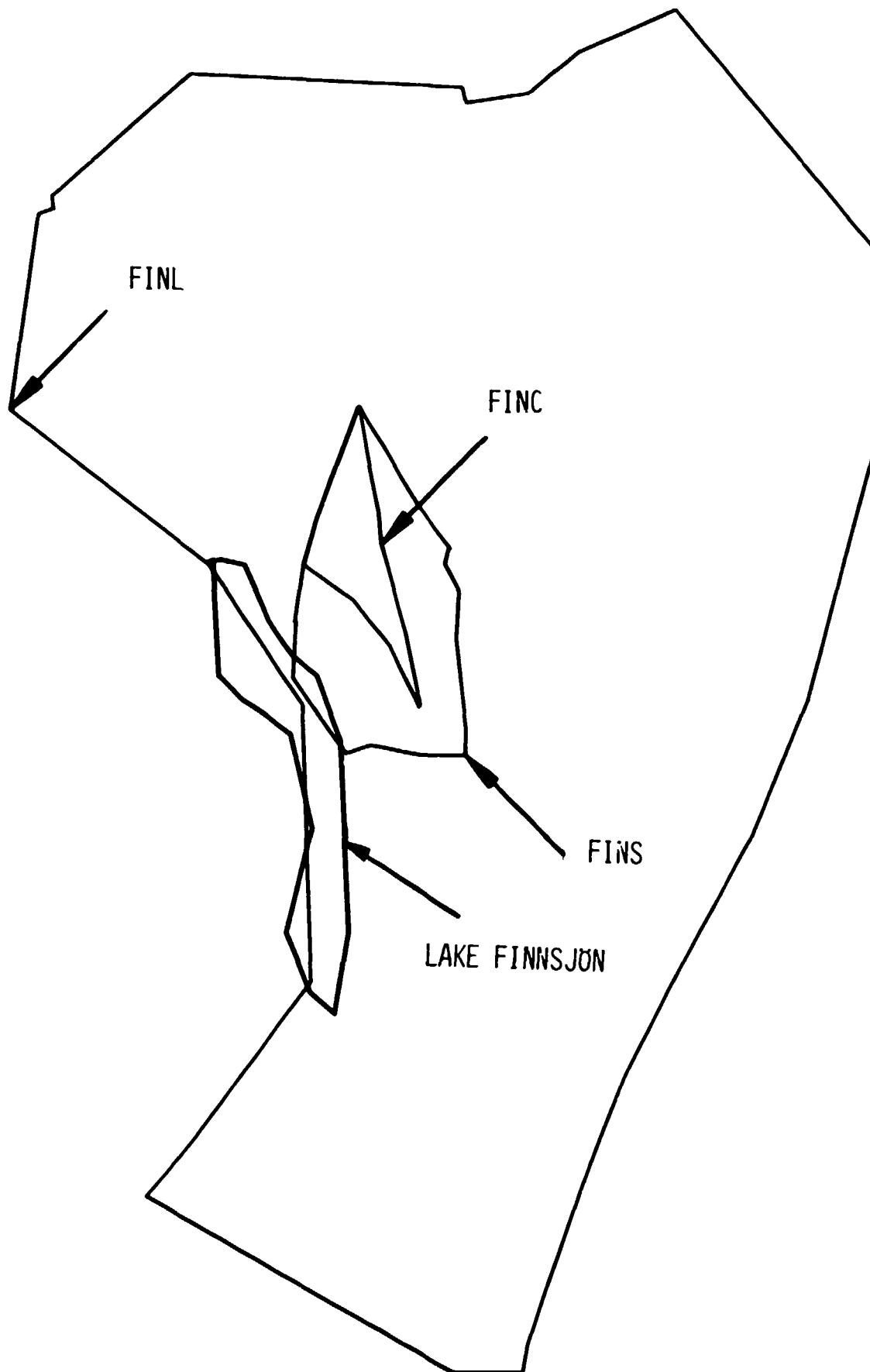
Fig 8-1.   Location and size of the different meshes at Finn-sjön. Results are given only for the FINC-mesh.
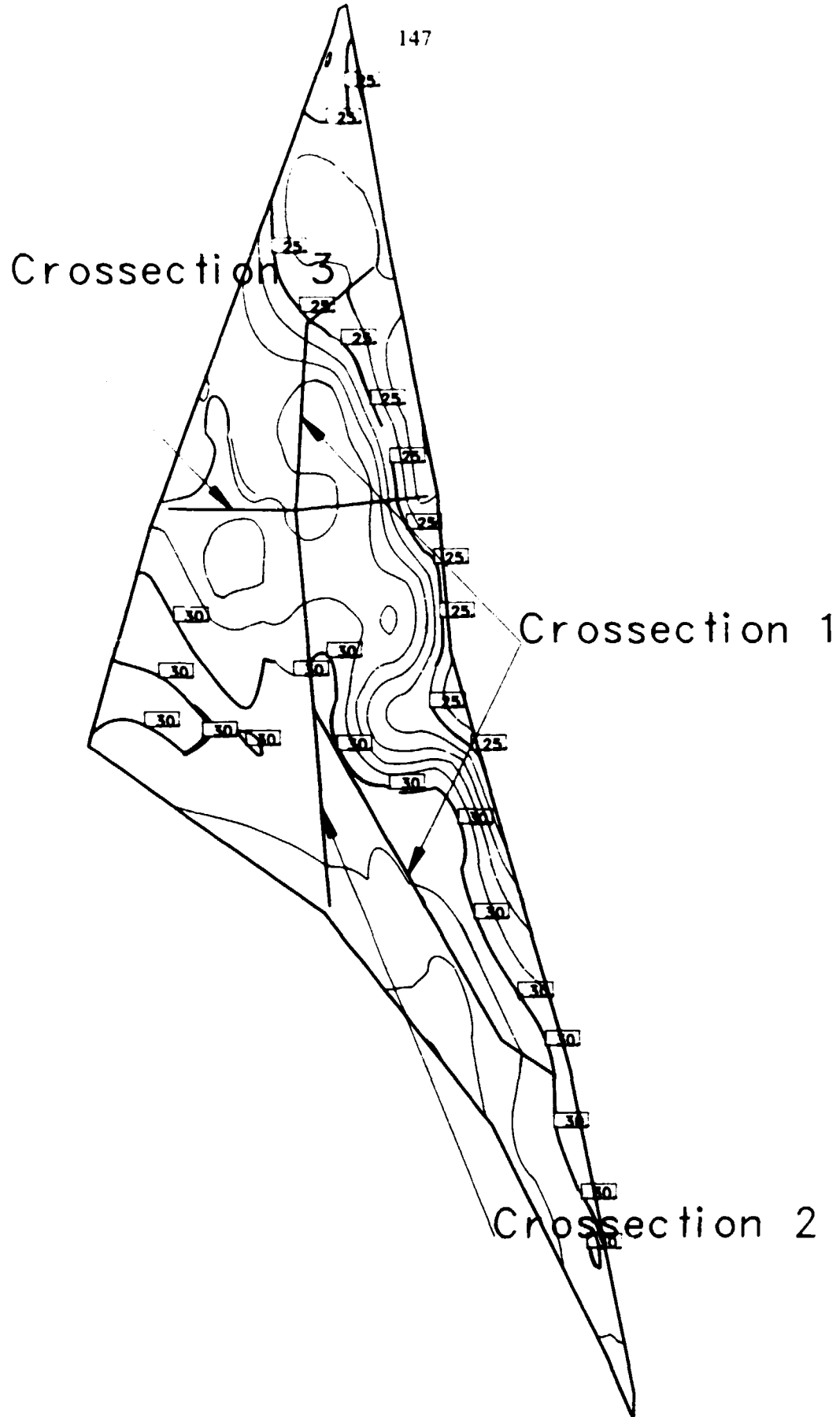
Fig 8-2.   Groundwater table of the FINC-mesh. The location of
            vertical cross sections used for presentation of re-
            sults are shown.
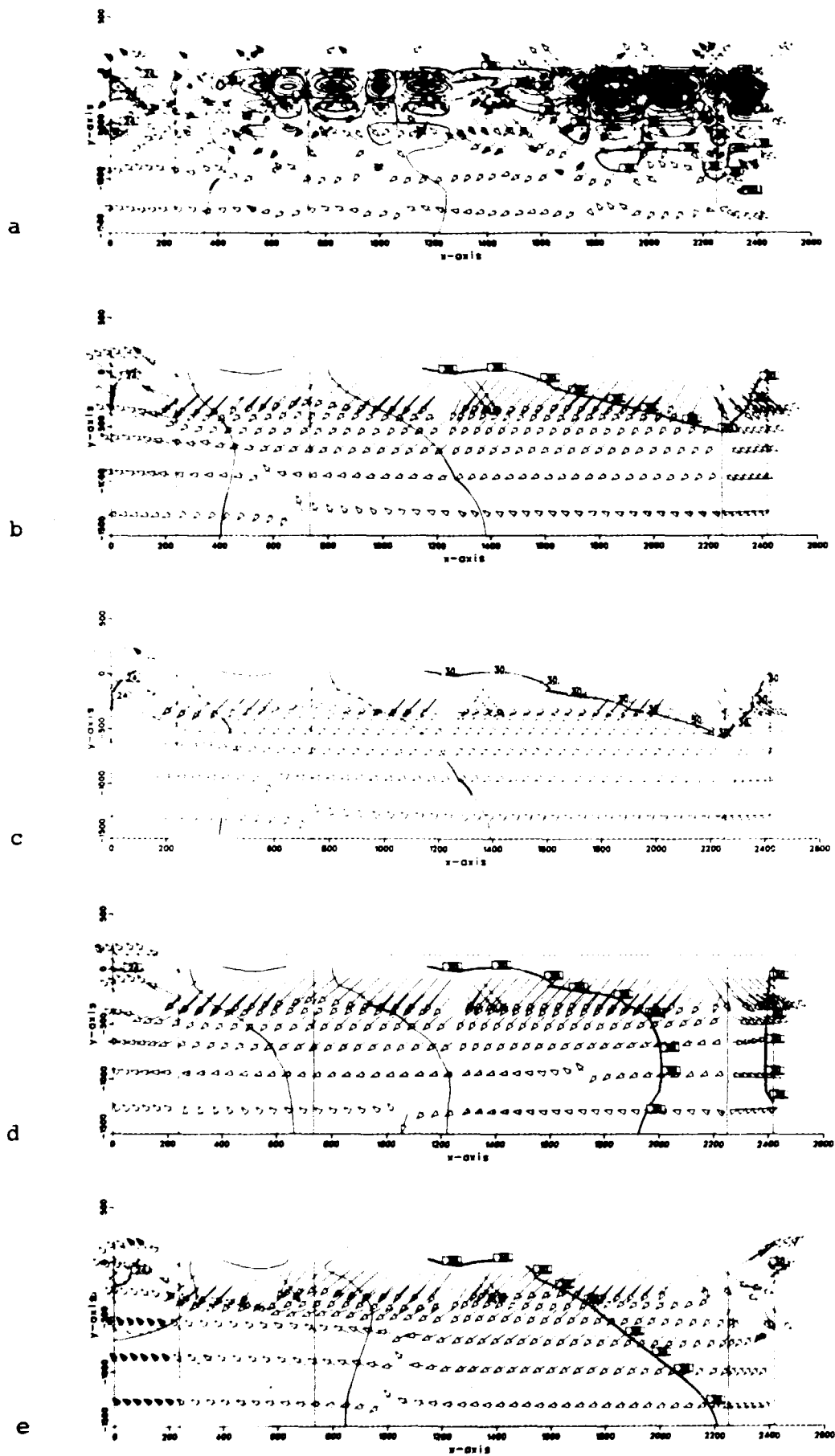
Fig 8-3. Isopotentials and projected flow vectors at cross
section no 1.
a = FINC   b = FINCL   c = FINCK
d = FINCHT   e = FINCL2
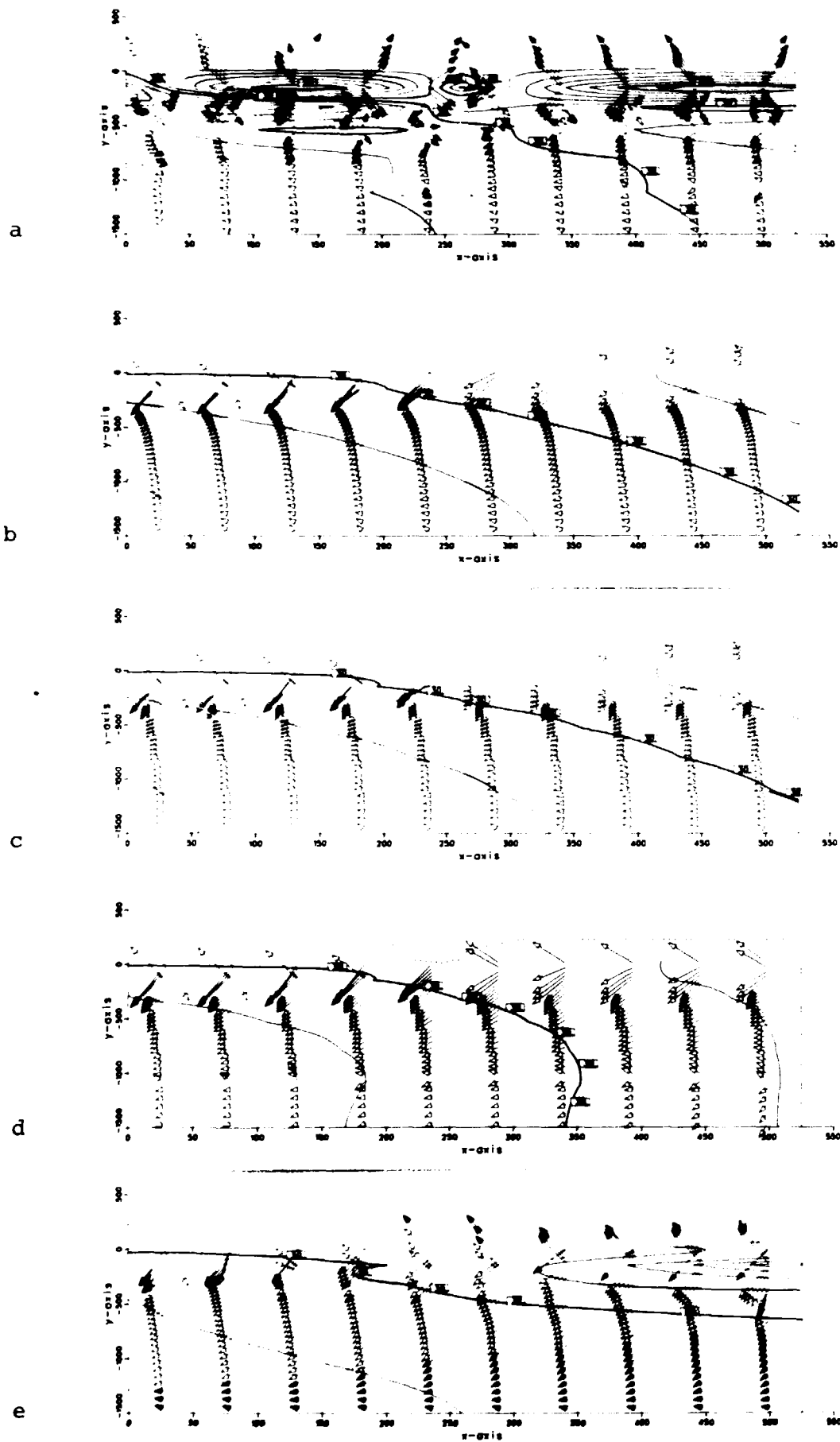
Fig 8-4. Isopotentials and projected flow vectors at cross section no 2.

a = FINC   b = FINCL   c = FINCK
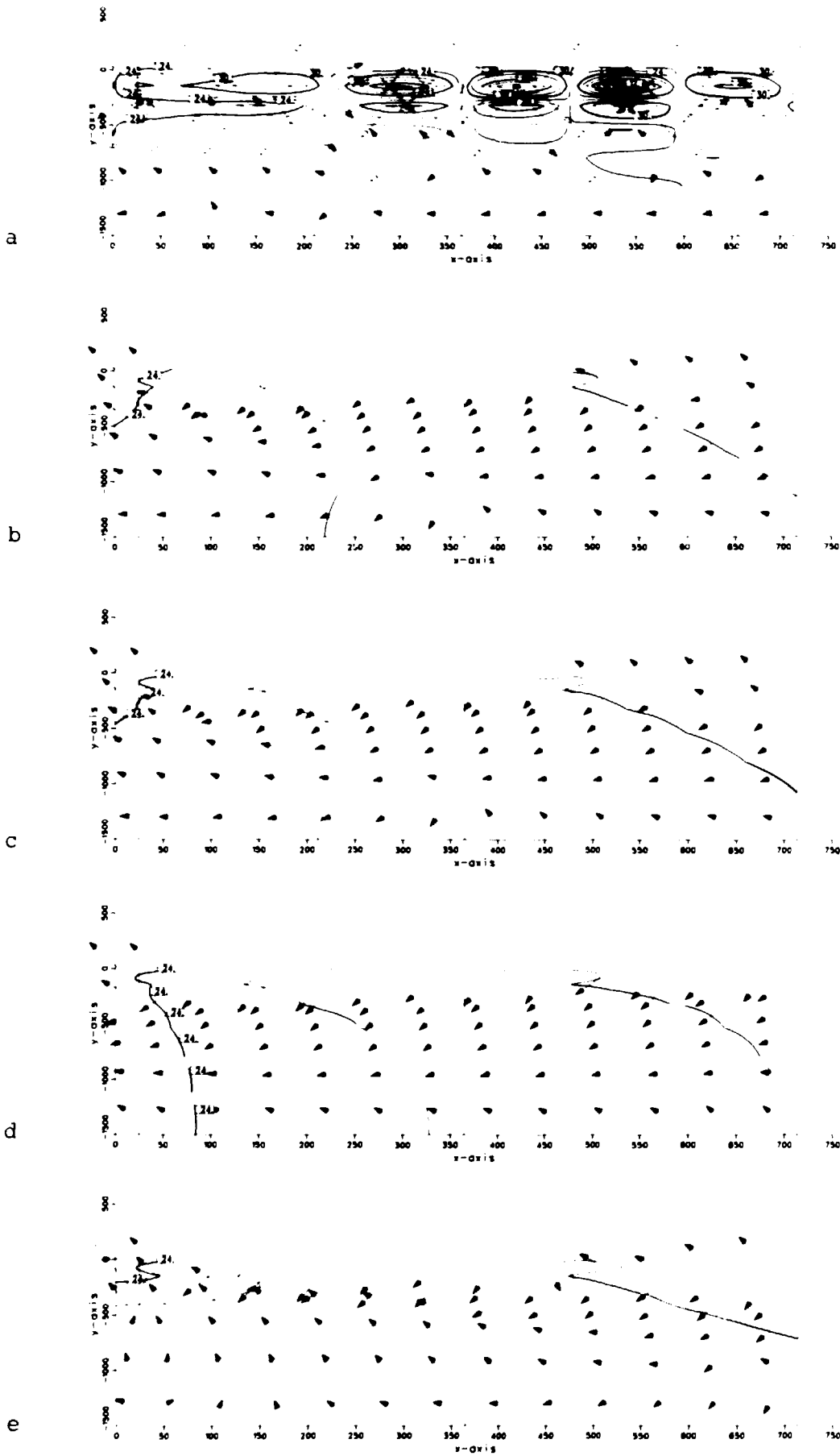
d = FINCHT   e = FINCL2

Fig 8-5.   Isopotentials and projected flow vectors at cross
            section no 3.
            a = FINC   b = FINCL   c = FINCK
            d = FINCHT   e = FINCL2
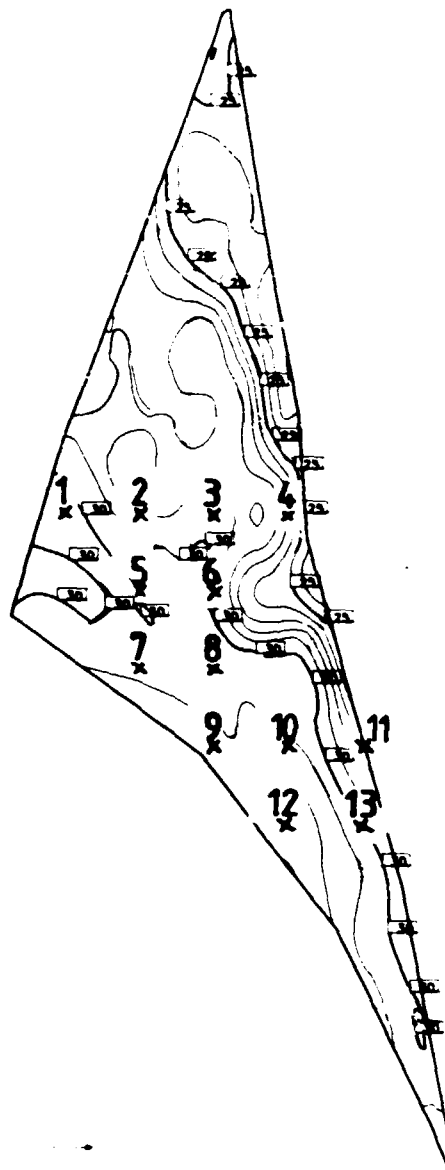
| Point	FLUXES 1/m²·yr				POTENTIALS m			
No	FINCL	FINCK	FINCHT	FINCL2	FINCL	FINCK	FINCHT	FINCL2
1	0.21	0.38	0.57	0.25	29.3	29.3	29.8	29.1
2	0.32	0.59	0.66	0.26	28.6	28.6	28.7	28.7
3	0.49	0.91	0.90	0.30	27.3	27.3	27.4	28.0
4	0.65	1.19	1.00	0.36	25.1	25.2	25.5	27.4
5	0.30	0.55	0.60	0.29	29.4	29.4	29.6	29.5
6	0.49	0.90	0.95	0.32	28.2	28.2	28.3	28.9
7	0.30	0.55	0.79	0.31	30.2	30.3	30.7	30.2
8	0.46	0.85	0.98	0.52	29.4	29.4	29.5	29.8
9	0.49	0.90	0.91	0.27	30.8	30.8	31.0	30.4
10	0.58	1.05	1.27	0.27	29.4	29.4	29.4	30.1
11	50.0	77.4	1.76	1.80	27.7	27.7	27.2	30.0
12	0.51	0.91	1.47	0.23	30.8	30.8	31.6	30.8
13	0.57	1.03	1.20	0.17	29.1	29.1	29.6	30.6

Fig 8-6.   Groundwater fluxes and potentials at -500 m. The locations of the grid points are indicated on the groundwater table map.
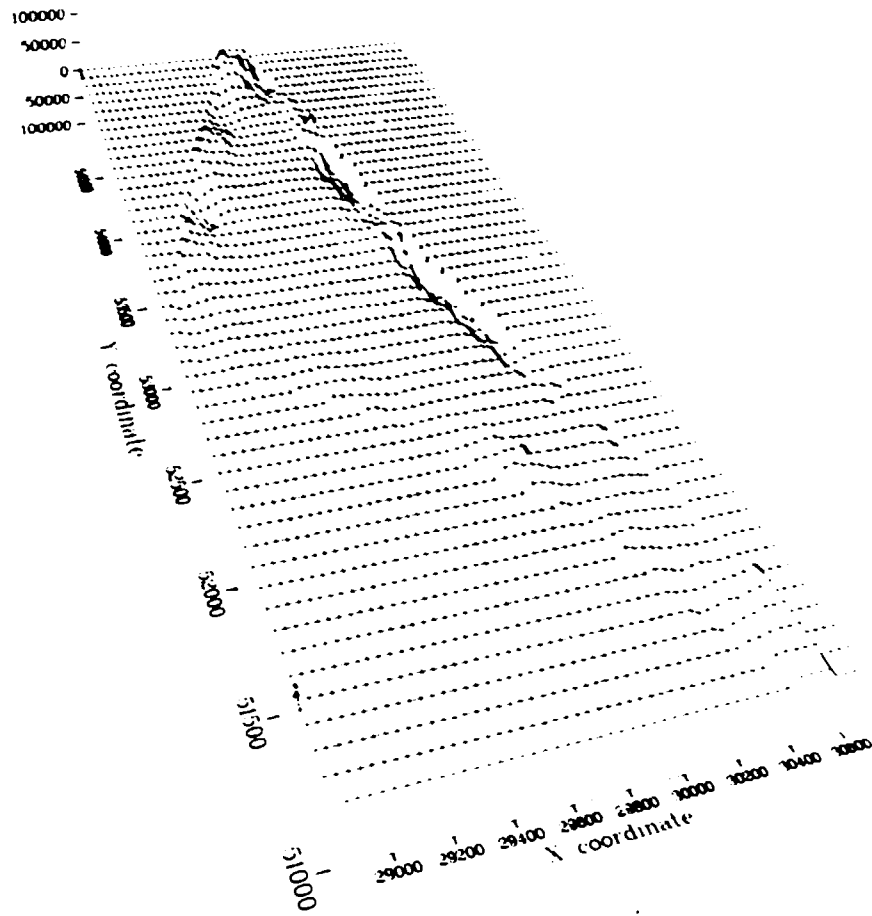
Fig 8-7.   Recharge rate in mm/yr, FINCL-run.
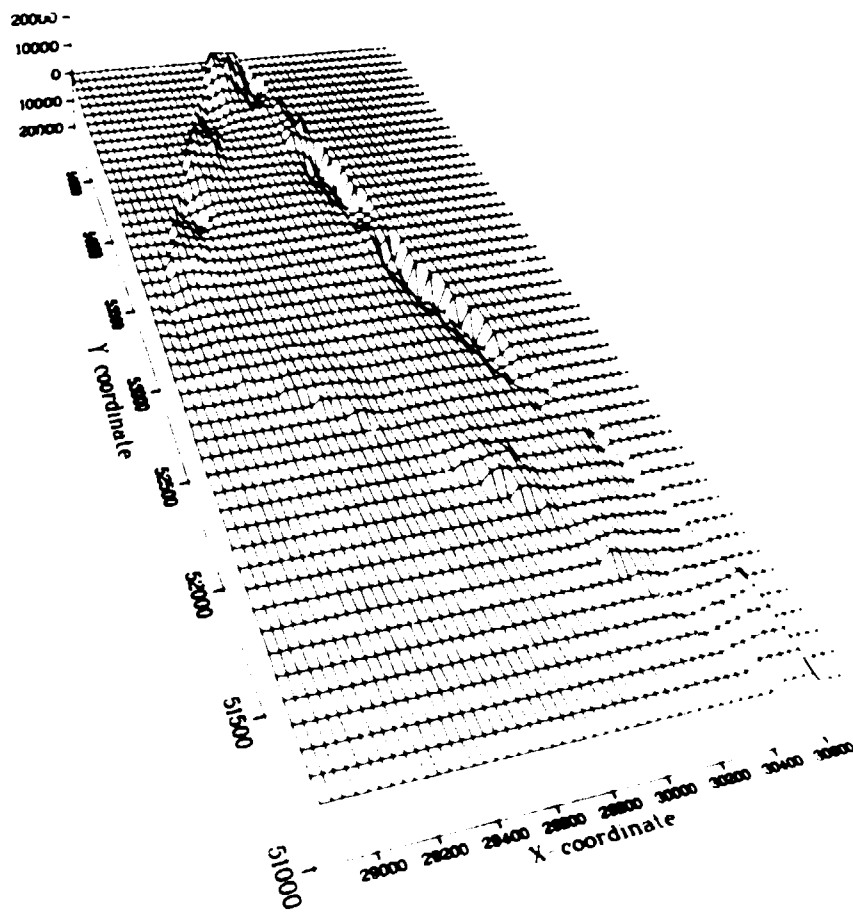
Fig 8-8.   Recharge rate in mm/yr, FINCK-run.
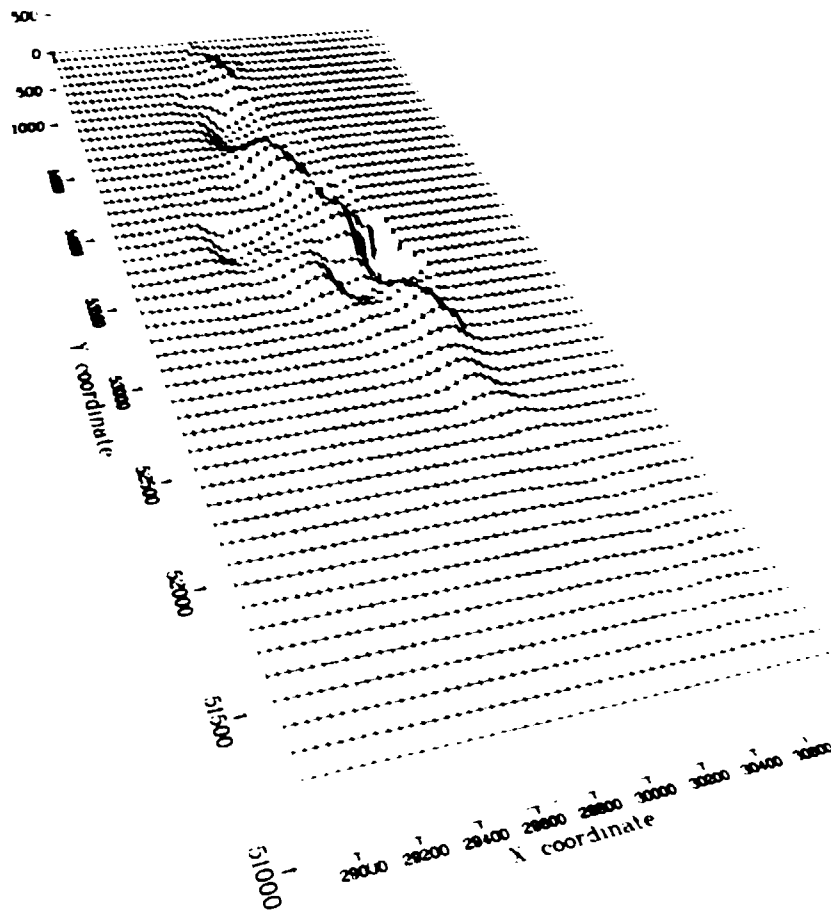
Fig 8-9.   Recharge rate in mm/yr, FINCHT-run.
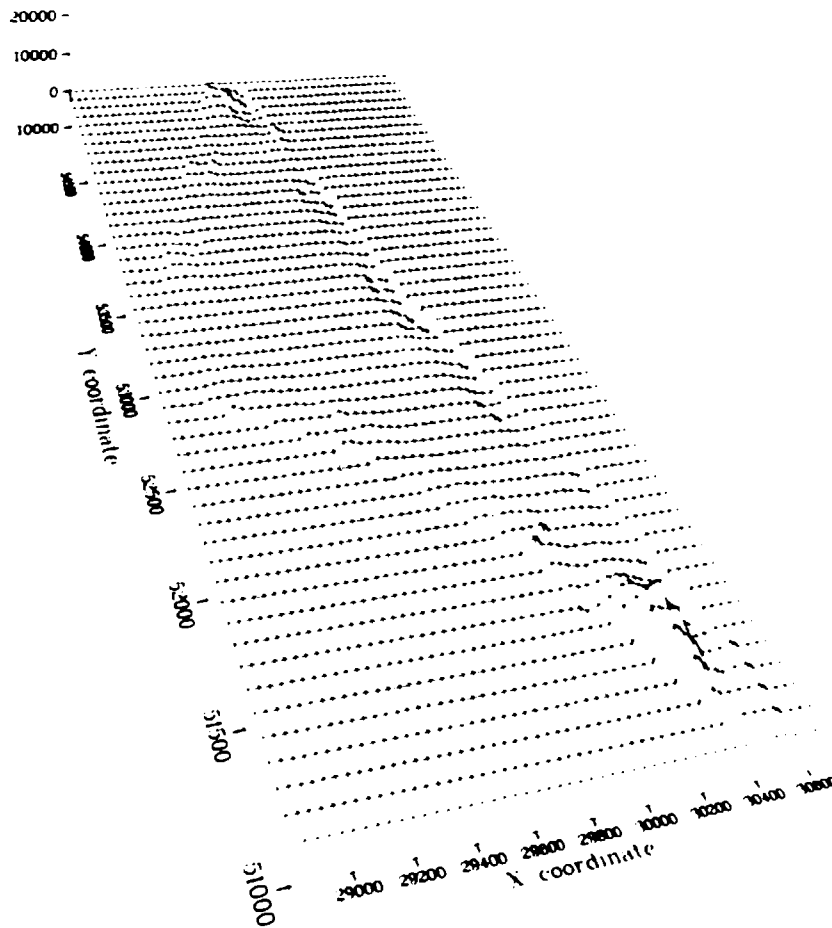
Fig 8-10.   Recharge rate in mm/yr, FINCL2-run.
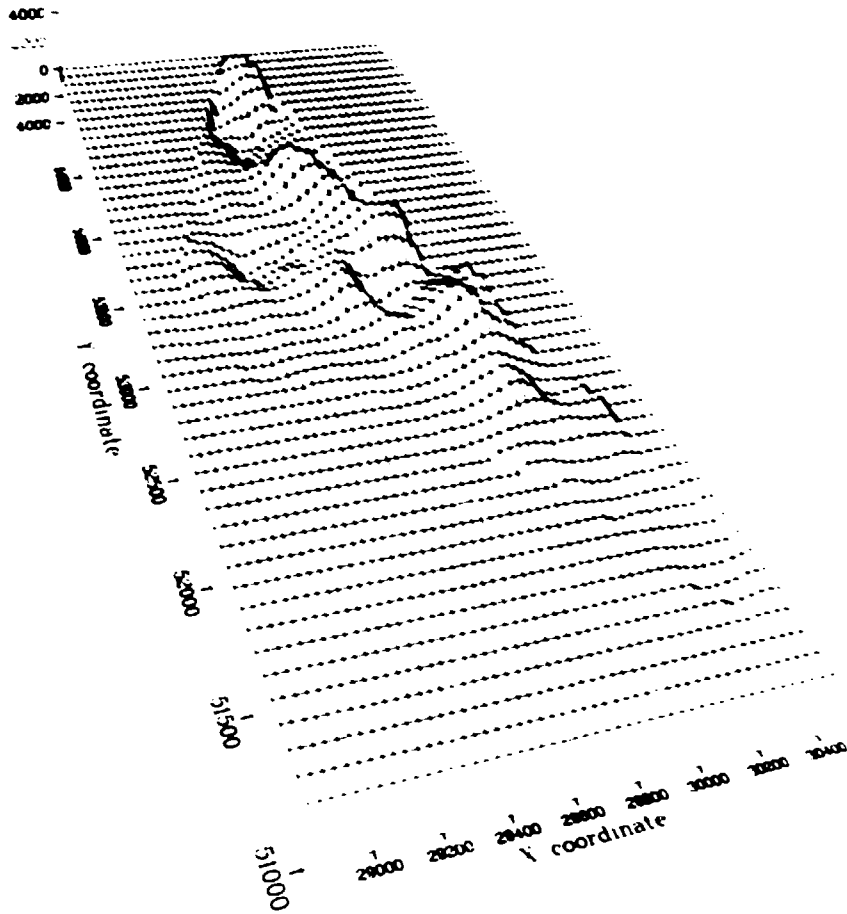
Fig 8-11.   Recharge   rate   in   mm/yr,   fracture   zones   excluded,
            FINCL-run.
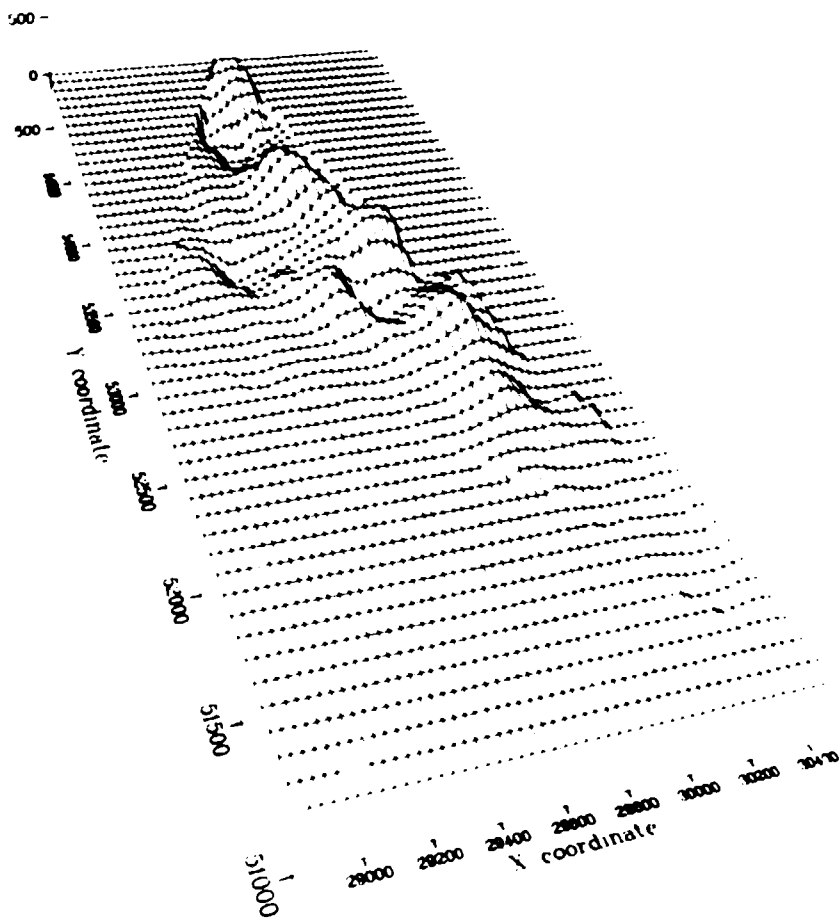
Fig 8-12.   Recharge   rate   in   mm/yr,   fracture   zones   excluded,
            FINCL-run.
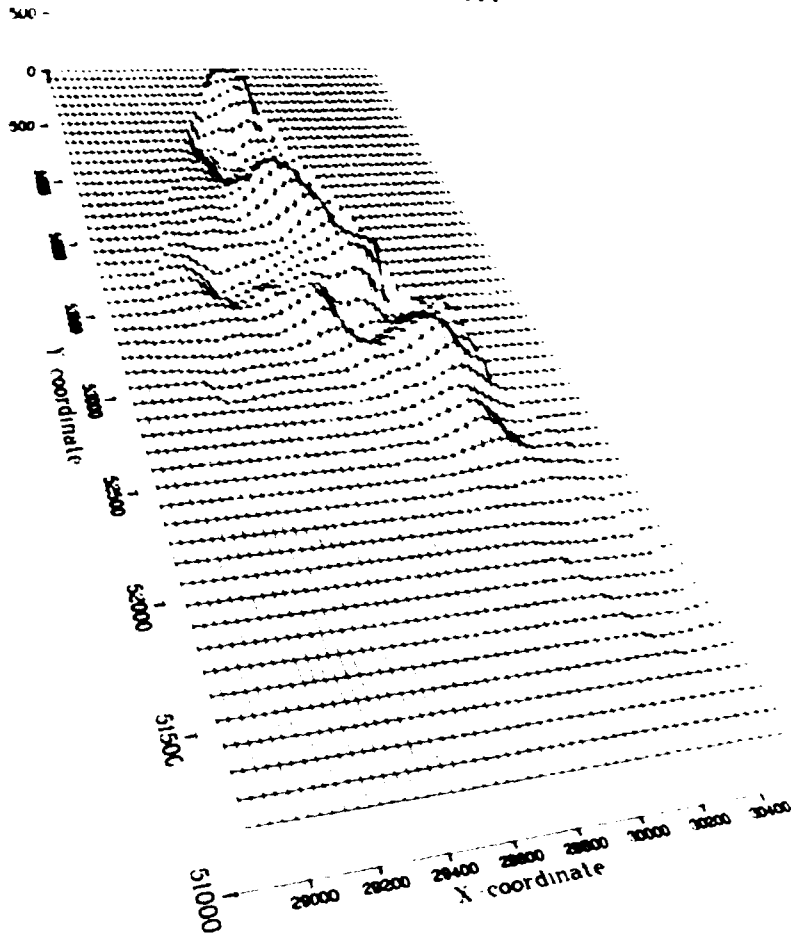
Fig 8-13.   Recharge rate in mm/yr, fracture zones excluded, FINCHT-run.
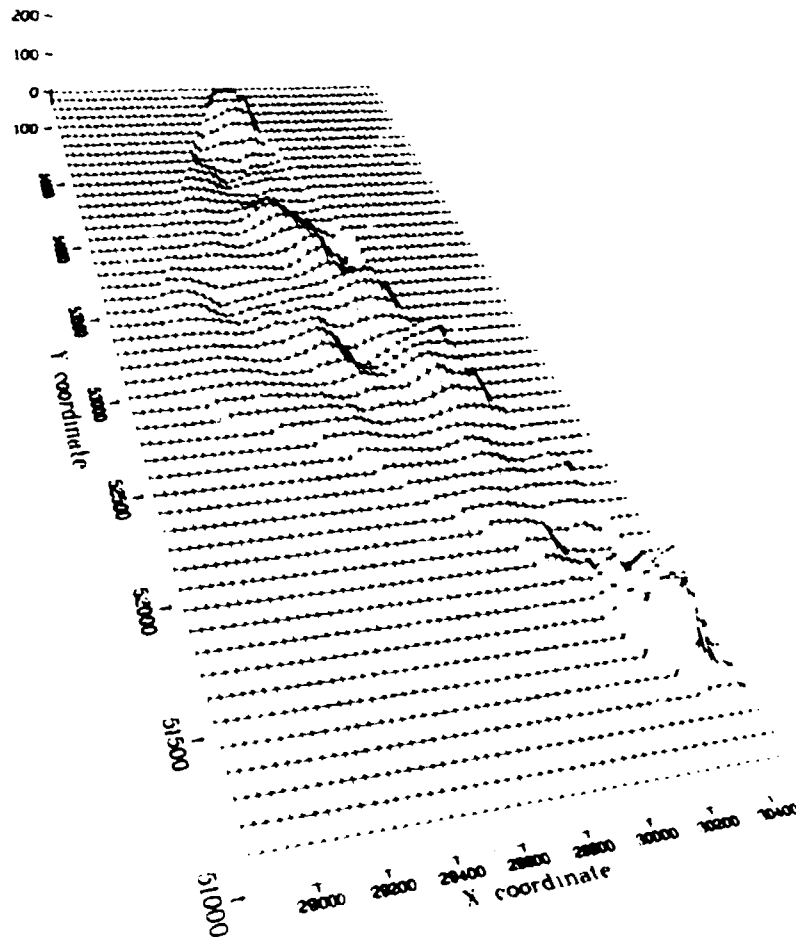
Fig 8-14.   Recharge rate in mm/yr, fracture zones excluded, FINCL2-run.
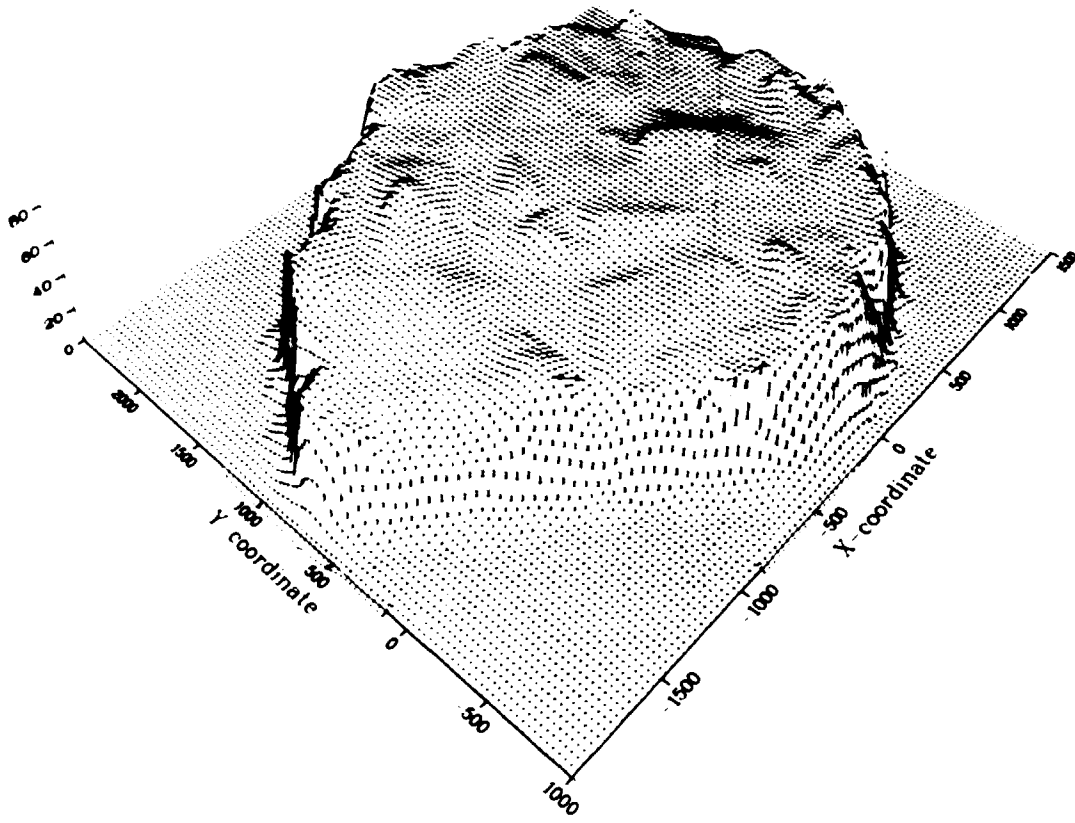
Fig 9-1.   Relief map of the groundwater table at Fjällveden.
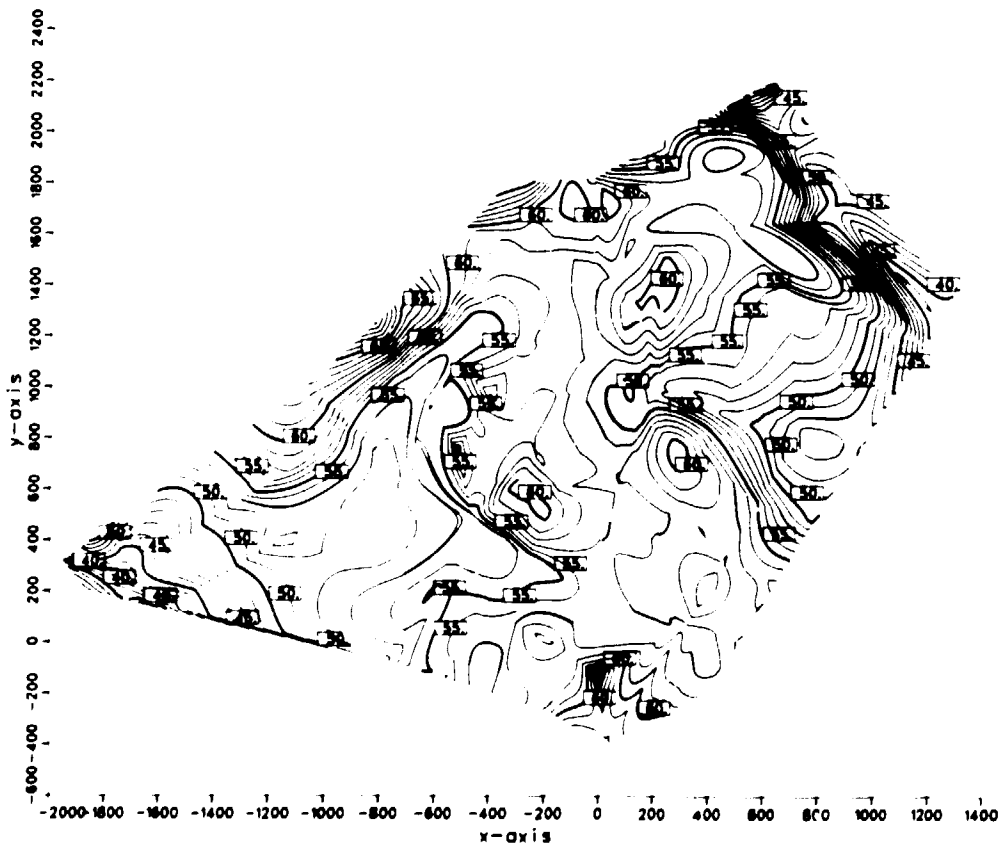
Fig 9-2.   Contour map of the groundwater table at Fjällveden.
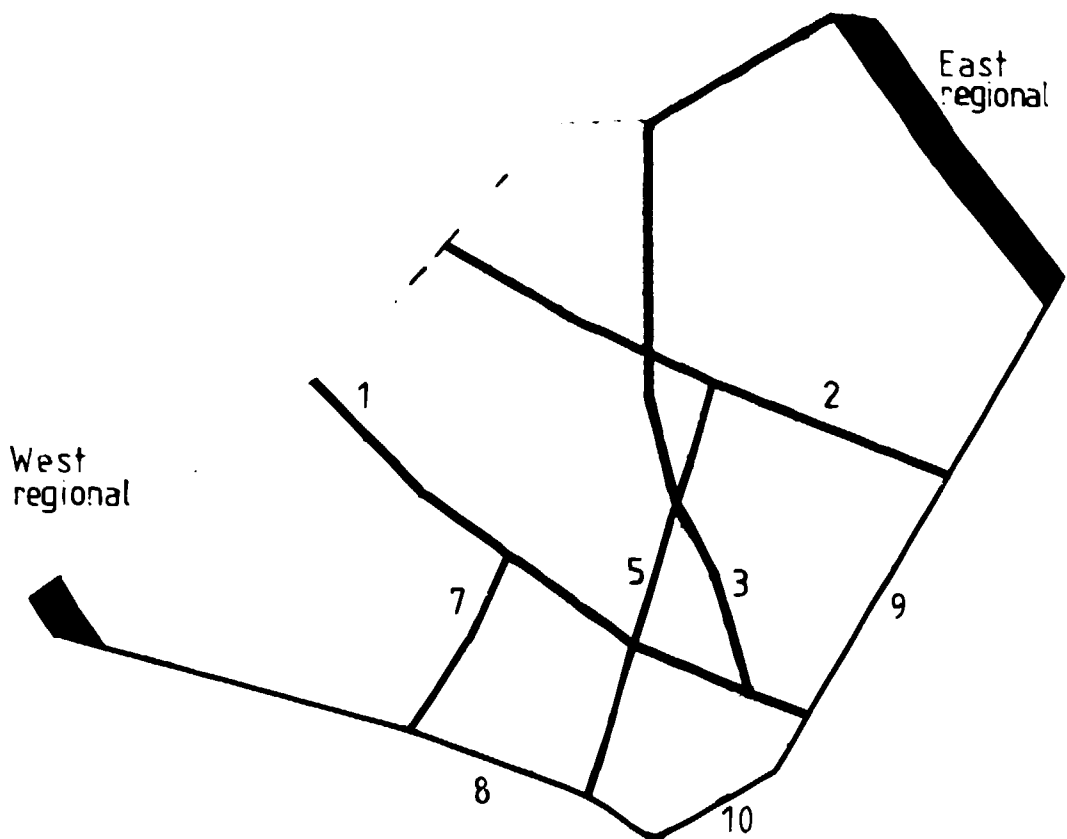
Fig 9-3. Fracture zones as modelled at Fjällveden.
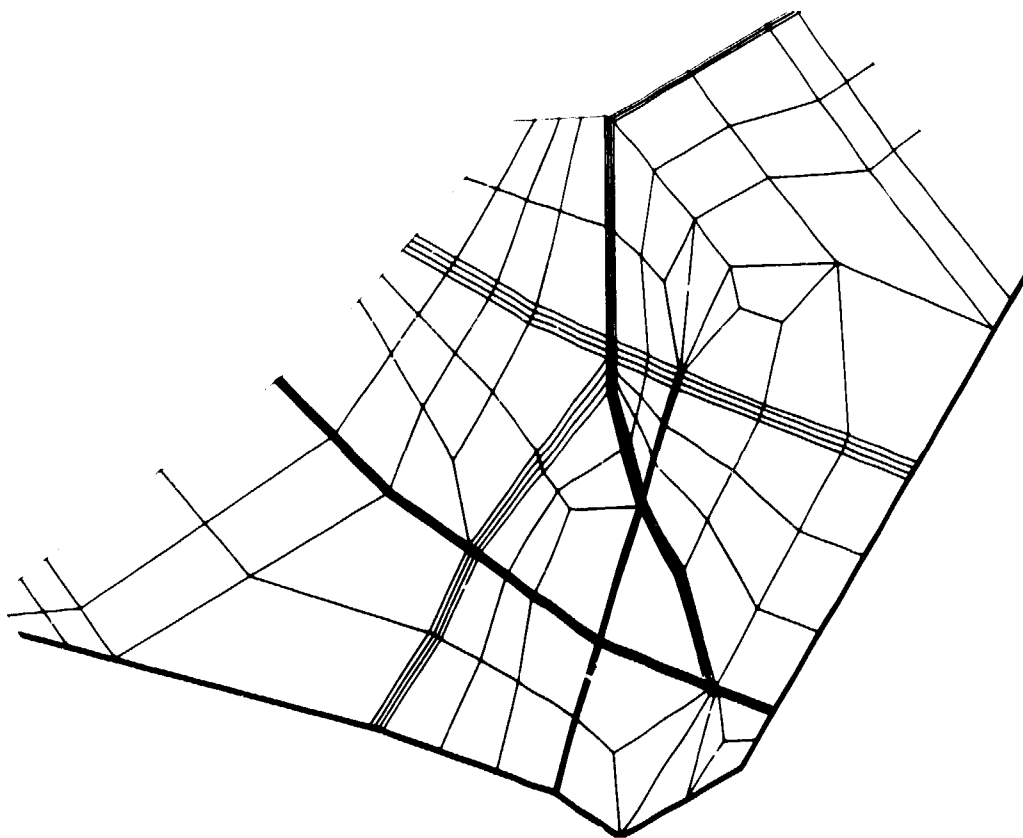
Fig 9-4. Top surface of the element mesh.

158
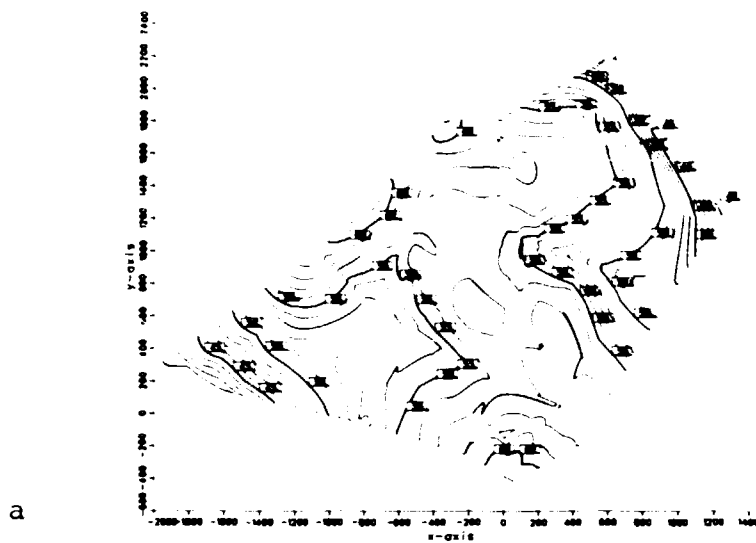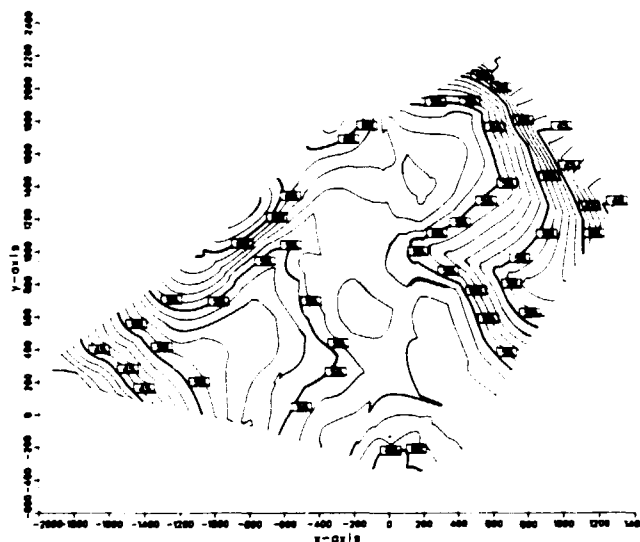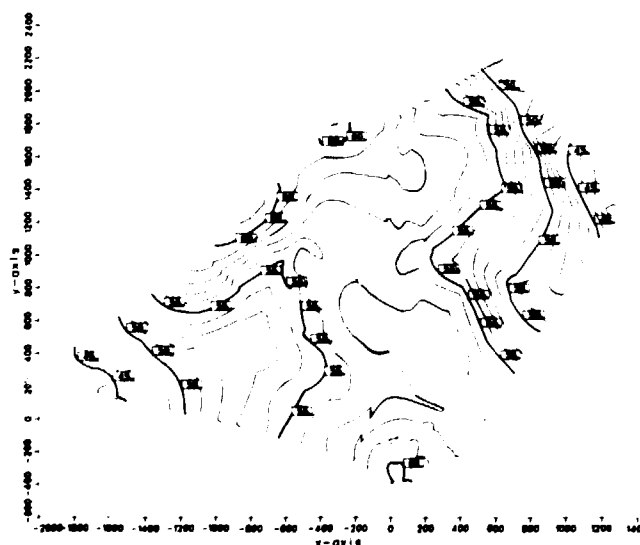
Fig 9-5.   Isopotential lines in a horisontal cross section at
            -100 m.
            a = FJEL   b = FJELA   c = FJELB
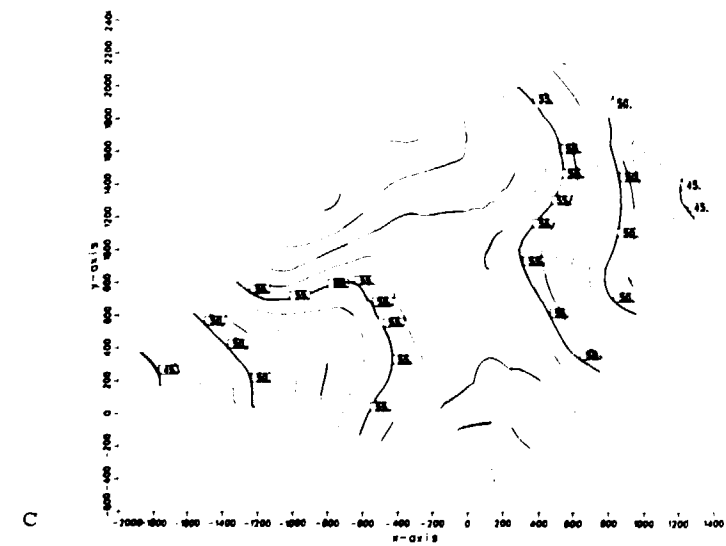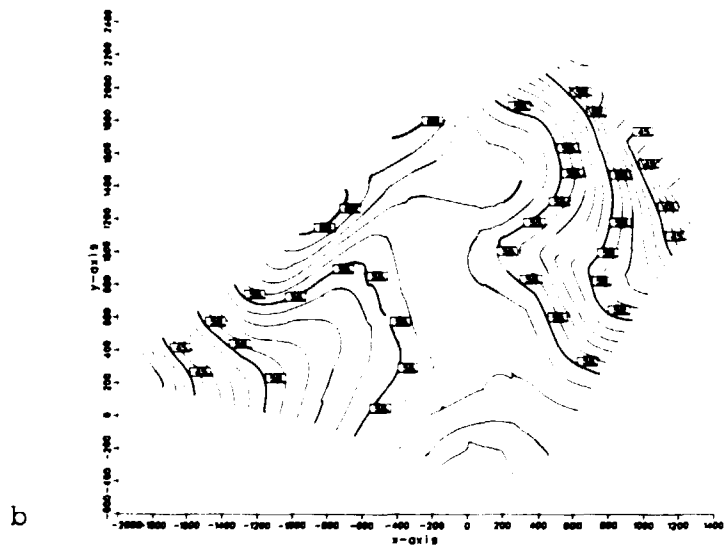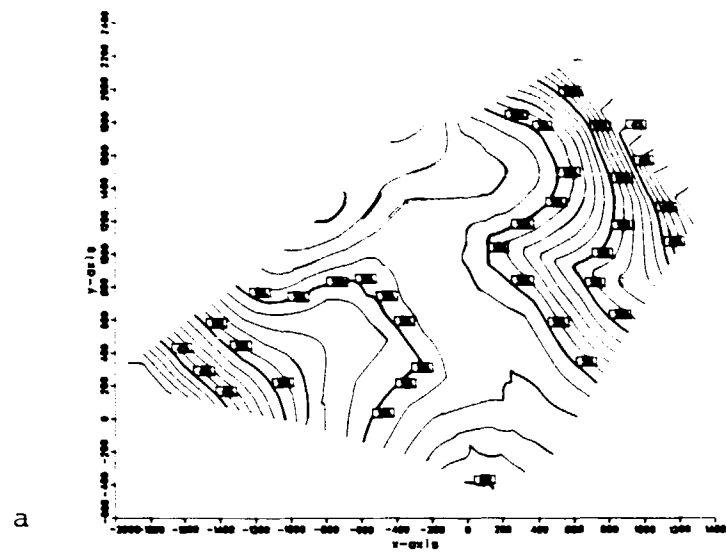
Fig 9-6.   Isopotential lines in a horisontal cross section at
            -260 m.

            a = FJEL   b = FJELA   c = FJELB
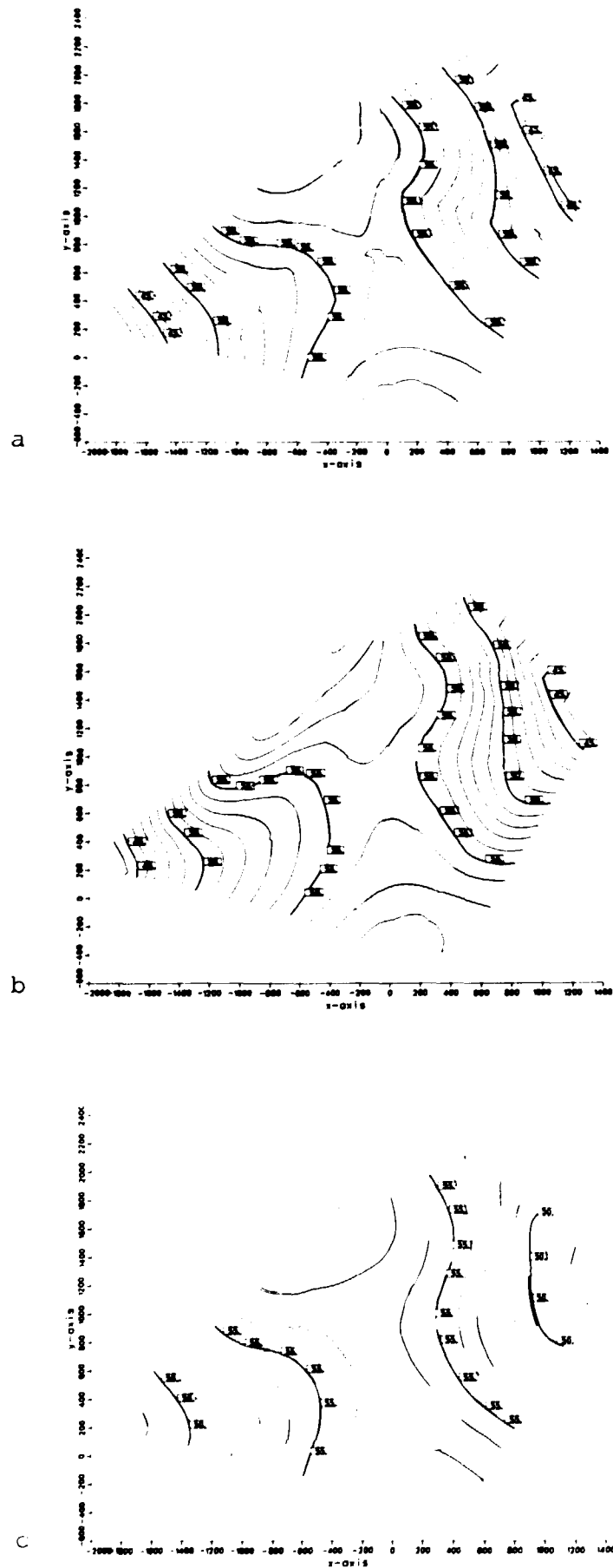
Fig 9-7.   Isopotential lines in a horisontal cross section at
            -500 m.
            a = FJEL   b = FJELA   c = FJELB
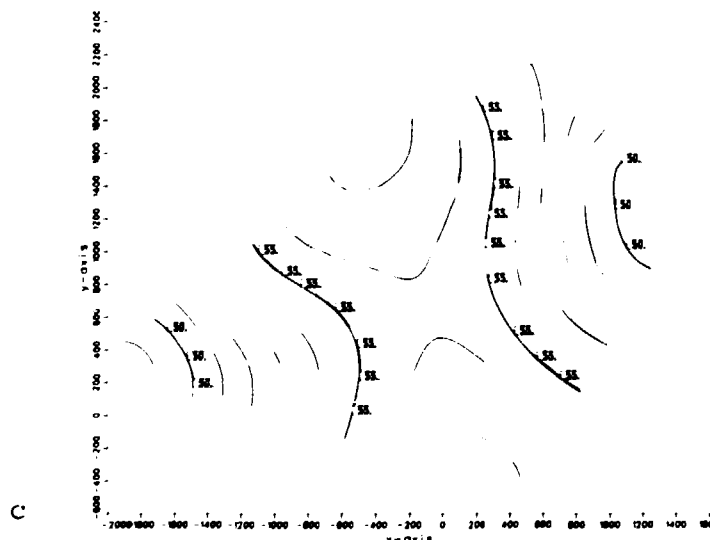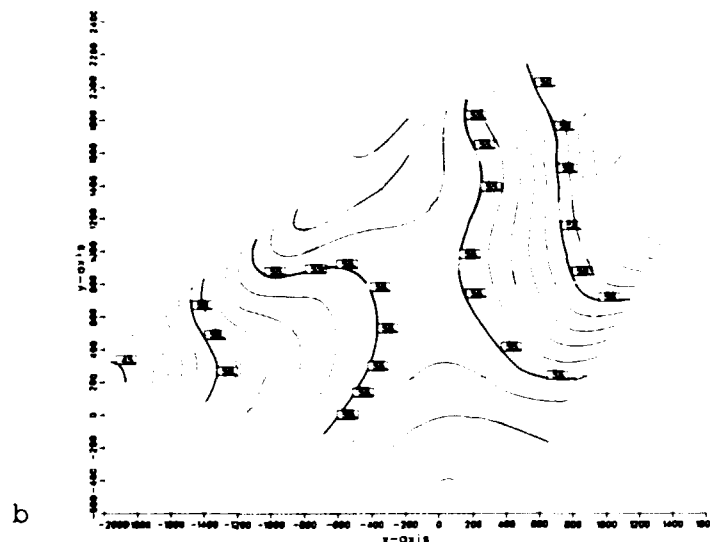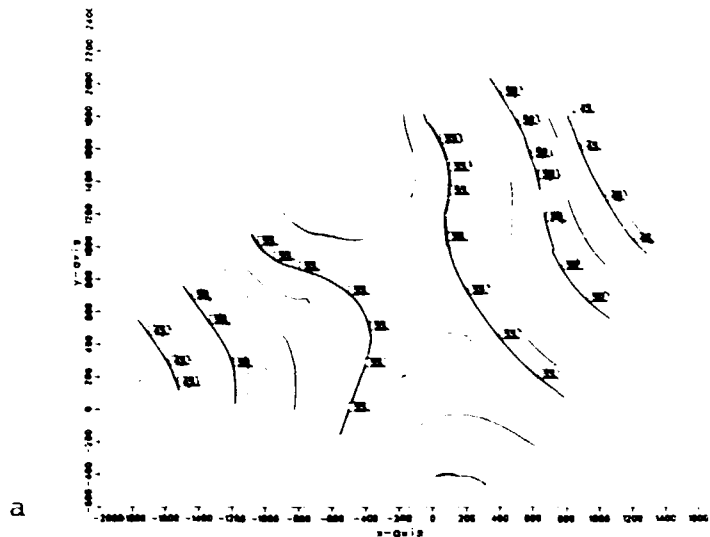
Fig 9-8. Isopotential lines in a horisontal cross section at
−830 m.

a = FJEL   b = FJELA   c = FJELB
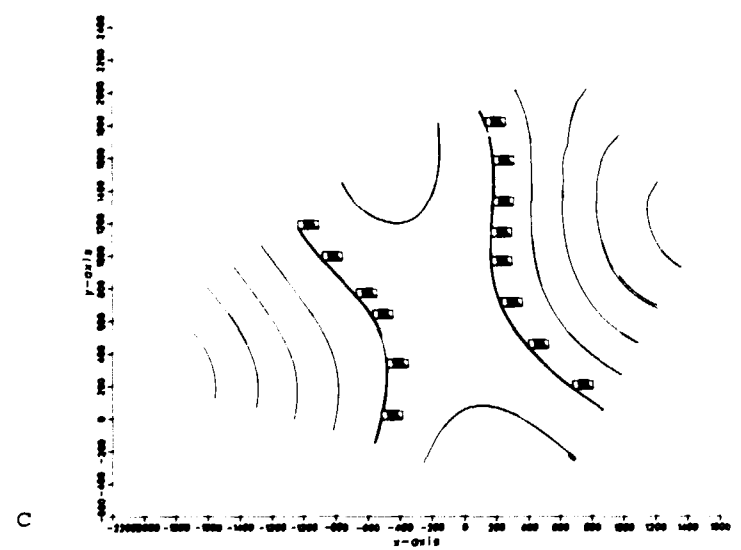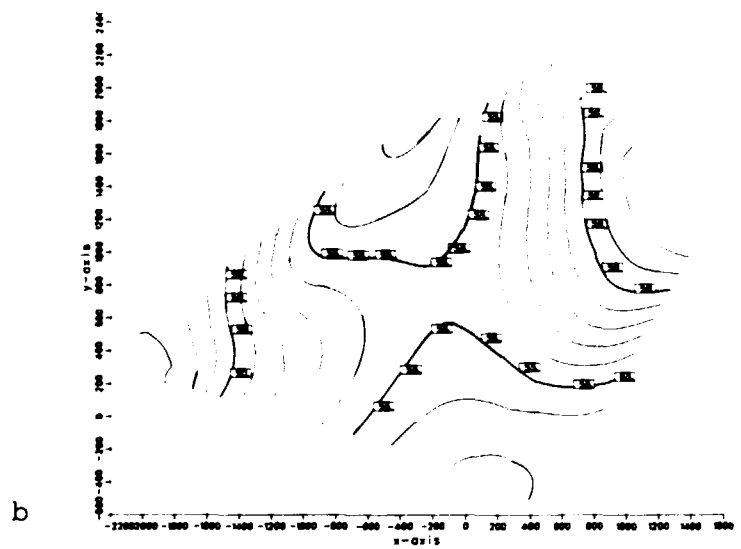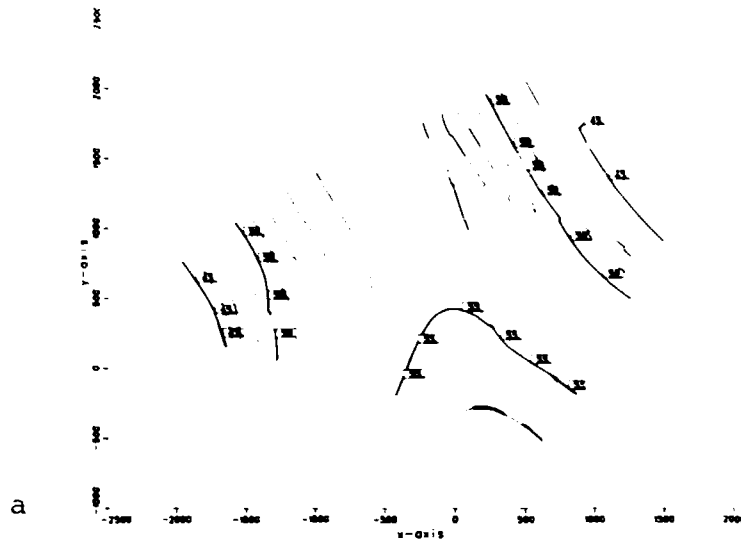
Fig 9-9.   Isopotential lines in a horisontal cross section at
            -1 170 m.
            a = FJEL   b = FJELA   c = FJELB

Fig 9-10.   Isopotential lines in a horisontal cross section at
            -1 500 m.
            a = FJEL   b = FJELA   c = FJELB
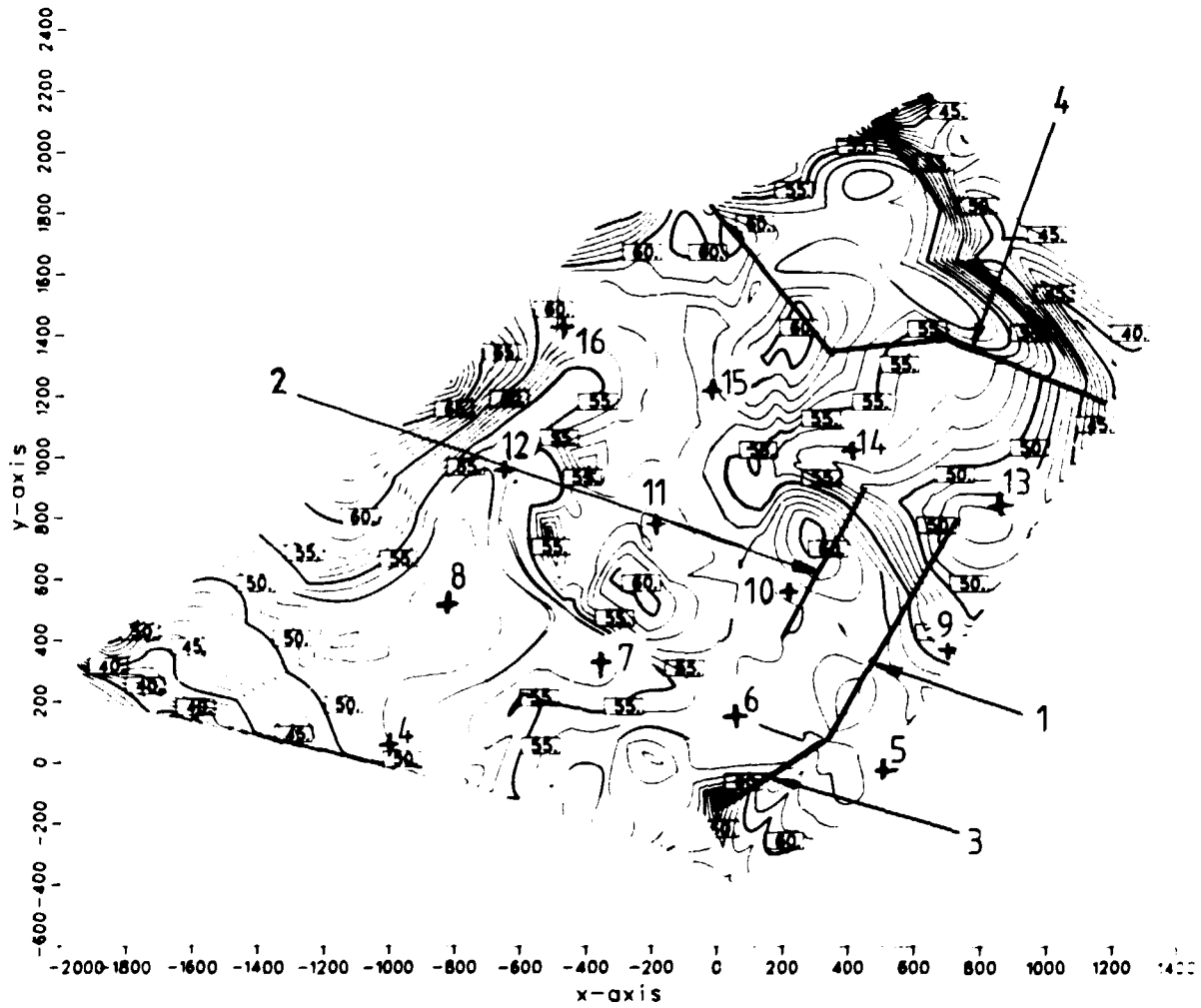
Fig 9-11. Locations of vertical cross sections at Fjällveden. The starting points of trajectories discussed in section 9.3.3 are also shown.
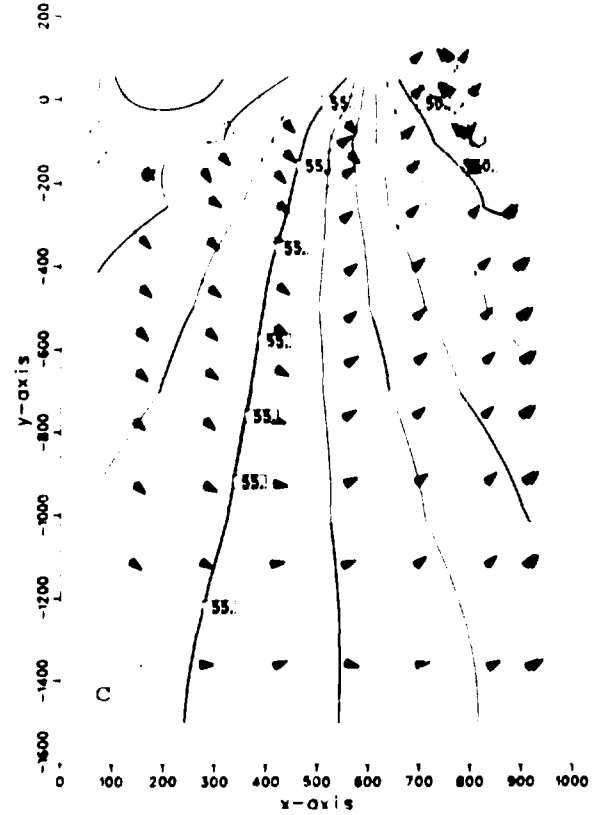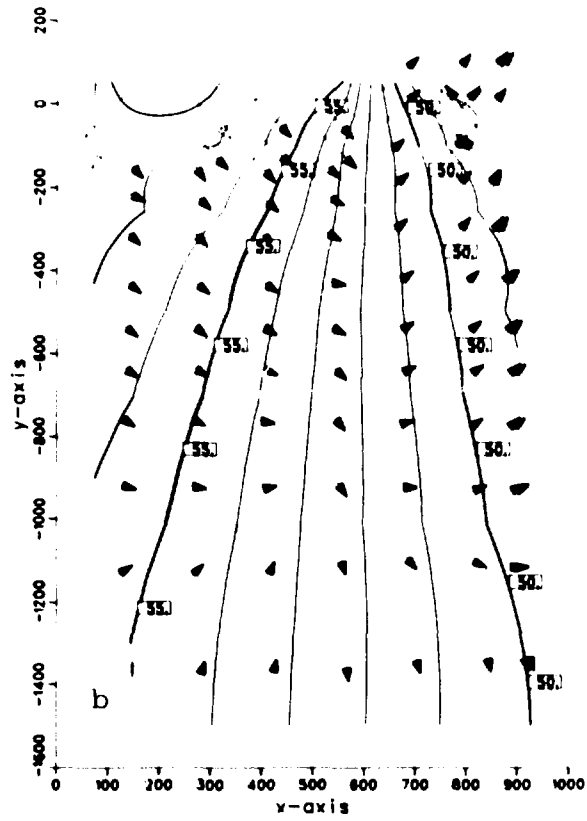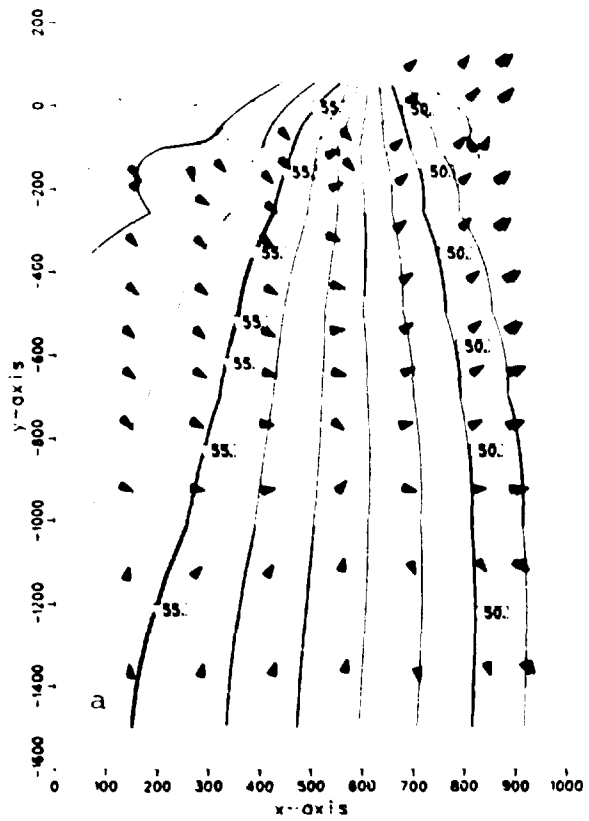
Fig 9-12. Isopotentials and projected flow vectors at vertical
           cross section no. 1.
           a = FJEL   b = FJELA   c = FJELB
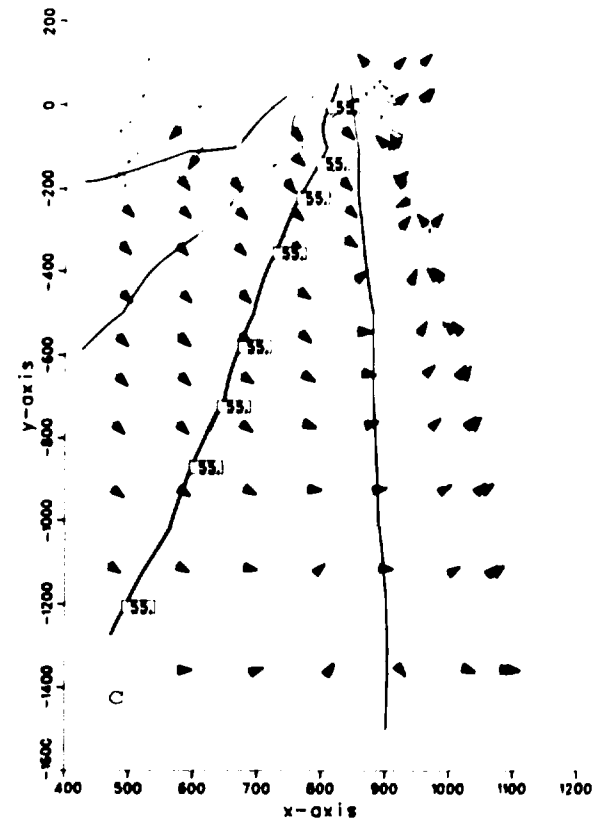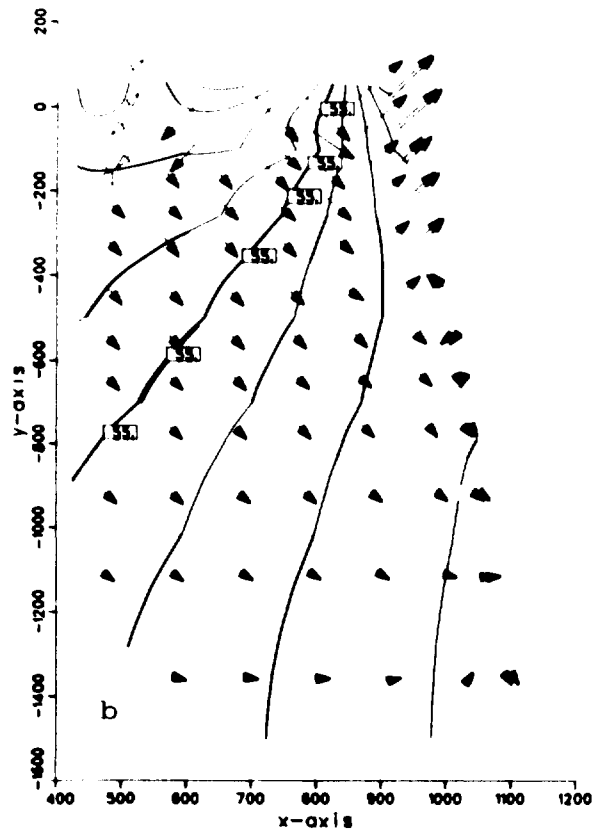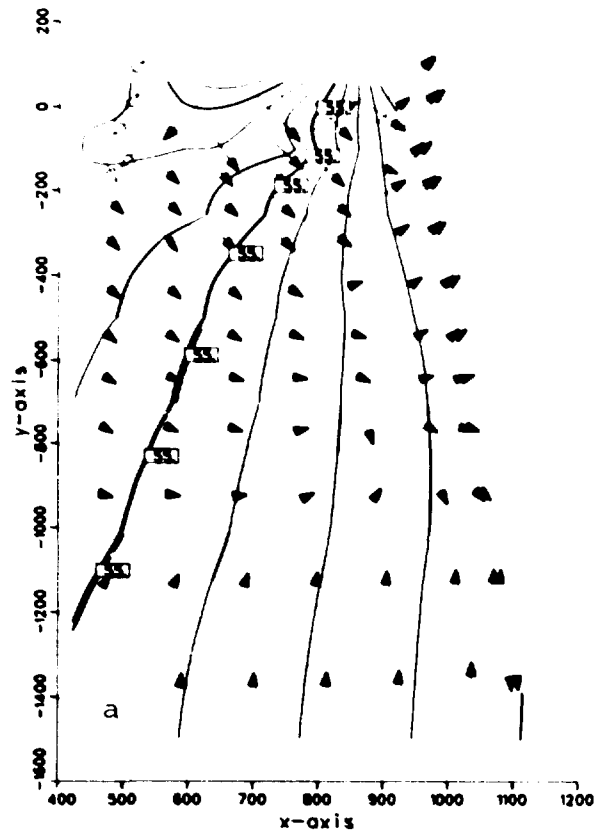
Fig 9-13.   Isopotentials and projected flow vectors at vertical
            cross section no. 2.
            a = FJEL   b = FJELA   c = FJELB
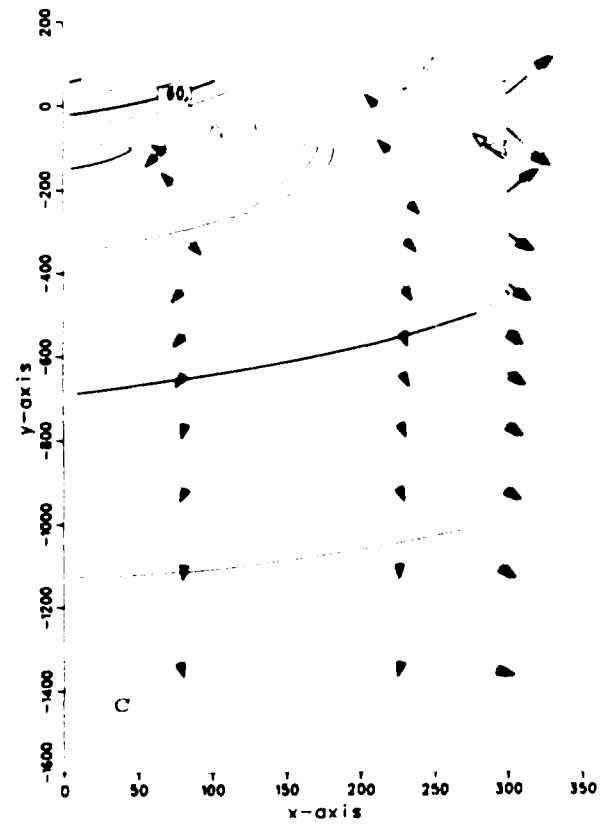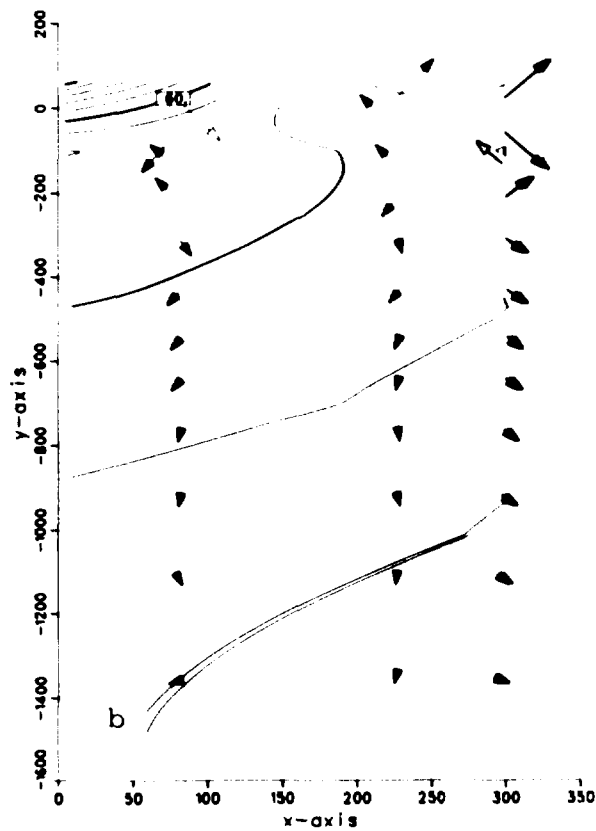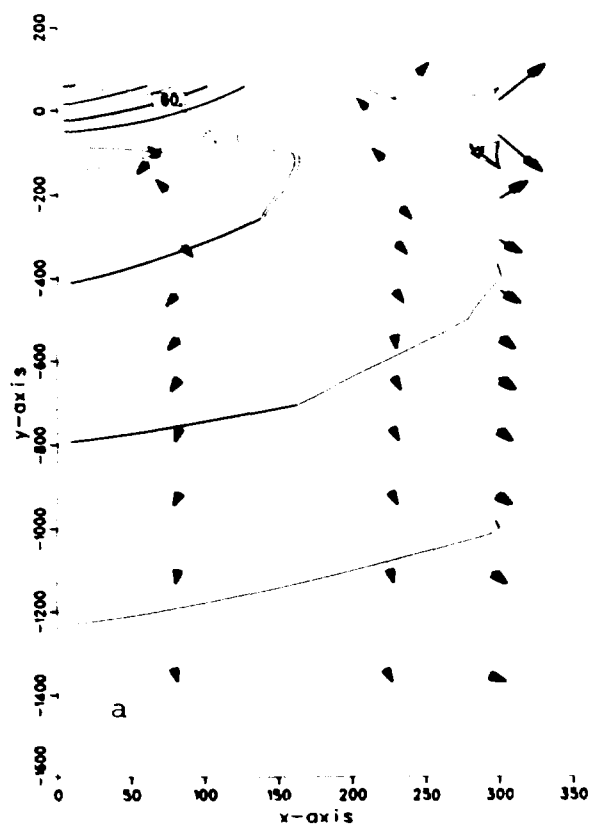
Fig 9-14.   Isopotentials and projected flow vectors at vertical
            cross section no. 3.
            a = FJEL   b = FJELA   c = FJELB
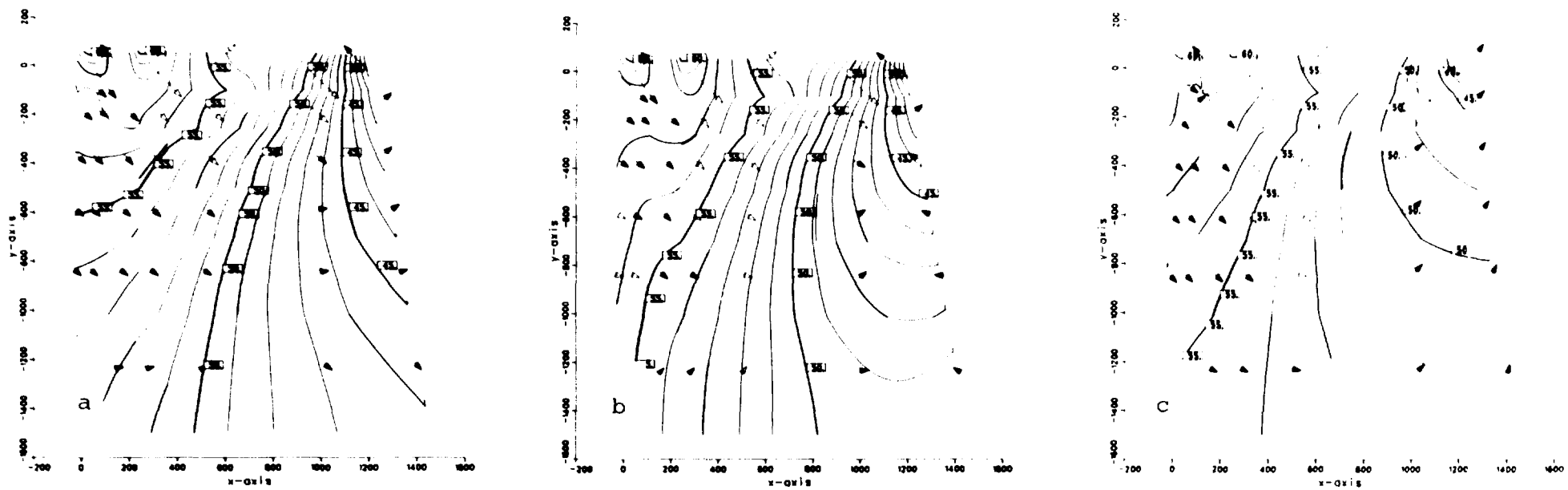
Fig 9-15.   Isopotentials and projected flow vectors at vertical
cross section no. 4.
a = FJEL   b = FJELA   c = FJELB
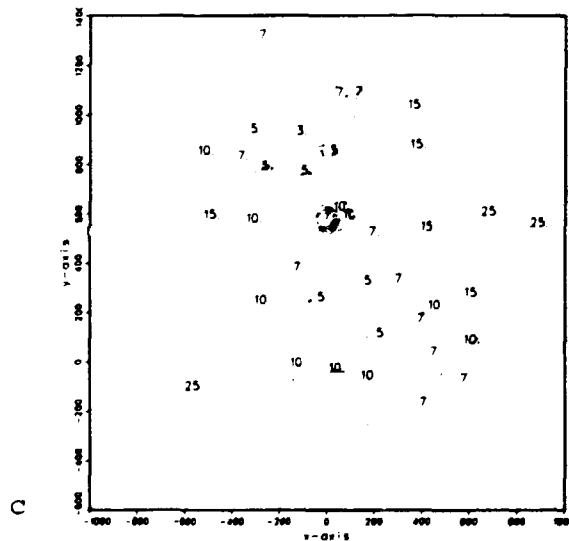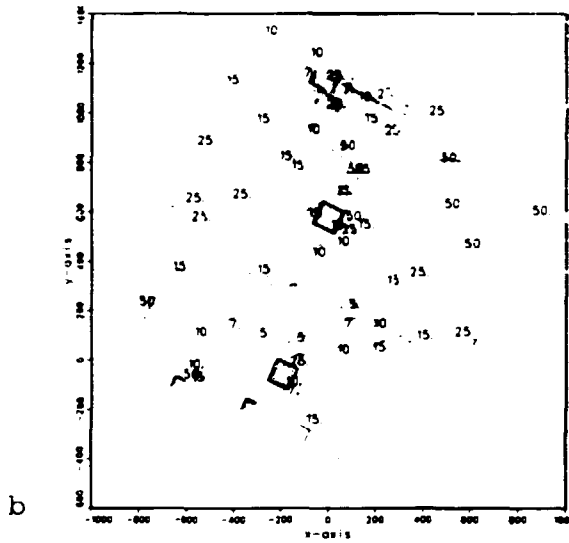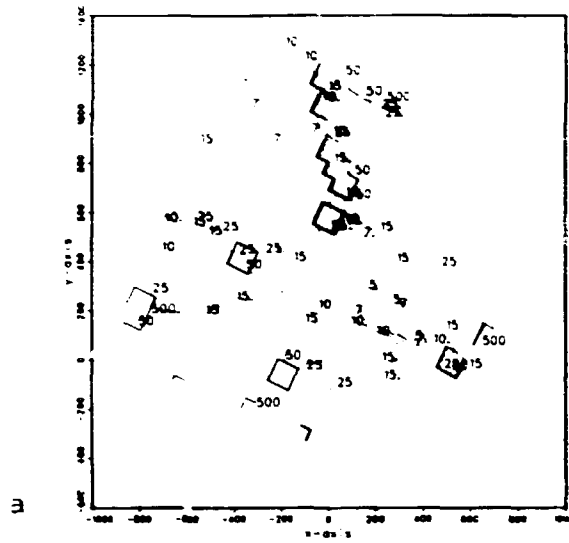
Fig 9-16. Fluxes at -400 m, (ml/m^2·yr).
a = FJEL   b = FJELA   c = FJELB
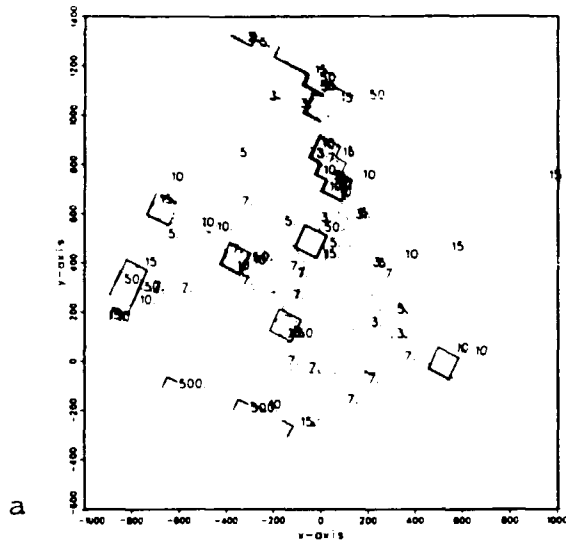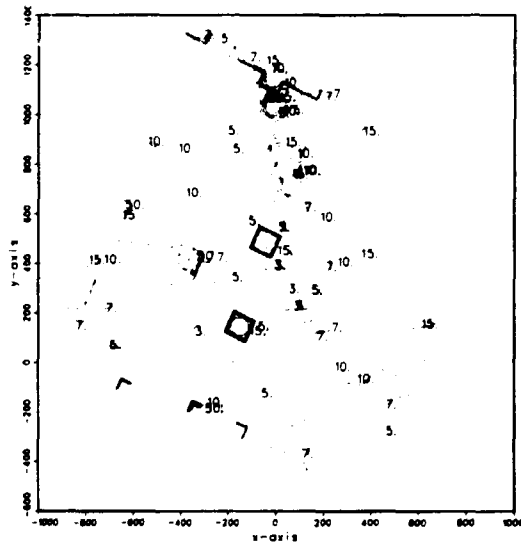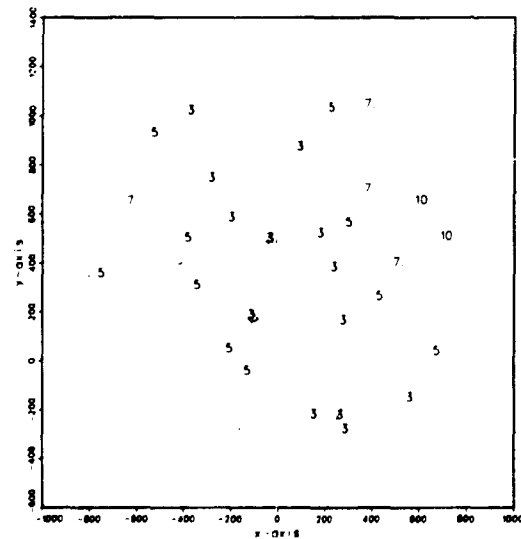
Fig 9-17.   Fluxes at -500 m, (ml/m$^2 \cdot$ yr).
a = FJEL   b = FJELA   c = FJELB
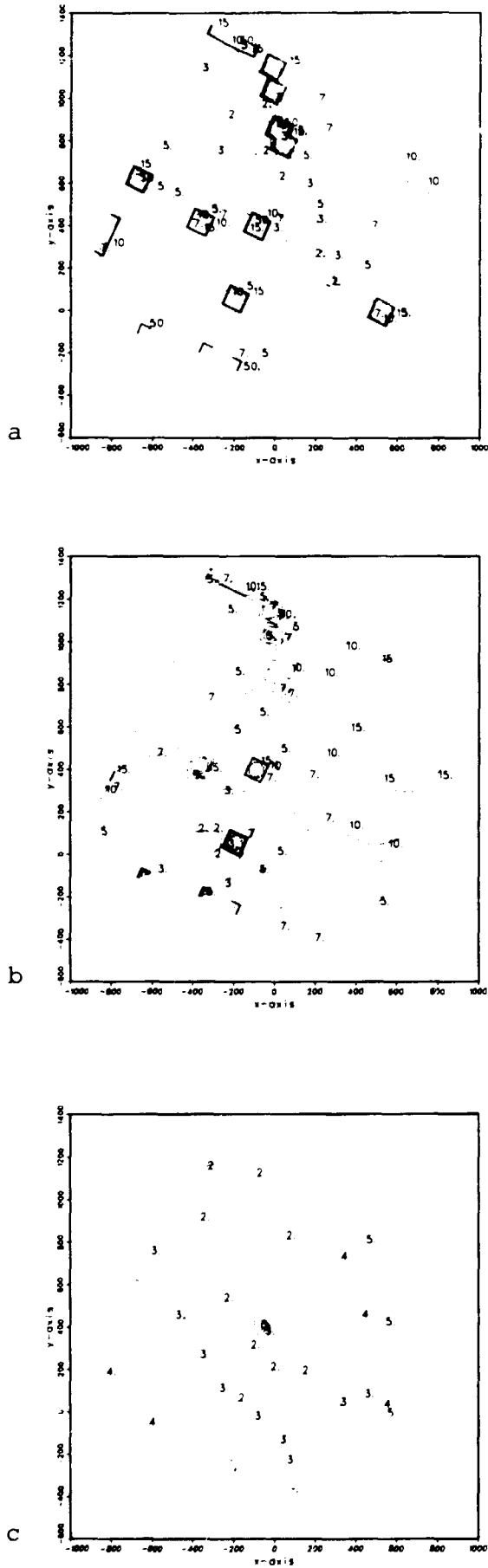
Fig 9-18.   Fluxes at -600 m, (ml/m^2·yr).
a = FJEL   b = FJELA   c = FJELB
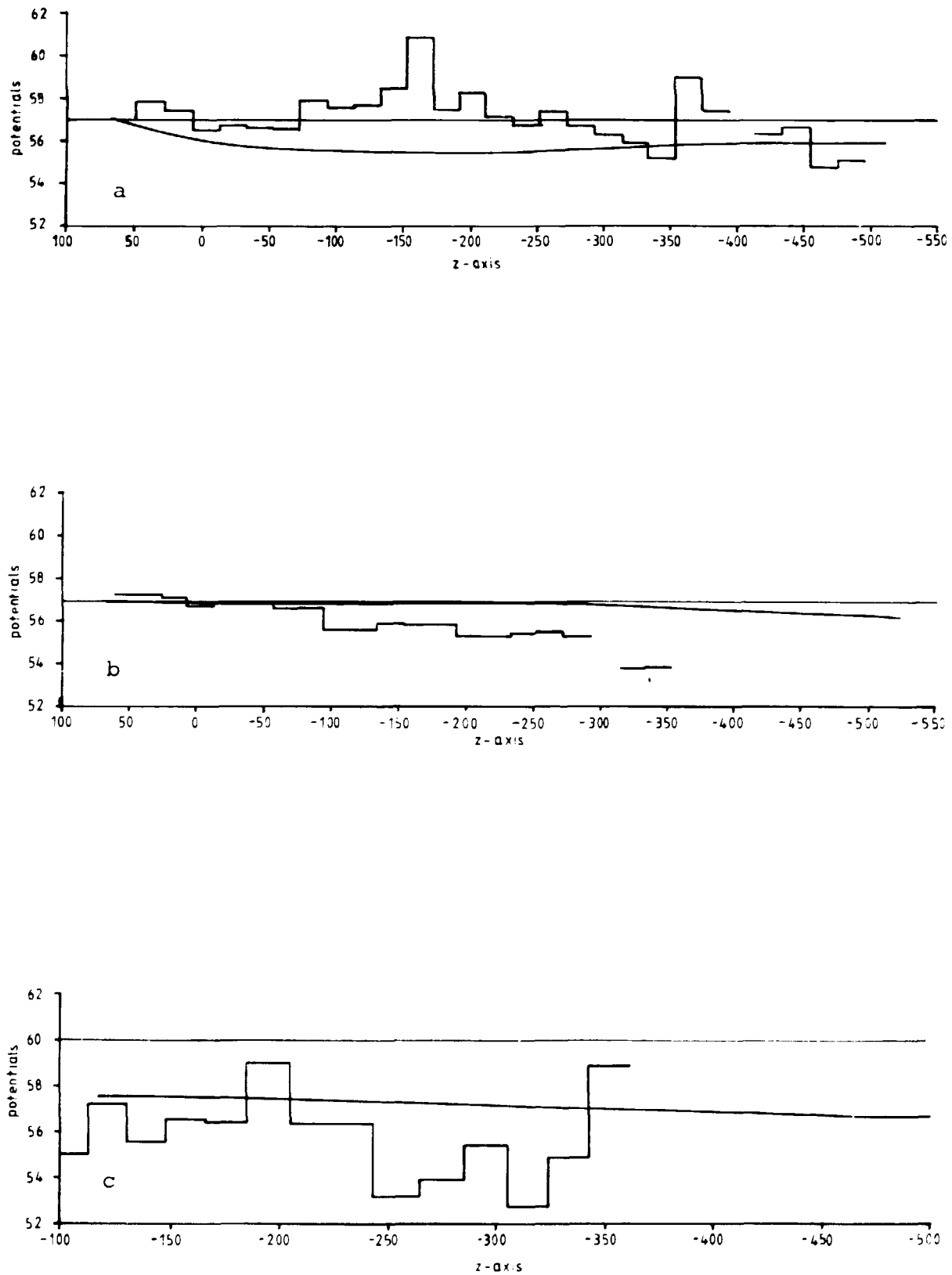
Fig 9-19.   Calculated potentials compared to measured at some bo-
re-holes. a = FJ 2, b = FJ 4, c = FJ 5. The upper
part of FJ 5 falls outside the calculated area. The-
refore the results are represented from about -100
m. The horisontal fall line starting at represents
the potential at the ordinate starting point of the
bore-hole. The step-wise line represents measured
data.
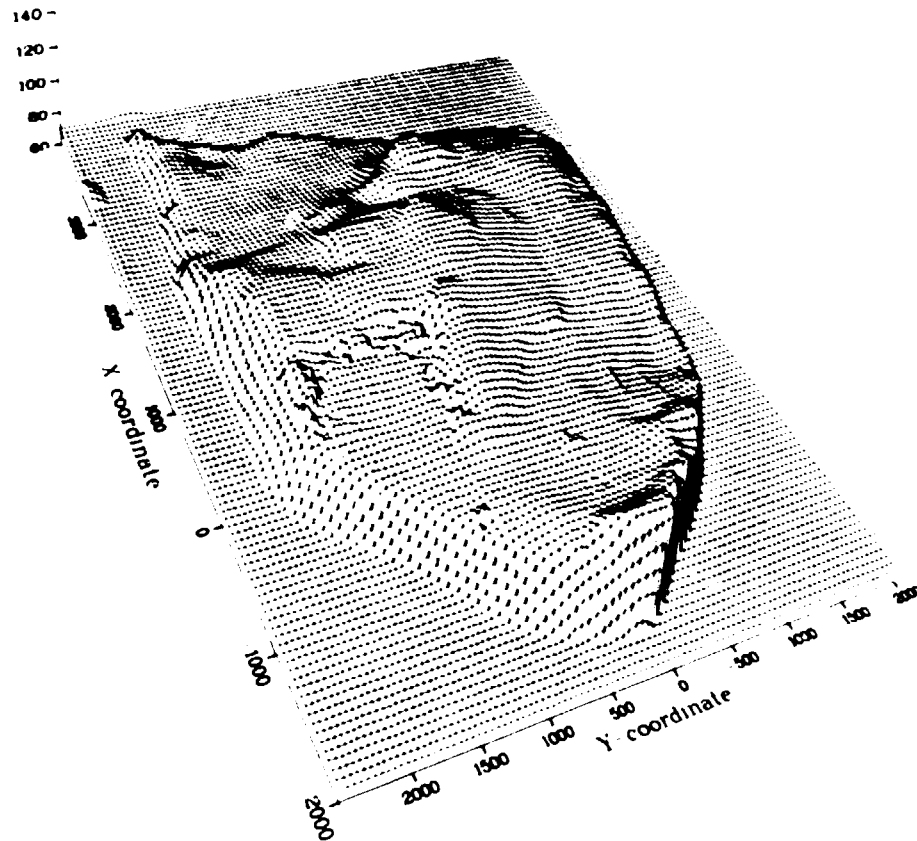
Fig 10-1.   Relief map of the groundwater table at Gideå.
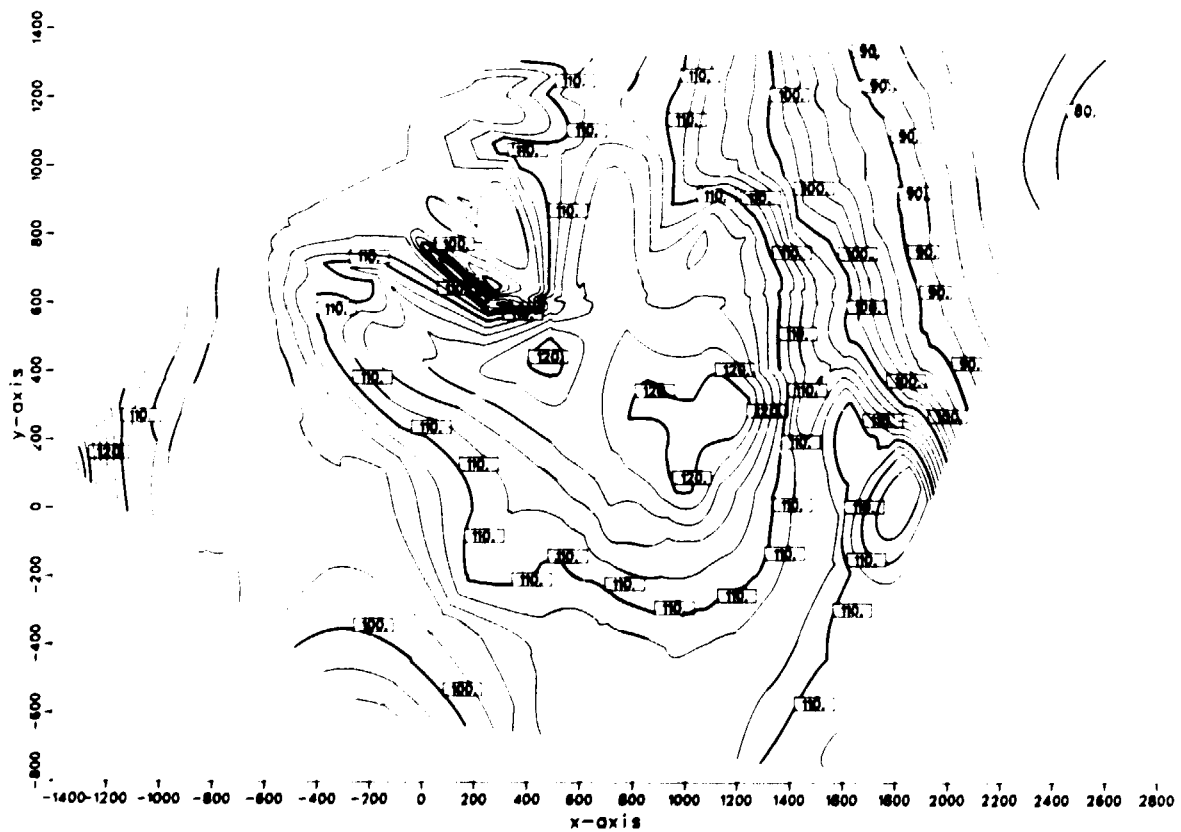
Fig 10-2.   Contour map of the groundwater table at Gideå.
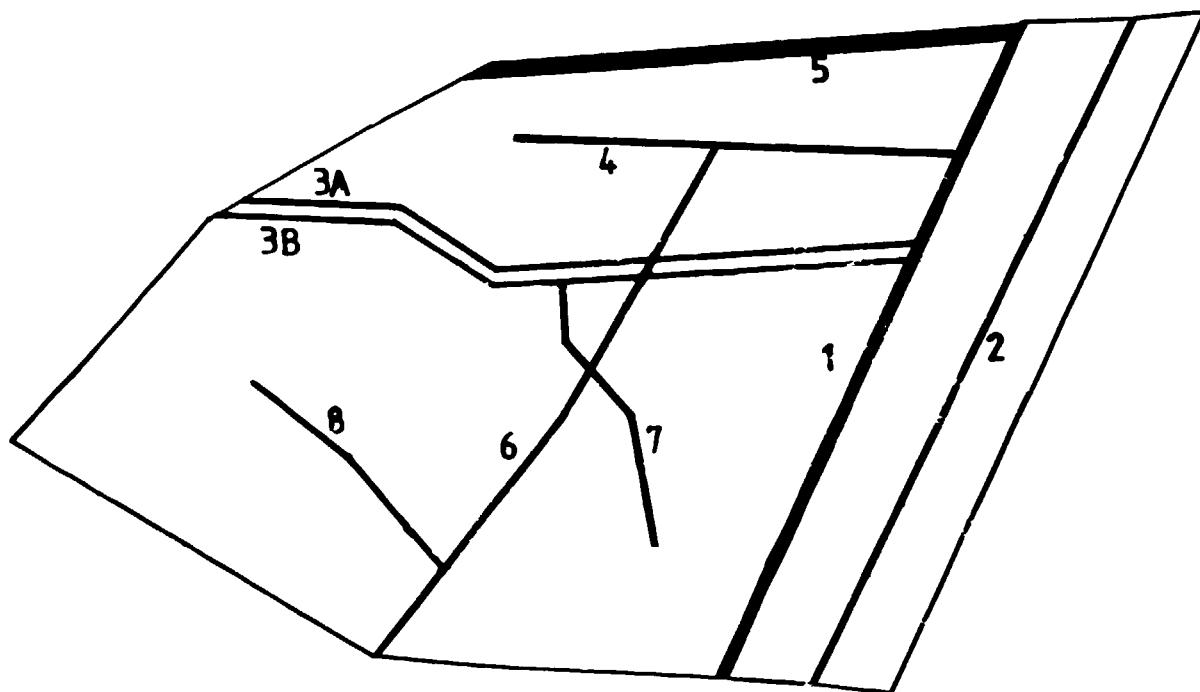
Fig 10-3.   Fracture zones at Gideå as modelled.
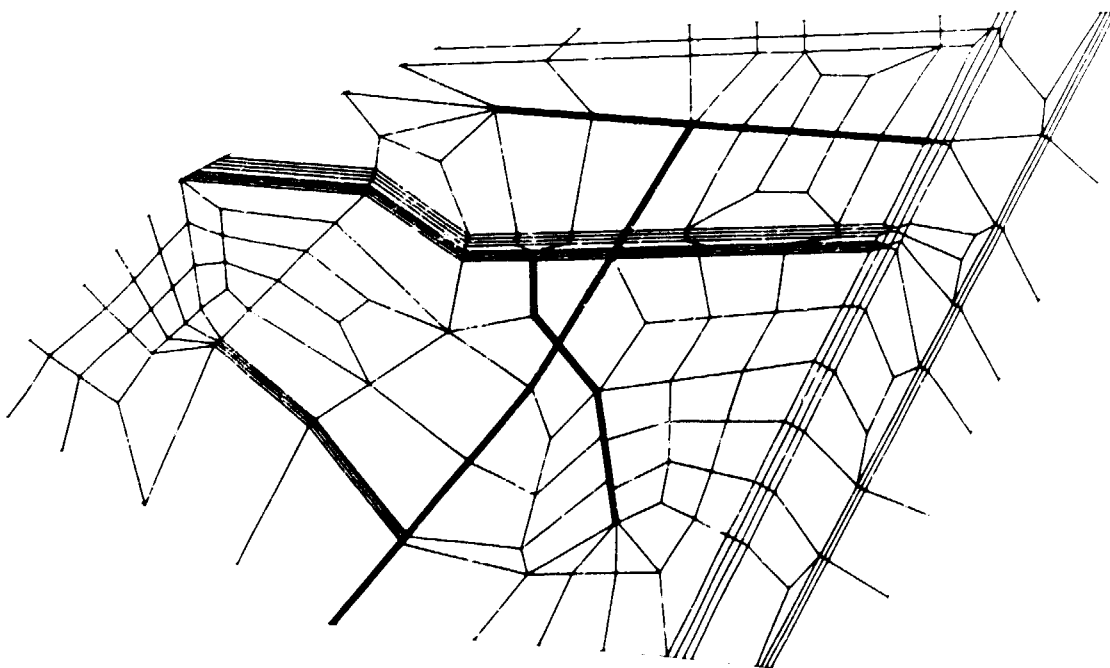
Fig 10-4.   Top surface of the element mesh.
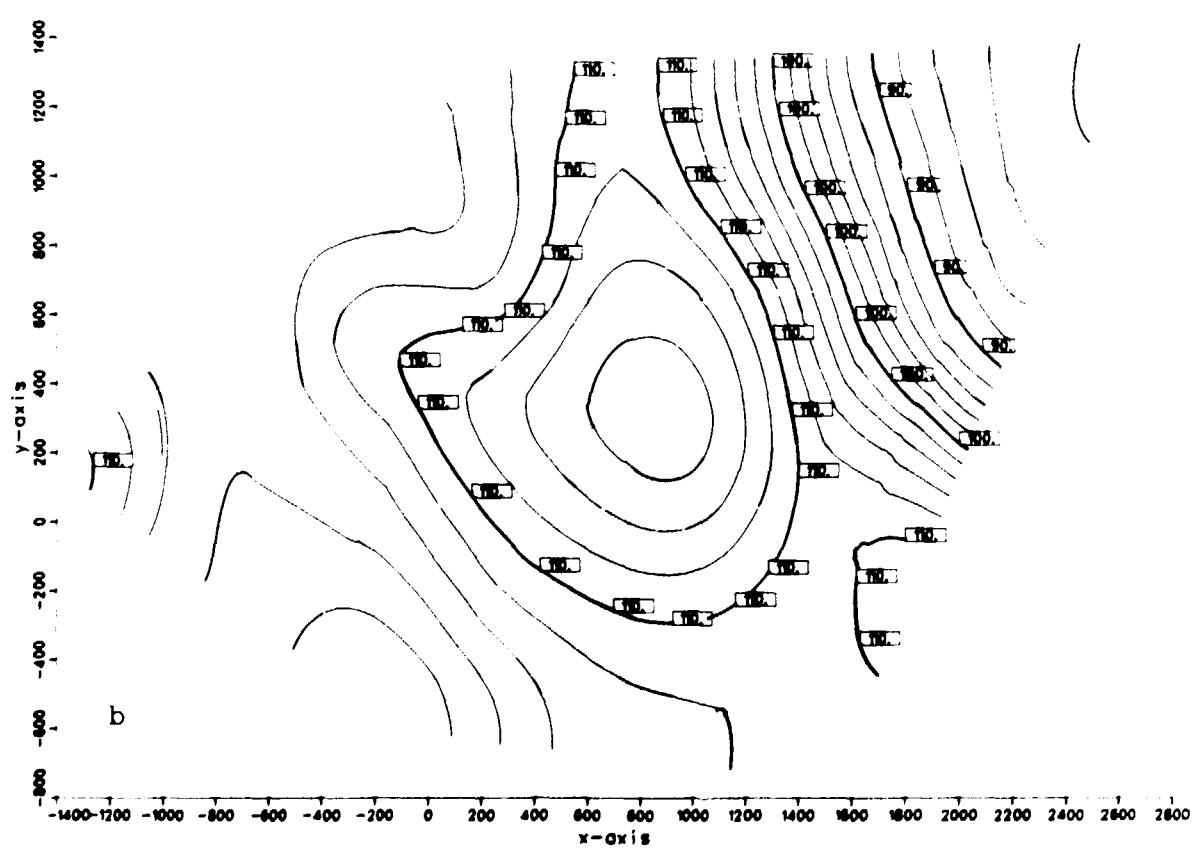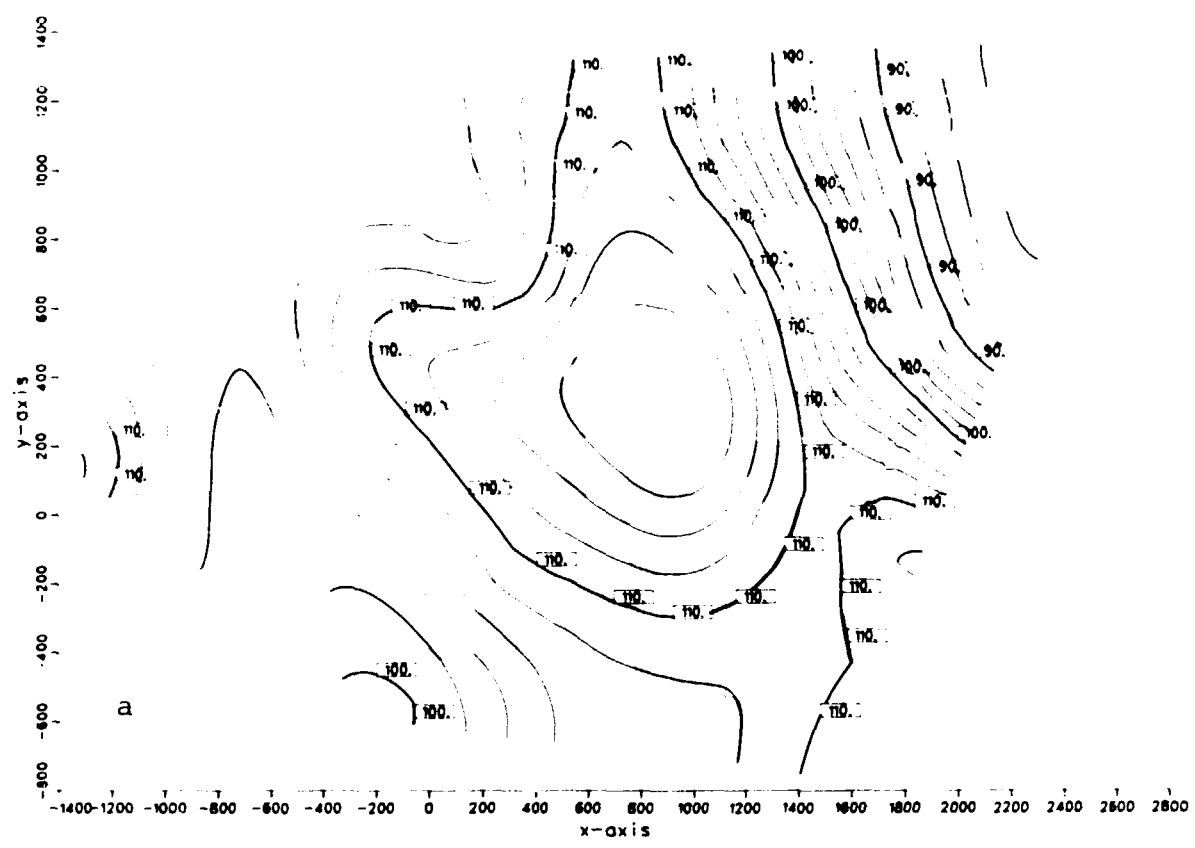
Fig 10-5.   Isopotential lines in a horisontal cross section at
            -150 m.
            a = GIDE   b = GIDEA
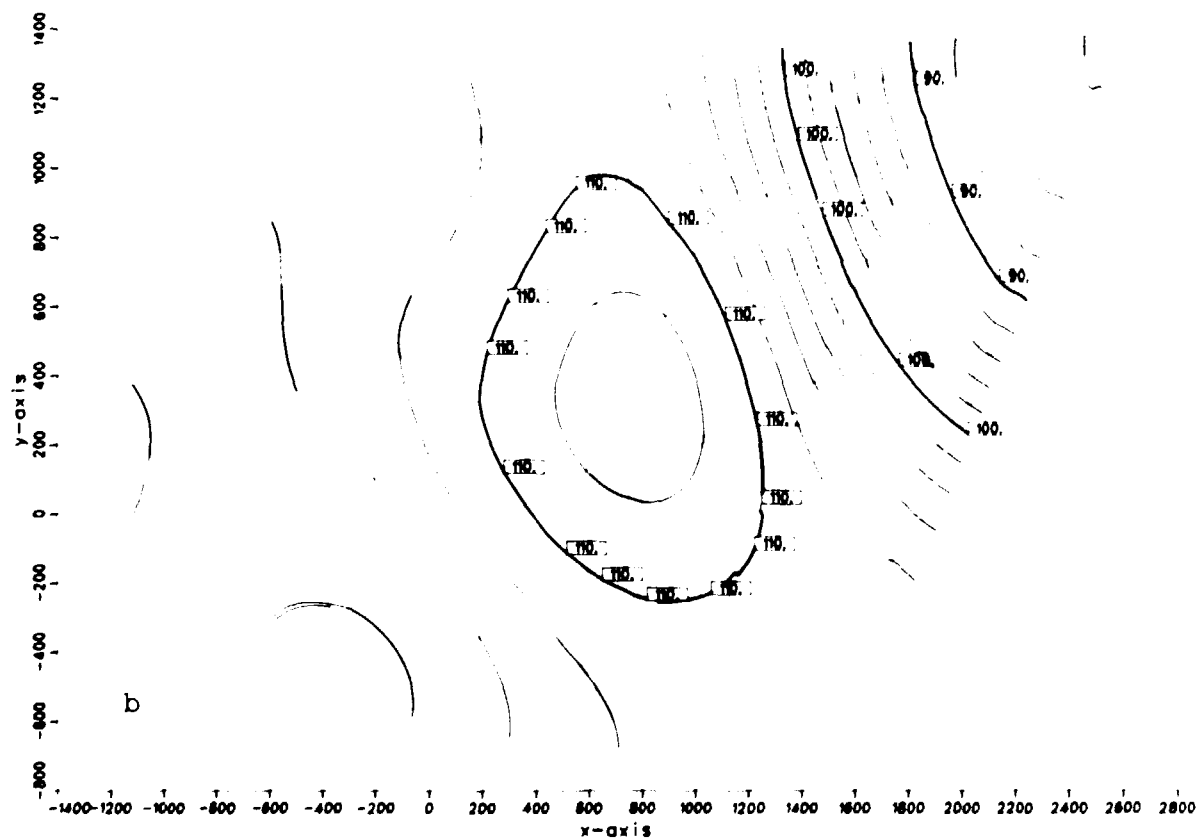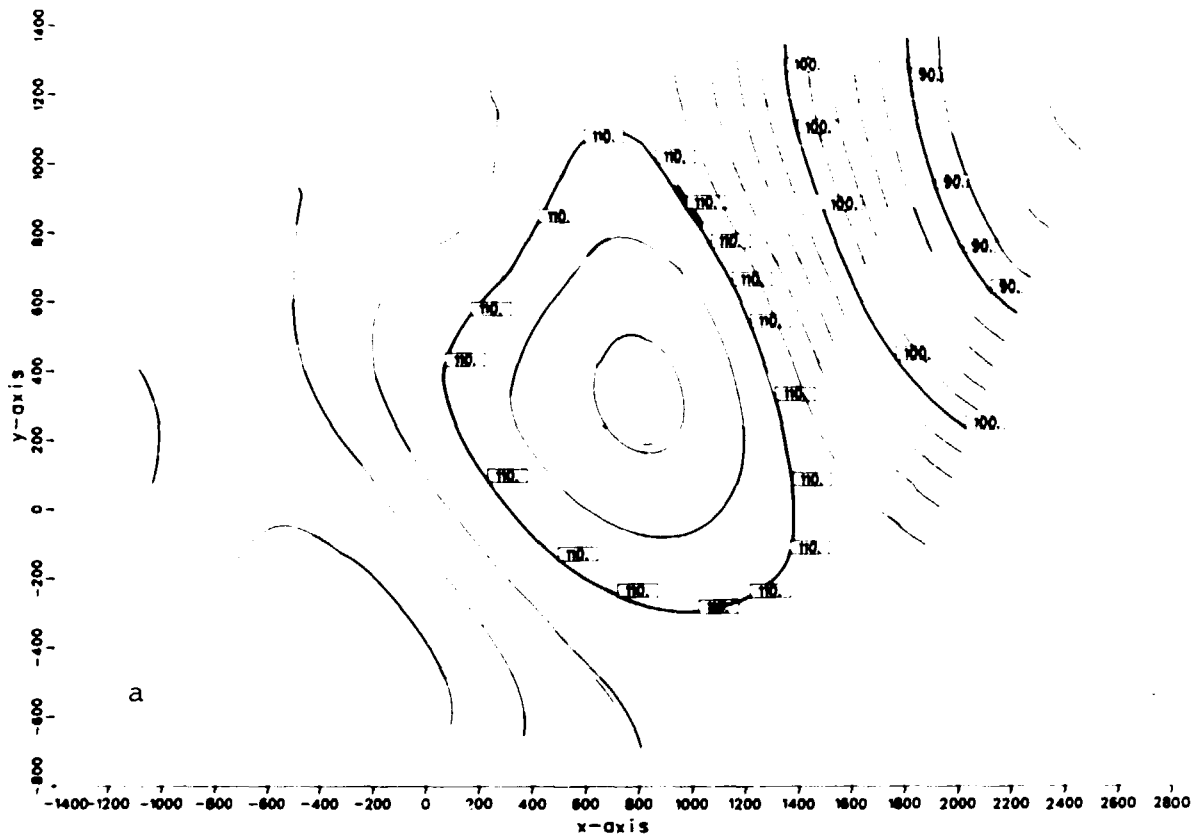
Fig 10-6.   Isopotential lines in a horisontal cross section at
            -500 m.
            a = GIDE   b = GIDEA
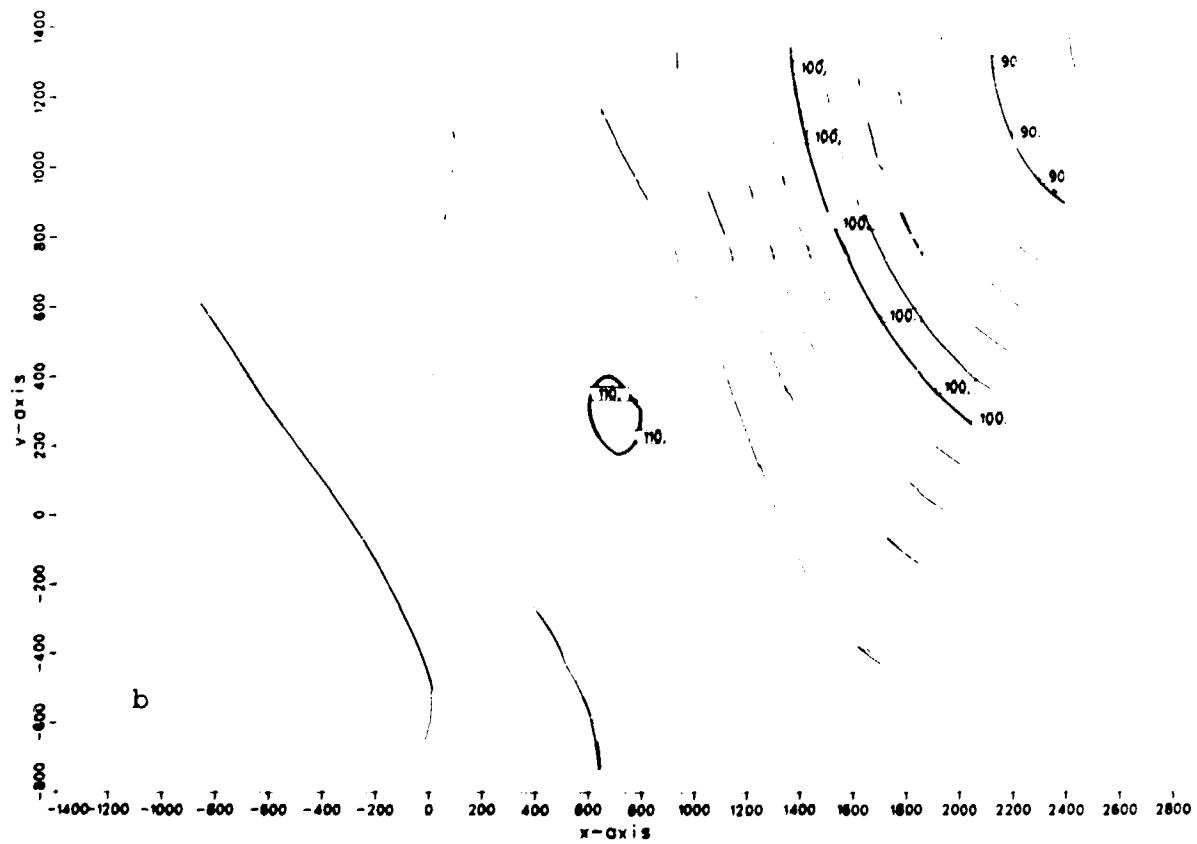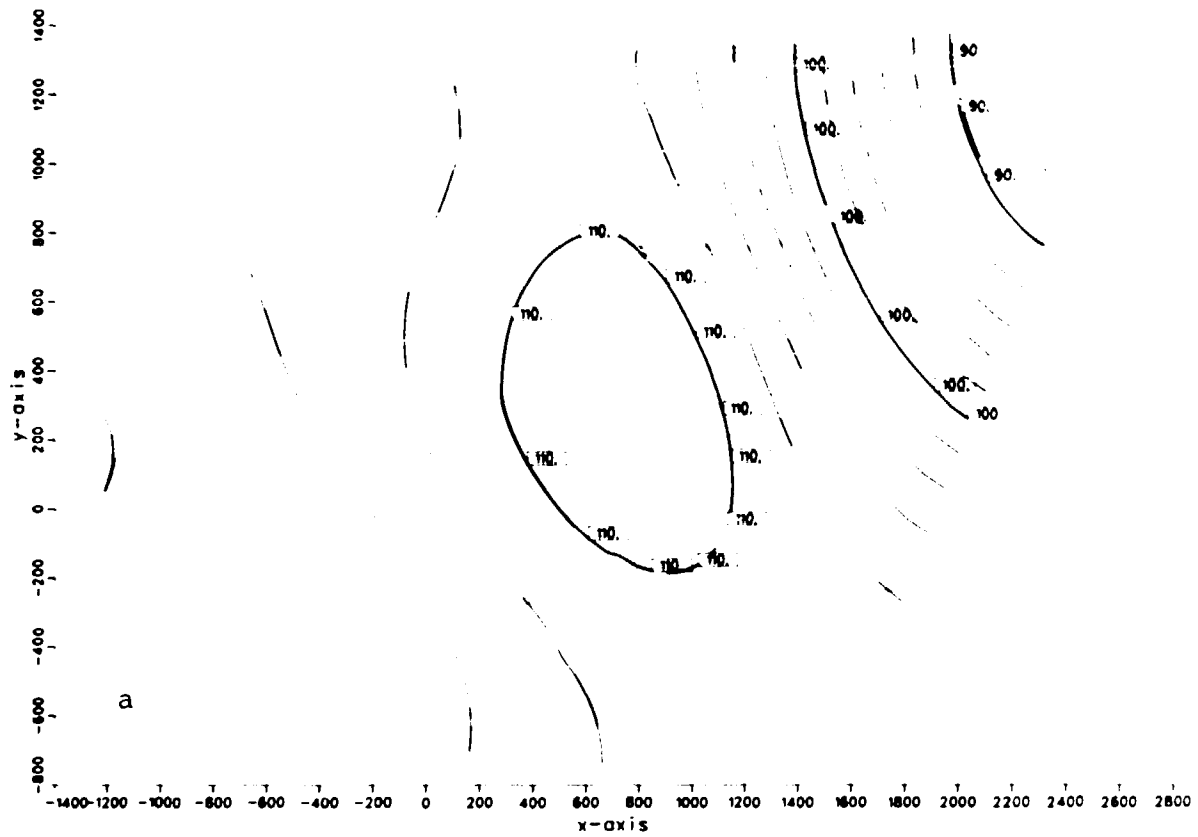
Fig 10-7.   Isopotential lines in a horisontal cross section at
             -750 m.
             a = GIDE   b = GIDEA
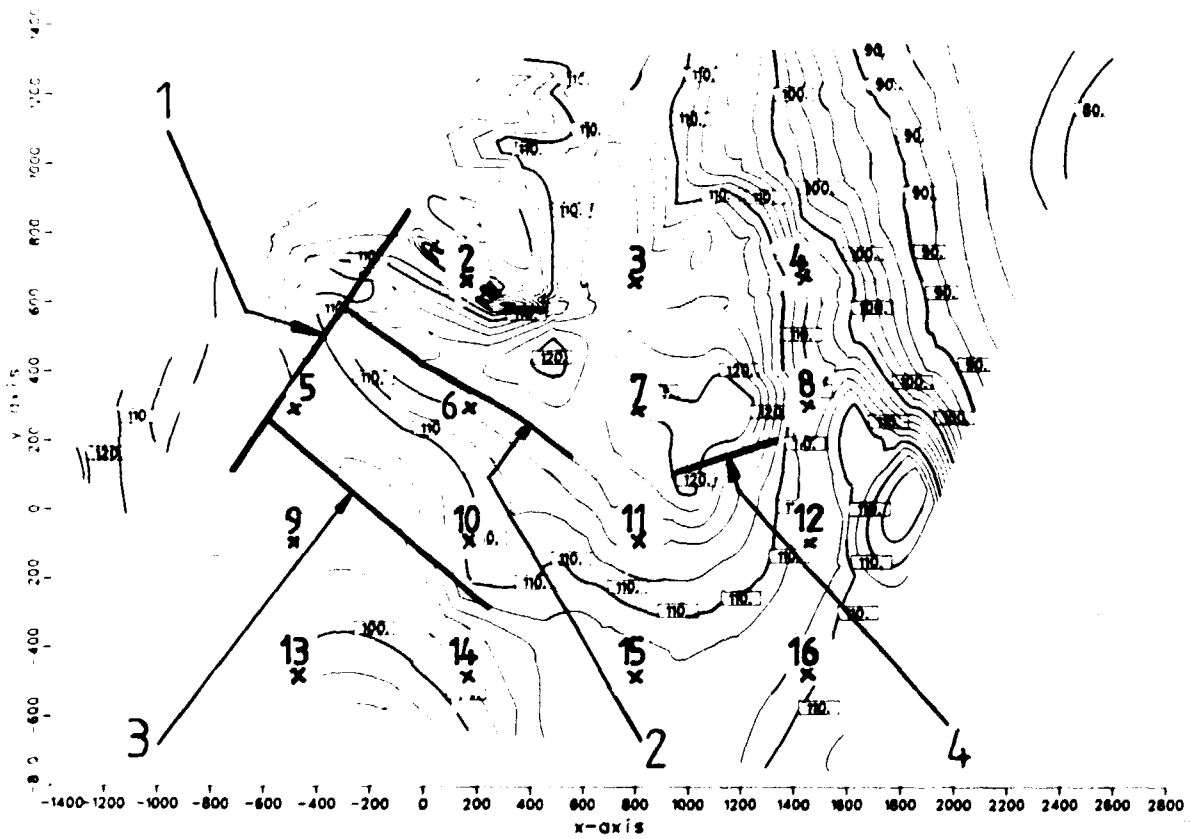
Fig 10-8.   Locations of vertical cross sections at Gideå. Star-
             ting points for trajectories discussed in section
             10.3.3 are also shown.
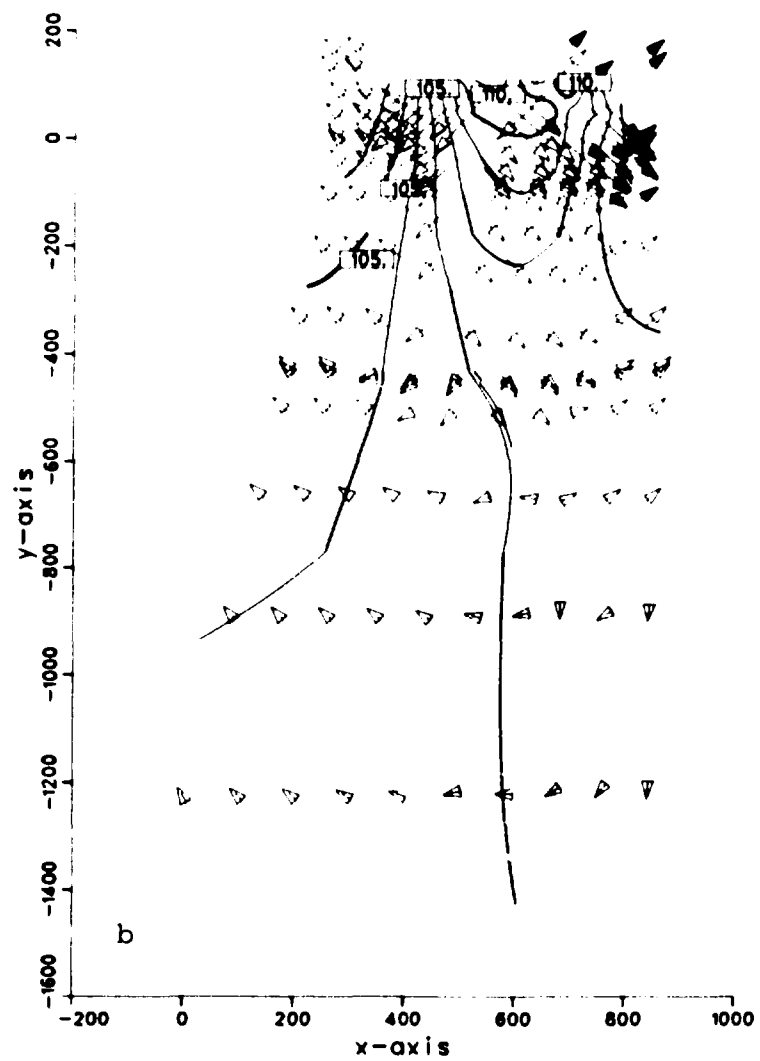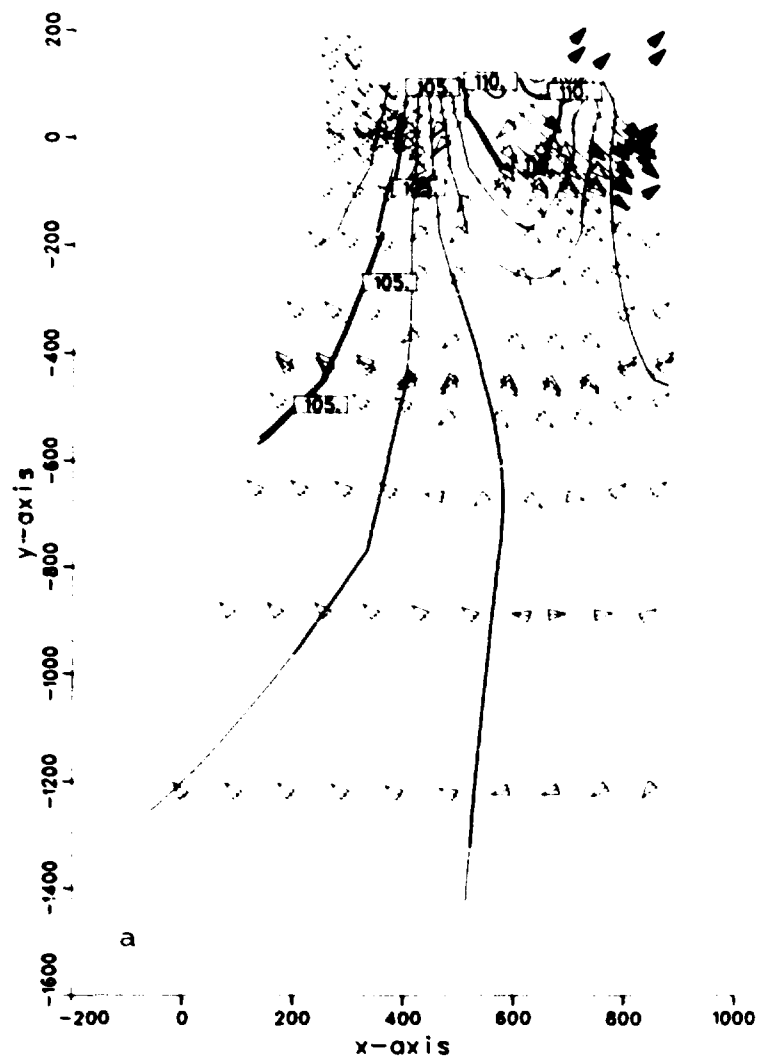
Fig 10-9.   Isopotentials and projected flow vectors at vertical
             cross section no. 1.
             a = GIDE   b = GIDEA
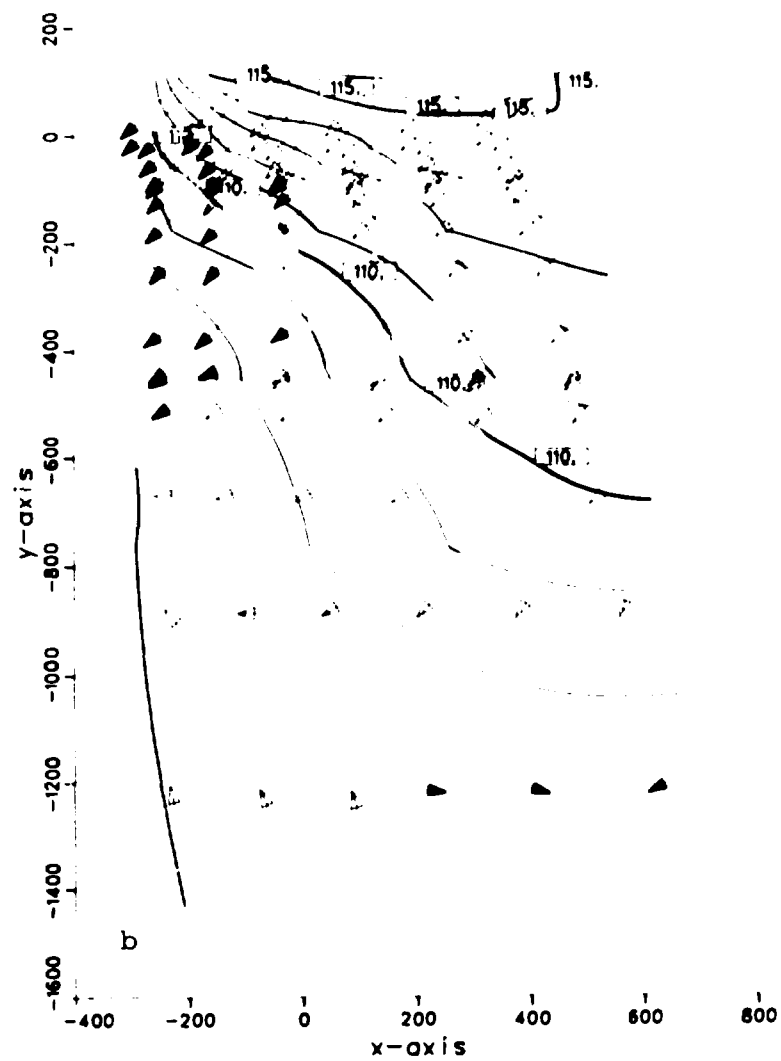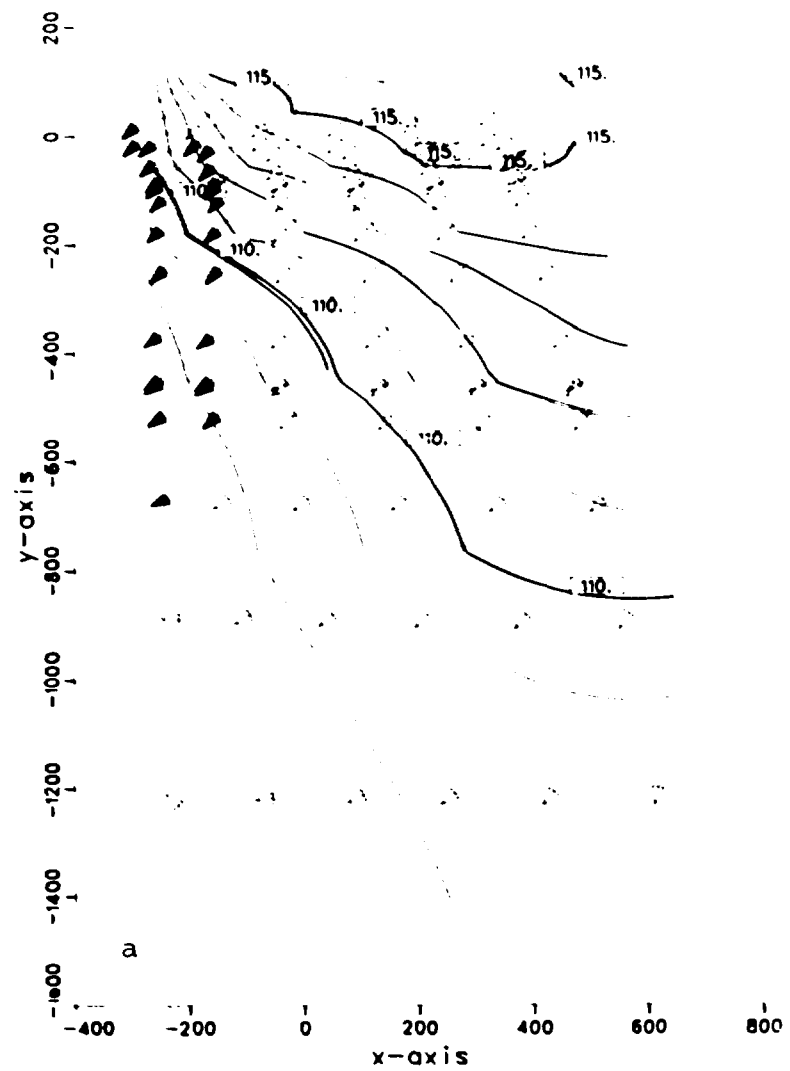
Fig 10-10. Isopotentials and projected flow vectors at vertical
cross section no. 2.
a = GIDE   b = GIDEA
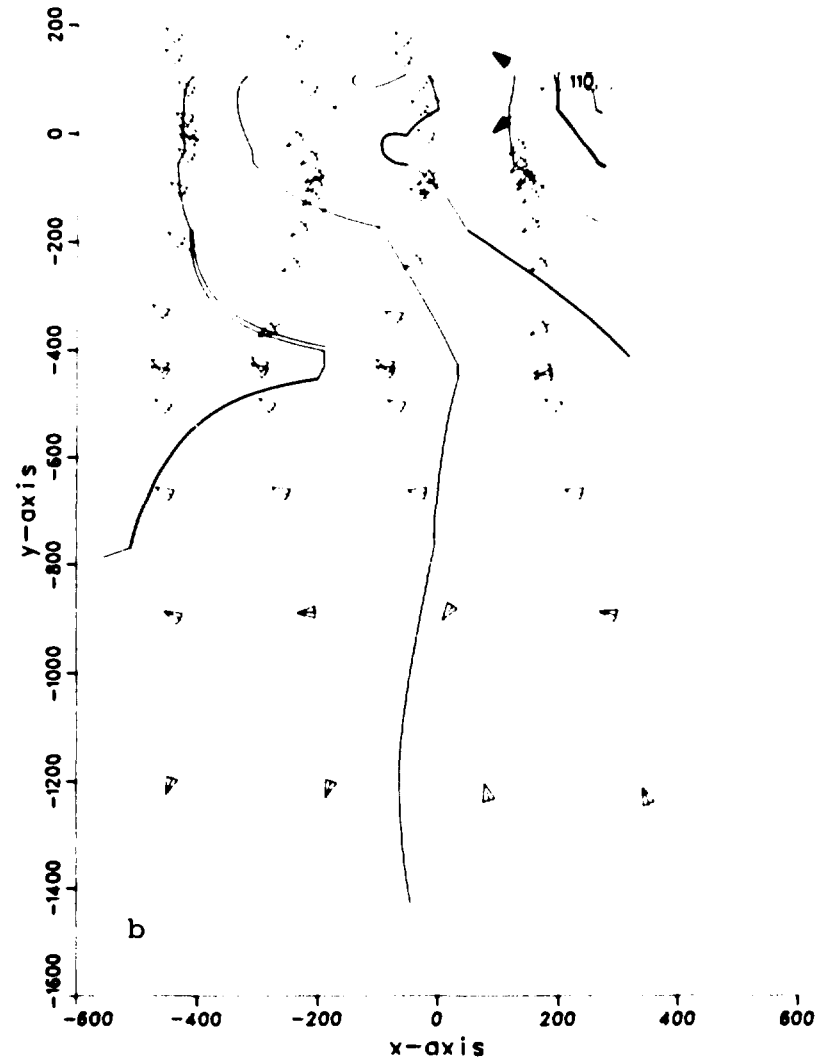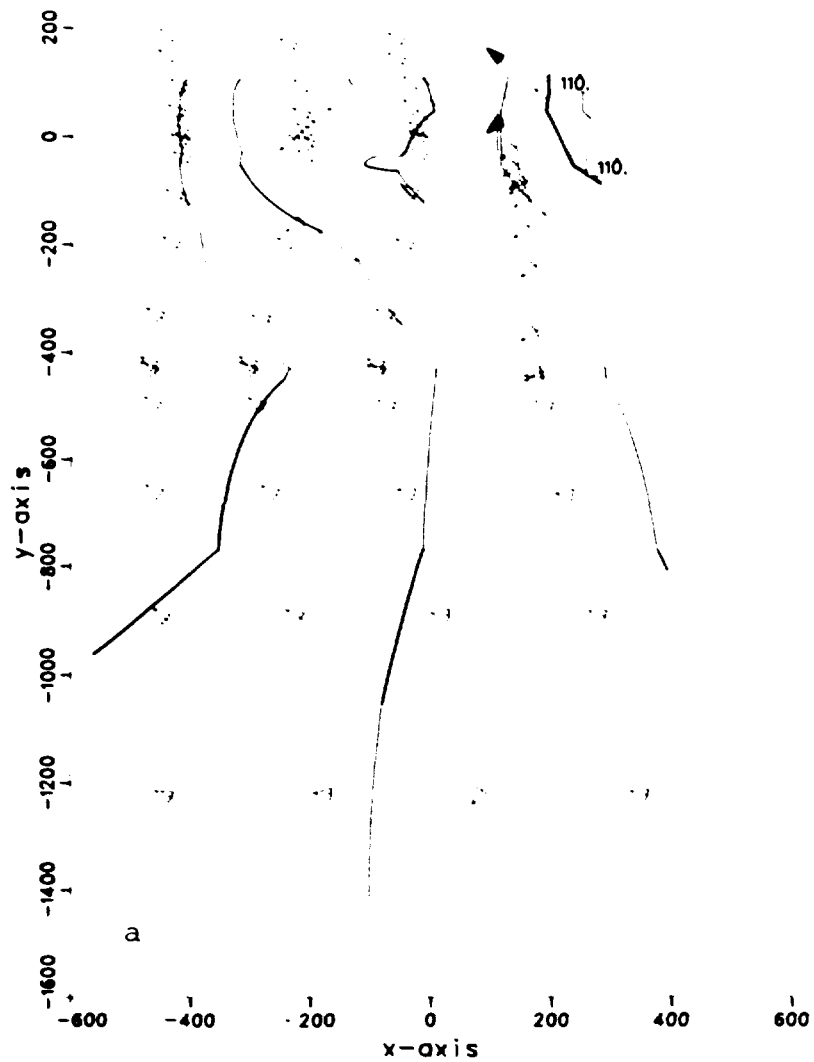
Fig 10-11. Isopotentials and projected flow vectors at vertical
cross section no. 3.

a = GIDE   b = GIDEA
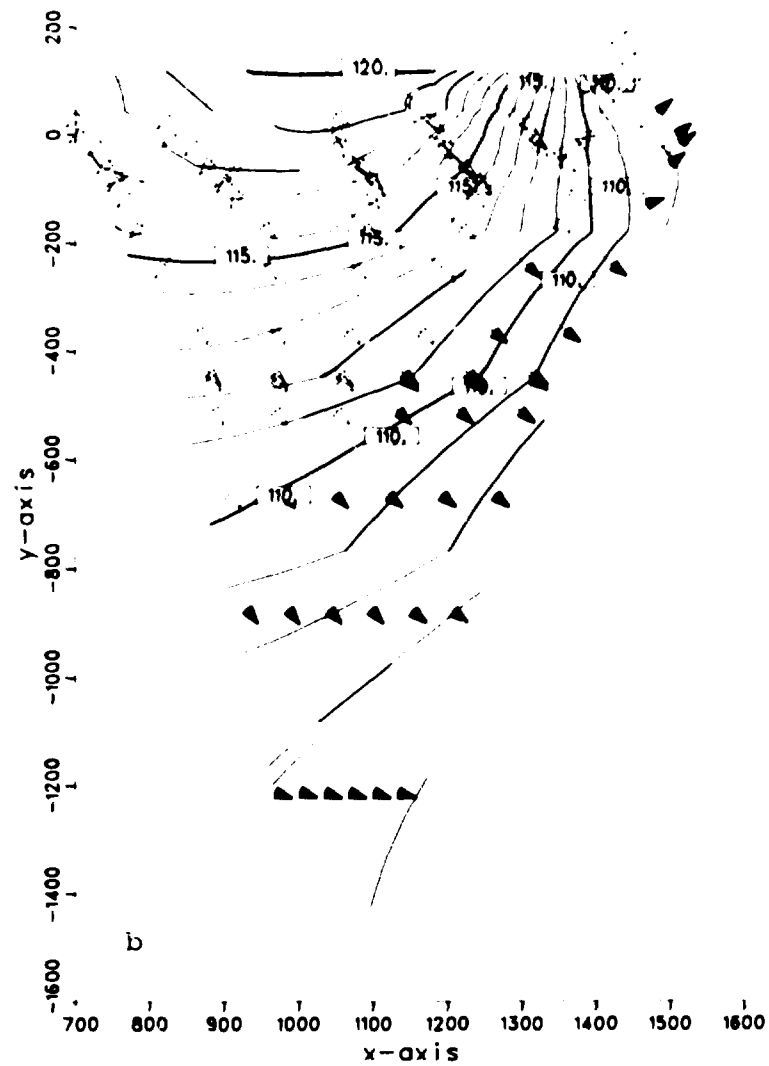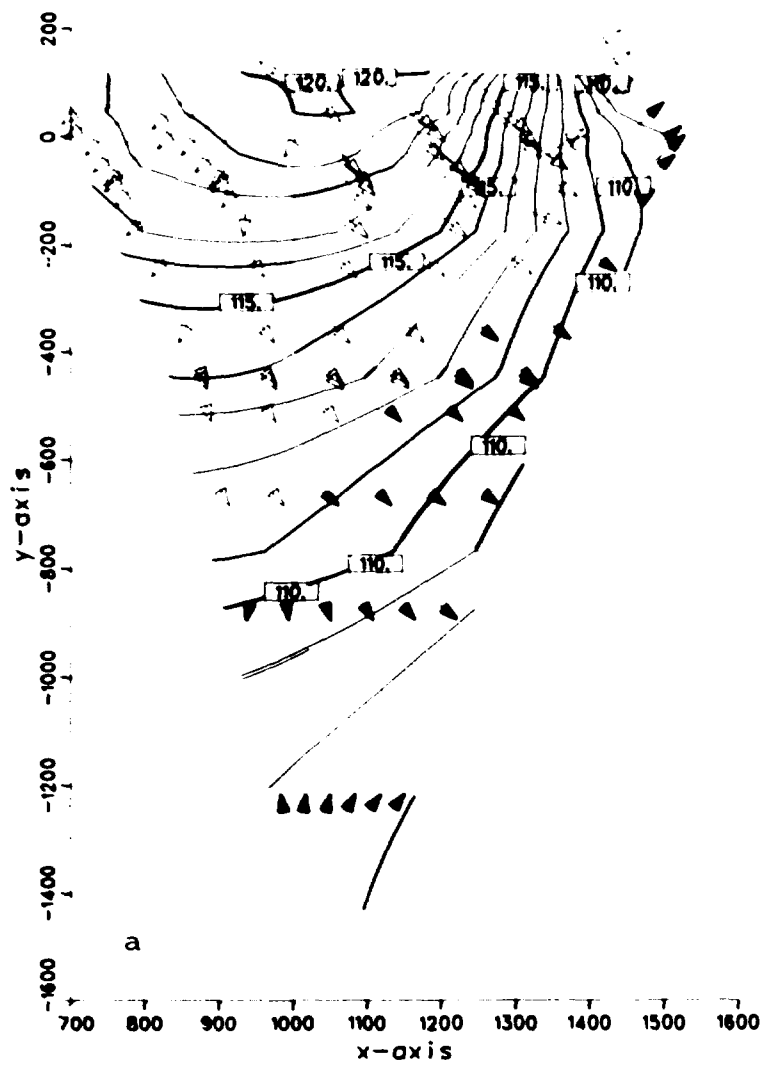
Fig 10-12.   Isopotentials and projected flow vectors at vertical
             cross section no. 4.
   a = GIDE   b = GIDEA
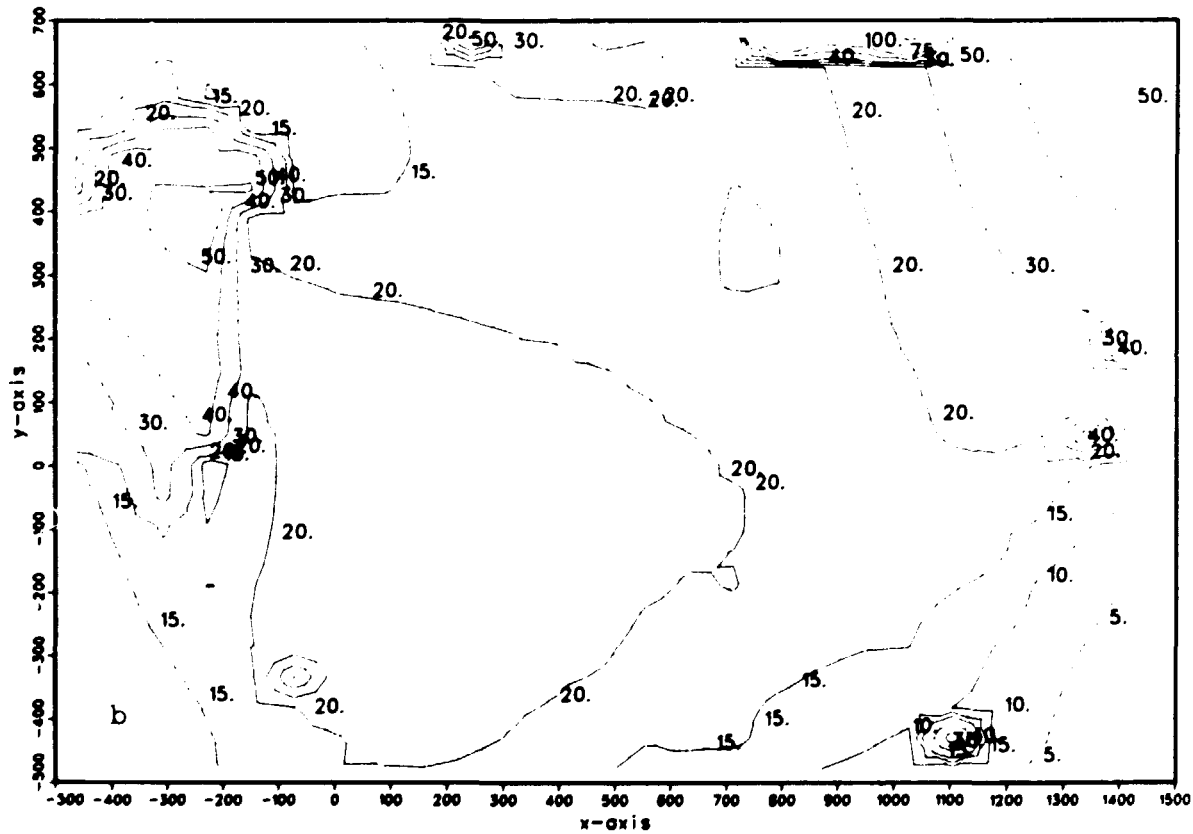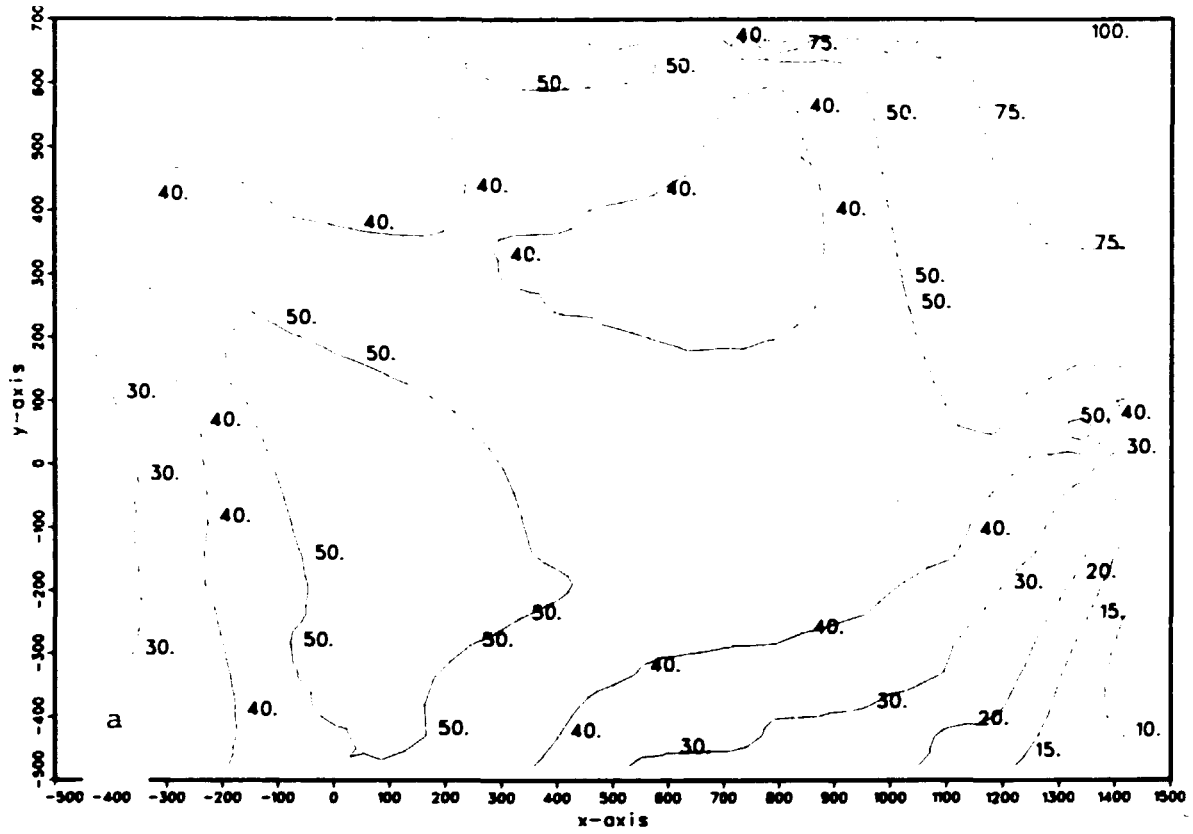
Fig 10-13. Fluxes at -400 m, (ml/m^2 · yr).
a = GIDE   b = GIDEA
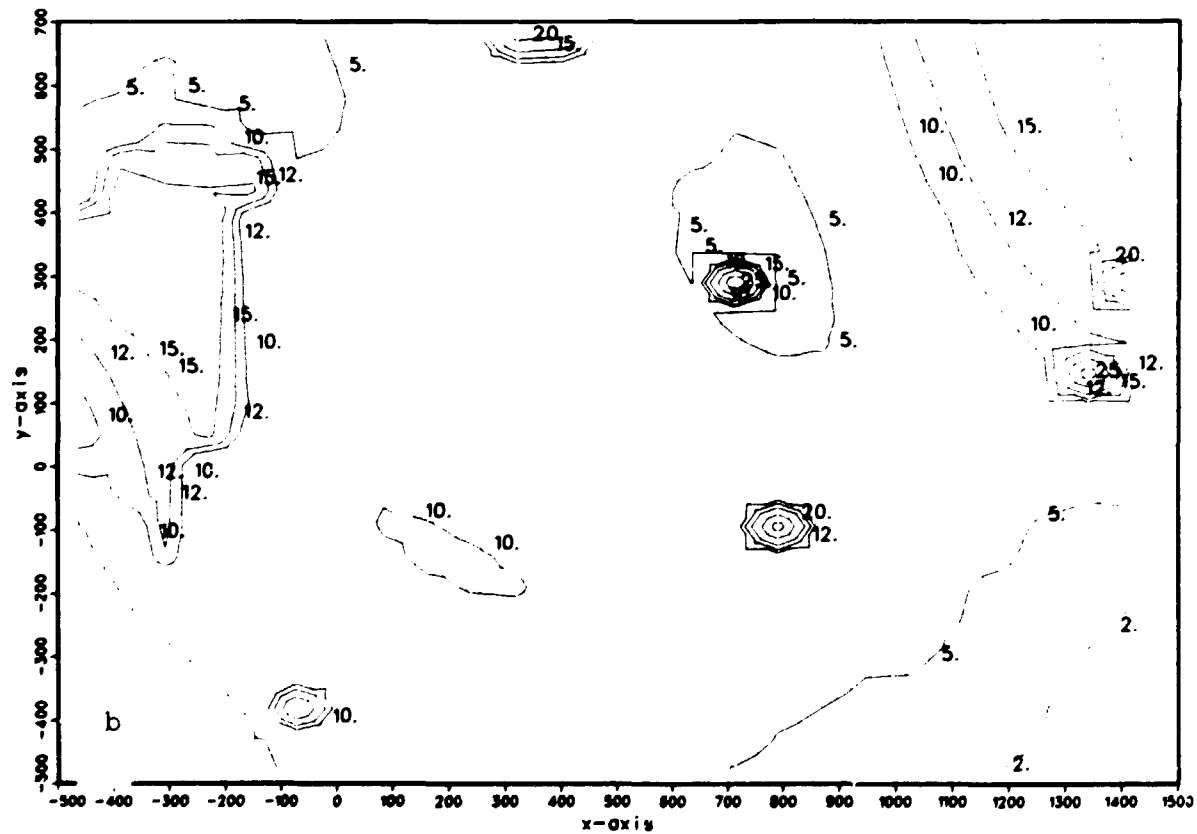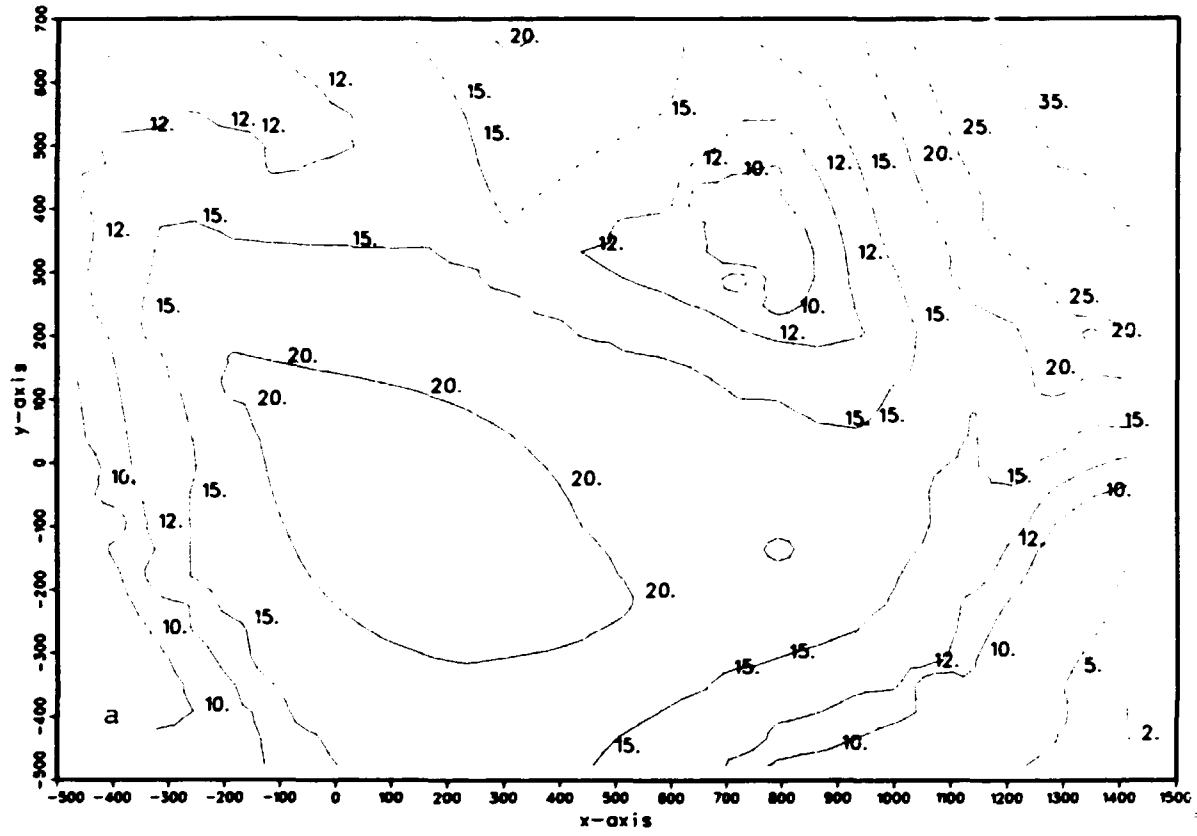
Fig 10-14. Fluxes at -500 m, $(ml/m^2 \cdot yr)$.
a = GIDE   b = GIDEA
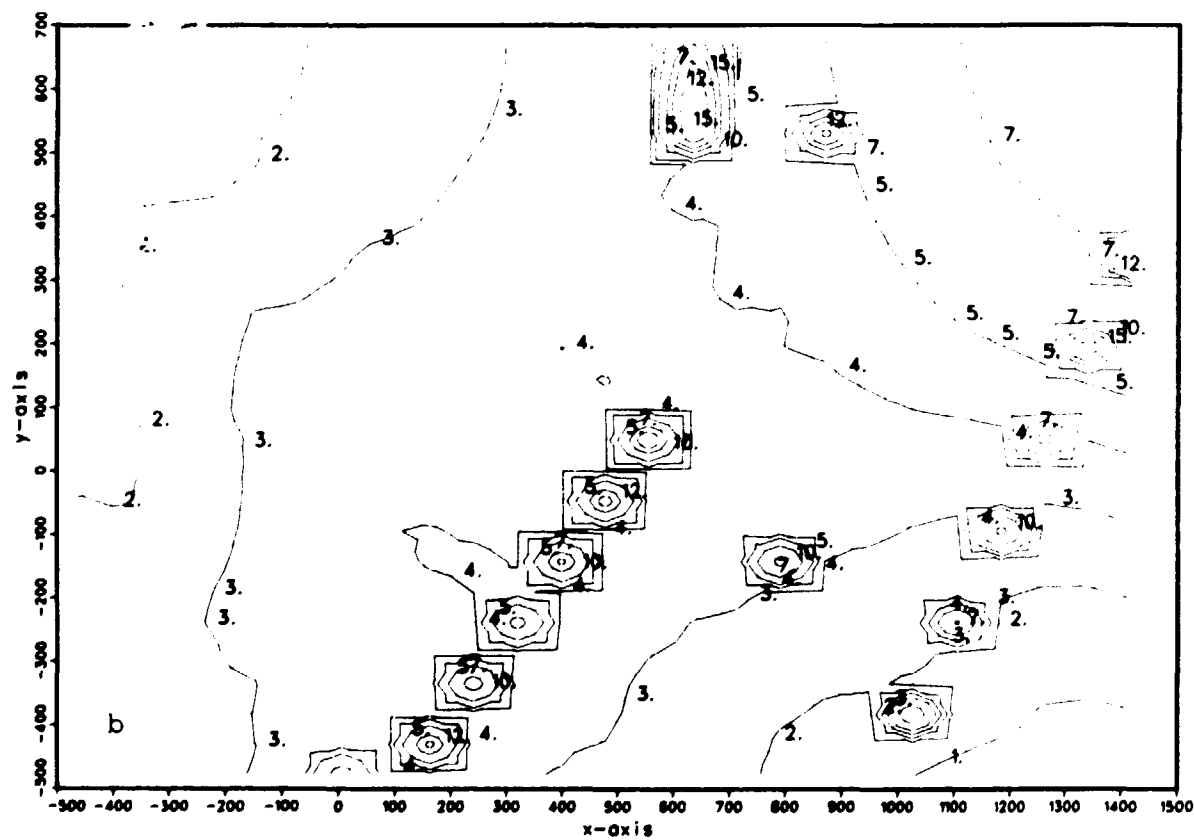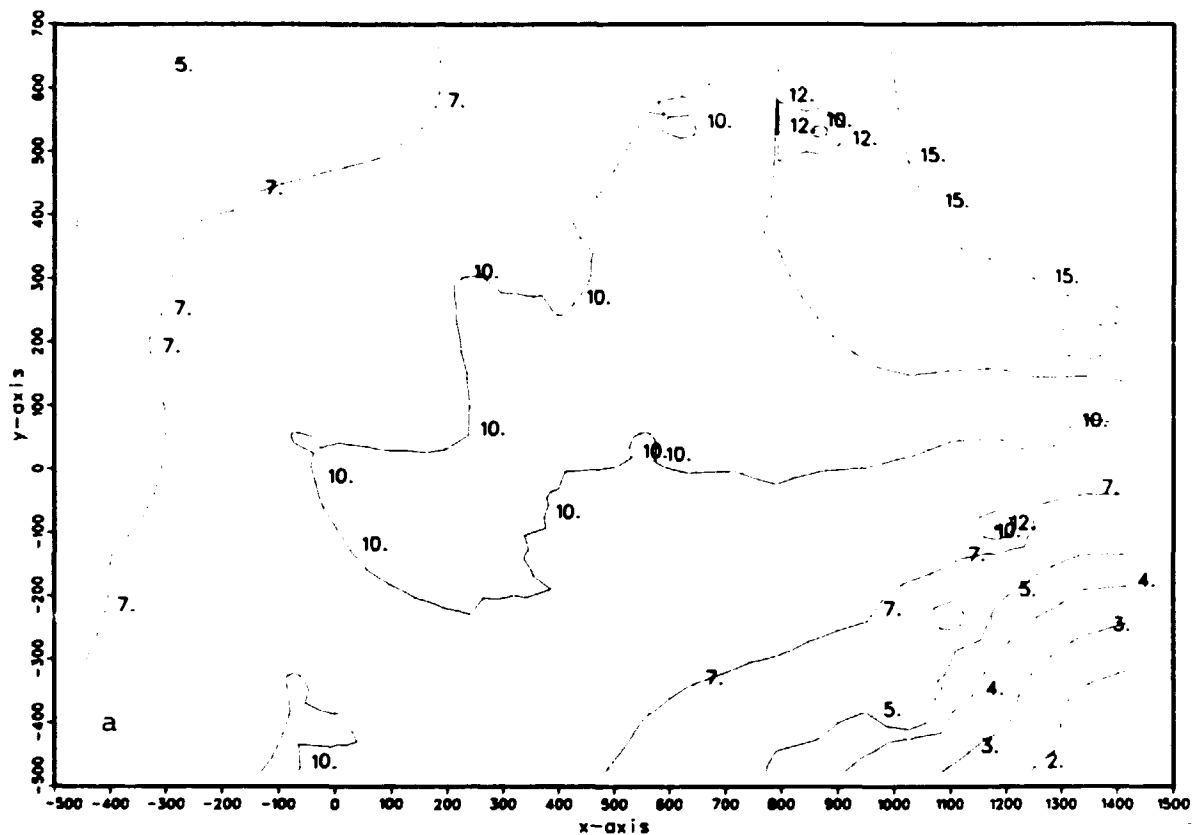
Fig 10-15. Fluxes at -600 m, (ml/m^2 · yr).
a = GIDE   b = GIDEA
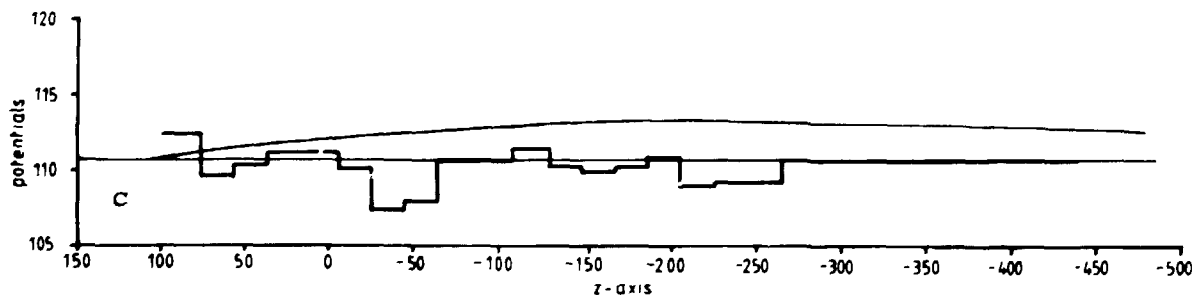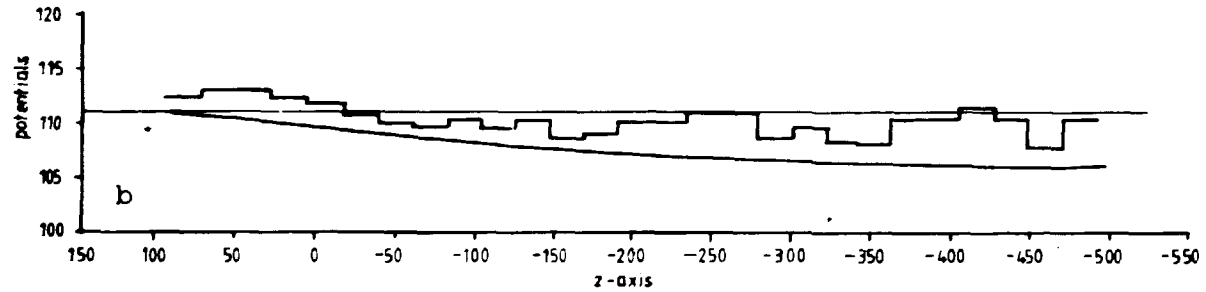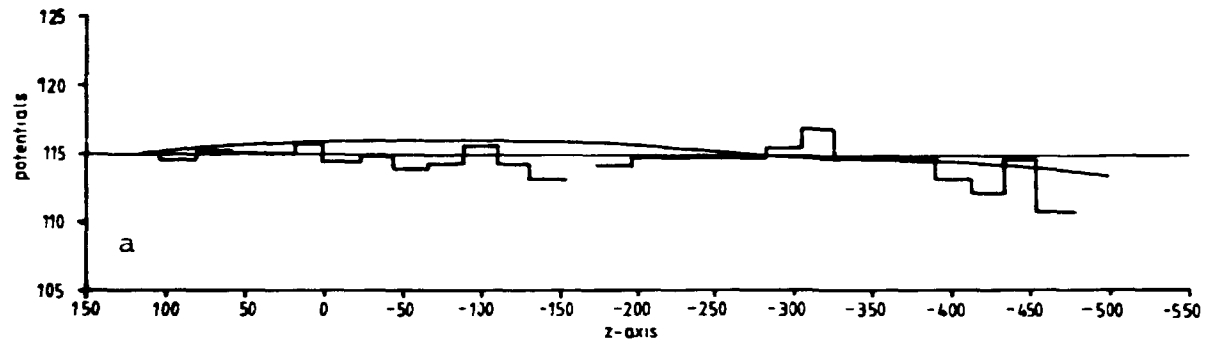
Fig 10-16. Calculated potentials compared to measured at some
bore-holes.
a = GI 3, b = GI 7, c = GI 8.

Note that long term observations are performed only
in bore-hole GI 7. The horisontal full line starting
at the ordinate represents the potential at the star-
ting point of the bore-hole. The step-wise lines re-
present measured data.
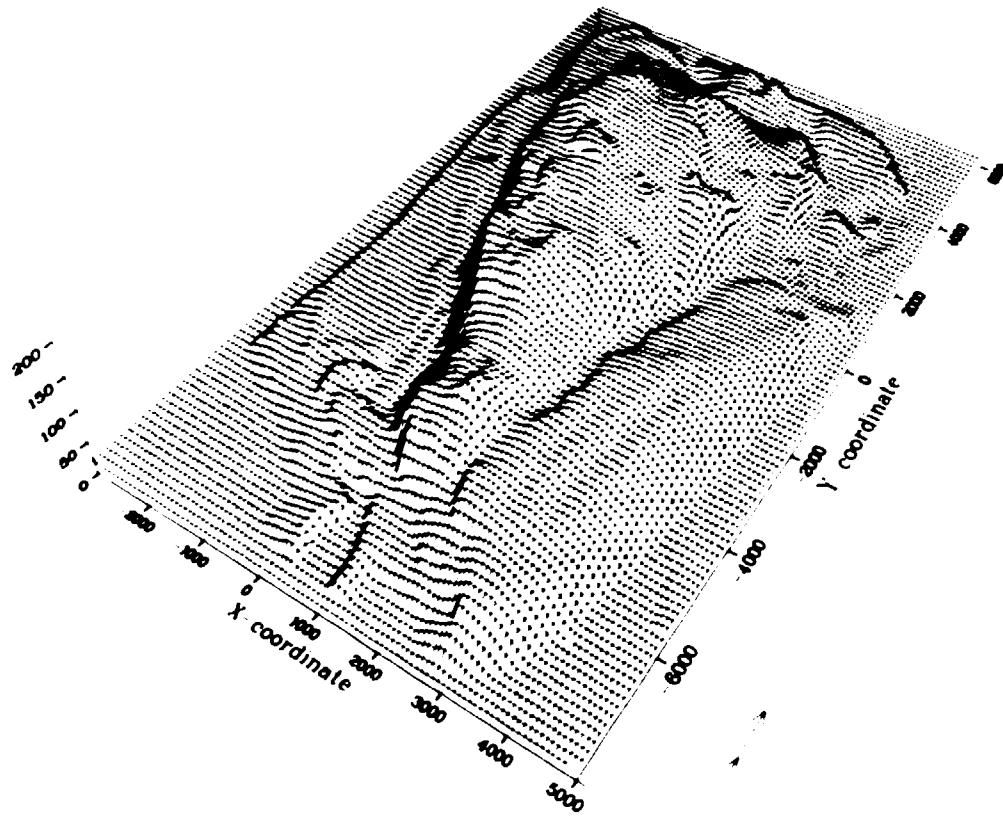
Fig 11-1.   Relief map of the groundwater table at regional area
             of Kamlunge.
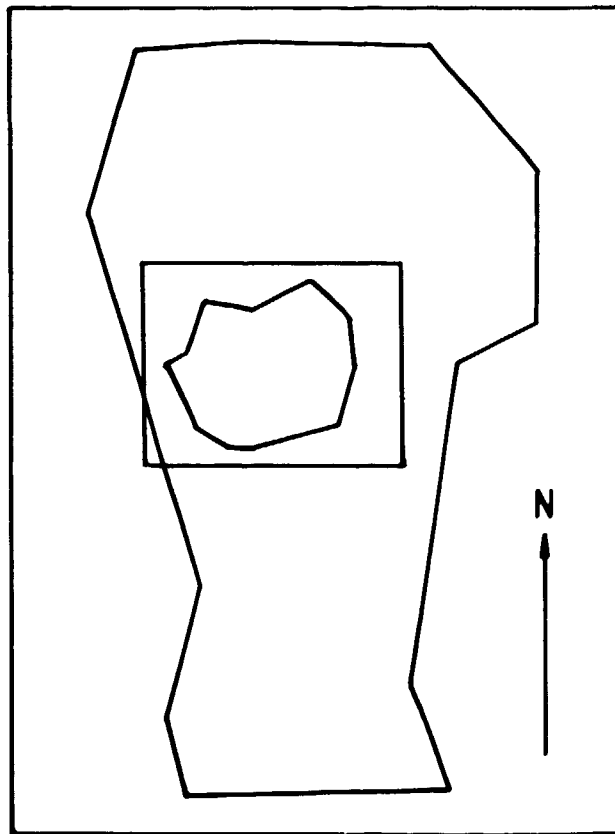
Fig 11-2.   Limits of the local area compared to the regional
             area.
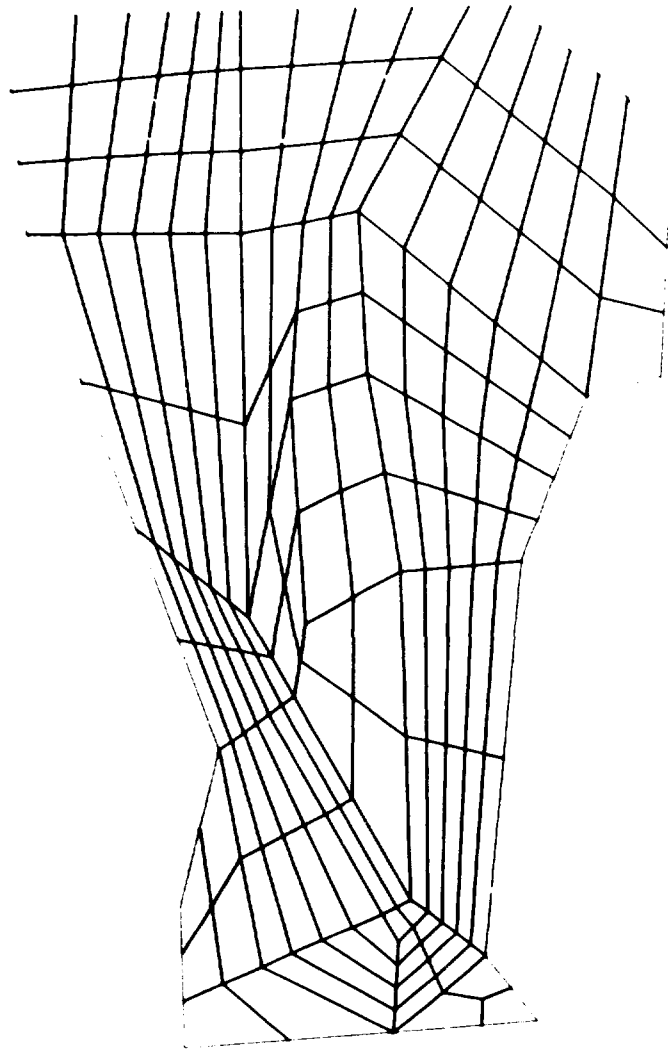
Fig 11-3.   Element mesh at the top surface of the
            regional area of Kamlunge.
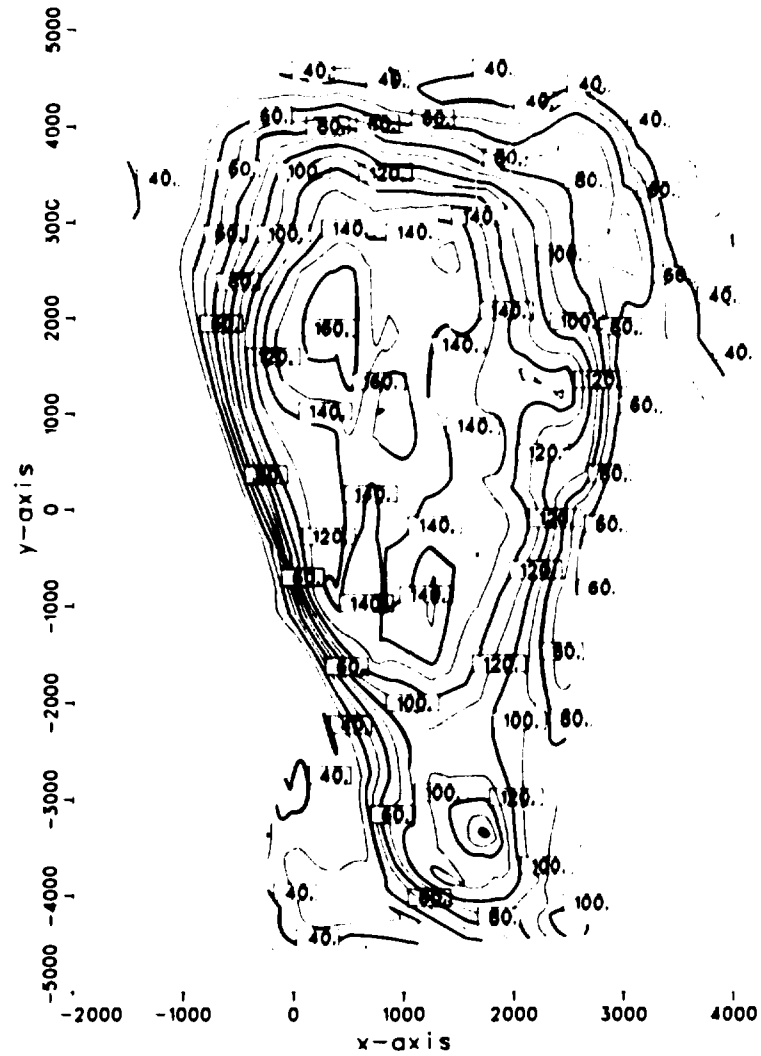
Fig 11-4.   Contour map of the groundwater table of the
            regional area at Kamlunge.

188
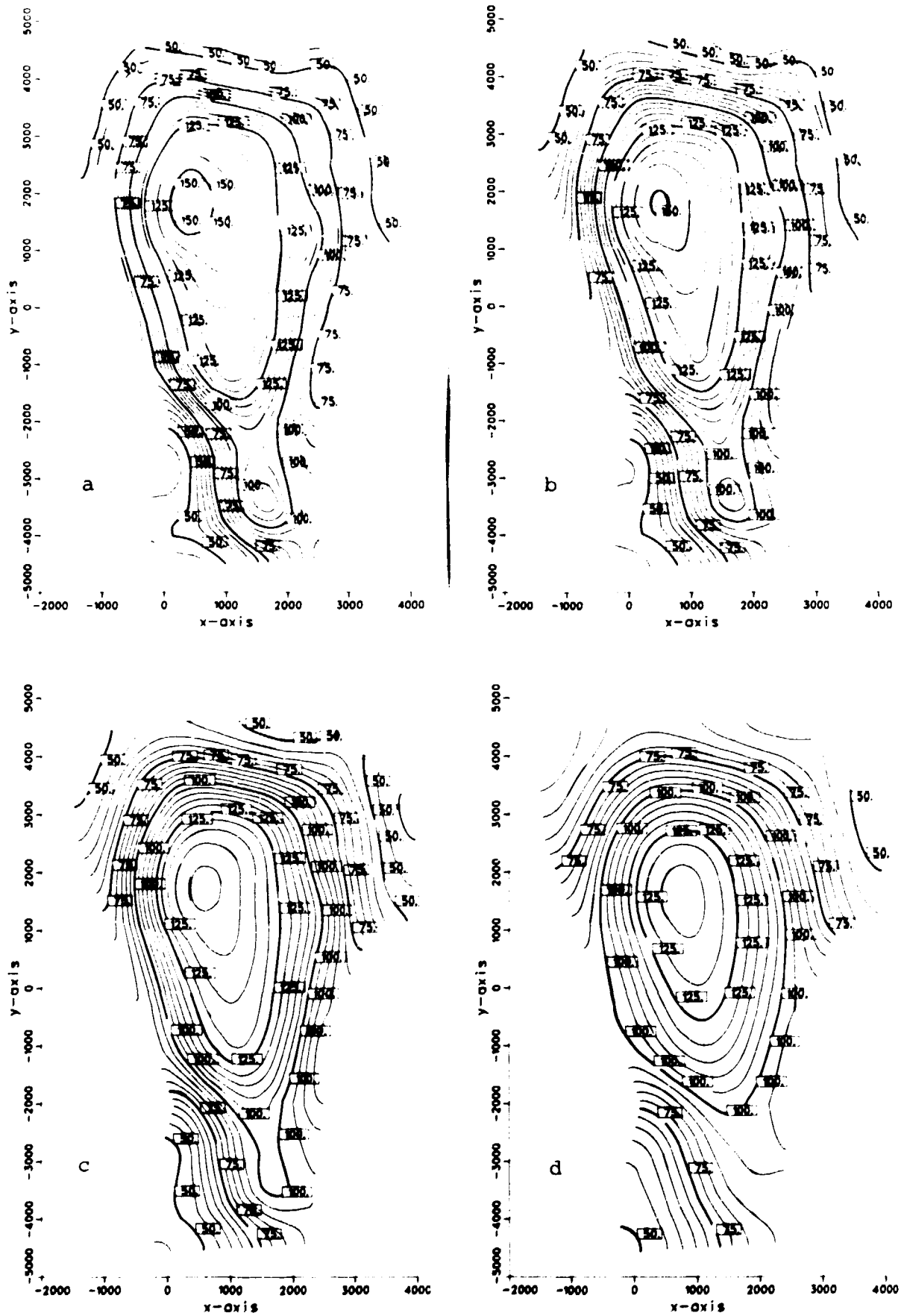
Fig 11-5.   Isopotential lines at different levels in the regio-
nal area.
a = -350 m, b = -520 m, c = -750 m, d = -1300 m.
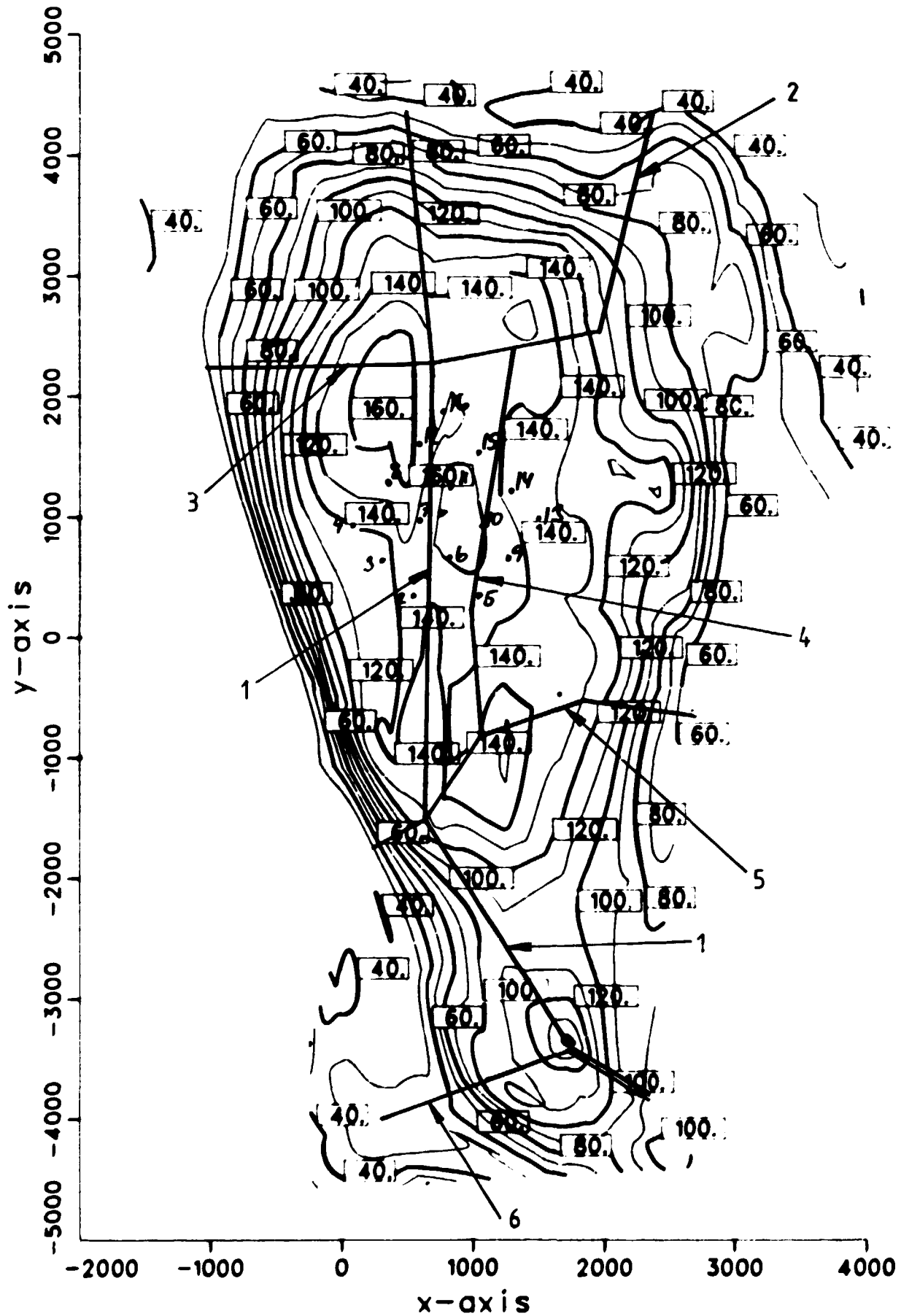
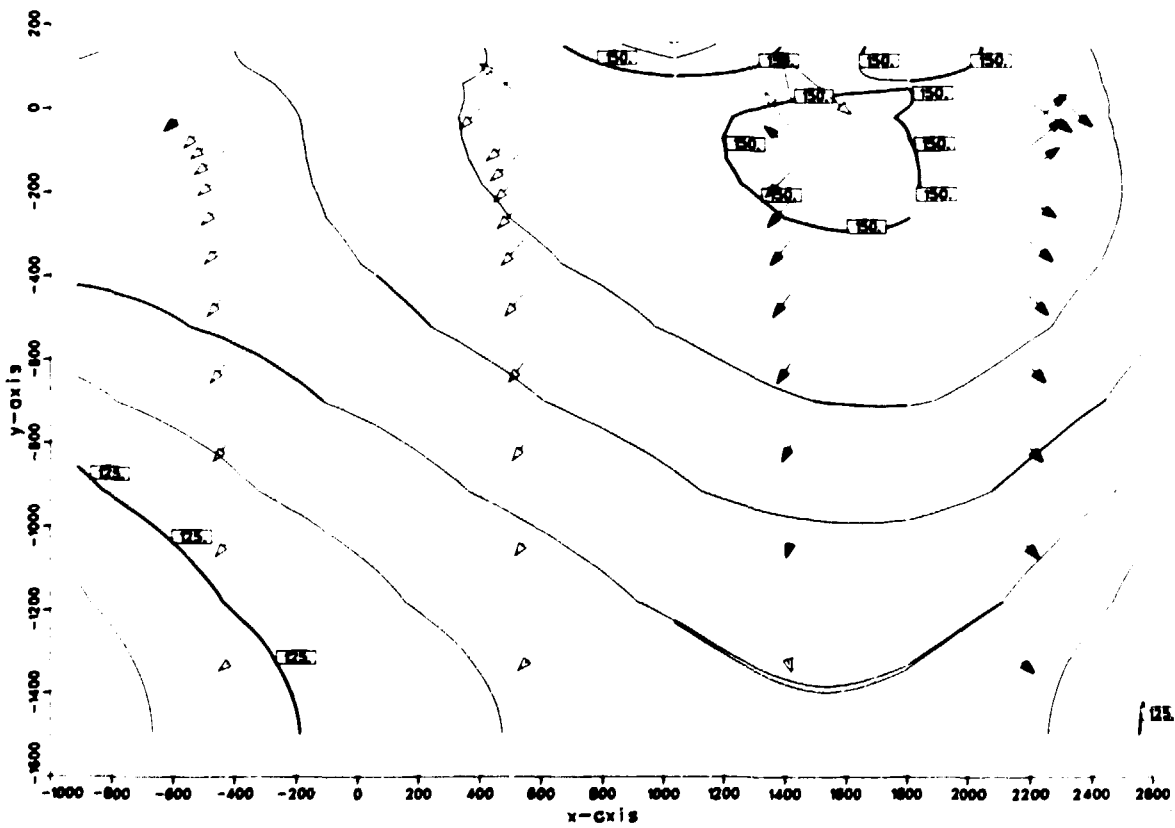Fig 11-6. Locations of vertical cross sections at regional area of Kamlunge. Starting points of trajectories discussed in section 11.2.5 are also shown.
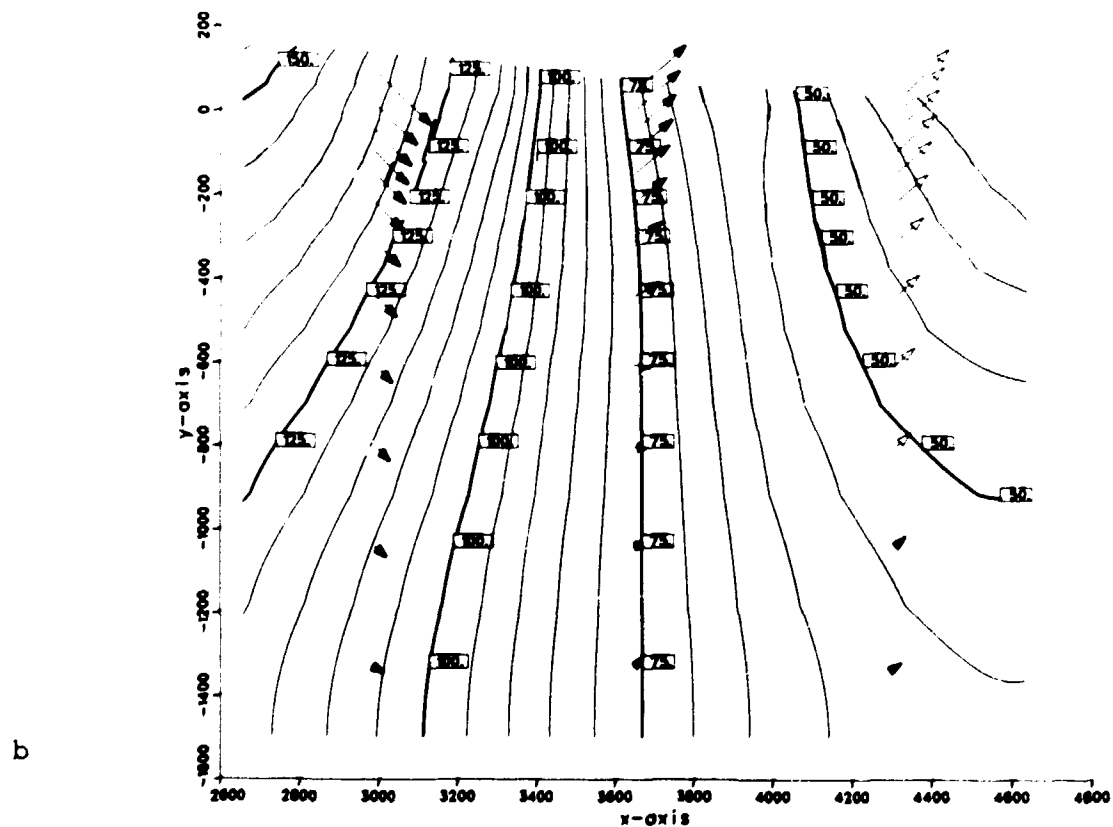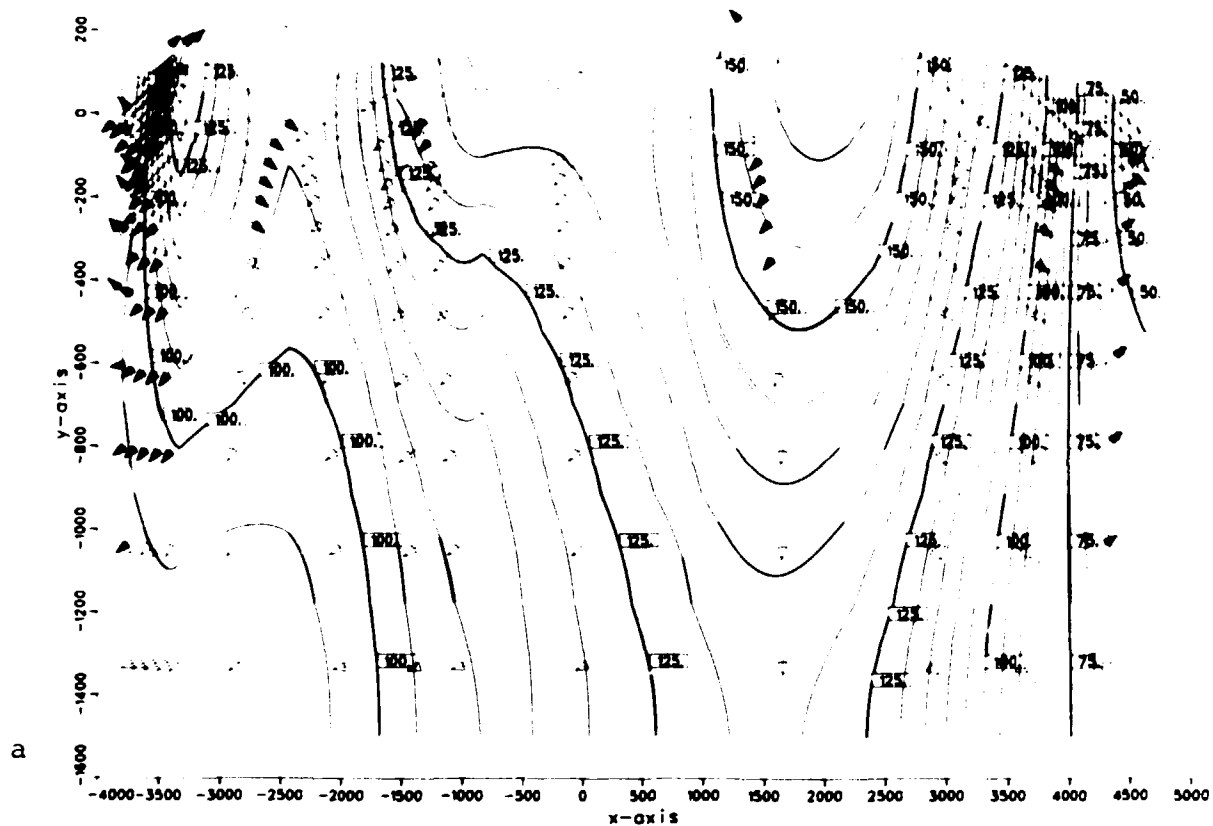
Fig 11-7.   Isopotentials and projected flow vectors at vertical
cross sections of the regional area at Kamlunge.
a = section no. 1, b = section no. 2.
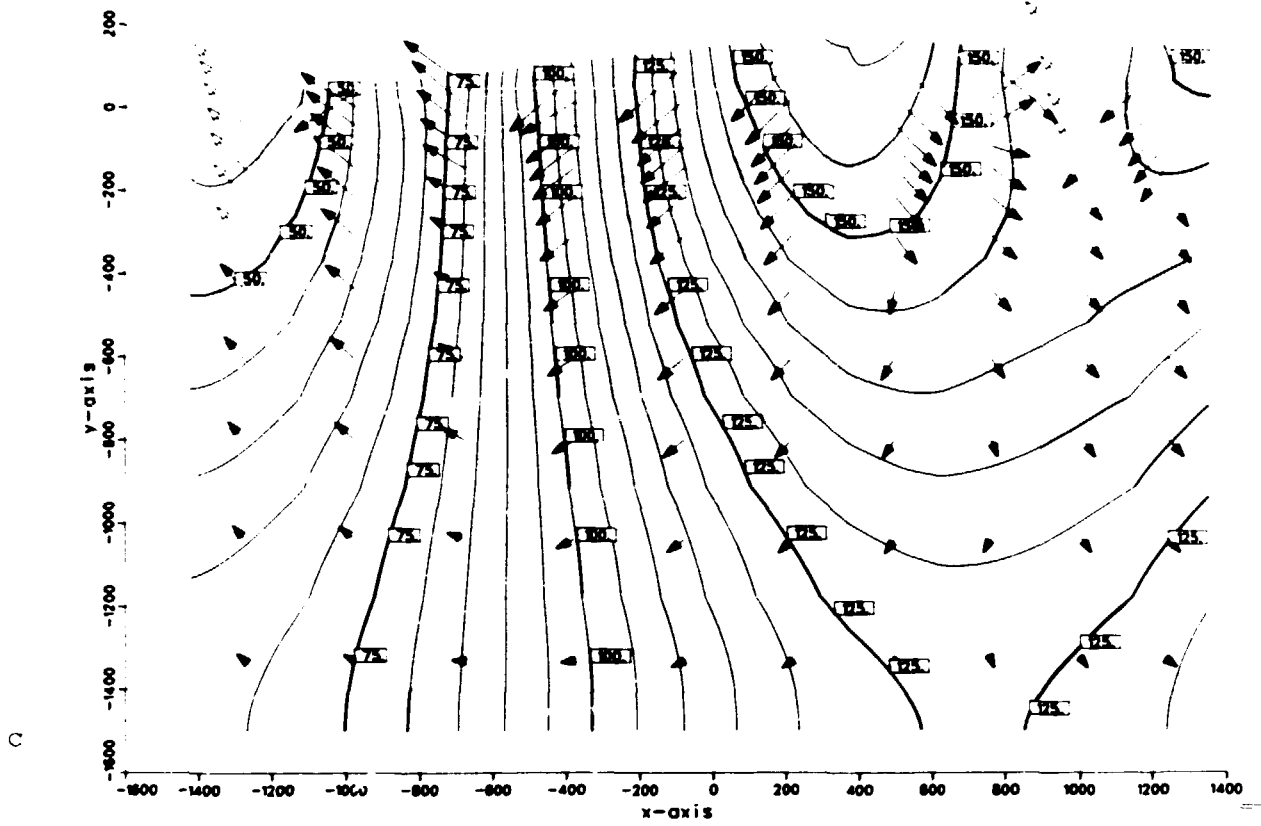
Fig 11-7. Isopotentials and projected flow vectors at vertical
cross sections of the regional area at Kamlunge.
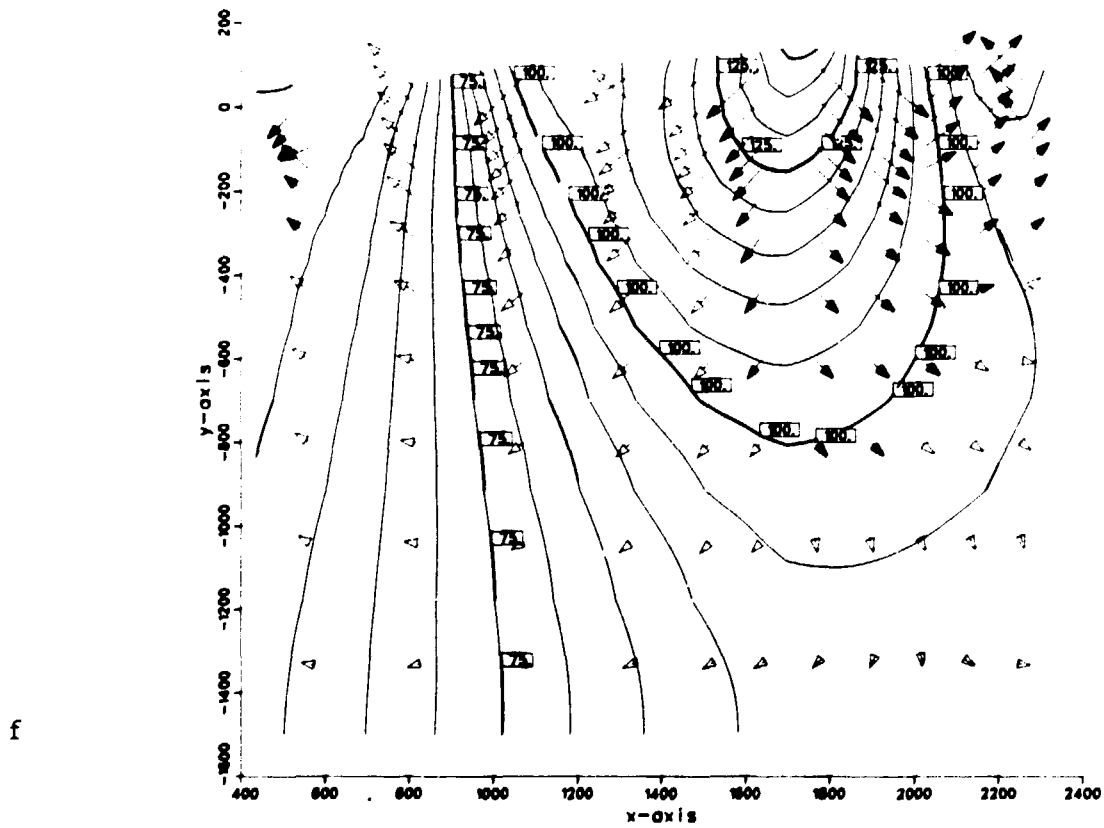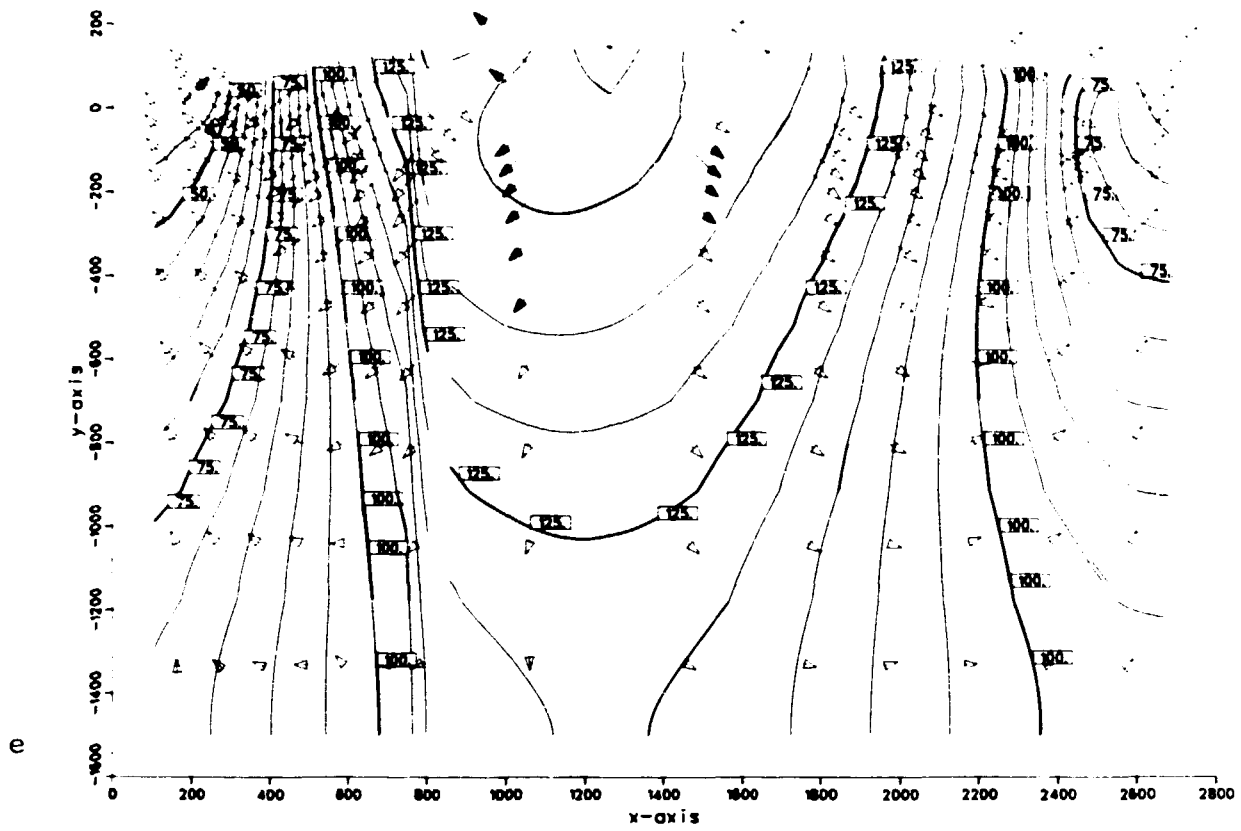c = section no. 3, d = section no. 4.

Fig 11-7.　Isopotentials and projected flow vectors at vertical
cross sections of the regional area at Kamlunge.
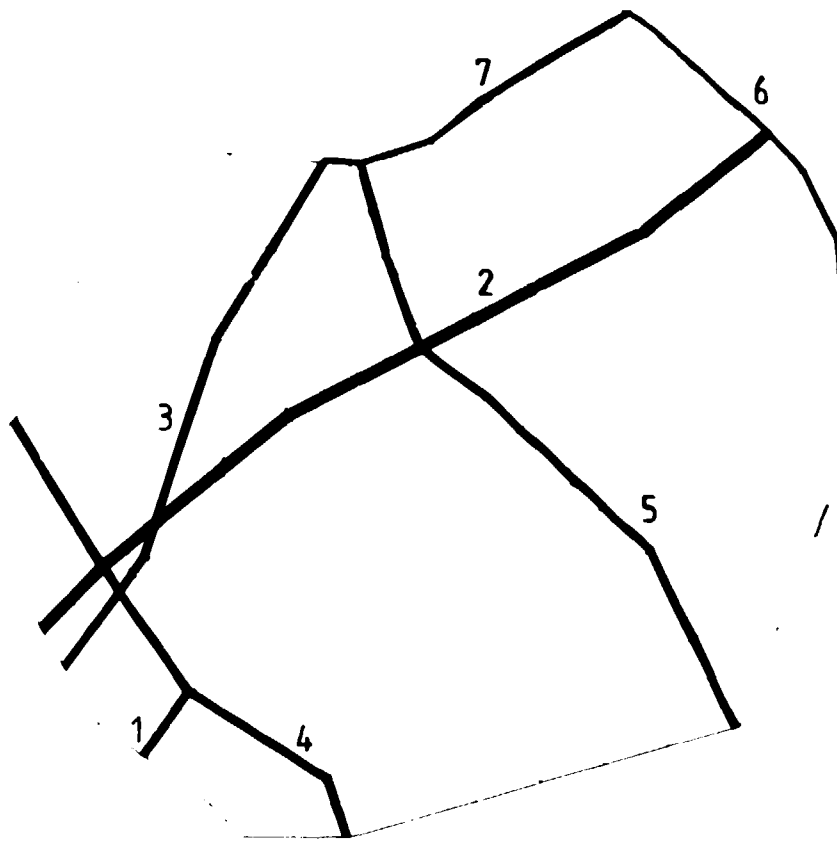e = section no. 5, f = section no. 6.

Fig 11-8. Fracture zones as modelled in the local area at Kam-
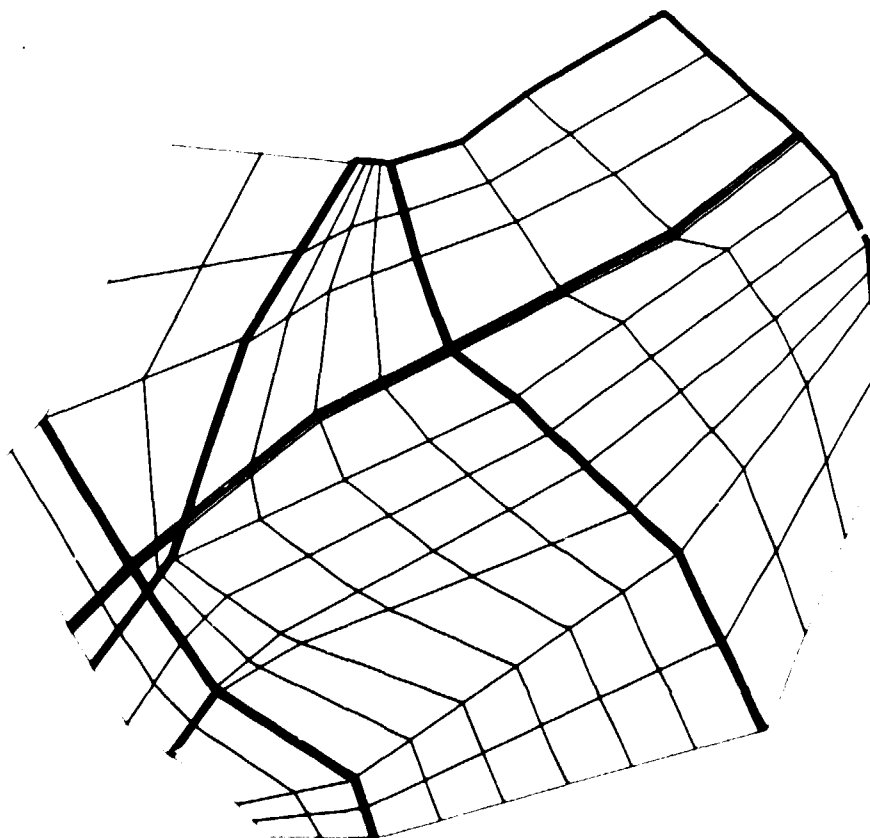lunge.

Fig 11-9. Top surface of the element mesh of the local area at
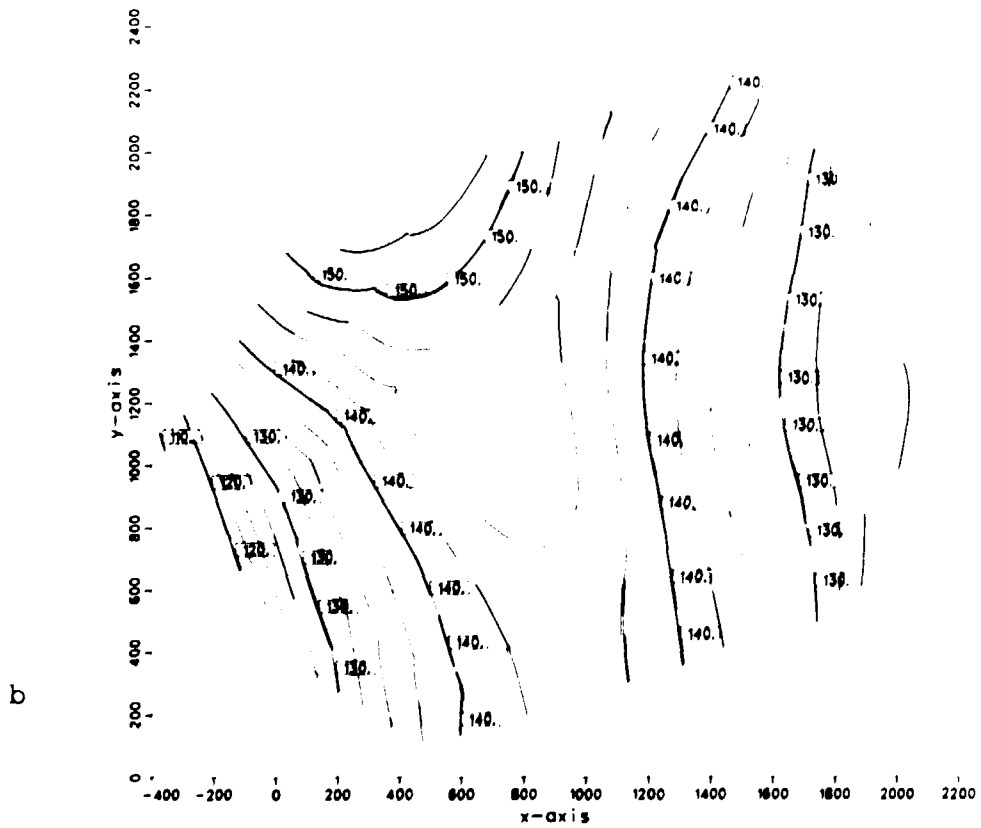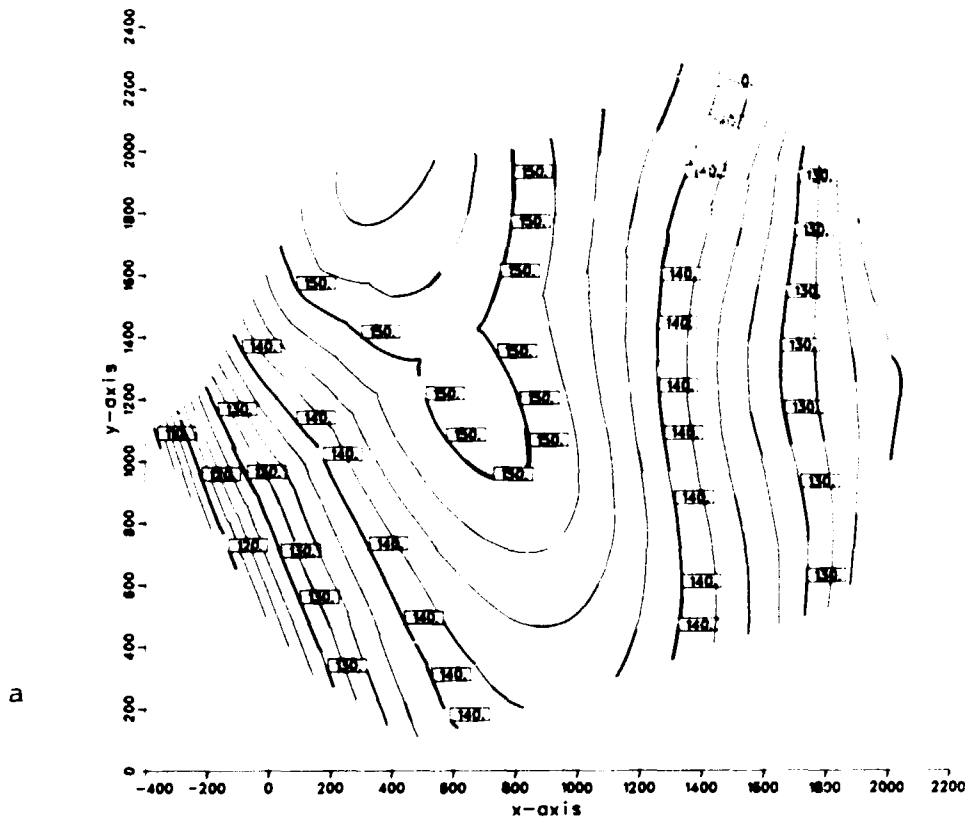Kamlunge.

Fig 11-10.   Isopotential lines in a horisontal cross section at
             -275 m.
             a = KAML, b = KAMS.
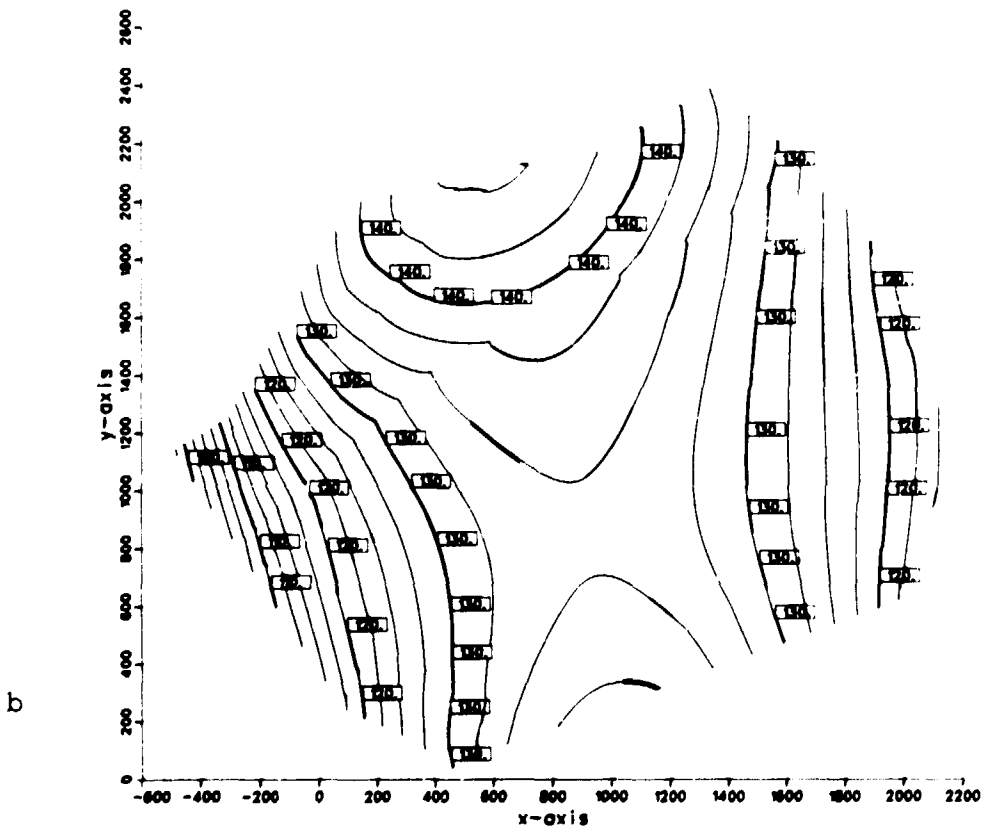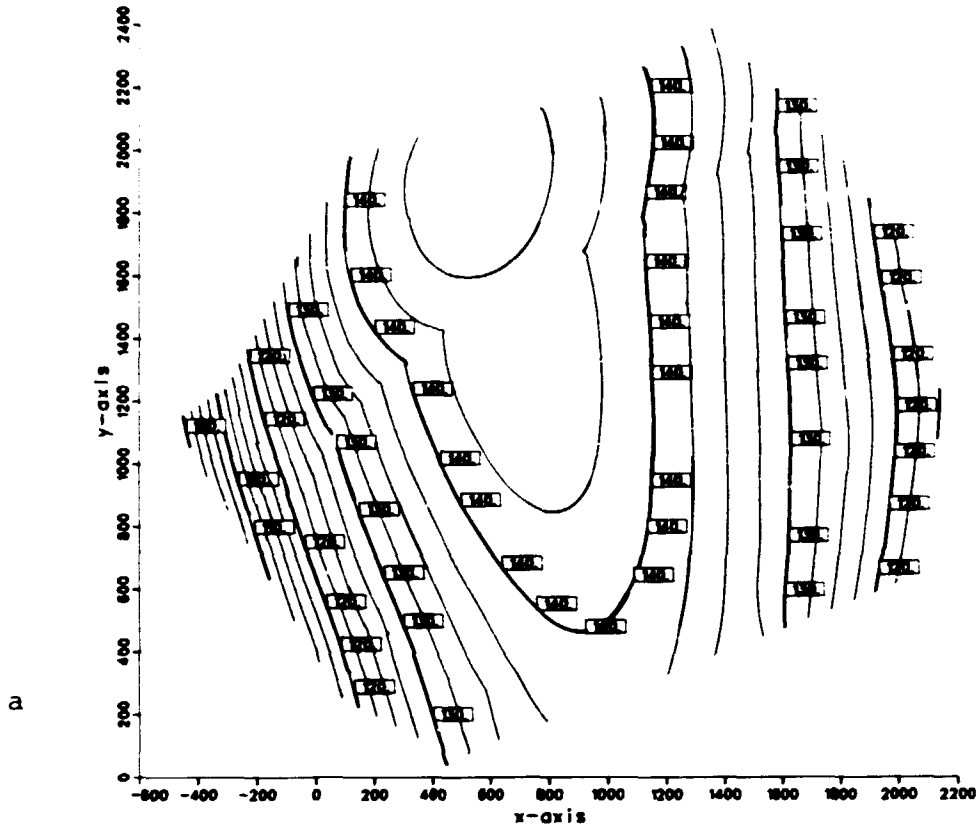
Fig 11-11.   Isopotential lines in a horisontal cross section at
             -650 m.
             a = KAML, b = KAMS.
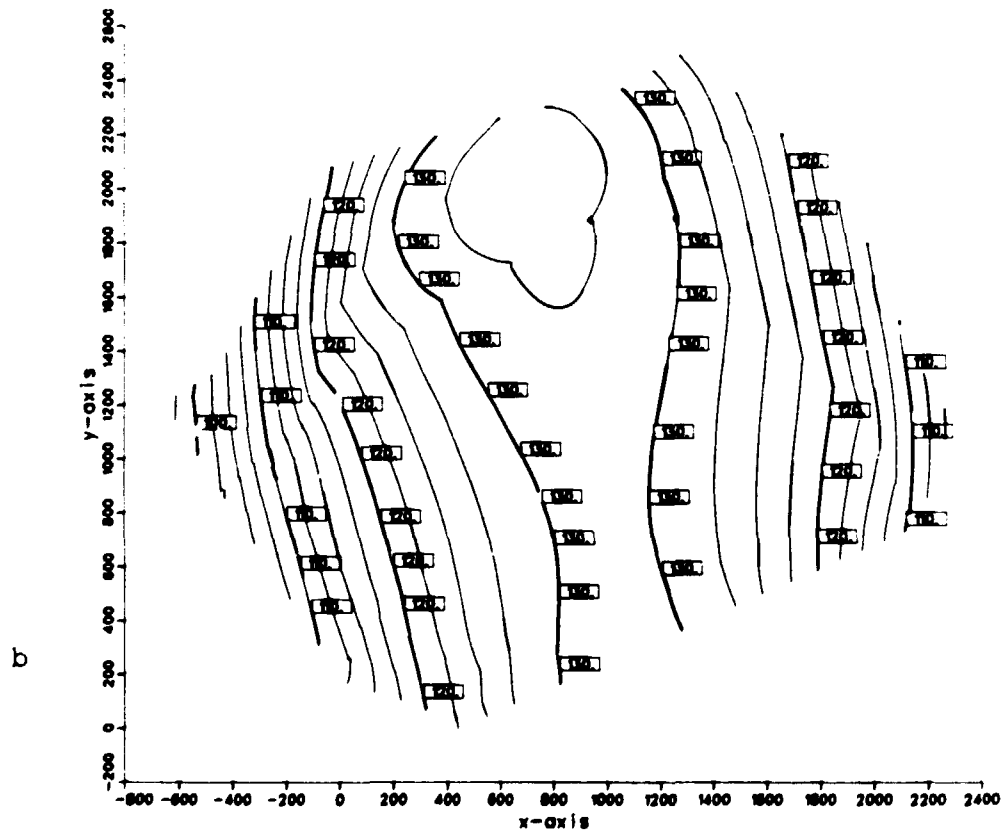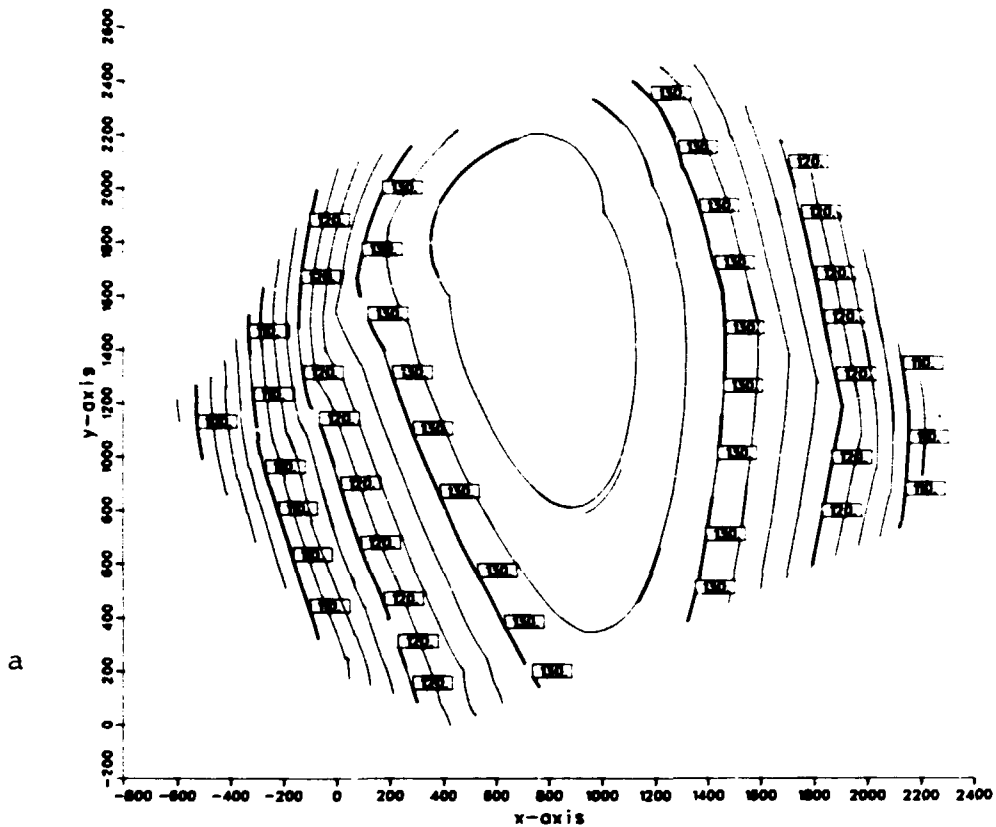
Fig 11-12. Isopotential lines in a horizontal cross section at
            -1150 m.
            a = KAML, b = KAMS.
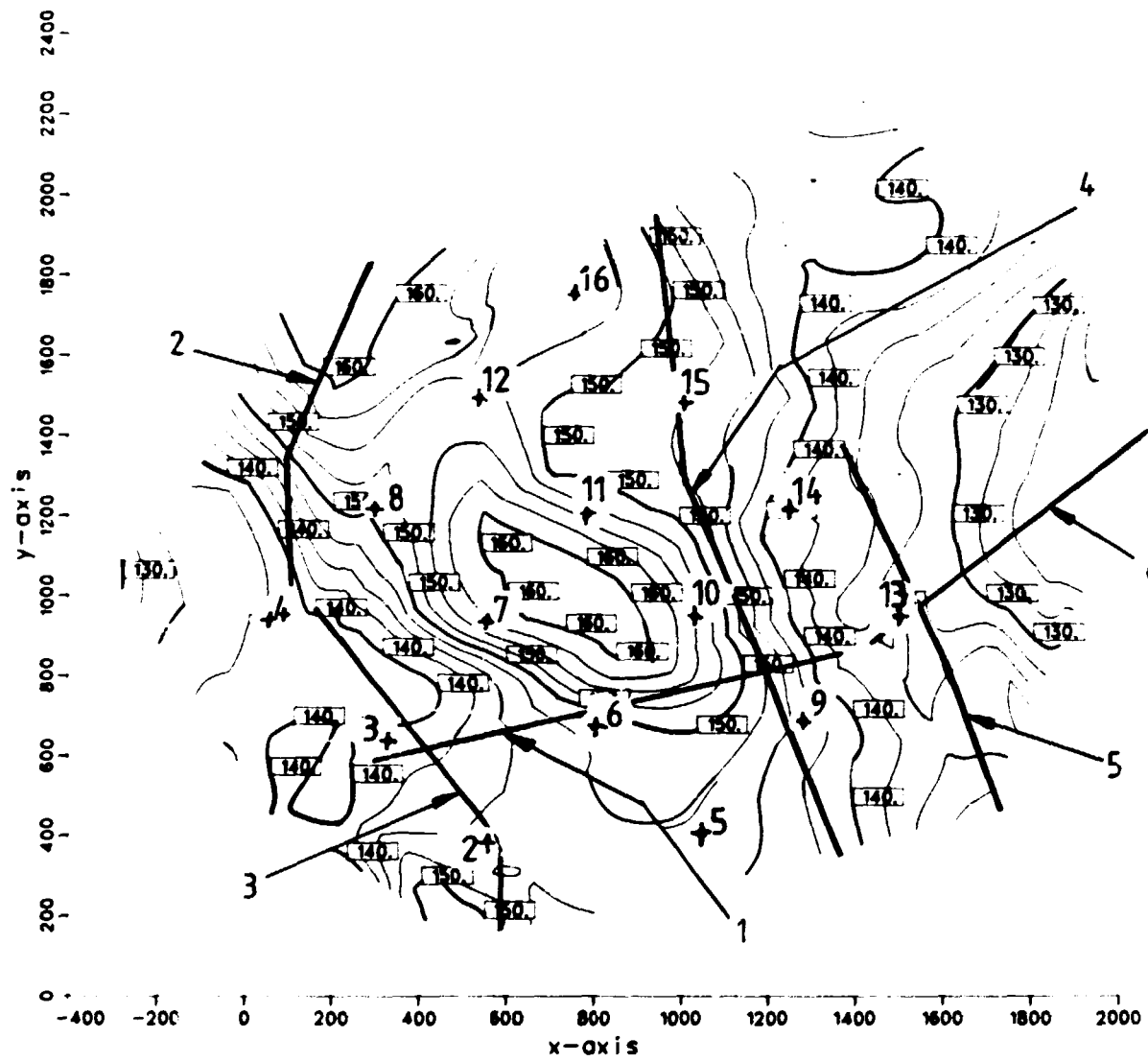
Fig 11-13. Locations of vertical cross sections at the local area at Kamlunge. Starting points of trajectories discussed in section 11.4.3 are also shown.
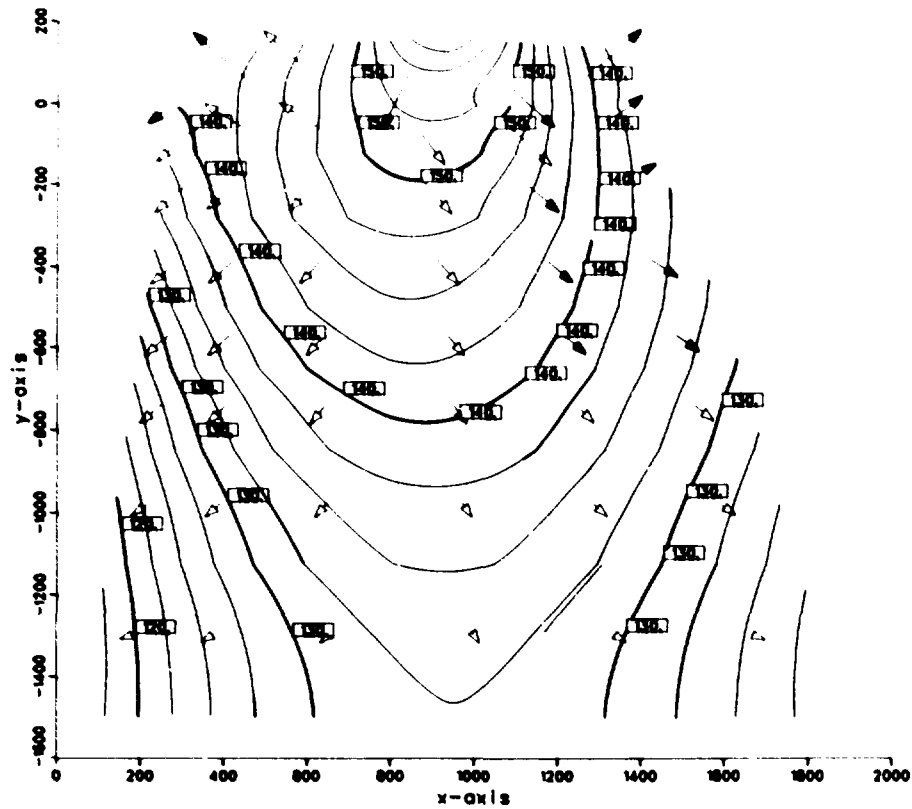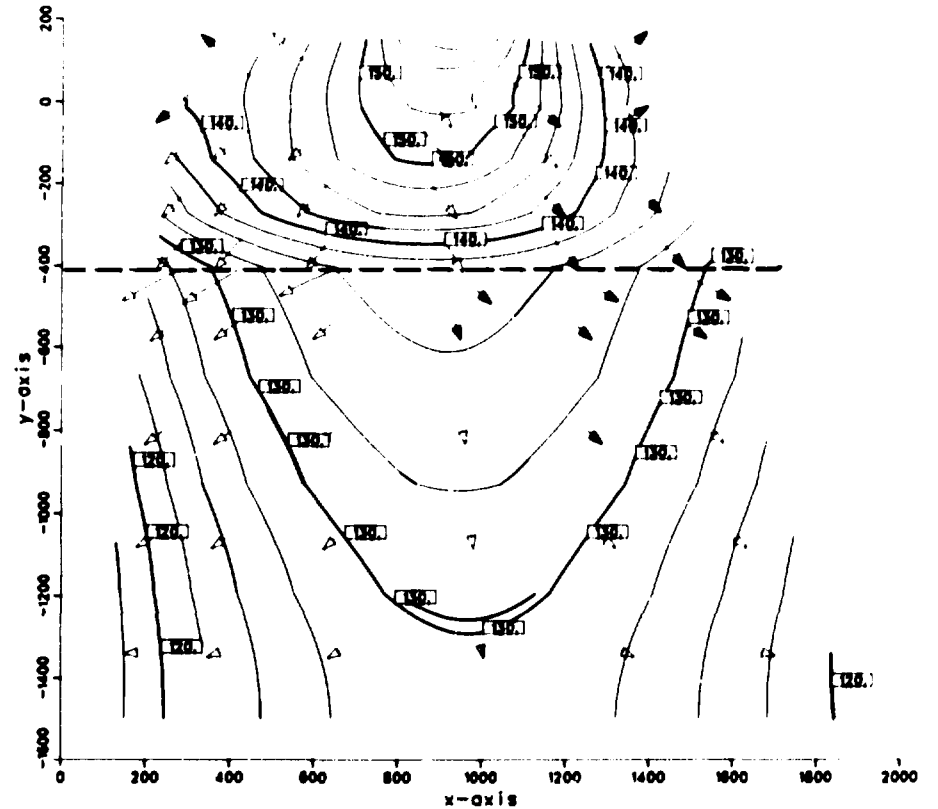
Fig 11-14. Isopotentials and projected flow vectors at vertical
section no. 1.
a = KAML, b = KAMS.
The dashed horisontal line denotes the horisontal fracture zone.
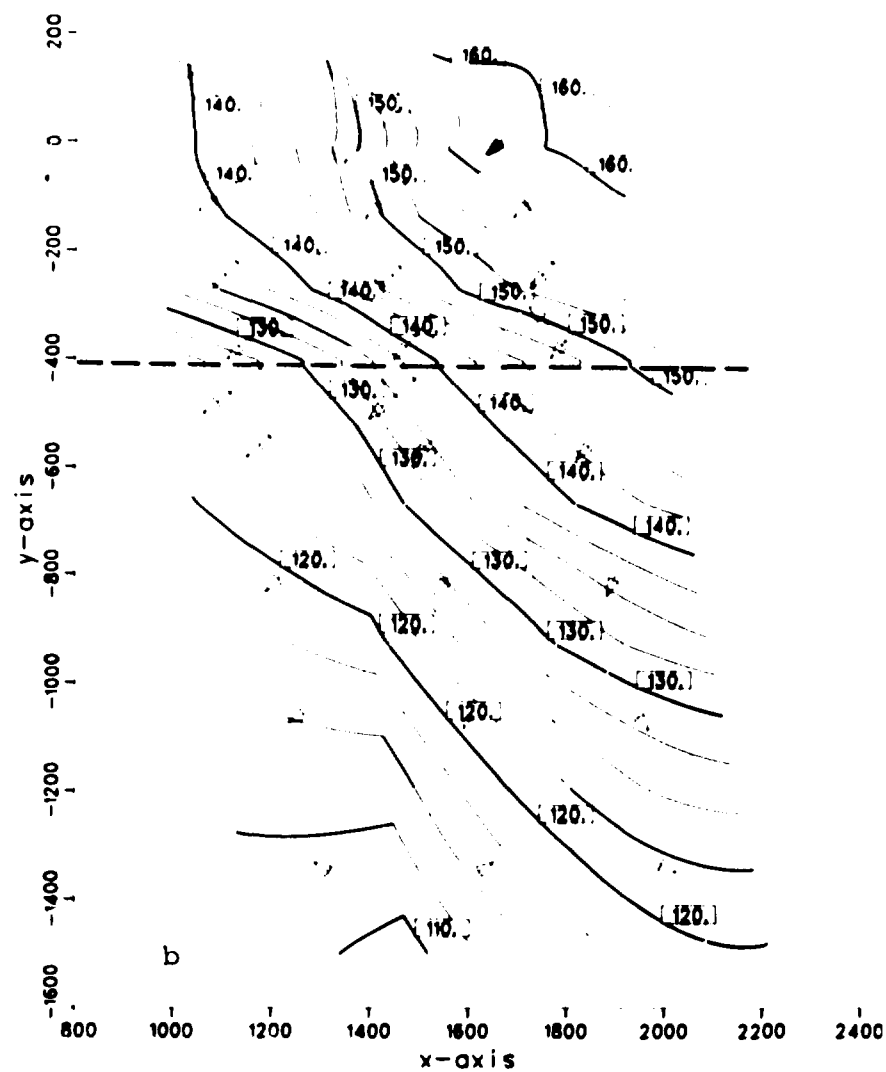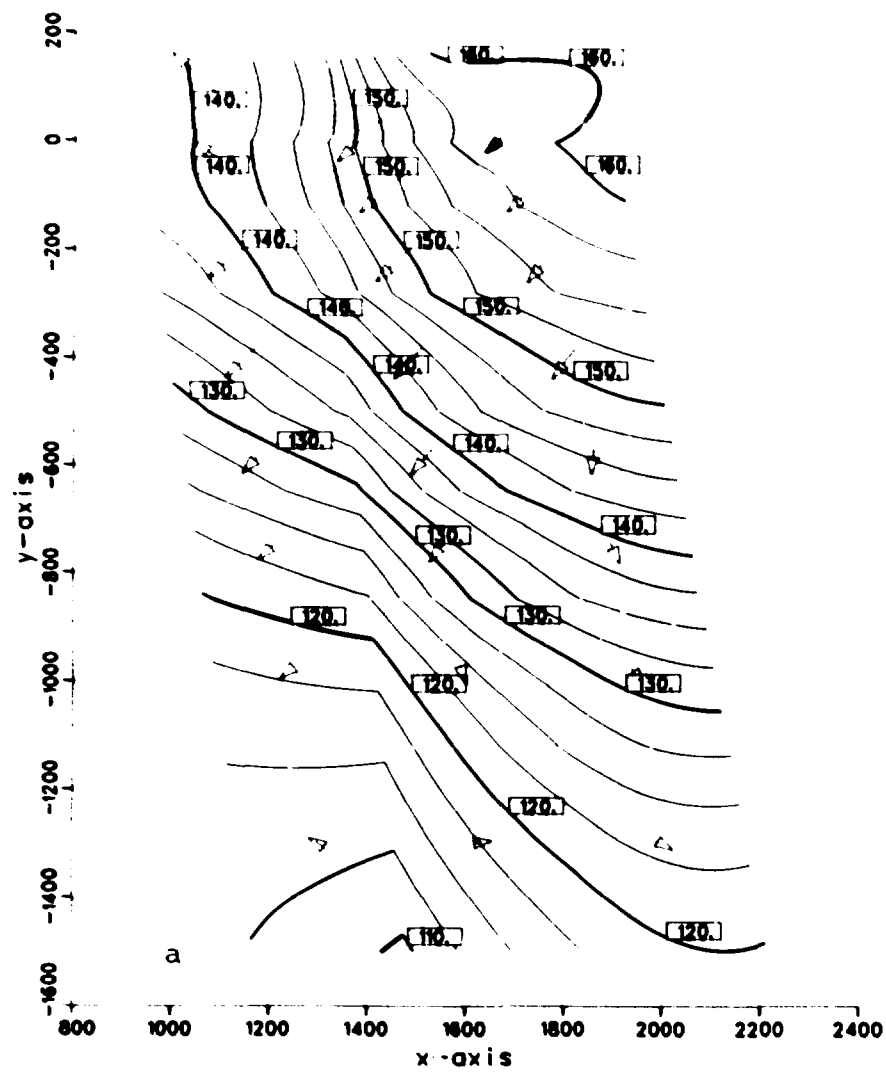
Fig 11-15. Isopotentials and projected flow vectors at vertical
section no. 2.
a = KAML, b = KAMS.
The dashed horisontal line denotes the horisontal fracture zone.
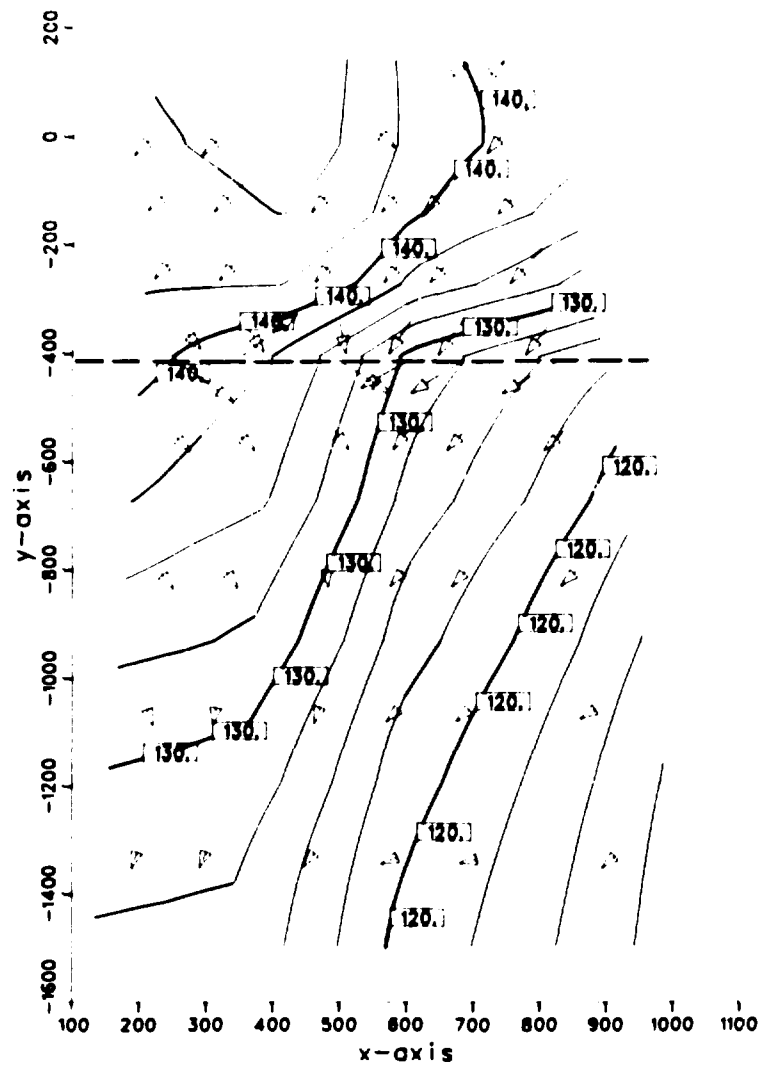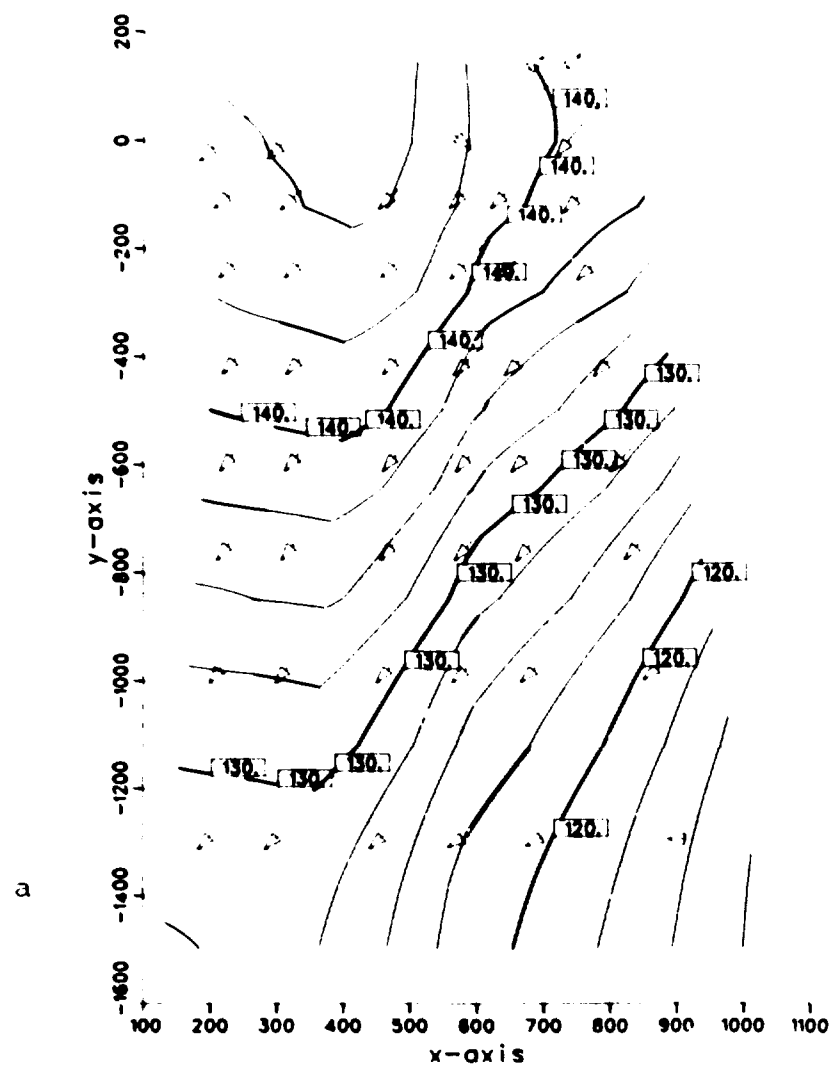
Fig 11-16. Isopotentials and projected flow vectors at vertical
            cross section no. 3.
            a = KAML, b = KAMS
            The dashed horisontal line denotes the horisontal fracture zone.
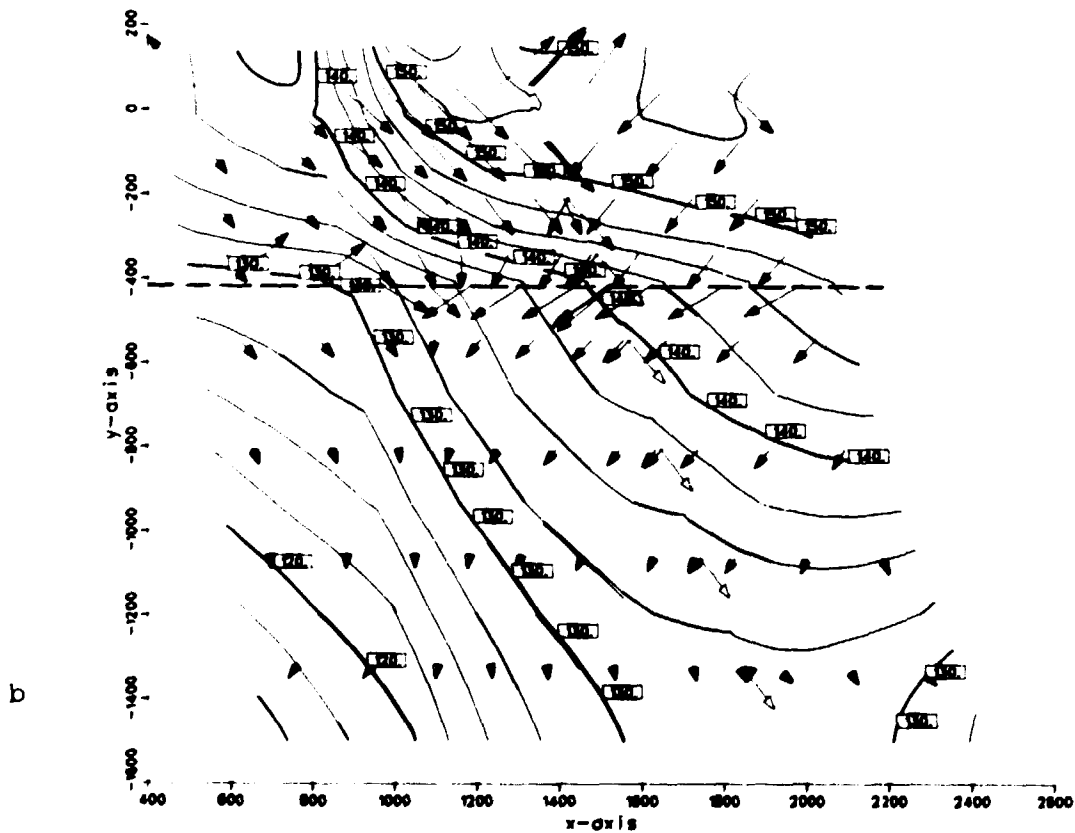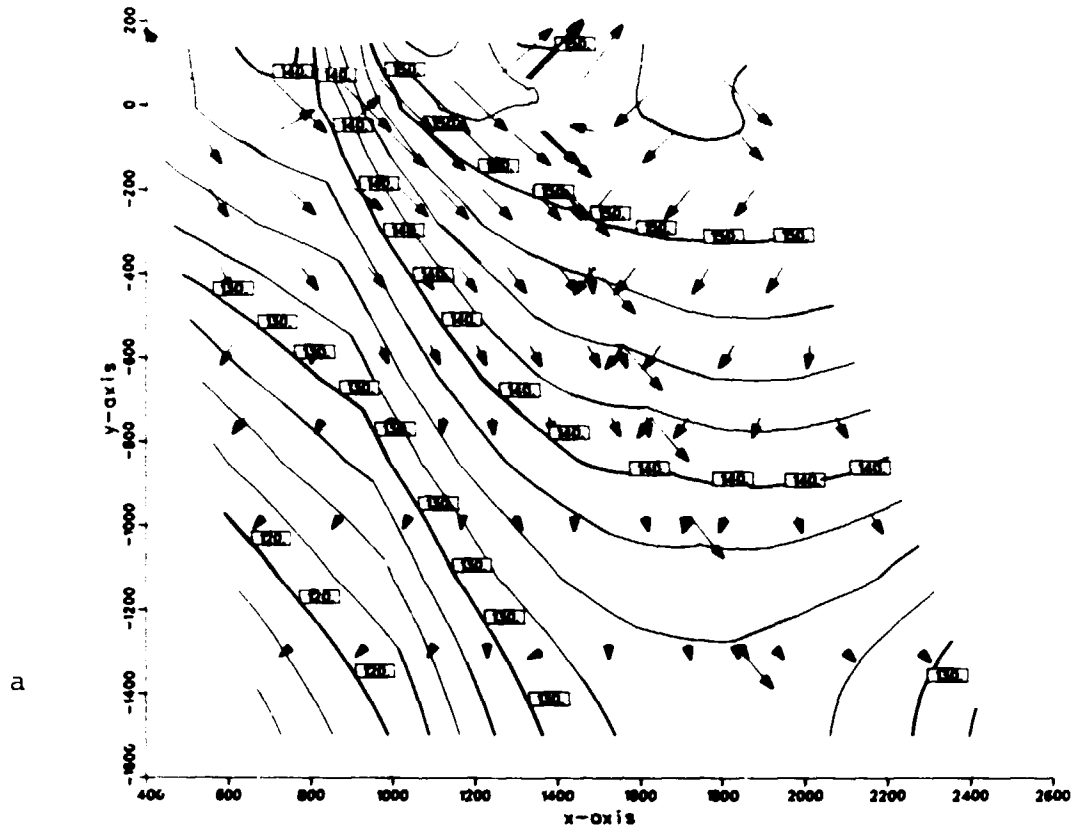
Fig 11-17. Isopotentials and projected flow vectors at vertical
            section no. 4.
            a = KAML, b = KAMS.
            The dashed horisontal line denotes the horisontal fracture zone.
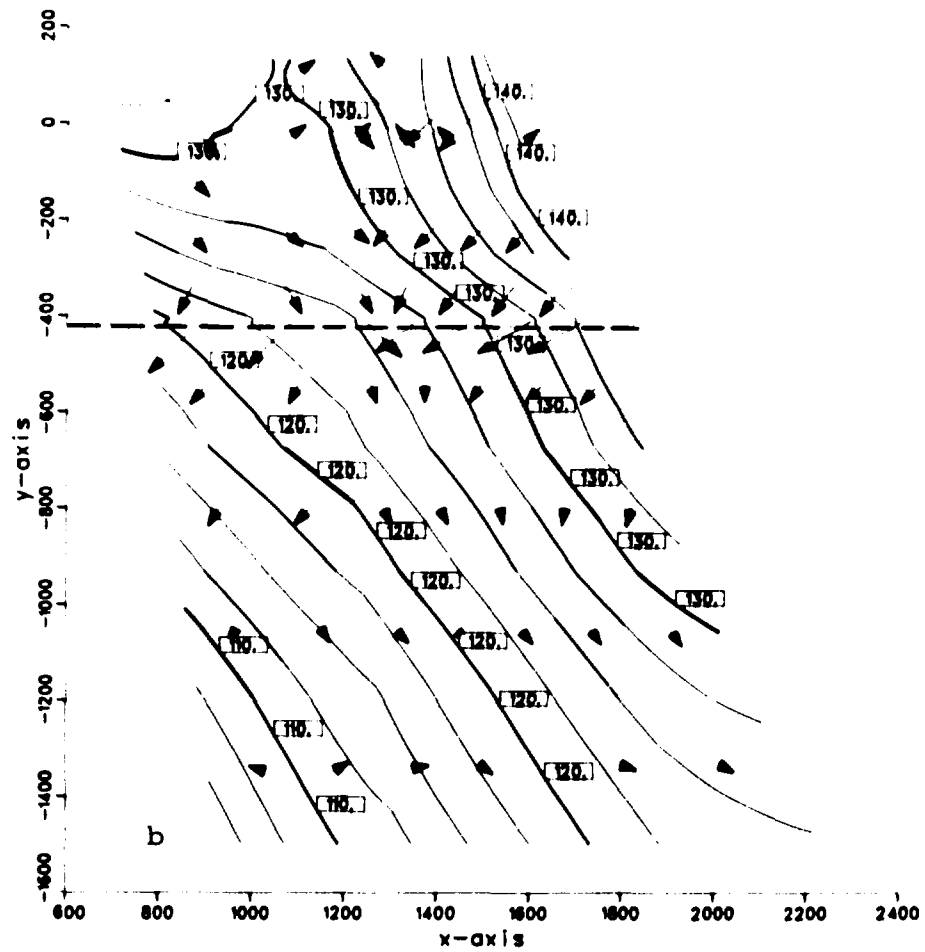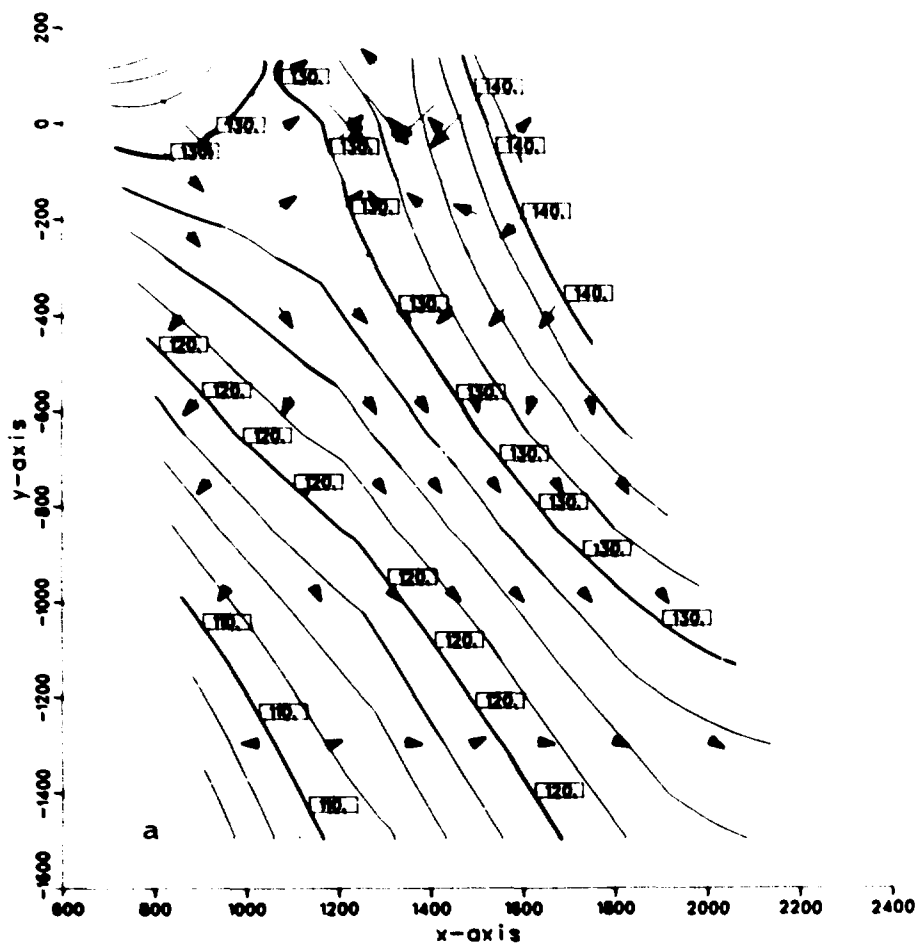
Fig 11-18. Isopotentials and projected flow vectors at vertical
            section no. 5.
            a = KAML, b = KAMS
            The dashed horisontal line denotes the horisontal fracture zone.
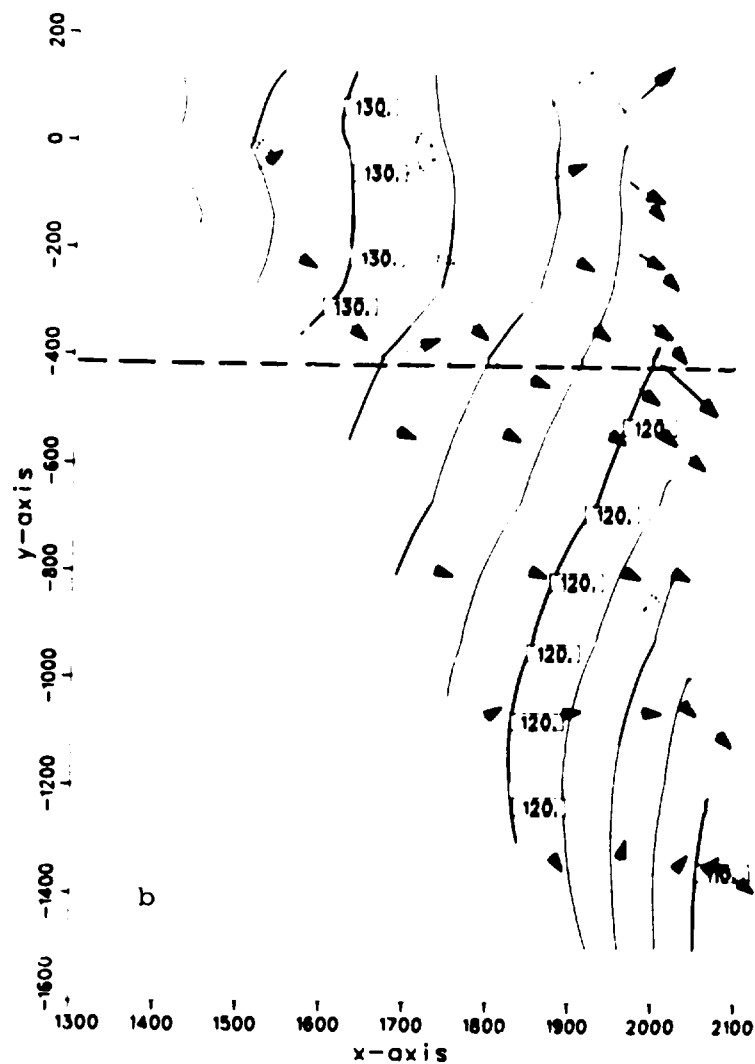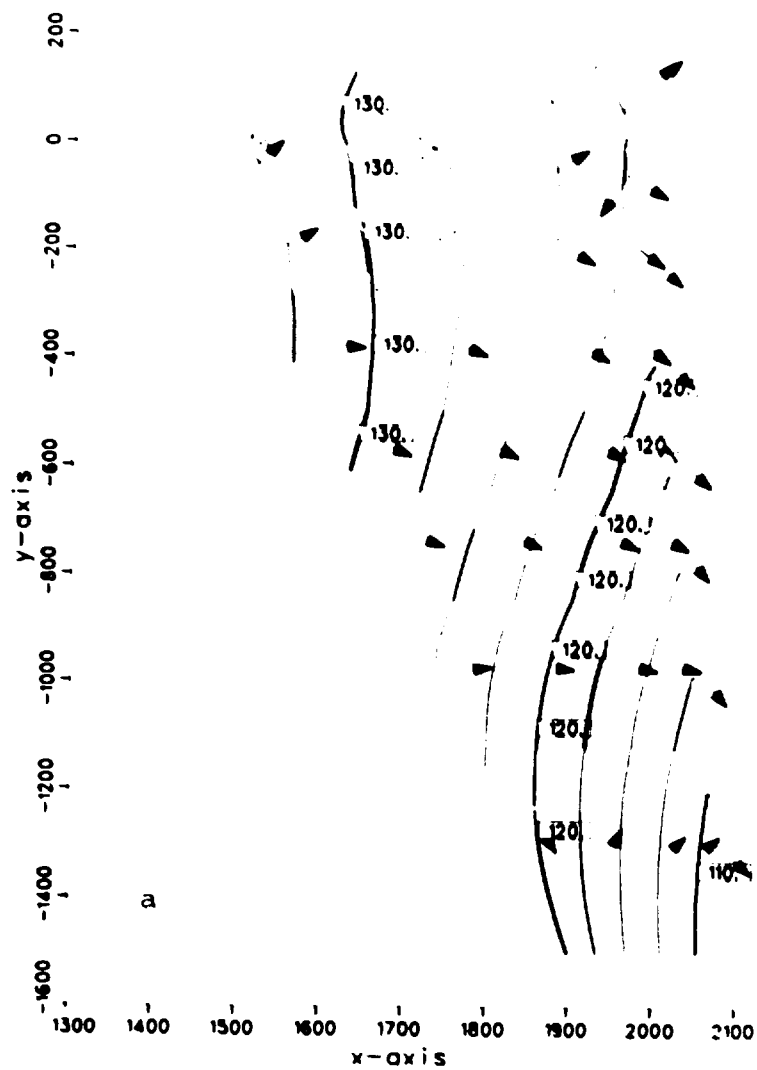
Fig 11-19. Isopotentials and projected flow vectors at vertical
section no. 6.
a = KAML, b = KAMS

The dashed horisontal line denotes the horisontal fracture zone.
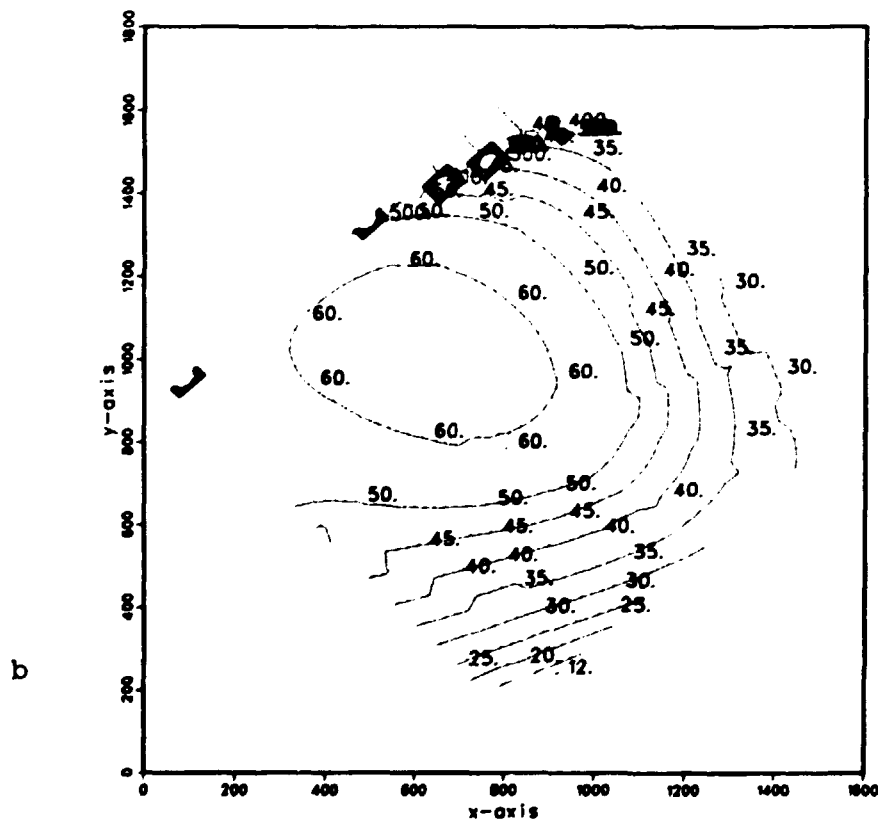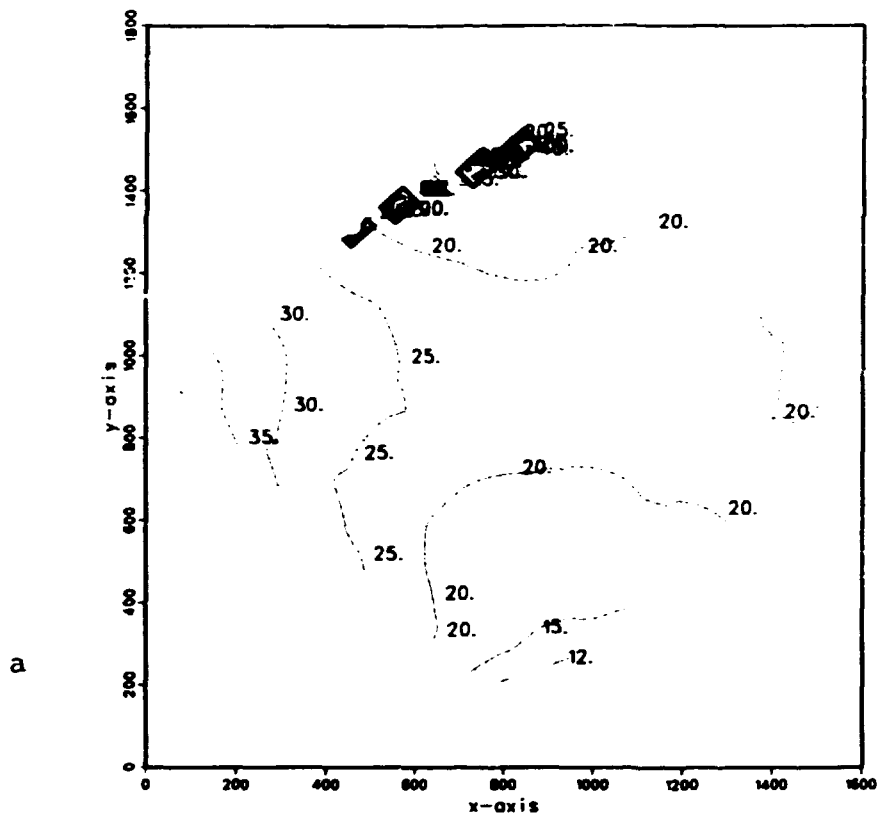
Fig 11-20. Fluxes at 450 m below ground surface $(ml/m^2 \cdot yr)$.
a = KAML, b = KAMS.
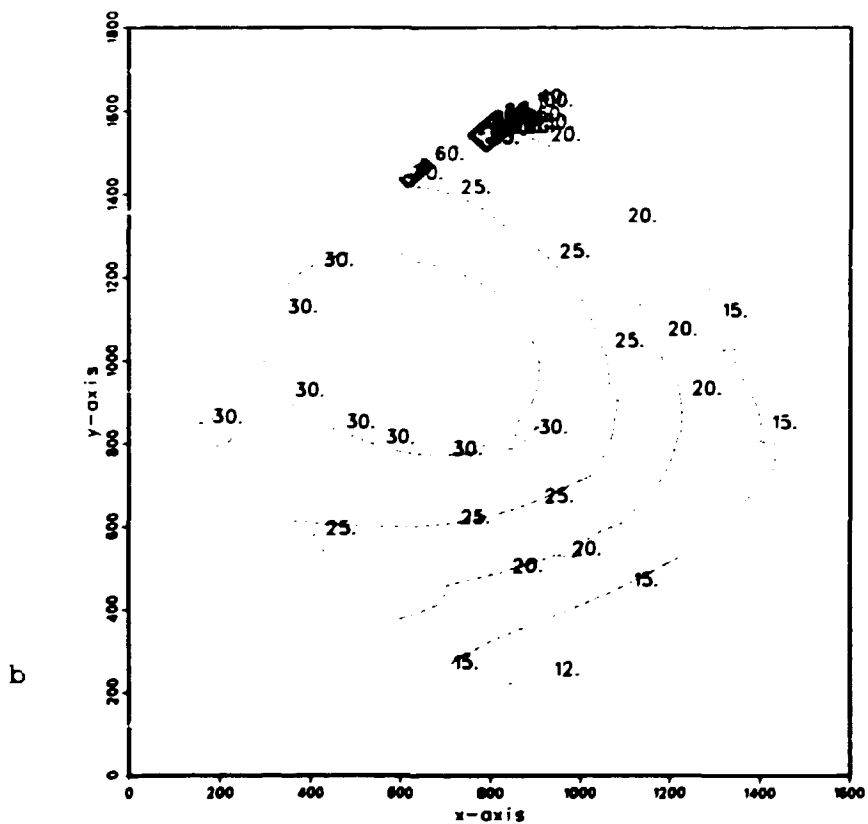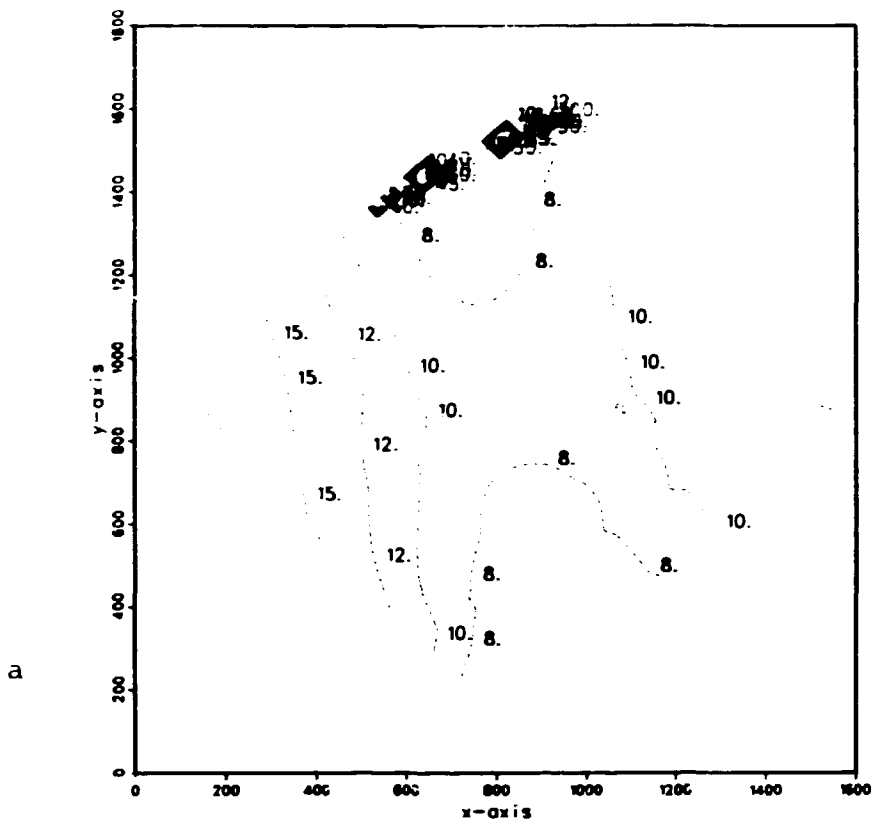
Fig 11-21. Fluxes at 550 m below ground surface $(ml/m^2 \cdot yr)$.
a = KAML, b = KAMS.
Cross section located just above the horisontal frac-
ture zone.
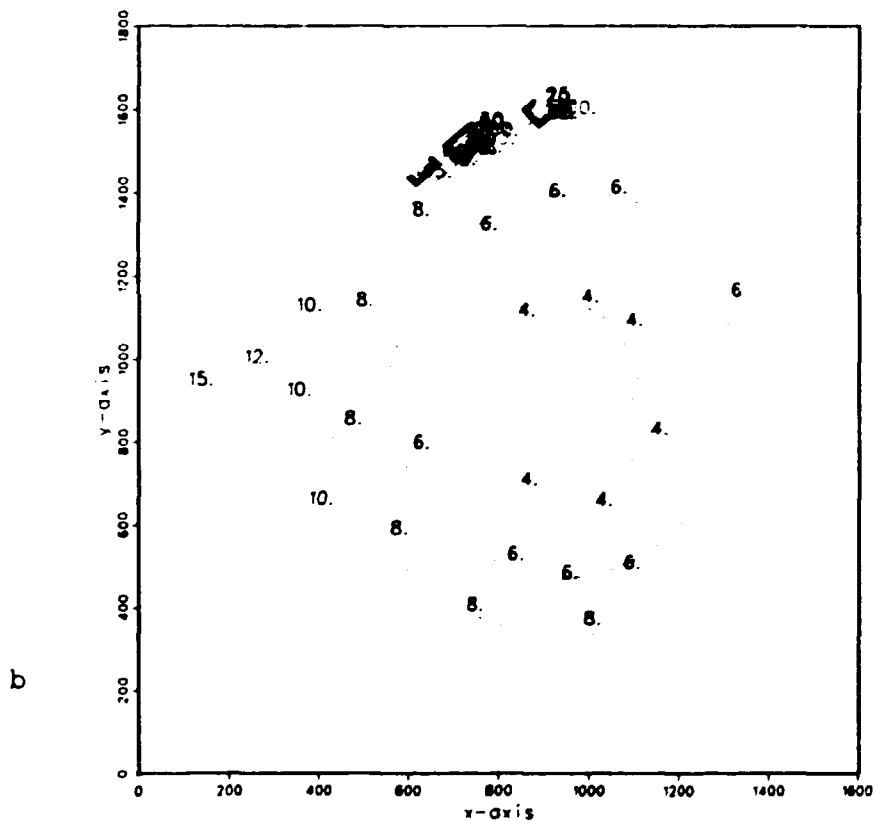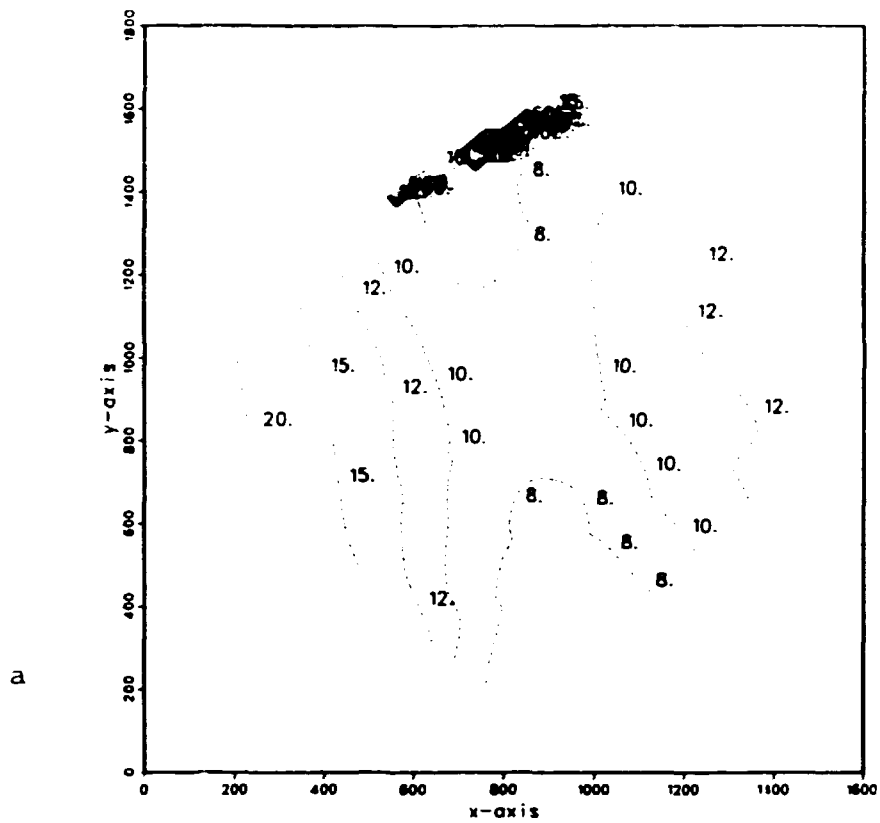
Fig 11-22. Fluxes at 570 m below ground surface ($ml/m^2 \cdot yr$).
a = KAML, b = KAMS.
Cross section located just below the horisontal frac-
ture zone.
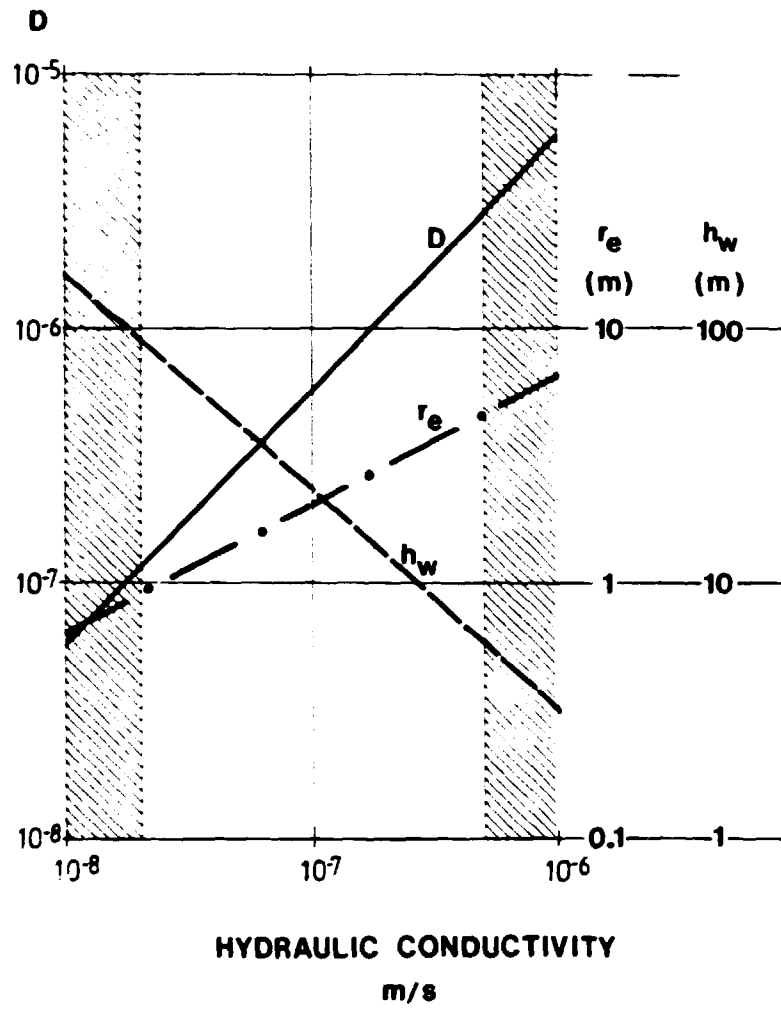
Figure 12.3.1. Drawdown h_w, influence radius r_e and
relation D between water from repository and
discharging well.

LIST OF KBS's TECHNICAL REPORTS

1977-78

TR 121   KBS Technical Reports 1 - 120.
          Summaries. Stockholm, May 1979.

1979

TR 79-28 The KBS Annual Report 1979.
          KBS Technical Reports 79-01--79-27.
          Summaries. Stockholm, March 1980.

1980

TR 80-26 The KBS Annual Report 1980.
          KBS Technical Reports 80-01--80-25.
          Summaries. Stockholm, March 1981.

1981

TR 81-17 The KBS Annual Report 1981.
          KBS Technical Reports 81-01--81-16
          Summaries. Stockholm, April 1982.

1983

TR 83-01 Radionuclide transport in a single fissure
          A laboratory study
          Trygve E Eriksen
          Department of Nuclear Chemistry
          The Royal Institute of Technology
          Stockholm, Sweden 1983-01-19

TR 83-02 The possible effects of alfa and beta radiolysis
          on the matrix dissolution of spent nuclear fuel
          I Grenthe
          I Puigdomènech
          J Bruno
          Department of Inorganic Chemistry
          Royal Institute of Technology
          Stockholm, Sweden January 1983

TR 83-03   Smectite alteration
           Proceedings of a colloquium at State University of
           New York at Buffalo, May 26-27, 1982
           Compiled by Duwayne M Anderson
           State University of New York at Buffalo
           February 15, 1983

TR 83-04   Stability of bentonite gels in crystalline rock -
           Physical aspects
           Roland Pusch
           Division Soil Mechanics, University of Luleå
           Luleå, Sweden, 1983-02-20

TR 83-05   Studies in pitting corrosion on archeological
           bronzes - Copper
           Åke Bresle
           Jozef Saers
           Birgit Arrhenius
           Archaeological Research Laboratory
           University of Stockholm
           Stockholm, Sweden 1983-01-02

TR 83-06   Investigation of the stress corrosion cracking of
           pure copper
           L A Benjamin
           D Hardie
           R N Parkins
           University of Newcastle upon Tyne
           Department of Metallurgy and Engineering Materials
           Newcastle upon Tyne, Great Britain, April 1983

TR 83-07   Sorption of radionuclides on geologic media -
           A literature survey. I: Fission Products
           K Andersson
           B Allard
           Department of Nuclear Chemistry
           Chalmers University of Technology
           Göteborg, Sweden 1983-01-31

TR 83-08   Formation and properties of actinide colloids
           U Olofsson
           B Allard
           M Bengtsson
           B Torstenfelt
           K Andersson
           Department of Nuclear Chemistry
           Chalmers University of Technology
           Göteborg, Sweden 1983-01-30

TR 83-09   Complexes of actinides with naturally occurring
           organic substances - Literature survey
           U Olofsson
           B Allard
           Department of Nucluear Chemistry
           Chalmers University of Technology
           Göteborg, Sweden 1983-02-15

TR 83-10   Radiolysis in nature:
           Evidence from the Oklo natural reactors
           David B Curtis
           Alexander J Gancarz
           New Mexico, USA February 1983

TR 83-11 Description of recipient areas related to final
storage of unreprocessed spent nuclear fuel
Björn Sundblad
Ulla Bergström
Studsvik Energiteknik AB
Nyköping, Sweden 1983-02-07

TR 83-12 Calculation of activity content and related
properties in PWR and BWR fuel using ORIGEN 2
Ove Edlund
Studsvik Energiteknik AB
Nyköping, Sweden 1983-03-07

TR 83-13 Sorption and diffusion studies of Cs and I in
concrete
K Andersson
B Torstenfelt
B Allard
Department of Nuclear Chemistry
Chalmers University of Technology
Göteborg, Sweden 1983-01-15

TR 83-14 The complexation of Eu(III) by fulvic acid
J A Marinsky
State University of New York at Buffalo, Buffalo,NY
1983-03-31

TR 83-15 Diffusion measurements in crystalline rocks
Kristina Skagius
Ivars Neretnieks
Royal Institute of Technology
Stockholm, Sweden 1983-03-11

TR 83-16 Stability of deep-sited smectite minerals in
crystalline rock - chemical aspects
Roland Pusch
Division of Soil Mechanics, University of Luleå
1983-03-30

TR 83-17 Analysis of groundwater from deep boreholes in
Gideå Sif Laurent .
Swedish Environmental Research Institute
Stockholm, Sweden 1983-03-09

TR 83-18 Migration experiments in Studsvik
O Landström
Studsvik Energiteknik AB
C-E Klockars
O Persson
E-L Tullborg
S Å Larson
Swedish Geological
K Andersson
B Allard
B Torstenfelt
Chalmers University of Technology
1983-01-31

TR 83-19   Analysis of groundwater from deep boreholes in
           Fjällveden
           Sif Laurent
           Swedish Environmental Research Institute
           Stockholm, Sweden 1983-03-29

TR 83-20   Encapsulation and handling of spent nuclear fuel
           for final disposal
           1   Welded copper canisters
           2   Pressed copper canisters (HIPOW)
           3   BWR Channels in Concrete
           B Lönnerberg, ASEA-ATOM
           H Larker, ASEA
           L Ageskog, VBB
           May 1983

TR 83-21   An analysis of the conditions of gas migration
           from a low-level radioactive waste repository
           C Braester
           Israel Institute of Technology, Haifa, Israel
           R Thunvik
           Royal Institute of Technology
           November 1982

TR 83-22   Calculated temperature field in and around a
           repository for spent nuclear fuel
           Taivo Tarandi, VBB
           Stockholm, Sweden April 1983

TR 83-23   Preparation of titanates and zeolites and their
           uses in radioactive waste management, particularly
           in the treatment of spent resins
           Å Hultgren, editor
           C Airola
           Studsvik Energiteknik AB
           S Forberg, Royal Institute of Technology
           L Fälth, University of Lund
           May 1983

TR 83-24   Corrosion resistance of a copper canister for
           spent nuclear fuel
           The Swedish Corrosion Research Institute and its
           reference group
           Stockholm, Sweden April 1983

TR 83-25   Feasibility study of EB welding of spent nuclear
           fuel canisters
           A Sanderson, T F Szluha, J Turner
           Welding Institute
           Cambridge, United Kingdom April 1983

TR 83-26   The KBS UO_2 leaching program
           Summary Report 1983-02-01
           Ronald Forsyth, Studsvik Energiteknik AB
           Nyköping, Sweden February 1983

TR 83-27   Radiation effects on the chemical environment
           in a radioactive waste repository
           Trygve Eriksen
           Royal Institute of Technology, Stockholm
           Arvid Jacobsson
           University of Luleå, Luleå
           Sweden 1983-07-01

TR 83-28 An analysis of selected parameters for the
BIOPATH-program
U Bergström
A-B Wilkens
Studsvik Energiteknik AB
Nyköping, Sweden 1983-06-08

TR 83-29 On the environmental impact of a repository for
spent nuclear fuel
Otto Brotzen
Stockholm, Sweden April 1983

TR 83-30 Encapsulation of spent nuclear fuel -
Safety Analysis
ES-konsult AB
Stockholm, Sweden April 1983

TR 83-31 Final disposal of spent nuclear fuel -
Standard programme for site investigations
Compiled by
Ulf Thoregren
Swedish Geological
April 1983

TR 83-32 Feasibility study of detection of defects in thick
welded copper
Tekniska Röntgencentralen AB
Stockholm, Sweden April 1983

TR 83-33 The interaction of bentonite and glass with
aqueous media
M Mosslehi
A Lambrosa
J A Marinsky
State University of New York
Buffalo, NY, USA April 1983

TR 83-34 Radionuclide diffusion and mobilities in compacted
bentonite
B Torstenfelt
B Allard
K Andersson
H Kipatsi
L Eliasson
U Olofsson
H Persson
Chalmers University of Technology
Göteborg, Sweden April 1983

TR 83-35 Actinide solution equilibria and solubilities in
geologic systems
B Allard
Chalmers University of Technology
Göteborg, Sweden 1983-04-10

TR 83-36 Iron content and reducing capacity of granites and
bentonite
B Torstenfelt
B Allard
W Johansson
T Ittner
Chalmers University of Technology
Göteborg, Sweden April 1983

TR 83-37 Surface migration in sorption processes
          A Rasmuson
          I Neretnieks
          Royal Institute of Technology
          Stockholm, Sweden March 1983

TR 83-38 Evaluation of some tracer tests in the granitic
          rock at Finnsjön
          L Moreno
          I Neretnieks
          Royal Institute of Technology, Stockholm
          C-E Klockars
          Swedish Geological, Uppsala
          April 1983

TR 83-39 Diffusion in the matrix of granitic rock
          Field test in the Stripa mine. Part 2
          L Birgersson
          I Neretnieks
          Royal Institute of Technology
          Stockholm, Sweden March 1983

TR 83-40 Redox conditions in groundwaters from
          Svartboberget, Gideå, Fjällveden and Kamlunge
          P Wikberg
          I Grenthe
          K Axelsen
          Royal Institute of Technology
          Stockholm, Sweden 1983-05-10

TR 83-41 Analysis of groundwater from deep boreholes in
          Svartboberget
          Sif Laurent
          Swedish Environmental Research Institute
          Stockholm, Sweden 1983-06-10

TR 83-42 Final disposal of high-level waste and spent
          nuclear fuel - foreign activities
          R Gelin
          Studsvik Energiteknik AB
          Nyköping, Sweden May 1983

TR 83-43 Final disposal of spent nuclear fuel - geological,
          hydrological and geophysical methods for site
          characterization
          K Ahlbom
          L Carlsson
          O Olsson
          Swedish Geological
          Sweden May 1983

TR 83-44 Final disposal of spent nuclear fuel - equipment
          for site characterization
          K Almén, K Hansson, B-E Johansson, G Nilsson
          Swedish Geological
          O Andersson, IPA-Konsult
          P Wikberg, Royal Institute of Technology
          H Åhagen, SKBF/KBS
          May 1983

TR 83-45   Model calculations of the groundwater flow at
           Finnsjön, Fjällveden, Gideå and Kamlunge
           L Carlsson
           A Winberg
           Swedish Geological, Göteborg
           B Grundfelt
           Kemakta Consultant Company, Stockholm
           May 1983

TR 83-46   Use of clays as buffers in radioactive repositories
           Roland Pusch
           University of Luleå
           Luleå May 25 1983

TR 83-47   Stress/strain/time properties of highly compacted
           bentonite
           Roland Pusch
           University of Luleå
           Luleå May 1983

TR 83-48   Model calculations of the migration of radio-
           nuclides from a repository for spent nuclear fuel
           A Bengtsson
           Kemakta Consultant Company, Stockholm
           M Magnusson
           I Neretnieks
           A Rasmuson
           Royal Institute of Technology, Stockholm
           May 1983

TR 83-49   Dose and dose commitment calculations from ground-
           waterborne radioactive elements released from a
           repository for spent nuclear fuel
           U Bergström
           Studsvik Energiteknik AB
           Nyköping, Sweden May 1983

TR 83-50   Calculation of fluxes through a repository caused
           by a local well
           R Thunvik
           Royal Institute of Technology
           Stockholm, Sweden May 1983

TR 83-51   GWHRT - A finite element solution to the coupled
           ground water flow and heat transport problem in
           three dimensions
           B Grundfelt
           Kemakta Consultant Company
           Stockholm, Sweden May 1983

TR 83-52   Evaluation of the geological, geophysical and
           hydrogeological conditions at Fjällveden
           K Ahlbom
           L Carlsson
           L-E Carlsten
           O Duran
           N-Å Larsson
           O Olsson
           Swedish Geological
           May 1983